AEDC-TR-72-158

cy.1

A MATHEMATICAL DESCRIPTION OF GAS-SURFACE INTERACTION BASED UPON RECIPROCITY

Max Kinslow
ARO, Inc.

February 1973

Approved for public release; distribution unlimited.

VON KÁRMÁN GAS DYNAMICS FACILITY
ARNOLD ENGINEERING DEVELOPMENT CENTER
AIR FORCE SYSTEMS COMMAND
ARNOLD AIR FORCE STATION, TENNESSEE

NOTICES

When U. S. Government drawings specifications, or other data are used for any purpose other than a definitely related Government procurement operation, the Government thereby incurs no responsibility nor any obligation whatsoever, and the fact that the Government may have formulated, furnished, or in any way supplied the said drawings, specifications, or other data, is not to be regarded by implication or otherwise, or in any manner licensing the holder or any other person or corporation, or conveying any rights or permission to manufacture, use, or sell any patented invention that may in any way be related thereto.

Qualified users may obtain copies of this report from the Defense Documentation Center.

References to named commercial products in this report are not to be considered in any sense as an endorsement of the product by the United States Air Force or the Government.

A MATHEMATICAL DESCRIPTION OF GAS-SURFACE INTERACTION BASED UPON RECIPROCITY

Max Kinslow
ARO, Inc.

FOREWORD

The research presented in this report was conducted by the Arnold Engineering Development Center (AEDC), Air Force Systems Command (AFSC), Arnold Air Force Station, Tennessee, in support of Program Element 64719F.

The results of the research were obtained by ARO, Inc. (a subsidiary of Sverdrup & Parcel and Associates, Inc.), contract operator of the AEDC, AFSC, under Contract F40600-73-C-0004. The research was conducted from July 1970 to July 1971 under ARO Project Nos. VW3121 and VW3126. The manuscript was submitted for publication on September 20, 1972.

The work reported herein was presented to the University of Tennessee in partial fulfillment of the requirements for the Ph.D. degree.

This technical report has been reviewed and is approved.

ROSS G. ROEPKE
Requirements Planning Division
Directorate of Technology

ROBERT O. DIETZ
Director of Technology

ABSTRACT

The general problem of the interaction between a monatomic gas and a solid surface is investigated from a mathematical point of view by the use of a scattering kernel. This general scattering kernel must fulfill the obvious conditions of normalization and non-negativity and has recently been shown to also satisfy the condition of detailed balancing or reciprocity. Previous gas-surface theories, both analytical and empirical, are considered in view of reciprocity. It is shown that most of these descriptions are satisfactory for gross gas-surface interactions but fail to describe the detailed interaction. By assuming a product solution in each of three coordinate systems, an infinite series of solutions is obtained. The first scattering kernel in each series is obtained in closed mathematical form, while the second and third are evaluated numerically. Recurrence relations are obtained for the coefficients in the infinite series for all solutions. It is shown that the first scattering kernel in rectangular coordinates adequately describes the experimentally observed results of gas-surface interaction. This solution has two parameters which describe the gas-surface interaction. It is shown that these parameters are related to a tangential and a normal thermal accommodation coefficient. The scattering kernels obtained are integrated, in some cases analytically and others numerically, with various weighting functions in order to obtain mean reflected properties, both global and local, such as molecular flux, speed, and energy. These various results are presented for typical gas-surface interaction parameters. It is shown that some combination of parameters describe general scattering characteristics. The theoretical results are in agreement with existing detailed measurements of reflected quantities such as intensities and mean speed, for a wide range of incident energy and direction.

TABLE OF CONTENTS

LIST OF FIGURES

FIGURE PAGE

FIGURE PAGE

FIGURE PAGE

LISTS OF SYMBOLS

LATIN

A_n	Weighting factor in Equation 21-a
A_r	Constant ≥ 1 related to α_r by Equation 204
A_x, A_y	Constant ≥ 1 related to α_x, α_y by Equations 196 and 197
A_ρ	Constant ≥ 1 related to α_ρ by Equation 208
a_{ij}	Constant used in Equation 19-a
a_k	Constant used in Equations 89 and 90
a	Dummy variable in Appendix B
B_n	Weighting factor in Equation 21-b
b_{ij}	Constant used in Equation 19-b
b	Dummy variable in Appendix B
C_n	Weighting factor in Equation 60
$c_{n,k}$	Constant used in Equation 22-a
$\tilde{c}_{n,k}$	Constant defined by Equation 33
c	Dummy variable in Appendix B
D_n	Weighting factor in Equation 71
d	Dummy variable in Appendix B
$d_{n,k}$	Constant used in Equation 22-b
$\tilde{d}_{n,k}$	Constant defined by Equation 43
dA	Detector sensing area, see Figure 27, Appendix A
d^3v	Incremental volume in velocity space, defined in Table I, page 18

$d\omega$	Solid angle, defined by Equation 156, see Figure 27, Appendix A
e	Kinetic energy per molecule, defined by Equation 140
e_w	Value of $\bar{e}$ for full accommodation to T_w
e_j	Constant defined by Equation 85
F	Function defined by Equations 11 and 211
f	Fraction of molecules reflected diffusely as defined by Maxwell [3]
f	Velocity distribution function at a point in space
f_r	Function defined by Equation 55
f_x, f_y	Functions defined by Equation 16
f_ρ	Function defined by Equation 68
$f(t)$	Arbitrary function used in Equations 94 and 110
G	Function defined by Equations 99 and 100
$g_{n,k}$	Constant defined by Equation 72
$\tilde{g}_{n,k}$	Constant defined by Equation 80
H	Function defined by Equations 113 and 114
h_j	Constants defined by Equation 101
I	Reflected molecular intensity given by Equation 160
I'	Relative molecular intensity
$\tilde{I}$	Dimensionless reflected intensity defined by Equation 161

i	Dummy variable
$\hat{j}$	Unit vector normal to surface
j	Dummy variable
$\hat{k}$	Arbitrary unit vector
k	Dummy variable
L	Distance between detector and surface element, see Figure 27, Appendix A
m	Molecular mass; also dummy variable
$\dot{N}$	Molecular beam intensity (number/unit time)
n	Integer ≥ 0, introduced in Equations 22 and 72
$P, P(\hat{v}', \hat{v})$	Scattering kernel
$P_x, P_x(v_x', v_x)$	Scattering kernel in x-coordinate direction, given by Equation 27-a
$P_x(v_x', v_x, \alpha_x)$	Same as P_x, with α_x as independent variable, used in Equation 211
$P_y, P_y(v_y', v_y)$	Scattering kernel in y-coordinate direction, given by Equation 27-b
$P_y(v_y', v_y, \alpha_y)$	Same as P_y, with α_y as independent variable, used in Equation 211
$P_z, P_z(v_z', v_z)$	Scattering kernel in z-coordinate direction, defined same as P_x
$P_z(v_z', v_z, \alpha_z)$	Same as P_z, with α_z as independent variable, used in Equation 211
$P_r, P_r(v_r', v_r)$	Scattering kernel in r-coordinate direction, given by Equation 59
$P_\rho, P_\rho(v', v)$	Scattering kernel in ρ-coordinate direction, given by Equation 74

$P_{x,n}, P_{z,n}$	Scattering kernel defined by Equation 26-a
$P_{y,n}$	Scattering kernel defined by Equation 26-b
$P_{r,n}$	Scattering kernel defined by Equation 61
$P_{\rho,n}$	Scattering kernel defined by Equation 77
P_1' and P_2	Scattering kernel defined by Equation 210
P_x	Scattering kernel defined by Equation 63
P_θ	Scattering kernel defined by Equation 124
P_φ	Scattering kernel defined by Equation 125
p	Variable in Equations 31 and 41
Q	Point of impact of molecular beam on surface
R	Gas constant per unit mass
r	Coordinate defined in Figure 1, Appendix A
S, S_x', etc.	Dimensionless velocity, $v/\sqrt{2RT_w}$, $v_x'/\sqrt{2RT_w}$, etc.
S_r	Reflected speed ratio defined by Equation 209
T	Temperature
T_r	Reflected static temperature in Section 1.3.6
T_w	Wall or surface temperature
t	Dummy variable
$\vec{u}$	Mean velocity of reflected Maxwellian in Section 1.3.6
$\vec{v}$	Reflected molecular velocity
$\vec{v'}$	Incident molecular velocity
v	Reflected speed $\lvert\vec{v}\rvert$
v'	Incident speed $\lvert\vec{v'}\rvert$
v_x, v_y', etc.	Velocity component in corresponding coordinate
W_n	Function defined by Equation 72
X_n	Function defined by Equation 22-a

x	Coordinate defined in Figure 1, Appendix A
Y_n	Function defined by Equation 22-b
y	Coordinate defined in Figure 1, Appendix A
z	Coordinate defined in Figure 1, Appendix A

GREEK

α	Thermal accommodation coefficient, defined by Equation 199
α_e	Local energy accommodation coefficient, defined by Equation 175
α_x, α_y, etc.	Accommodation coefficient in corresponding coordinate direction
β	Weighting factor in Section 1.2.1
ΔH	Heat of adsorption in Section 4.1
θ	Coordinate defined in Figure 1, Appendix A
θ_i	Value of θ for incident molecule
θ_m	Value of θ for which I is a maximum
μ	Ratio of masses of gas and surface atoms as used by Baule [10]
ν	Order of Bessel function (Appendix B)
ρ	Coordinate direction defined in Figure 1, Appendix A
ρ	Density of reflected gas molecules, defined in Equation 165
$\tilde{\rho}$	Dimensionless density defined by Equation 166
τ	Period of Fourier series in Section 2.3.2
φ	Coordinate defined in Figure 1, Appendix A

φ_i	Value of φ for incident molecule
Ω	$\psi_i - \psi$, used in Section 2.4
ψ	Coordinate defined in Figure 1, Appendix A

SUPERSCRIPTS

+	Refers to molecules directed toward the surface
-	Refers to molecules directed away from the surface

SUBSCRIPTS

i,j,k,m	Dummy variables
x,y,z	Refers to components in rectangular coordinates
r	Component in cylindrical coordinates
ρ	Component in spherical coordinates

OTHERS

$\overline{(\ )}$	Mean or average quantity
$\vec{(\ )}$	Signifies a vector quantity

FUNCTIONS

erf(t)	Error function
exp(t)	Exponential function
$I_\nu(t)$	Bessel function
$M_{a,b}(t)$	Whittaker function
M(a,b,t)	Kummer function
m!	Factorial
$\delta(t)$	Dirac delta function
$\Gamma(t)$	Gamma function

I. INTRODUCTION

The interaction of a gas with a solid surface is very important in several fields of science. The aerodynamicist would like to know the gross interaction effects such as the total momentum and energy exchange under conditions such as the flight of an artificial satellite through the rarefied upper atmosphere. The mathematician, working in the field of kinetic theory, desires a mathematical description of the gas-surface interaction for a boundary condition to the Boltzmann equation. Theoretical and experimental results on gas-surface interaction help the physical chemist better understand the complex process of surface catalyticity and help the physicist understand the surface structure and the gas-solid interaction potentials.

In general, the knowledge and understanding of gas-surface interaction phenomena are less advanced than that in the bulk gas, this in spite of the fact that most experimentation in the bulk gas is influenced to a large extent by solid boundaries. It is, in general, true that the knowledge of the interface phenomena between two disciplines proceeds slower than that in either. Usually, it is necessary to resort to empirical methods for descriptions of these phenomena, e.g., heat transfer coefficients.

Many times in this paper and other papers the terms "reflected gas" and "reemitted gas" are used interchangeably

to mean the gas after it has interacted with the surface, irrespective of the type of interaction.

1.1 HISTORICAL BACKGROUND

It is now approaching 100 years since Knudt and Warburg [1][1] in 1875 proposed, based upon measurements of the damping of a vibrating disk in a rarefied gas, that under certain conditions a gas may slip adjacent to a solid boundary. They speculated that something analogous may occur in rarefied gases when heat is being conducted, namely, a temperature jump at a solid boundary. Prior to this time it had been assumed that a gas in contact with a solid surface has identical velocity and temperature as the surface, i.e., the zero slip condition. Osborne Reynolds [2] in 1879 introduced a factor of slip between mean tangential velocities of incident and reflected molecules. He recognized that this factor somehow depended upon the nature of the gas-surface interaction. He also realized that incomplete molecular accommodation is not a prerequisite for velocity slip or temperature jump at a surface. However, this factor, the inverse of which he considered a coefficient of roughness, concerns macroscopic properties.

Maxwell [3] later that same year was the first to propose a gas surface interaction model based upon the kinetic theory of gases, which he pioneered [4]. He showed that both

---

[1]Numbers in brackets refer to similarly numbered references in the List of References.

a perfectly elastic smooth surface and a surface of such properties that the gas being reflected has the same distribution of velocities as if it were emitted from a static gas at the surface temperature (complete accommodation) do not disturb a gas in equilibrium with the surface. He proposed:

> . . . to treat the surface as something intermediate between a perfectly reflecting and a perfectly absorbing surface, and, in particular, to suppose that of every unit of area a portion f absorbs all the incident molecules, and afterwards allows them to evaporate with velocities corresponding to those in still gas at the temperature of the solid, while a portion 1-f perfectly reflects all the molecules incident upon it.

Even today the gas-surface model of Maxwell is probably the most widely used for calculating gross gas-surface effects. It is interesting that his original paper [3] did not contain any mention of the gas-surface interaction; this was added in an appendix at the insistence of a referee.

Smoluchowski [5] was the first to measure the heat transfer between rarefied gases and a surface and to show that there is indeed a temperature jump. He also recognized the need for parameters to indicate the degree that gas molecules, upon an encounter with a surface, assume the conditions of the surface. These parameters, which can be defined for each molecular quantity that can be affected by the encounter, are known as accommodation coefficients. However, the thermal accommodation coefficient as defined by him, was awkward since it could vary over all positive numbers. His unlucky choice of the definition of this factor, caused Knudsen [6] to be widely recognized

as the originator of the thermal accommodation coefficient, α, which he defines to vary between zero and unity. Knudsen experimentally determined α for several different gas-surface combinations and found that it varied from 0.26 for hydrogen in contact with polished platinum up to approximately 0.87 for the heavier gases such as nitrogen.

Both Smoluchowski and Knudsen defined accommodation in terms of temperature since they were especially interested in flows close to equilibrium for which temperature could be defined. Any definition of thermal accommodation involving temperature implicitly assumes that the incident and reflected gas has a temperature associated with it, i.e., it has a Maxwellian velocity distribution. Recently Kuscer, et al [7] read into Knudsen's definition of α the assumption that for a gas with a Maxwellian distribution incident upon a surface, that the reflected distribution is also Maxwellian at a temperature determined from the definition of the accommodation coefficient. This hypothesis, which Kuscer [7] refers to as "Knudsen's assumption" will be compared to theoretical results later. However, Knudsen himself recognized that for departures from equilibrium the reflected molecules may not have a Maxwellian velocity distribution and that the definition of α must be written in terms of energy.

The experimental results of Smoluchowski [5] and Knudsen [6] and also those of Soddy and Berry [8] and Blodgett and Langmuir [9] for the thermal accommodation of

various gas-surface interactions indicated two general trends. First, as was probably expected, α was lower for polished surfaces than for rough surfaces. Second, α was lower for lighter gases and approached unity for heavier gases.

Baule [10] in 1914 was the first to attempt a microscopic analysis of gas-surface interactions. He assumed that both the gas molecules and the surface atom behave as hard spheres with a mass ratio μ. The result that he obtained for the case of a zero temperature solid was:

$$\alpha = 2\mu/(1+\mu)^2$$

This result was in qualitative agreement with the variation of α with gas molecular weight for $\mu < 1$. In general, however, this simple theory could not be expected to contribute to a better understanding of gas-surface interactions since neither the surface structure nor the interaction potential is modeled in a realistic way.

Following Baule, several other microscopic gas-surface theories were proposed based upon both classical and the newly developed quantum mechanics. Most of the early analyses were of necessity one-dimensional treatments which were either simple and not very meaningful or complex and not amenable to mathematical solutions. Only with the introduction of large analogue and digital computers has it been possible to propose and solve more realistic three-dimensional models.

As the theoretical models advanced so did the experimental capabilities. The experimental results presented in [5, 6, 8 and 9] were based upon near equilibrium conditions, where the gas incident upon the surface had a near Maxwellian velocity distribution with a temperature close to the surface temperature. Beginning around 1930 there was renewed interest in experimental gas surface interactions, which was prompted by the prediction of diffraction effects by quantum theory. Unidirectional molecular beams were generated by the use of an effusive orifice or Knudsen source. Most notable among the experimental investigators of this period was Estermann [11, 12].

It was not until 1951 that Kantrowitz and Gray [13] suggested an improvement on molecular beam generation. Their aerodynamic nozzle and skimmer permitted a several fold increase in molecular flux as well as a more nearly monoenergetic beam.

Molecular detection techniques have also improved to the point such that today the velocity distribution function of molecules reflected from a surface can be determined, thus permitting the determination of desired gas-surface parameters.

The earlier theoretical gas-surface models were required to reproduce only the gross accommodation coefficients of which α was the most important. However, with improved experimental techniques, it was necessary that the theoretical results be able to describe these more detailed

experimental data. The most important of these was the distribution of reflected molecular flux as a function of reflected direction, usually referred to as the "spatial distribution."

The most complete classical model at present is probably that of Oman, et al [14]. This model requires a statistical or Monte Carlo approach in order to obtain a solution and is therefore not convenient for a mathematical description of the gas-surface interaction. There are many other analyses such as the "hard cube" model of Logan and Stickney [15] and the "soft cube" model of Logan and Keck [16]. These models are either too complicated for a general description of the gas-surface interaction or do not adequately describe it. For a more complete discussion of gas-surface interaction theories see the review paper by Goodman [17]. Recently, Busby [18] has proposed a gas-surface model that utilizes a potential well at the surface in order to explain the observed capture coefficient of a molecular beam incident upon a highly cooled surface.

In order to represent the gas-surface interaction in mathematical terms, an alternate approach has been to propose empirical descriptions. As has been pointed out, Maxwell [3] proposed a model of this sort. More recently, Nocilla [19, 20] has extended the Maxwell model to assume that the reemitted velocity distribution is equivalent to the free molecule effusive flow of a gas with mean velocity and temperatures to be determined by fitting the experimental

data. Hurlbut and Sherman [21] have applied this model to calculate aerodynamic forces on simple bodies in free molecule flow. Epstein [22] proposes an empirical reflection model that matches the variation of α with temperature by determining three arbitrary constants. These empirical models will be discussed in more detail later.

It has been widely recognized since Maxwell that any gas-surface model, either analytical or empirical, must preserve a Maxwellian velocity distribution at the surface temperature, i.e., at equilibrium the surface does not disturb the gas. This condition has recently been strengthened by showing that not only is the Maxwellian distribution maintained at a surface globally but also the principal of detailed balancing is satisfied. These conditions will be discussed in more detail in the next section.

1.2 RECIPROCITY AND GAS-SURFACE INTERACTION

The time independent interaction between a monatomic gas and a solid boundary is expressed mathematically by means of a function $P(\vec{v}', \vec{v})$ which relates the probability of reflected molecular velocity $\vec{v}$, to that of the incident molecular velocity, $\vec{v}'$, and the boundary or wall properties. Thus, for given wall conditions, a molecule with velocity $\vec{v}'$ impinging upon the surface will have a probability of $P(\vec{v}', \vec{v})d^3v$ that it will be scattered into the velocity increment d^3v about $\vec{v}$. $P(\vec{v}', \vec{v})$ is known as a scattering kernel because of the role it plays in Equation 3.

The scattering kernel $P(\hat{v}', \hat{v})$, which is defined only for $\hat{v}'$ directed toward the surface and $\hat{v}$ directed away is non-negative and for the case of no mass exchange with the surface is normalized in half velocity space. These requirements are expressed mathematically as:

$$P(\hat{v}', \hat{v}) \geq 0, \quad \hat{v}' \cdot \hat{j} < 0, \quad \hat{v} \cdot \hat{j} > 0 \tag{1}$$

$$\int_{\hat{v}\hat{j}>0} P(\hat{v}', \hat{v}) \, d^3v = 1 \tag{2}$$

See the List of Symbols and Figure 1, Appendix A, for the definition of symbols. It should be pointed out that the orientation of the x,z axes for an isotropic surface is arbitrary and is usually chosen such that v_z' is zero. If the surface is not isotropic but has differences in structure in various directions then the x and z axes should be defined to align with the structure of the surface in order to simplify the equations.

The use of the scattering kernel, as has been pointed out by Shidlovskiy [23] is the most general representation of the boundary conditions at a solid surface. The use of the scattering kernel is desirable in order to completely specify the boundary conditions for the Boltzmann equation when solid boundaries are involved.

The velocity distribution function,[2] f, in a gas adjacent to a solid boundary may be considered to consist of two parts, those molecules with velocities directed toward the solid surface or wall and those with velocities directed away from the wall. Thus:

$$f = f^+ + f^-$$

where: $f^+ \equiv 0, \ \vec{v}\cdot\vec{j} > 0$

$$f^- \equiv 0, \ \vec{v}'\cdot\vec{j} < 0$$

Using the scattering kernel it can be shown (Cercignani [24], page 51) that the distribution of reflected molecules is related to the distribution of incident molecules by:

$$f^+(\vec{v}) = -(\vec{v}\cdot\vec{j})^{-1} \int_{\vec{v}\cdot\vec{j}<0} (\vec{v}'\cdot\vec{j}) P(\vec{v}', \vec{v}) f^-(\vec{v}') \, d^3v' \qquad (3)$$

From consideration of a gas in equilibrium with a surface, it is obvious that if $f^-(\vec{v}')$ is a static Maxwellian distribution at the wall temperature, T_w, then $f^+(\vec{v})$ is also a Maxwellian at T_w. This fact restricts somewhat the functions that are suitable for describing gas-surface interactions.

---

[2]The velocity distribution function as used in this paper is defined as a probability density in velocity space at a point in physical space. This is the normal kinetic theory definition of f. However, most authors in the field of molecular beams and gas-surface interaction define a velocity distribution function in terms of flux of molecules instead of molecular density. This frequently causes confusion since many times the definition used is not clearly stated.

However, from an equilibrium consideration it can be shown that not only is the Maxwellian distribution maintained by the molecular interactions as a whole, but each encounter is compensated by an inverse encounter. In other words, the general principle of "detailed balancing" is applicable to gas-surface interaction as well as in the gas itself. Cercignani [24] recently pointed out the importance of detailed balancing for the description of the gas-surface interaction. Kuscer and Summerfield [25] obtained the same results based upon an analogy with slow neutrons and referred to it as the "reciprocity relation."

This reciprocity relation in terms of present nomenclature is:

$$-(\vec{v}' \cdot \vec{j}) \exp(-\vec{v}'^{2}/2RT_w) P(\vec{v}', \vec{v}) = (\vec{v} \cdot \vec{j}) \exp(-\vec{v}^2/2RT_w) P(-\vec{v}, -\vec{v}') \quad (4)$$

The interaction of a molecule with the surface, which is described by $P(\vec{v}', \vec{v})$, takes place on an individual statistical basis and is independent of whether the gas is in equilibrium with the wall or not as long as the surface is in equilibrium with itself. Therefore, Equation 4 applies independent of the thermodynamic state of the gas or the details of what happens on a microscopic scale during the gas-surface interaction.

It may be surprising that detailed balancing holds between gas molecules only when the gas is at equilibrium but is still applicable for molecular encounters with the

surface under any conditions of the gas. It might help to think of detailed balancing as an interaction between a test particle and an equilibrium reservoir. The test particle is a molecule with velocity $\vec{v}'$ before the encounter and velocity $\vec{v}$ after the encounter. The reservoir in one case is the equilibrium gas and in the other is the surface. For non-equilibrium conditions in the gas the reservoir consisting of gas molecules ceases to exist while the surface is assumed to remain unchanged.[3] It should be pointed out that under varying molecular fluxes to a surface that the characteristics of the surface may change. For example, under the condition of high flux, a relatively large amount of gas may be adsorbed on the surface and therefore change its characteristics. In the present context it is assumed that the effective surface is invariant with incident gas properties. For two derivations of reciprocity, both classical and quantum mechanical; see the paper by Kuscer [26].

Equations 1, 2 and 4 are the basic relations that must be satisfied by the scattering kernel. Notice that Equations 2 and 4 are linear in the scattering kernel. Thus, if P_1 and P_2 satisfy Equations 1, 2 and 4 then $P_3 = \beta P_1 + (1-\beta) P_2$ satisfies Equations 2 and 4 for all values of β and satisfies Equation 1 for $0 \leq \beta \leq 1$. On the other

[3]If the gas adjacent to a wall were in such a state of non-equilibrium that the equilibrium of the wall were destroyed, then Equation 4 would no longer be valid, e.g., for extremely high rates of heat transfer.

hand, if P_1 and/or P_2 do not satisfy Equation 1 it may be possible for some values of β that P_3 satisfies Equations 1, 2 and 4. Therefore, in the analysis that follows individual scattering kernels are not disqualified because of failure to fulfill Equation 1 since a linear combination with others may.

It can also be shown that if P_1 satisfies Equation 4 then P_2 also satisfies the reciprocity relation, where P_2 is given by:

$$P_2(\vec{v}', \vec{v}) = P_1[2(\vec{v}' \cdot \vec{j})\vec{j} - \vec{v}', \vec{v}] \tag{5}$$

Equation 5 is simply a reflection of P_2 about the normal velocity and it is easy to show that Equations 1 and 2 are also fulfilled. Thus, if a forward scattering kernel satisfies reciprocity then a backscattering kernel also satisfies reciprocity.

1.3 SOME SCATTERING KERNELS IN VIEW OF RECIPROCITY

1.3.1 Complete Accommodation

The scattering kernel for complete accommodation of a gas to a surface is the same as the effusive flow of a gas at T_w as assumed by Maxwell [3]. The kernel becomes

$$P(\vec{v}', \vec{v}) = (2/\pi)(2RT_w)^{-2}(\vec{v} \cdot \vec{j}) \exp(-v^2/2RT_w) \tag{6}$$

1.3.2 Specular Reflections

The scattering kernel for specular reflection is:

$$P(\hat{v}', \hat{v}) = \delta(v_x' - v_x)\delta(v_y' + v_y)\delta(v_z' - v_z) \tag{7}$$

where: $\delta(t)$ is the Dirac delta function and has the following properties:

$$\delta(t) = 0, \quad t \neq 0$$
$$\int_{-\infty}^{\infty} \delta(t) = 1 \tag{8}$$

1.3.3 Diffuse Elastic Scattering

The scattering kernel for diffuse elastic scattering from a surface, also called Lambert scattering by analogy with light reflected from a rough surface, is:

$$P(\hat{v}', \hat{v}) = v_y \, \delta(v' + v)/(\pi v^3) \tag{9}$$

1.3.4 Back Scattered Model

Berman and Maegley [27] have recently (1972) proposed a back scattering model in order to explain the experimentally observed fact that the flow of a rarefied gas through a tube may be less that predicted for complete accommodations. Many years earlier Gaede [28] in 1913 had observed the same phenomenon and concluded that based upon Maxwell's model that the amount of specular reflectivity should be negative. The back scattering model is:

$$P(\hat{v}', \hat{v}) = \delta(v_x' + v_x)\delta(v_y' + v_y)\delta(v_z' + v_z) \tag{10}$$

This expression can be obtained from Equation 7 by the application of Equation 5. The microscopic observation

of back scattering is very difficult since any molecular detector tends to disturb the incident molecules.

1.3.5 Epstein's Scattering Model [22]

As mentioned earlier, Epstein [22] has proposed an empirical scattering kernel. His expression, in terms of present nomenclature, is:

$$P(\vec{v}',\vec{v}) = v_y \exp(-v^2/2RT_w)F(\vec{v}')F(\vec{v})/[\int_{v_y>0} v_y \exp(-v^2/2RT_w)\cdot$$

$$F(\vec{v})d^3v'] + \delta(v_x'-v_x)\delta(v_y'+v_y)\delta(v_z'-v_z)[1-F(\vec{v}')] \qquad (11)$$

By substitution it can be shown that Equation 11 satisfies Equation 4 if $F(\vec{v}) = F(-\vec{v})$ and satisfies Equation 1 if $0 \leq F(\vec{v}) \leq 1$, otherwise $F(\vec{v})$ is an arbitrary function and satisfies Equation 2 for any $F(\vec{v})$. For the limits of $F(\vec{v}) \equiv 0$ and $F(\vec{v}) \equiv 1$, Equation 11 reduces to specular and diffuse scattering, respectively.

1.3.6 Nocilla's Scattering Model [19, 20]

Nocilla's normalized reflection model in terms of present nomenclature is:

$$P(\vec{v}',\vec{v}) = (2/\pi)(2RT_r)^{-2} v_y \exp[-(\vec{v}-\vec{u})^2/2RT_r]/[(\pi)^{1/2}(u_y/$$

$$\sqrt{2RT_r})\{1+\mathrm{erf}(u_y/\sqrt{2RT_r})\}+\exp(-u_y^2/2RT_r)] \qquad (12)$$

where: $T_r = T_r(\vec{v}')$

$\vec{u} = \vec{u}(\vec{v}')$

The quantities T_r and $\bar{u}$ are the temperature and mean velocity of the assumed reemitted Maxwellian. For $T_r = T_w$ and $\hat{u} = 0$ Equation 12 reduces to Equation 6 and for $T_r \rightarrow 0$ and $\hat{u} = \hat{v}' - 2(\hat{v}\cdot\hat{j})\hat{j}$ Equation 12 approaches Equation 7. It is difficult to ascertain if Nocilla's model satisfies Equation 4. However, Kuscer [7] has stated that, in general, Equation 12 does not satisfy reciprocity.

1.3.7 Summary

By direct substitution and inspection it can be seen that Equations 6, 7, 9 and 10, as well as Equation 11 satisfy the reciprocity condition as expressed in Equation 4 as well as satisfying Equations 1 and 2. Note that all these kernels except Equation 6 are discontinuous in velocity space and would therefore not be suitable for describing a real microscopic gas-surface interaction. It is widely recognized [24, 25, 26] that Equations 1, 2 and 4 are necessary conditions which must be satisfied by the scattering kernel for any surface.

Any physical model of the gas-surface interaction such as those given in [14, 15 and 16], is solved exactly, would satisfy Equations 1, 2 and 4. However, when approximations are made, as is usually done, the results do not necessarily fulfill reciprocity, although Equations 1 and 2 can be satisfied. While agreement with data can be achieved over a limited range by a suitable choice of model parameters, these models cannot be extended with confidence outside the range of known validity.

1.4 COORDINATE SYSTEMS

In the analysis that follows, the scattering kernel is solved as a product solution in three different coordinate systems; rectangular, cylindrical and spherical. After giving the relations among the various coordinate systems the three developments will be presented in Section II.

Referring to Figure 1, Appendix A, the coordinates in each system are:

Coordinate System	Coordinates
rectangular	x,y,z
cylindrical	y,r,ψ
spherical	ρ,θ,φ

The cylindrical and spherical systems are not identical with those normally encountered. These coordinates were chosen to match those commonly used by gas-surface experimentalists [18, 29].

The relations between velocity components and angles in these coordinate systems are shown in Table I, page 18. Also given is the expression for an incremental volume in velocity space.

TABLE I
RELATIONS BETWEEN VELOCITY COMPONENTS

Coordinate System		Rectangular	Cylindrical	Spherical
Rectangular	$v_x =$	v_x	$v_r\cos\psi$	$v_\rho\cos\varphi\sin\theta$
	$v_y =$	v_y	v_y	$v_\rho\cos\varphi\cos\theta$
	$v_z =$	v_z	$v_r\sin\psi$	$v_\rho\sin\varphi$
Cylindrical	$v_y =$	v_y	v_y	$v_\rho\cos\varphi\cos\theta$
	$v_r =$	$\sqrt{v_x^2+v_z^2}$	v_r	$v_\rho\sqrt{1-\cos^2\varphi\cos^2\theta}$
	$\psi =$	$\mathrm{Tan}^{-1}(v_z/v_z)$	ψ	$\mathrm{Tan}^{-1}(\mathrm{Tan}\varphi/\sin\theta)$
Spherical	$v_\rho =$	$\sqrt{v_x^2+v_y^2+v_z^2}$	$\sqrt{v_r^2+v_y^2}$	v_ρ
	$\theta =$	$\mathrm{Tan}^{-1}(v_x/v_y)$	$\mathrm{Tan}^{-1}(v_r\cos\psi/v_y$	θ
	$\varphi =$	$\mathrm{Tan}^{-1}\left(v_z/\sqrt{v_x^2+v_y^2}\right)$	$\mathrm{Sin}^{-1}\left(v_r\sin\psi/\sqrt{v_r^2+v_y^2}\right)$	φ
Incremental Volume in Velocity Space	$d^3v =$	$dv_x dv_y dv_z$	$v_r d\psi dv_r dv_y$	$v_\rho^2\cos\varphi dv_\rho d\theta d\psi$

II. THEORETICAL DEVELOPMENT

Some mathematical solutions to Equations 1, 2 and 4 will be obtained in this section. The questions may arise as to how a scattering kernel can be determined without considering the physics of the gas-surface interactions. The situation is similar to that in a gas at equilibrium, detailed balancing is valid and the molecular velocity distribution is obtained independently of the physical interaction between molecules. At the wall, however, a molecule interacts for only a finite length of time and therefore accommodation is incomplete. In any case, the set of functions that satisfy Equations 1, 2 and 4 contains all solutions to any physical model of the surface.

Borrowing from Maxwell the idea that each velocity component in a gas is independent, it is assumed that the interaction of each velocity component with the surface is independent. This is equivalent to assuming that $P(\vec{v}', \vec{v})$ can be represented by a product of independent probability functions, one for each coordinate direction.

2.1 RECTANGULAR COORDINATE SYSTEM

As has been previously stated, it is assumed that the scattering kernel $P(\vec{v}', \vec{v})$ can be written as a product solution in rectangular coordinates as follows:

$$P(\vec{v}', \vec{v}) = P_x(v_x', v_x) P_y(v_y', v_y) P_z(v_z', v_z) \tag{13}$$

Substituting this expression into Equations 2 and 4 and, since the coordinates are independent, equating the terms containing each coordinate, gives for the normalization and reciprocity relations, respectively:

$$\int_{-\infty}^{\infty} P_x(v_x', v_x)\, dv_x = 1 \tag{14-a}$$

$$\int_{0}^{\infty} P_y(v_y', v_y)\, dv_y = 1 \tag{14-b}$$

$$\int_{-\infty}^{\infty} P_z(v_z', v_z)\, dv_z = 1 \tag{14-c}$$

and:

$$\exp(-v_x'^2/2RT_w) P_x(v_x', v_x) = \exp(-v_x^2/2RT_w) P_x(-v_x, -v_x') \tag{15-a}$$

$$-v_y' \exp(-v_y'^2/2RT_w) P_y(v_y', v_y) = v_y \exp(-v_y^2/2RT_w) P_y(-v_y, -v_y') \tag{15-b}$$

$$\exp(-v_z'^2/2RT_w) P_z(v_z', v_z) = \exp(-v_z^2/2RT_w) P_z(-v_z, -v_z') \tag{15-c}$$

Notice that the equations for x and z are identical, therefore only the analyses for x and y will be presented in detail.

From a consideration of Equations 1 and 13 it is obvious that $P_x(v_x', v_x)$, $P_y(v_y', v_y)$, and $P_z(v_z', v_z)$ must be

non-negative. New functions are defined as follows:

$$f_x(v_x', v_x) = P_x(v_x', v_x)\exp[(A_x^2-1)v_x'^2/2RT_w+A_x^2 v_x^2/2RT_w] \tag{16-a}$$

$$f_y(v_y', v_y) = \frac{P_y(v_y', v_y)}{v_y}\exp[(A_y^2-1)v_y'^2/2RT_w+A_y^2 v_y^2/2RT_w] \tag{16-b}$$

where A_x and A_y are constants equal to or greater than unity. f_x and f_y were defined to simplify the reciprocity relation.

Substituting Equation 16 into Equations 14 and 15 yields for the normalization conditions:

$$\int_{-\infty}^{\infty} f_x(v_x', v_x)\exp[-(A_x^2-1)v_x'^2/2RT_w-A_x^2 v_x^2/2RT_w]\, dv_x = 1 \tag{17-a}$$

$$\int_{0}^{\infty} v_y f_y(v_y', v_y)\exp[-(A_y^2-1)v_y'^2/2RT_w-A_y^2 v_y^2/2RT_w]\, dv_y = 1 \tag{17-b}$$

and for the reciprocity relation:

$$f_x(v_x', v_x) = f_x(-v_x, -v_x') \tag{18-a}$$

$$f_y(v_y', v_y) = f_y(-v_y, -v_y') \tag{18-b}$$

From Equations 1 and 16 it can be seen that $f_x(v_x', v_x)$ and $f_y(v_y', v_y)$ must also be non-negative.

Let $f_x(v_x', v_x)$ and $f_y(v_y', v_y)$ be represented by double infinite series as follows:

$$f_x(v_x', v_x) = \sum_{j=0}^{\infty} \sum_{i=0}^{\infty} a_{ij} v_x'^{i} v_x^{j} \tag{19-a}$$

$$f_y(v_y', v_y) = \sum_{j=0}^{\infty} \sum_{i=0}^{\infty} b_{ij} v_y'^{i} v_y^{j} \tag{19-b}$$

Reciprocity requires that:

$$a_{ij} = (-1)^{i+j} a_{ji} \tag{20-a}$$

$$b_{ij} = (-1)^{i+j} b_{ji} \tag{20-b}$$

Taking advantage of the fact that reciprocity imposes a certain kind of symmetry on the coefficients in the expressions for f_x and f_y, the infinite series in Equation 19 can be rewritten as a double sum on the diagonals of the array of terms as follows:

$$f_x(v_x', v_x) = \sum_{n=0}^{\infty} A_n X_n (v_x', v_x) \tag{21-a}$$

$$f_y(v_y', v_y) = \sum_{n=0}^{\infty} B_n Y_n (v_y', v_y) \tag{21-b}$$

where:

$$X_n(v_x', v_x) = \sum_{k=0}^{\infty} c_{n,k} (v_x' v_x)^k [v_x^n + (-v_x')^n] \tag{22-a}$$

$$Y_n(v_y', v_y) = \sum_{k=0}^{\infty} d_{n,k}(v_y' v_y)^k [v_y^n + (-v_y')^n] \qquad (22\text{-b})$$

with:

$$c_{0,k} = \frac{a_{k,k}}{2A_0}$$

$$d_{0,k} = \frac{b_{k,k}}{2B_0}$$

$$\left.\begin{aligned} c_{n,k} &= \frac{a_{k,n+k}}{A_n} \\ d_{n,k} &= \frac{b_{k,k+n}}{B_n} \end{aligned}\right\} n = 1, 2, \ldots .$$

By inspection it can be seen that Equation 22 automatically satisfies, for arbitrary non-negative integer value of n, the reciprocity relation as expressed in Equation 18. The only restriction upon Equation 21 is that it be non-negative and be normalized according to Equation 17.

In order to shorten the equations, the arguments of variables will be hereafter omitted unless needed for clarity. Also, velocities will be non-dimensionalized by $\sqrt{2RT_w}$, e.g.:

$$\begin{aligned} S_x' &= v_x/\sqrt{2RT_w} \\ S_x &= v_x/\sqrt{2RT_w} \\ S &= v/\sqrt{2RT_w} \end{aligned} \qquad (23)$$

etc.

It is now assumed that each X_n and Y_n is individually normalized by Equation 17 as follows:

$$\sqrt{2RT_w} \int_{-\infty}^{\infty} X_n \exp[-(A_x^2-1)S_x'^2 - A_x^2 S_x^2] \, dS_x = 1 \quad (24\text{-a})$$

$$(2RT_w) \int_{0}^{\infty} S_y Y_n \exp[-(A_y^2-1)S_y'^2 - A_y^2 S_y^2] \, dS_y = 1 \quad (24\text{-b})$$

Overall normalization is satisfied by requiring that:

$$\sum_{n=0}^{\infty} A_n = 1 \quad (25\text{-a})$$

$$\sum_{n=0}^{\infty} B_n = 1 \quad (25\text{-b})$$

where A_n and B_n are arbitrary, subject to the above. It will become apparent that if for some n, X_n or Y_n is not normalizable then the corresponding A_n or B_n must be zero in order to preserve the overall normalization.

It is not necessary that X_n, Y_n, A_n or B_n be non-negative but only that f_x and f_y and therefore P be non-negative.

Each X_n or Y_n that satisfies the above conditions leads to a scattering kernel in the corresponding coordinate direction by the use of Equations 21 and 16. Thus:

$$P_{x,n} = X_n \exp[-(A_x^2-1)S_x'^2 - A_x^2 S_x^2] \quad (26\text{-a})$$

$$P_{y,n} = \sqrt{2RT_w}\, S_y Y_n \exp[-(A_y^2-1)S_y'^2 - A_y^2 S_y^2] \qquad (26\text{-b})$$

and:

$$P_x = \sum_{n=0}^{\infty} A_n\, P_{x,n} \qquad (27\text{-a})$$

$$P_y = \sum_{n=0}^{\infty} B_n\, P_{y,n} \qquad (27\text{-b})$$

Letting:

$$\tilde{c}_{n,k} = c_{n,k}\, (\sqrt{2RT_w/A_x})^{n+2k+1} \qquad (28\text{-a})$$

and:

$$\tilde{d}_{n,k} = d_{n,k}\, (\sqrt{2RT_w/A_y})^{n+2k+2} \qquad (28\text{-b})$$

and substituting in Equation 22 gives:

$$X_n = (2RT_w)^{1/2} \sum_{k=0}^{\infty} A_x^{n+2k+1}\, \tilde{c}_{n,k} (S_x' S_x)^k\, [S_x^n + (-S_x')^n] \qquad (29\text{-a})$$

$$Y_n = (2RT_w)^{-1} \sum_{k=0}^{\infty} A_y^{n+2k+2}\, \tilde{d}_{n,k} (S_y' S_y)^k\, [S_y^n + (-S_y')^n] \qquad (29\text{-b})$$

2.1.1 The Evaluation of $P_{x,n}$

Substituting Equation 29-a into Equation 24-a yields:

$$\int_{-\infty}^{\infty} \sum_{k=0}^{\infty} A_x^{n+2k+1} \tilde{c}_{n,k} (S_x' S_x)^k [S_x^n + (-S_x')^n] \exp(-A_x^2 S_x^2)\, dS_x =$$

$$\exp[(A_x^2 - 1) S_x'^2] \tag{30}$$

Integrating term by term on the left hand side where each term is of the form:

$$\int_{-\infty}^{\infty} t^m \exp(-p^2 t^2)\, dt = \begin{cases} 0 \text{ if } m \text{ is odd} \\ \Gamma(m/2 + 1/2)/p^{m+1} \text{ if } m \text{ is even} \end{cases} \tag{31}$$

and expanding the right hand side in an infinite series, gives the following power series in S_x':

$$\sum_{k=0}^{\infty} A_x^{2k} \tilde{c}_{2n,2k} S_x'^{2k} \Gamma(k + n + 1/2) - \sum_{k=0}^{\infty} A_x^{2n+2k} \tilde{c}_{2n,2k}$$

$$(S_x')^{2k+2n} \Gamma(k + 1/2) = \sum_{k=0}^{\infty} \frac{(A_x^2 - 1)^k S_x'^{2k}}{k!} \tag{32}$$

for even indices of $\tilde{c}_{n,k}$. Referring to Equation 30, for the first index and the second index odd the coefficients are arbitrary since the integrals and the right hand side of Equation 32 are zero. If the first index is odd, the integrated form of Equation 30 cannot be satisfied, because there are only odd powers of S_x' on the left hand side and only even powers on the right side. Therefore, $X_{2n+1}(v_x', v_x')$ cannot be normalized and A_{2n+1} must be zero. The only case that must be investigated is that given by Equation 32.

Equating the coefficients of like powers of S_x' in Equation 32 yields:

$$\tilde{c}_{n,k} = \left(\frac{A_x^2-1}{A_x^2}\right)^{\frac{k}{2}} \frac{1}{(k/2)!\ \Gamma(k/2 + n/2 + 1/2)} \qquad k < n$$

$$\tilde{c}_{n,k} = \left(\frac{A_x^2-1}{A_x^2}\right)^{\frac{k}{2}} \frac{1}{(k/2)!\ \Gamma(k/2 + n/2 + 1/2)} -$$

$$\tilde{c}_{n,k-n} \frac{\Gamma(k/2 - n/2 + 1/2)}{\Gamma(k/2 + n/2 + 1/2)} \qquad k \geq n \qquad (33)$$

for k,n even. For odd k, $\tilde{c}_{n,k}$ is arbitrary. However, it is assumed that Equation 33 also gives the odd coefficients. Given values of A_x and even n, and using Equations 26-a, 29-a and 33, $P_{x,n}$ can be determined as a function of S_x' and S_x. The case of n=0 can be solved analytically. For n=0 Equation 33 becomes:

$$\tilde{c}_{0,k} = \frac{1}{2}\left(\frac{A_x^2-1}{A_x^2}\right)^{\frac{k}{2}} \frac{1}{\Gamma(k/2 + 1)\ \Gamma(k/2 + 1/2)} \qquad (34)$$

using the fact that $(k/2)! = \Gamma(k/2 + 1)$. Equation 6.1.17 of [30] permits writing:

$$\Gamma(k/2 + 1)\ \Gamma(k/2 + 1/2) = \frac{\pi\ \Gamma(k+1)}{2^k} = \frac{\pi\ k!}{2^k} \qquad (35)$$

Substituting Equation 35 in Equation 34, Equation 29-a becomes:

$$X_0 = (2\pi RT_w)^{-1/2} A_x \sum_{k=0}^{\infty} \frac{(A_x^2-1)^{k/2} A_x^k}{k!} (2S_x' S_x)^k \qquad (36)$$

By inspection it can be seen that this is the expansion of the exponential function, therefore Equation 36 becomes:

$$X_0 = (2\pi RT_w)^{-1/2} A_x \exp[2(A_x^2-1)^{1/2} A_x S_x' S_x] \qquad (37)$$

Substituting in Equation 26-2 gives:

$$\sqrt{2RT_w}\, P_{x,0} = \pi^{-1/2} A_x \exp - \left\{(A_x^2-1)^{1/2} S_x' - A_x S_x\right\}^2 \qquad (38)$$

This equation contains most of the experimentally observed properties of gas-surface interactions. For the case of $A_x=1$ Equation 38 reduces to the fully accommodated diffuse reflection and for $A_x \rightarrow \infty$ approaches $\delta(S_x'-S_x)$ which is specular reflection. This specular limit can be shown from a consideration of Equation 21.9-18b in [31]. It will be shown later (Section 3.3) that A_x is related to the thermal accommodation coefficient, α, and is in fact, for n=0, given by the following:

$$A_x = (\alpha_x)^{-1/2} \qquad (39)$$

The x subscript was added to α to allow the accommodation coefficient to vary with coordinate direction. Figure 2, Appendix A, illustrates the results of Equation 38

with $\sqrt{2RT_w}\ P_{x,0}$ given as a function of S_x, S_x' and α_x.

For n greater than zero (n=2,4,6,...) it was necessary to solve Equations 26-a, 29-a and 33 numerically. A computer program was written to solve these equations. The results are shown for $\sqrt{2RT_w}\ P_{x,n}$ in Figures 3 and 4, Appendix A, for n=2 and 4, respectively.

2.1.2 The Evaluation of $P_{y,n}$

Substituting Equation 29-b into Equation 24-b yields:

$$\int_0^\infty S_y \sum_{k=0}^{\infty} A_y^{n+2k+2}\, \tilde{d}_{n,k} (S_y' S_y)^k [S_y^n + (-S_y')^n] \exp(-A_y^2 S_y^2)\, dS_y =$$

$$\exp[(A_y^2 - 1) S_y'^2] \qquad (40)$$

As was done for the x coordinate the left hand side can be integrated term by term. Each term is of the form:

$$\int_0^\infty t^m \exp(-p^2 t^2)\, dt = \Gamma(m+1/2)/2p^{m+1} \qquad (41)$$

Performing the integration and expressing the right hand side as an infinite series, Equation 40 becomes:

$$\frac{1}{2} \sum_{k=0}^{\infty} (-1)^n A_y^{n+k}\, \tilde{d}_{n,k}\, S_y'^{k+n}\, \Gamma(k/2 + 1) +$$

$$\frac{1}{2} \sum_{k=0}^{\infty} A_y^k\, \tilde{d}_{n,k}\, S_y'^k\, \Gamma(k/2 + n/2 + 1) =$$

$$\sum_{k=0}^{\infty} \frac{(A_y^2-1)^k \, S_y'^{2k}}{k!} \tag{42}$$

Since this equation holds for arbitrary value of S_y' the coefficient of like power of S_y' can be equated, and solving for $\tilde{d}_{n,k}$ yields:

$$\tilde{d}_{n,k} = \left(\frac{A_y^2-1}{A_y^2}\right)^{k/2} \frac{2}{\Gamma(k/2 + n/2 + 1)(k/2)!} \qquad k \text{ even, } < n$$

$$\tilde{d}_{n,k} = 0 \qquad k \text{ odd, } < n$$

$$\tilde{d}_{n,k} = \left(\frac{A_y^2-1}{A_y^2}\right)^{k/2} \frac{2}{\Gamma(k/2 + n/2 + 1)(k/2)!} -$$

$$(-1)^n \, \tilde{d}_{n,k-n} \frac{\Gamma(k/2 - n/2 + 1)}{\Gamma(k/2 + n/2 + 1)} \qquad k \text{ even, } \geq n$$

$$\tilde{d}_{n,k} = -(-1)^n \, \tilde{d}_{n,k-n} \frac{\Gamma(k/2 - n/2 + 1)}{\Gamma(k/2 + n/2 + 1)} \qquad k \text{ odd, } \geq n \tag{43}$$

Using Equations 26-b, 29-b and 43 $P_{y,n}$ $2RT_w$ can be determined as a function of S_y, S_y' and A_y for given values of n. As was true for $P_{x,0}$, $P_{y,0}$ can be obtained in closed form. For n=0 Equation 43 becomes:

$$\tilde{d}_{0,k} = \left(\frac{A_y^2-1}{A_y^2}\right)^{k/2} \frac{}{\Gamma(k/2 + 1)(k/2)!} \qquad \text{for } k = 0, 2, 4, \ldots$$

$$\tilde{d}_{0,k} = 0 \qquad \text{for } k = 1, 3, 5, \ldots \tag{44}$$

Substituting Equation 44 in Equation 29-b yields,

$$Y_0 = (RT_w)^{-1} \sum_{k=0}^{\infty} (A_y^2-1)^k A_y^{2k} \frac{(S_y' S_y)^{2k}}{\Gamma(k+1)\, k!} \tag{45}$$

From inspection (see Equation 9.6.10 in [30]) it can be seen that Equation 45 is the expansion of the modified Bessel function of the first kind, I_0. Equation 45 therefore becomes:

$$Y_0 = A_y^2 (RT_w)^{-1} I_0 (-2\sqrt{A_y^2-1}\, A_y S_y' S_y) \tag{46}$$

Substituting Equation 46 in Equation 26-b gives:[4]

$$P_{y,0}\sqrt{2RT_w} = 2A_y^2 S_y I_0(2A_y\sqrt{A_y^2-1}\, S_y' S_y) \cdot$$

$$\exp[-(A_y^2-1)\, S_y'^2 - A_y^2 S_y^2] \tag{47}$$

As was the case for $P_{x,0}$, Equation 47 contains most of the experimentally observed properties of gas-surface interaction. For the limit of $A_y=1$ Equation 47 reduces to the fully accommodated diffuse reflection and for $A_y \to \infty$, using the asymptotic expansion for I_0, Equation 47 reduces to:

$$P_{y,0}\sqrt{2RT_w} \to \frac{A_y}{\sqrt{\pi}} \sqrt{\frac{S_y}{-S_y'}}\ \exp[-A_y^2(S_y' + S_y)^2] \tag{48}$$

or as was shown for $P_{x,0}$:

---

[4]After the present analysis was complete, it was found that Kuscer et al [7] had obtained, in a completely different manner, a result similar to that given in Equations 38 and 47.

$$P_{y,0}\sqrt{2RT_w} \rightarrow \delta(S_y' + S_y) \tag{49}$$

Thus for $A_y \rightarrow \infty$, $S_y = -S_y'$, which is also specular reflection.

Figure 5, Appendix A, illustrates the results of Equation 47 with $\sqrt{2RT_w}\, P_{y,0}$ given as a function of S_y, S_y' and α_y. For n=1, 2, Equations 26-b, 29-b and 43 were solved numerically. The results for $P_{y,n}$ are shown in Figures 6 and 7, Appendix A, for n=1 and 2, respectively, as a function of S_y, S_y' and α_y where:

$$\alpha_y = A_y^{-2} \tag{50}$$

2.2 CYLINDRICAL COORDINATE SYSTEM

Keeping in mind the cylindrical coordinates y, r, and ψ as given in Figure 1, Appendix A and Table I, page 18, the scattering kernel is now assumed to be representable as follows:

$$P(\vec{v}', \vec{v}) = P_y(v_y', v_y)\; P_r(v_r', v_r)\; P_\psi(\psi_1, \psi) \tag{51}$$

In cylindrical coordinates Equation 2 becomes:

$$\int_{-\pi}^{\pi} \int_{0}^{\infty} \int_{0}^{\infty} P(\vec{v}', \vec{v})\; v_r\; dv_y\; dv_r\; d\psi = 1 \tag{52}$$

Substituting Equation 51 into Equation 52 the following are obtained for the normalization relation for each coordinate, respectively:

$$\int_0^\infty P_y \, dv_y = 1 \tag{53-a}$$

$$\int_0^\infty v_r \, P_r \, dv_r = 1 \tag{53-b}$$

$$\int_{-\pi}^{\pi} P_\psi \, d\psi = 1 \tag{53-c}$$

The reciprocity relation given by Equation 4 becomes in cylindrical coordinates with the applications of Equation 51:

$$-v_y' \exp(-S_y'^2) \, P_y(v_y', v_y) = v_y \exp(-S_y^2) \, P_y(-v_y, -v_y') \tag{54-a}$$

$$\exp(-S_r'^2) \, P_r(v_r', v_r) = \exp(-S_r^2) \, P_r(-v_r, -v_r') \tag{54-b}$$

$$P_x(\psi_i, \psi) = P_\psi(\psi, \psi_i) \tag{54-c}$$

Notice that Equations 53-a and 54-a are identical to Equations 14-b and 15-b, respectively. Therefore, the results for the y coordinate in cylindrical and rectangular coordinates are the same.

2.2.1 The Evaluation of $P_{r,n}$

A function, $f_r(v_r', v_r)$, is defined as follows:

$$f_r(v_r', v_r) = P_r \exp[(A_r^2 - 1) S_r'^2 + A_r^2 \, S_r^2] \tag{55}$$

Utilizing this relation, Equations 53-b and 54-b become, as a function of f_r, respectively:

$$\int_0^\infty v_r f_r \exp[-(A_r^2-1)S_r'^2 - A_r^2 S_r^2]\, dv_r = 1 \tag{56}$$

$$f_r(v_r', v_r) = f_r(-v_r, -f_r') \tag{57}$$

These two equations are the same as Equation 17-b and 18-b except for the subscripts. This leads to the conclusion:

$$f_r(v_r', v_r) \equiv f_y(v_r', v_r) \tag{58}$$

Assuming that P_r is given by a linear combination of individual kernels as was done in Equation 27, permits writing:

$$P_r = \sum_{n=0}^{\infty} C_n P_{r,n} \tag{59}$$

Subject to:

$$\sum_{n=0}^{\infty} C_n = 1 \tag{60}$$

where, from a consideration of Equations 58, 55 and 16-b:

$$P_{r,n}(v_r', v_r) = \frac{P_{y,n}(v_r', v_r)}{v_r} \tag{61}$$

For n=0, in view of Equation 47, Equation 61 becomes:

$$(2RT_w)P_{r,0} = 2A_r^2\, I_o(2A_r\sqrt{A_r^2-1}\, S_r' S_r) \exp[-(A_r^2-1)S_r'^2 - A_r^2 S_r^2] \tag{62}$$

The results of this equation are shown in Figure 8, Appendix A. The numerical calculation for n=1, and 2 are shown in Figures 9 and 10, Appendix A, respectively.

2.2.2 The Evaluation of P_ψ

From a consideration of Equation 62 and Figures 8, 9, and 10, Appendix A, it can be seen that, in general, $P_{r,n}$ is finite at $v_r=0$. In view of this and since for normal reflected velocities ($v_r=0$) the reflected probability is independent of ψ, the only solution is for P_ψ to be equal to a constant. From Equation 53-c it is found that:

$$P_\psi = \frac{1}{2\pi} \tag{63}$$

which also satisfies Equation 45-c.

2.3 SPHERICAL COORDINATE SYSTEM

Using the spherical coordinates as given in Figure 1, Appendix A, and Table I, page 18, the scattering kernel is now assumed to be representable as follows:

$$P(v',v) = P_\rho(v',v)\ P_\theta(\theta_i,\theta)\ P_\varphi(\varphi_i,\varphi) \tag{64}$$

Note that the ρ subscript is not needed on the velocity components since the velocity vectors coincide with the coordinate direction and the velocity component is therefore equal to the molecular speed when the velocity is directed away from the surface and to its negative when directed

toward the surface. In spherical coordinates Equation 2 becomes:

$$\int_0^{\infty} \int_{-\pi/2}^{\pi/2} \int_{-\pi/2}^{\pi/2} P\, v^2 \cos\varphi \, d\varphi \, d\theta \, dv = 1 \qquad (65)$$

Substituting Equation 64 into Equation 65 the following normalization relations are obtained for each coordinate, respectively:

$$\int_0^{\infty} P_\rho \, v^2 \, dv = 1 \qquad (66\text{-a})$$

$$\int_{-\pi/2}^{\pi/2} P_\theta \, d\theta = 1 \qquad (66\text{-b})$$

$$\int_{-\pi/2}^{\pi/2} P_\varphi \cos\varphi \, d\varphi = 1 \qquad (66\text{-c})$$

In spherical coordinates, after the application of Equation 64, Equation 4, the reciprocity relation, becomes:

$$-v' \exp(-S'^2) \, P_\rho(v', v) = v \exp(-S^2) \, P_\rho(-v, -v') \qquad (67\text{-a})$$

$$\cos\theta_i \, P_\theta(\theta_i, \theta) = \cos\theta \, P_\theta(\theta, \theta_i) \qquad (67\text{-b})$$

$$\cos\varphi_i \, P_\varphi(\varphi_i, \varphi) = \cos\varphi \, P_\varphi(\varphi, \varphi_i) \qquad (67\text{-c})$$

From Equations 1 and 64 it can be seen that P_ρ, P_θ and P_φ must be non-negative. This requirement along with Equations 66 and 67 are the conditions that must be satisfied by P_ρ, P_θ and P_φ.

2.3.1 The Evaluation of $P_{\rho,n}$

The development of the solution for P_ρ will closely parallel the solution for P_x and P_y. A function f_ρ is defined as follows:

$$f_\rho(v',v) = \frac{P_\rho}{v} \exp[(A_\rho{}^2-1)\ S'^2 + A_\rho{}^2\ S^2] \tag{68}$$

Equations 66-a and 67-a become, in terms of f_ρ, respectively:

$$\int_0^\infty v^3\ f_\rho \exp[-(A_\rho{}^2-1)\ S'^2 - A_\rho{}^2\ S^2]\ dv = 1 \tag{69}$$

and:

$$f_\rho(v',v) = f_\rho(-v,-v') \tag{70}$$

It is now assumed that f_ρ can be represented as:

$$f_\rho = \sum_{n=0}^{\infty} D_n\ W_n(v',v) \tag{71}$$

where:

$$W_n(v',v) = \sum_{k=0}^{\infty} g_{n,k}\ (v'v)^k[v^n + (-v')^n] \tag{72}$$

and the D_n's are arbitrary constants subject to:

$$\sum_{n=0}^{\infty} D_n = 1 \tag{73}$$

Notice that the assumed form for W_n and therefore f_ρ as expressed in Equations 71 and 72 automatically satisfies the reciprocity relation given in Equation 70. Therefore the only constraints upon f_ρ are the normalization conditions given by Equation 69 and the condition of being non-negative.

Assuming that P_ρ is given by a linear combination of individual kernels as was done in Equation 27, yields:

$$P_\rho = \sum_{n=0}^{\infty} D_n \, P_{\rho,n} \tag{74}$$

Equation 72 becomes, in terms of S and S':

$$W_n = \sum_{k=0}^{\infty} \tilde{g}_{n,k} \, (S'S)^k [S^n + (-S')^n] A_\rho^{2k+n+4} \tag{75}$$

where:

$$\tilde{g}_{n,k} = g_{n,k} \left(\frac{\sqrt{2RT_w}}{A_\rho} \right)^{n+2k+4} \tag{76}$$

For $D_n = 1$ and $D_j = 0$ $(j \neq n)$ Equations 71, 74 and 75 may be used along with the dimensionless speeds to permit writing Equation 68 as follows:

$$(2RT_w)^{3/2} P_{\rho,n} = S \exp[-(A_\rho^2-1)S'^2 - A_\rho^2 S^2] \cdot$$

$$\sum_{k=0}^{\infty} \tilde{g}_{n,k} (S'S)^k [S^n + (-S')^n] A_\rho^{n+2k+4} \tag{77}$$

Substituting Equations 71 and 72 into Equation 69 gives:

$$A_\rho^{n+2k+4} \int_0^\infty S^3 \sum_{k=0}^{\infty} \tilde{g}_{n,k} (S'S)^k [S^n + (-S')^n] \exp(-A_\rho^2 S^2)\, dS$$

$$= \exp[(A_\rho^2-1)S'^2] \tag{78}$$

Equation 78 can be integrated term by term on the left hand side where each term is of the form given by Equation 41. Performing this integration and expanding the right hand side as an infinite series, Equation 78 becomes:

$$\frac{1}{2} \sum_{k=0}^{\infty} A_\rho^k \tilde{g}_{n,k} S_y'^k \Gamma(k/2 + n/2 + 2) +$$

$$\frac{(-1)^n}{2} \sum_{k=0}^{\infty} A_\rho^{k+m} \tilde{g}_{n,k} (S')^{k+n} \Gamma(k/2 + 2) =$$

$$\sum_{k=0}^{\infty} (A_\gamma^2-1)^k S'^{2k} \tag{79}$$

Since this equation is valid for arbitrary values of S', the coefficients of like powers of S' can be equated. Solving this set of equations for $\tilde{g}_{n,k}$ gives:

$$\tilde{g}_{n,k} = \left(\frac{A_\rho{}^2-1}{A_\rho{}^2}\right)^{k/2} \frac{2}{(k/2)!\ \Gamma(k/2 + n/2 + 2)} \qquad k \text{ even, } < n$$

$$\tilde{g}_{n,k} = 0 \qquad k \text{ odd, } < n$$

$$\tilde{g}_{n,k} = \left(\frac{A_\rho{}^2-1}{A_\rho{}^2}\right)^{k/2} \frac{2}{(k/2)!\ \Gamma(k/2 + n/2 + 2)} -$$

$$(-1)^n\ \tilde{g}_{n,k-n}\ \frac{\Gamma(k/2 - n/2 + 2)}{\Gamma(k/2 + n/2 + 2)} \qquad k \text{ even, } \geq n$$

$$\tilde{g}_{n,k} = -(-1)^n\ \tilde{g}_{n,k-n}\ \frac{\Gamma(k/2 - n/2 + 2)}{\Gamma(k/2 + n/2 + 2)} \qquad k \text{ odd, } \geq n \qquad (80)$$

Using Equations 77 and 80, $P_{\rho,n}(2RT_w)^{3/2}$ can be determined as a function of S,S' and A_ρ for given values of n. As was the result for $P_{x,0}$, $P_{r,0}$, $P_{\rho,0}$ can be obtained in closed form. For n=0 Equation 80 becomes:

$$\tilde{g}_{0,k} = \left(\frac{A_\rho{}^2-1}{A_\rho{}^2}\right)^{k/2} \frac{1}{(k/2)!\ \Gamma(k/2 + 2)} \qquad \text{even k}$$

$$\tilde{g}_{0,k} = 0 \qquad \text{odd k} \qquad (81)$$

Substituting Equation 81 into Equation 77 yields:

$$(2RT_w)^{3/2}\ P_{\rho,0} = S\ \exp[-(A_\rho{}^2-1)S'^2 - A_\rho{}^2\ S^2].$$

$$2A_\rho^4 \sum_{k=0}^{\infty} (A_\rho^2-1)^k \frac{(S'S)^{2k} A_\rho^{2k}}{k!\ \Gamma(k+2)} \tag{82}$$

From Equation 9.6.10 of [30] it can be seen that this last sum is equal to:

$$\frac{I_1(-2S'S\ A_\rho\sqrt{A_\rho^2-1})}{-S'S\ A_\rho\sqrt{A_\rho^2-1}}$$

Equation 82 therefore becomes:

$$(2RT_w)^{3/2} P_{\rho,0} = \frac{2A_\rho^3}{\sqrt{A_\rho^2-1}\ (-S')} \exp\left[-(A_\rho^2-1)S'^2 - A_\rho^2 S^2\right] \cdot$$

$$I_1(-2S'SA_\rho\sqrt{A_\rho^2-1}) \tag{83}$$

Equation 83 is plotted in Figure 11, Appendix A, with $(2RT_w)^{3/2} P_{\rho,0}$ given as a function of S for various values of S' and α_ρ, where:

$$\alpha_\rho = \frac{1}{A_\rho^2} \tag{84}$$

For n greater than zero (n=1,2) Equations 77 and 80 were solved numerically. The results for $(2RT_w)^{3/2} P_{\rho,1}$ and $(2RT_w)^{3/2} P_{\rho,2}$ are shown in Figures 12 and 13, Appendix A, respectively.

2.3.2 The Evaluation of P_θ

It is assumed that P_θ is given by the following infinite series:

$$P_\theta = \cos\theta \sum_{j=0}^{\infty} e_j \cos[j(\theta_i + \theta)] \tag{85}$$

This form was chosen because each term on the right hand side automatically satisfied Equation 67-b. Substituting Equation 85 into Equation 66-b gives for the normalization condition:

$$\int_{-\pi/2}^{\pi/2} \cos\theta \sum_{j=0}^{\infty} e_j \cos[j(\theta_i + \theta)]\, d\theta = 1 \tag{86}$$

Each term in this equation is of the form:

$$\int_{-\pi/2}^{\pi/2} \cos\theta \cos[j(\theta_i + \theta)]\, d\theta$$

By using the trigonometric identity for the cosine of the sum of two angles this integral becomes:

$$\int_{-\pi/2}^{\pi/2} \cos\theta[\cos j\theta_i \cos j\theta - \sin j\theta_i \sin j\theta]\, d\theta$$

which, after integrating, yields:

$$\cos(j\theta_i)\left[\frac{\sin(j-1)\pi/2}{j-1} + \frac{\sin(j+1)\pi/2}{j+1}\right]$$

which may be reduced to:

$$\frac{-2\cos(j\theta_i)\cos(j\pi/2)}{j^2-1}$$

This expression is zero for all odd values of j except j=1 where it is of the form zero over zero which must be evaluated by l'Hopital's rule. The final result is:

$$\int_{-\pi/2}^{\pi/2} \cos\theta \cos[j(\theta_i+\theta)]\, d\theta = \begin{cases} 2 & , j = 0 \\ \pi/2 \cos\theta_i & , j = 1 \\ \dfrac{-2(-1)^{j/2}\cos(j\theta_i)}{(j^2-1)} & , j \text{ even} \\ 0 & , j \text{ odd}, > 1 \end{cases} \tag{87}$$

Since the integral is zero for j odd, > 1 the corresponding e_j is arbitrary since that term does not contribute to the sum in Equation 86.

Substituting Equation 87 into Equation 86 gives the following:

$$2e_0 + \pi/2\, e_1 \cos\theta_i - 2\sum_{k=1}^{\infty} e_{2k} \frac{(-1)^k \cos 2k\theta_i}{(4k^2-1)} = 1 \tag{88}$$

By inspection it can be seen that this equation is equivalent to the equation for the Fourier expansions of

$1-(\pi/2)\ e_1 \cos\theta_i$ over the period $-\pi/2$ to $\pi/2$. The Fourier series is:

$$1 - \pi/2\ e_1 \cos\theta_i = a_0/2 + \sum_{k=1}^{\infty} a_k \cos 2k\,\theta_i \qquad (89)$$

where the Fourier coefficients are:

$$a_k = 2/\pi \int_{-\pi/2}^{\pi/2} (1-\pi/2\ e_1 \cos\theta_i) \cos 2k\,\theta_i\, d\theta_i \qquad (90)$$

Notice that the terms containing $\sin 2k\theta_i$ are missing from Equation 89 because the left hand side is an even function of θ_i.

Equation 90 can be integrated to give:

$$\left.\begin{aligned} a_o &= 2(1-e_1) \\ a_{2k-1} &= 0 \\ a_{2k} &= \frac{(-1)^k 2e_1}{(4k^2-1)} \end{aligned}\right\} k = 1,2,3,.... \qquad (91)$$

Substituting Equation 89 into Equation 88, using Equation 91 and equating like coefficients of $\cos 2k\theta_i$ gives:

$$e_0 = \frac{1-e_1}{2} \qquad (92)$$

$$e_{2k} = -e_1 \quad , \qquad k \geq 1$$

It has already been shown that the odd e's greater than 1 are arbitrary.

Utilizing Equation 92, Equation 85 becomes:

$$P_\theta = \cos\theta\left[\frac{1-e_1}{2} + e_1\cos(\lambda_i+\theta) - e_1\sum_{k=1}^{\infty}\cos 2k(\theta_i+\theta) + \sum_{k=1}^{\infty} e_{2k+1}\cos(2k+1)(\theta_i+\theta)\right] \quad (93)$$

By inspection, it can be seen that the first sum in Equation 93 will not converge by the normal definition since the coefficients are constant. It can be seen that the value of the sum at $\theta_i+\theta=0$ is unbounded since all terms are "in phase" at this point. However, at other values of $\theta_i+\theta$, the sum oscillates from positive to negative with unlimited frequency and over any interval is of unbounded variation. This sum is indeed a badly behaved function. However, in the mean, this sum acts similar to a Dirac delta function. The Fourier coefficients for the delta functions will now be determined.

Any real function, f(t), defined over the finite interval $-\tau/2 < t < \tau/2$, defines a Fourier series if:

$$\int_{-\tau/2}^{\tau/2} |f(t)|\, dt \quad (94)$$

is bounded (see [31], Sections 4.11-2b). The Fourier series is defined as:

$$\frac{1}{2} a_0 + \sum_{k=1}^{\infty} a_k \cos (2\pi kt/\tau) \tag{95}$$

if f(t) is symmetric about t=0, the expression for a_k is:

$$a_k = 2/\tau \int_{-\tau/2}^{\tau/2} f(t) \cos (2\pi kt/\tau)\, dt \tag{96}$$

The delta function $\delta(t)$ satisfied the above condition. In fact, if we let the interval be $-\pi/2 \leq t \leq \pi/2$, expression 94 becomes:

$$\int_{-\pi/2}^{\pi/2} \left|\delta(t)\right| \, dt = 1 \tag{97}$$

Equation 96 gives for the Fourier coefficients of the delta function:

$$a_k = 2/\pi \int_{-\pi/2}^{\pi/2} \delta(t) \cos (2kt)\, dt \tag{98}$$

$$= 2/\pi$$

Thus, the Fourier coefficients of the even cosine terms are constants; this is true also for the coefficients of the first sum in Equation 93. Notice that the Fourier series given by Equations 95 and 98 does not converge uniformly to the delta function over any subinterval.

Convergence is guaranteed only for a function of bounded variation (see [31], Section 4.11-4) and the delta function is unbounded.

While it is true that the Fourier series of the delta function is not equal to the delta function itself, it may be that they both satisfy the same integral relation as given in Equation 86. Therefore, substituting for the series of even terms in Equation 93 the delta function and re-writing the series of odd terms gives:

$$P_\theta = \cos\theta\left[\frac{1+e_1}{2} + e_1 \cos(\theta_i+\theta) - e_1\,\pi/2\,\delta(\theta_i+\theta) + G(\theta_i+\theta)\right] \tag{99}$$

where $G(\theta_i+\theta)$ is the sum of odd terms in Equation 93 and is an arbitrary function subject to the following conditions:

$$G(\theta) = G(-\theta)$$

$$G(\theta) = -G(\pi-\theta)$$

$$\int_{-\pi/2}^{\pi/2} \cos\theta\, G(\theta_i+\theta)\, d\theta = 0 \tag{100}$$

Equation 99 does indeed satisfy Equation 66-b for arbitrary e_1 and G subject to Equation 100. However, e_1 and G are still limited such that P_θ is non-negative. It will be shown in Section 2.4.3 that e_1 and G are further restricted.

2.3.3 The Evaluation of P_ϕ

Similar to what was done for P_θ it is assumed that P_φ is given by the following series:

$$P_{\varphi} = \cos \varphi \sum_{j=0}^{\infty} h_j \cos [j(\varphi_i+\varphi)] \tag{101}$$

The reciprocity relation as expressed in Equation 67-c is satisfied by Equation 101 for arbitrary h_j's. Substituting Equation 101 into Equation 66-c gives for the normalization relation:

$$\int_{-\pi/2}^{\pi/2} \cos^2 \varphi \sum_{j=0}^{\infty} h_j \cos [j(\varphi_i+\varphi)] \, d\varphi = 1 \tag{102}$$

Each term in the infinite series contains an integral of the form:

$$\int_{-\pi/2}^{\pi/2} \cos^2 \varphi \cos [j(\varphi_i+\varphi)] \, d\varphi$$

which becomes, after using the trigonometric identity for the cosine of the sum of angles:

$$\cos j\varphi_i \int_{-\pi/2}^{\pi/2} \cos^2 \varphi \cos j\varphi \, d\varphi - \sin j\varphi_i \int_{-\pi/2}^{\pi/2} \cos^2\varphi \sin j\varphi \, d\varphi$$

The second integral is zero from symmetry. Integrating the remaining term gives:

$$\frac{4 \cos j \varphi_i \sin (j \pi/2)}{j(4-j^2)}$$

This expression is zero for all even values of j except j=1, 2 where it is of the form zero over zero in which case it must be evaluated by l'Hopital's rule. The final result for the integral is:

$$\int_{-\pi/2}^{\pi/2} \cos^2 \varphi \cos\left[j(\varphi_i+\varphi)\right] d\varphi = \pi/2 \quad , \qquad j = 0$$

$$= \frac{4 \cos \varphi_i}{3} \quad , \qquad j = 1$$

$$= \pi/4 \cos 2\varphi_i \quad , \qquad j = 2$$

$$= 4/15 \cos 3\varphi_i \quad , \qquad j = 3$$

$$= 0 \quad , \qquad \text{even } j, \geq 4$$

$$= \frac{(-1)^{(j+1)/2}\, 4}{j(j^2-4)} \cos j\varphi_i \quad , \qquad \text{odd } j \tag{103}$$

Since the integral in Equation 102 is zero for even j's greater than two, the corresponding h_j is arbitrary since it does not contribute to the sum in Equation 102.

Substituting Equation 103 into Equation 102 for each term in the series, gives:

$$\pi/2\ h_0 + \pi/4\ h_2 \cos 2\varphi_i - \sum_{k=0}^{\infty} (-1)^k \cdot$$

$$h_{2k+1} \frac{4 \cos(2k+1)\varphi_i}{(2k+1)(2k-1)(2k+3)} = 1 \tag{104}$$

Equation 104 is equivalent to the Fourier expansion of $1-\pi/2\ h_0 - \pi/4\ h_2 \cos 2\varphi_i$ over the range $-\pi/2 \leq \varphi_i \leq \pi/2$. Because there are only odd multiples of φ_i in the series in Equation 104 the Fourier series must be skew-symmetric about $\pm\pi/2$. The Fourier series is:

$$1-\pi/2\ h_0 - \pi/4\ h_2 \cos 2\varphi_i = a_0/2 + \sum_{k=1}^{\infty} a_k \cos k\varphi_i \qquad (105)$$

where:

$$a_k = (-1)^{(k-1)/2} \left(\frac{4/\pi - 2h_0}{k} + \frac{k\ h_2}{k^2-4} \right) \quad , \quad \text{odd } k$$

$$= 0 \quad , \quad \text{even } k.$$

Equating Equations 104 and 105 and solving for h_k gives for odd k:

$$h_k = +4/\pi - 2h_0 - k^2\ [1/\pi - h_o/2 + h_2/4] \qquad (106)$$

A necessary, though not sufficient, condition for the convergence of P_φ, as given by Equation 101, is for h_k to be bounded as $k \rightarrow \infty$. This fact requires that the coefficient of k^2 in Equation 106 be zero, i.e.:

$$h_2 = 2h_0 - 4/\pi \qquad (107)$$

Equation 106 therefore becomes:

$$h_k = 4/\pi - 2h_0 \quad , \quad \text{even } k \tag{108}$$

Utilizing Equations 107 and 108 and the fact that the even h_k's for k greater than 2 are arbitrary, Equation 101 becomes:

$$P_\varphi = \cos\varphi[h_0 - (4/\pi-2h_0)\cos 2(\varphi_i+\varphi) +$$

$$(4/\pi-2h_0)\sum_{k=1}^{\infty}\cos(2k-1)(\varphi_i+\varphi) +$$

$$\sum_{k=1}^{\infty} h_{2k+2}\cos(2k+2)(\varphi_i+\varphi)] \tag{109}$$

Notice that the first infinite sum in Equation 109 has constant coefficients as was the case in Equation 93. However, the series in Equation 93 contained even multiples of the angles, while Equation 109 contains only odd multiples.

In Section 2.3.2 the Fourier coefficients of the delta function were shown to be equal to a constant for the even cosine terms and zero for the other terms. It will now be shown that a Fourier series for the delta function can be developed that contains only odd cosine terms. Let f(t) be defined as follows:

$$f(t) = \delta(t) - \delta(t+\pi) - \delta(t-\pi) \tag{110}$$

By inspection it can be seen that Equation 110 is equivalent to $\delta(t)$ over the range $-\pi < t < \pi$. From Equation 96 with $\tau = 2\pi$ and using Equation 110 there is obtained:

$$a_k = 1/\pi \int_{-\pi}^{\pi} [\delta(t)-\delta(t+\pi) - \delta(t-\pi)] \cos kt \, dt \qquad (111)$$

With the help of Equation 21.9-10a from [31], Equation 111 may be integrated to give:

$$a_k = 0 \quad , \qquad k \text{ - even}$$

$$a_k = 2/\pi \, , \qquad k \text{ - odd} \qquad (112)$$

As was done for P_θ, the series in Equation 109 can be rewritten in terms of the delta function and an arbitrary function $H(\varphi_i+\varphi)$ as follows:

$$P_\varphi = \cos \varphi [h_0 - (4/\pi-2h_0) \cos 2(\varphi_i+\varphi) +$$

$$(4/\pi-2h_0)(\pi/2) \, \delta(\varphi_i+\varphi) + H(\varphi_i+\varphi)] \qquad (113)$$

where $H(\varphi_i+\varphi)$ is subject to the conditions:

$$H(\varphi) = H(-\varphi)$$

$$H(\varphi) = H(\pi-\varphi)$$

$$\int_{-\pi/2}^{\pi/2} \cos^2 \varphi \, H(\varphi+\varphi_i) \, d\varphi = 0 \qquad (114)$$

Equation 113 satisfies Equation 66-c for arbitrary value of h_0 and H subject to the conditions set forth in Equation 114 and such that P_φ is non-negative. It will be shown in Section 2.4.3 that h_0 and H have additional restrictions on them.

2.4 INVARIANCE OF KERNEL UNDER ROTATION OF COORDINATE SYSTEM

Any mathematical description of the scattering kernel must be of the form such that $P(\hat{v}', \hat{v})$ is invariant with respect to a rotation of the coordinate system about the surface normal. This condition, like the non-negativity of the scattering kernel, is one that is difficult to apply a priori but is simple to verify after a solution is obtained. The scattering kernel as given by Equations 13, 51 and 64 must therefore be invariant as the coordinate systems are rotated (e.g., as ψ is varied). Referring to Figure 1, Appendix A, it can be seen that as the x, z axes are rotated about the y axis that v_x', v_z', v_x, v_z, ψ_i, ψ, θ_i, θ, φ_i, and φ vary, while v_y', v_y, v_r', v_r, v_ρ', and v_ρ are invariant. In order to prove that a scattering kernel satisfies this condition it is necessary to show that it is invariant with ψ for all possible incident and reflected velocities. On the other hand a scattering kernel can be disqualified by demonstrating one example that fails to hold. Each of the three kernels in each coordinate system will be

scrutinized in order to eliminate those that are unsatisfactory and thereby simplify the equations.

2.4.1 Check of Equations in Rectangular Coordinates

The complete scattering kernel is given by Equation 13 with the coordinate kernels given by Equation 27. Remember that the form for the z coordinate is identical with that for the x coordinate. $P(\hat{v}', \hat{v})$ must be independent of the orientation of the x, z axes for arbitrary values of A_n and, in particular, for A_n=1 with all other A's equal to zero.

For n=0, in the x and z coordinates, using Equation 38 for $P_{x,0}$ and $P_{z,0}$, Equation 13 becomes:

$$P = P_y(\pi/2RT_w)A_xA_z \exp\left\{-\left[(A_x^2-1)^{1/2} S_x'-A_xS_x\right]^2 - \left[(A_z^2-1)^{1/2} S_z'-A_zS_z\right]^2\right\} \quad (115)$$

The expression for P_y was not required since it is a constant with the rotation of the coordinate system since v_y and v_y' do not change. Equation 115 can be written in terms of the single independent variable ψ by the use of Table I, page 18, which gives:

$$P = \pi/2RT_wP_{y,0}A_xA_z \exp\left\{-[(A_x^2-1)^{1/2} S_r'\cos(\Omega+\psi) - A_xS_r\cos\psi]^2 - [(A_z^2-1)^{1/2} S_r'\sin(\Omega+\psi) - A_zS_r\sin\psi]^2\right\} \quad (116)$$

where $\Omega = \psi_i - \psi$

Notice that Ω is independent of the rotation of the axis since both ψ_i and ψ vary in the same manner.

The scattering kernel given by Equation 116 is invariant with ψ only if the coefficients of terms containing ψ vanish. Expanding the argument of the exponential function in Equation 116, collecting terms with like variations of ψ, and equating the coefficients to zero, it can be shown that Equation 116 is invariant with ψ if and only if $A_x = A_z$. For this condition Equation 116 becomes:

$$P = (\pi/2RT_w)\ P_y A_x^2 \exp[-(A_x^2-1)\ S_r'^2 +$$

$$2S_r' S_r A_x (A_x^2-1)^{1/2} \cos\Omega - A_x^2 S_r^2] \qquad (117)$$

Thus Equation 116 is a valid scattering kernel only for an isotropic surface.

For n greater than zero it is easy to show that the scattering kernel from Equation 13, using the numerical results from Figures 4 and 5, Appendix A, is not invariant with rotation. Looking at the results for n = 2 and 4 it can be seen that for each value of α_x, P_x (and therefore P_z) is equal to zero at one or more values of S_x for each value of S_x'. A consequence of the assumed product solution of P is that the zeroes form an intersecting grid of infinite straight lines in the v_x, v_z (or S_x, S_y) plane. It is easy to see that as the coordinate system is rotated the zeroes

of P turn also and remain orthogonal to the axis, therefore P is not invariant with rotation for at least n = 2 and 4. It is assumed that $P_{x,n}$ for n greater than 4 is also an unsuitable kernel.

It can be concluded that A_0 must be equal to unity with the other A_n's equal to zero, while B_n is still arbitrary subject to the previously stated conditions. The final results for P_x and P_z are therefore given by Equation 38 with $A_x = A_z$.

2.4.2 Check of Equations in Cylindrical Coordinates

Equation 51 gives the scattering kernel in cylindrical coordinates with the individual kernels given by Equations 27-b, 59 and 63. It is obvious that P_r, like P_y, is invariant with rotation of the x, z axes since v_r and v_r' do not change. From Equation 63 P_ψ is equal to a constant and is consequently independent of the orientation. Therefore, Equation 51 as derived satisfies the invariance with rotation condition.

2.4.3 Check of Equations in Spherical Coordinates

The scattering kernel in spherical coordinate is given by Equation 64. Because the speeds v' and v are not affected by the coordinate system, P_ρ is invariant. Using Equations 99 and 113 in Equation 64 yields:

$$P = P_\rho \cos\theta \cos\varphi[(1-e_1)/2 + e_1 \cos(\theta_i+\theta) - e_1 \pi/2\, \delta(\theta_i+\theta) +$$

$$G(\theta_i+\theta)][h_0 - (4/\pi-2h_0) \cos 2(\varphi_i+\varphi) +$$

$$(4/\pi-2h_0)\ (\pi/2)\ \delta(\varphi_i+\varphi) + H(\varphi_i+\varphi)\ ] \tag{118}$$

From Figure 1, Appendix A, and Table I, page 18, it can be seen that:

$$\cos\ \theta\ \cos\ \varphi = \frac{S_y}{S} \tag{119}$$

which is invariant with changes in ψ. Therefore, the product of the two bracket terms in Equation 118 must be invariant with axis rotation.

It will now be shown that e_1 and $4/\pi-2h_0$ must be zero in order to maintain the invariance of P. The term $\delta(\theta_i+\theta)$ is infinite along the arc $\theta = -\theta_i$ and $\delta(\varphi_i+\varphi)$ is infinite along the arc $\varphi = -\varphi_i$. Since neither of the bracketed terms is identically equal to zero over any range of θ or φ, P is infinite (except possibly for isolated points) along $\theta = -\theta_i$ and $\varphi = -\varphi_i$. (Note that being infinite does not disqualify a term.) However, as the x, z axes are rotated, the loci of constant θ and φ rotate about the point where $\theta = -\theta_i$ and $\varphi = -\varphi_i$. This means that the curves where P is infinite moves in phase space and therefore P cannot be invariant unless the coefficients of the delta function are zero. This means that:

$$e_1 = 0 \tag{120}$$

and,

$$h_0 = 2/\pi \tag{121}$$

In a similar manner it will be shown that G and H in Equation 118 must be identically zero. From Equation 100 it can be seen that:

$$G(\pi/2) = -G(\pi/2) = 0 \tag{122}$$

Since e_1 is zero from Equation 120 and from Equation 122 $G(\theta+\theta_i)$ is zero for $\theta+\theta_i = \pi/2$ the first bracket term in Equation 118 becomes 1/2 for $\theta = \pi/2-\theta_i$. Since it has been shown that the product of the two bracketed terms must be a constant, the second term must be a constant for arbitrary value of φ and φ_i. The only solution for G and H is therefore:

$$\begin{aligned} G &\equiv 0 \\ H &\equiv 0 \end{aligned} \tag{123}$$

Equations 99 and 113 become, respectively:

$$P_\theta = \frac{\cos\ \theta}{2} \tag{124}$$

$$P_\varphi = \frac{2\ \cos\ \varphi}{\pi} \tag{125}$$

The scattering kernel in spherical coordinates that satisfies all necessary conditions is given by Equations 64, 74, 124 and 125. For the case of $D_n = 1$, $D_i=0$ $i\neq n$ and $A_p \longrightarrow \infty$ it can be shown that the scattering kernel in spherical coordinates approaches that for diffuse elastic scattering as given by Equation 9.

III. APPLICATION OF THEORETICAL RESULTS

In Section I the most general description of gas-surface interaction, that of the scattering kernel, was introduced and in Section II several scattering kernels were developed that satisfy all required conditions including that of reciprocity. However, the scattering kernel itself is far too detailed to be of much practical use since it gives the probability density as a function of six independent velocity components as well as characteristics of the surface. Usually it is some moment of the reflected molecular distribution such as the molecular flux distribution, mean velocities, or total energy that is desired. In this section several of these important moments will be obtained, some in closed mathematical form and others from numerical integration.

3.1 REFLECTED GLOBAL PROPERTIES

Mean reflected molecular properties are determined by integrating the desired properties over some group of reflected molecules. Global properties are determined by integrating over all reflected molecules. Total energy and momentum exchange between a gas and a surface are important quantities which are determined in the remainder of this section.

3.1.1 Mean Reflected Velocity Components

In order to determine the momentum exchange between a gas and a surface it is necessary to know the mean velocities of reflected molecules. The mean velocity component in a given direction, say in the direction of a unit vector $\hat{k}$ of reemitted molecules is given by:

$$\overline{\hat{v}\cdot\hat{k}} = \bar{v}_k = \int_{v\cdot n>0} \hat{k}\cdot\vec{v}\, P\, d^3v \tag{126}$$

3.1.1.1 The Determination of $\bar{S}_x$

In rectangular coordinates, using Table I, page 18, and Equation 126, the mean velocity component in the direction of the x coordinate, $\bar{v}_x$, is:

$$\bar{v}_x = \int_{-\infty}^{\infty} \int_{0}^{\infty} \int_{-\infty}^{\infty} v_x\, P\, dv_x dv_y dv_z \tag{127}$$

Since it has been assumed that P is given as a product solution in Equation 13, Equation 127 can be separated into the product of three integrals as follows:

$$\bar{v}_x = \int_{-\infty}^{\infty} v_x P_x dv_x \int_{0}^{\infty} P_y dv_y \int_{-\infty}^{\infty} P_z dv_z \tag{128}$$

It can be seen that the last two of these integrals are unity from Equations 14-b and 14-c. Using this fact and the result of Section 2.4.1 that P_x is given by Equation 38, Equation 128 becomes in terms of dimensionless velocities:

$$\bar{S}_x = \frac{A_x}{\sqrt{\pi}} \int_{-\infty}^{\infty} S_x \exp[-(A_x^2-1)^{1/2} S_x'-A_x S_x^2] \, dS_x \tag{129}$$

Integrating yields:

$$\bar{S}_x = \frac{\sqrt{A_x^2-1}}{A_x} S_x' \tag{130}$$

or in terms of α_x:

$$\bar{S}_x = \sqrt{1-\alpha_x} S_x' \tag{131}$$

Thus, the mean reflected x component of velocity is proportional to the x component of the incident velocity.

In both cylindrical and spherical coordinates, $\bar{S}_x$ is zero from symmetry.

3.1.1.2 The Determination of $\bar{S}_y$

Again using Table I, page 18, and Equation 126, the mean velocity component in the y direction, $\bar{v}_y$, is:

$$\bar{v}_y = \int_{-\infty}^{\infty} \int_{0}^{\infty} \int_{-\infty}^{\infty} v_y \, P dv_x \, dv_y \, dv_z \tag{132}$$

for the rectangular coordinate solution. As was the case for $\bar{v}_x$, Equation 132 reduces to:

$$\bar{v}_y = \int_{0}^{\infty} v_y \, P_y \, dv_y \tag{133}$$

Where P_y is given by Equation 27-b. Equation 133 can be evaluated for each $P_{y,n}$. For n=0, using Equation 47,

Equation 133 becomes in terms of dimensionless velocities:

$$\bar{S}_y = 2A_y^2 \int_0^\infty S_y^2 \, I_0[2A_y\sqrt{A_y^2-1}\, S_y' S_y] \exp[-(A_y^2-1)S_y'^2 - A_y^2 S_y^2] \, dS_y \tag{134}$$

Using the results of Appendix B, Equation 134 becomes:

$$\bar{S}_y = \frac{\sqrt{\pi}}{2 A_y} \exp[-(A_y^2-1)S_y'^2] \, M[3/2, \; 1, \; (A_y^2-1)S_y'] \tag{135}$$

where M is the confluent hypergeometric function of Kummer.

The result of Equation 135 is shown in Figure 14, Appendix A, with $\bar{S}_y$ given as a function of S_y' for various values of α_y.

For n greater than zero it was necessary to evaluate Equation 133 numerically. Using the numerical results for $P_{y,n}$ obtained in Section 2.1.2, Equation 133 was integrated. The results for n=1 and 2 are shown in Figures 15 and 16, Appendix A, respectively, for given values of α_y.

The result of $\bar{S}_y$ in cylindrical coordinates is exactly the same as that given above since it was shown in Section 2.2 that P_y is common to both.

The solution for P in spherical coordinates from Equation 64 yields for the mean normal velocity:

$$\bar{v}_y = \int_0^\infty \int_{-\pi/2}^{\pi/2} \int_{-\pi/2}^{\pi/2} v^3 \cos^2 \varphi \cos \theta \, P_\rho P_\theta P_\varphi \, d\theta d\varphi dv \tag{136}$$

Use of Table I, page 18, was required to express v_y and d^3v in spherical coordinates.

Separating variables and substituting Equations 124 and 125 for P_θ and P_φ, respectively, Equation 136 becomes:

$$\bar{v}_y = \int_0^\infty v^3 P_\rho \, dv \int_{-\pi/2}^{\pi/2} \frac{\cos^2\theta}{2} \, d\theta \int_{-\pi/2}^{\pi/2} \frac{2\cos^2\varphi}{\pi} \, d\varphi \qquad (137)$$

Where P_ρ is given by Equation 74 and $\bar{v}_y$ must be evaluated for n=0,1,2, etc.

For n=0 (D_n=1), using Equation 83 for $P_{\rho,0}$ and performing the two angular integrations, Equation 137 gives for the dimensionless mean reflected normal component:

$$\bar{S}_y = \frac{4 A_\rho^3}{3\sqrt{A_\rho^2-1}\,(-S')} \int_0^\infty S^3 \exp[-(A_\rho^2-1)S'^2 - A_\rho^2 S^2] \, I_1[-2S'S A_\rho\sqrt{A_\rho^2-1}] \, dS \qquad (138)$$

Using the result of Appendix B. Equation 138 becomes,

$$\bar{S}_y = \frac{\pi}{2A_\rho} \exp[-(A_\rho^2-1)S'^2] M[5/2,2,S'^2(A_\rho^2-1)] \qquad (139)$$

The result of Equation 139 is shown in Figure 17, Appendix A, with $\bar{S}_y$ plotted as a function of S' for various values of α_ρ. The numerical results for n=1 and 2 are shown in Figures 18 and 19, Appendix A, respectively.

3.1.2 Mean Energy of Reflected Molecules

The exchange of energy between a gas and a surface is perhaps the most important, or at least the most investigated, gas-surface phenomenon. The kinetic energy, e, of a reemitted molecule is given by:

$$e = \frac{mv^2}{2} \tag{140}$$

The mean reflected energy is:

$$\bar{e} = \int_{\vec{v}\cdot\vec{n}<0} e\ P\ d^3\bar{v} = \frac{m}{2}\ \overline{v^2} \tag{141}$$

The evaluation of $\bar{e}$ thus requires the determination of the mean square of the reflected velocities.

3.1.2.1 The Determination of $\overline{S^2}$ in Rectangular Coordinates

In rectangular coordinates the square of the velocity is given by:

$$v^2 = v_x^2 + v_y^2 + v_z^2 \tag{142}$$

Substituting this expression into Equations 131 and 132 and using Equation 5, the mean square of the velocity of reflected molecules becomes:

$$\overline{v^2} = \int_{-\infty}^{\infty}\int_{0}^{\infty}\int_{-\infty}^{\infty} (v_x^2 + v_y^2 + v_z^2)\ P_x P_y P_z dv_x dv_y dv_z \tag{143}$$

Separating variables and utilizing the normalization conditions (Equation 6) Equation 134 becomes:

$$\overline{v^2} = \int_{-\infty}^{\infty} v_x^2 P_x dv_x + \int_{0}^{\infty} v_y^2 P_y dv_y + \int_{-\infty}^{\infty} v_z^2 P_z dv_z \qquad (144)$$

which is equivalent to:

$$\overline{v^2} = \overline{v_x^2} + \overline{v_y^2} + \overline{v_z^2} \qquad (145)$$

In terms of dimensionless velocities the terms on the right hand of Equation 145 become:

$$\overline{S_x^2} = \int_{-\infty}^{\infty} S_x^2 \quad 2RT_w \, P_x dS_x \qquad (146\text{-a})$$

$$\overline{S_y^2} = \int_{0}^{\infty} S_y^2 \quad 2RT_w \, P_y dS_y \qquad (146\text{-b})$$

where the form of $\overline{S_z^2}$ is identical to that of $\overline{S_x^2}$.

For n=0, Equations 29 and 38 may be utilized for $\sqrt{2RT_w}\, P_x$ and $\sqrt{2RT_w}\, P_y$, respectively, in Equation 146 and integrated to yield:

$$\overline{S_x^2} = \frac{A_x^{-2}}{2} + S_x'^2 \, (1-A_x^{-2}) \qquad (147\text{-a})$$

$$\overline{S_y^2} = A_y^{-2} + S_y'^2 \, (1-A_y^{-2}) \qquad (147\text{-b})$$

Use was made of Appendix B for obtaining Equation 147-b. Figure 20, Appendix A. presents Equation 147-a with $\sqrt{\overline{S_x^2}}$ plotted as a function of S_x' for various values of α_x. Figure 21, Appendix A. similarly shows the results of Equation 147-b.

For n greater than unity it has been shown (Section 2.4.1) that $A_n = 0$ and therefore the complete scattering kernel in the x and z coordinates is given by Equation 38. In the y direction, the numerical results for n greater than unity as shown in Figures 6 and 7, Appendix A, was substituted in Equation 146-b and numerically integrated. These results for n=1 and 2 are shown in Figures 22 and 23, Appendix A.

3.1.2.2 The Determination of $\overline{S_2}$ in Cylindrical Coordinates

In cylindrical coordinates the square of the molecular velocity is given by:

$$v^2 = v_r^2 + v_y^2 \tag{148}$$

Substituting Equation 148 into Equations 140 and 141 and using Equation 51 yields:

$$\overline{v^2} = \int_{-\pi}^{\pi} \int_{0}^{\infty} \int_{0}^{\infty} (v_r^2 + v_y^2)\, P_y P_r P_\psi v_r \, dv_y \, dv_r \, d\psi \tag{149}$$

After separation of variables and the utilization of the normalization conditions as expressed in Equation 53, Equation 149 becomes:

$$\overline{v^2} = \int_{0}^{\infty} v_r^3 P_r \, dv_r + \int_{0}^{\infty} v_y^2 P_y \, dv_y \tag{150}$$

which is the same as:

$$\overline{v^2} = \overline{v_r^2} + \overline{v_y^2} \tag{151}$$

The results for $\overline{v_y^2}$ are identical to those in rectangular coordinates and already presented in Figures 21, 22 and 23, Appendix A, as $\sqrt{S_y^2}$.

In terms of dimensionless velocities the first term on the right hand side of Equation 151, after using Equation 62 and integrating, becomes for n=0:

$$\overline{S_r^2} = A_r^{-2} + S_r'^2(1-A_r^{-2}) \tag{152}$$

which is of the same form as Equation 147-b. In fact, from an inspection of Equations 61, 146-b, and the expression for $\overline{v_r^2}$, it can be seen that the results for $\overline{v_y^2}$ and $\overline{v_r^2}$ are equivalent for all values of n. Thus Figures 21, 22 and 23, Appendix A, also give the results for $\sqrt{\overline{S_r^2}}$.

3.1.2.3 The Determination of $\overline{S^2}$ in Spherical Coordinates

From Table I, page 18, it can be seen that the square of the molecular velocity in spherical coordinates is simply:

$$v^2 \equiv v_\rho^2 \tag{153}$$

Equation 141, after integrating over θ and φ becomes:

$$\overline{v^2} = \int_0^\infty v^4 \, P \, dv \tag{154}$$

For n=0, using Equation 83 and Appendix B, Equation 154 becomes in terms of dimensionless velocity:

$$\overline{S^2} = 2A_\rho^{-2} + S'^2(1-A_\rho^{-2}) \tag{155}$$

Equation 155 is plotted in Figure 24, Appendix A, as $\sqrt{\overline{S^2}}$ as a function of S' for various values of α_ρ. For n greater than 1 it was necessary to numerically integrate Equation 154 using the numerical results for P_ρ shown in Figures 12 and 13, Appendix A. The results are presented, using the same parameters as for n=0, in Figures 25 and 26, Appendix A, for n=1 and 2, respectively.

3.2 REFLECTED DIRECTIONAL PROPERTIES

In Section 3.1 the reflected global properties of velocity components and energy were determined based upon the theoretical results of Section II. We will now turn our attention to the determination of local or directional properties.

Consider the detector shown in Figure 27, Appendix A. The type of detector is immaterial, it could measure molecular flux, density, velocity, etc. The detector, located a distance L from the point of impact, Q, of the molecular beam, has a sensing area, dA, which subtends a solid angle of $d\omega$ when viewed from A. The solid angle is given by:

$$d\omega = \frac{dA}{L^2} \tag{156}$$

Because all reflected molecules are assumed to emanate from the origin, all molecules within $d\omega$ at θ and φ in physical space are also within the same solid angle in velocity space. Thus, the molecular properties at the detector are determined by integrating the desired properties over all molecules within $d\omega$.

Previous results in this paper have been presented (e.g., Figures 2-26, Appendix A, inclusive) for each of three coordinate systems for various values of n. Inasmuch as the scattering kernel with n=0 in rectangular coordinates embodies most of the experimentally observed gas-surface phenomena, the results which follow will be presented in detail only for this case, since more independent variables are involved because the coordinates directions are not separable as was true for the global properties.

Important directional properties which will be investigated are molecular flux, density, speed and energy.

3.2.1 Molecular Flux Distribution

The easiest reflected quantity to measure is molecular flux. Referring to Figure 27, Appendix A, the number of reflected molecules with speed between v and

v + dv entering the detector during time dt will now be determined. The number of molecules reflected during time dt with speeds between v and v + dv within $d\omega$ is:

$$\dot{N}P\ v^2\ d\omega\ dv\ dt \tag{157}$$

Notice that $v^2\ d\omega\ dv$ is simply the incremental volume in velocity space. These molecules are spread out over a length vdt within $d\omega$ in physical space. The number per unit volume in physical space is that given by Equation 157 divided by the increments volume, $L^2 d\omega v dt$, which yields:

$$d\rho = \frac{\dot{N}P v dv}{L^2} \tag{158}$$

During the time dt, molecules with velocity v contained in the volume dA vdt, will enter the detector. This volume multiplied by the incremental density given by Equation 158 and dividing by dt in order to obtain an intensity yields:

$$dI = \frac{\dot{N}P\ v^2 dv dA}{L^2} \tag{159}$$

dI is therefore the total number of molecules with speeds between v and v + dv that enter the detector per unit time. Equation 159 may be integrated over all reflected speeds to obtain the total number of molecules scattered into the detector per unit time. Thus:

$$I = \frac{\dot{N}dA}{L^2} \int_0^\infty P\, v^2 dv \tag{160}$$

A dimensionless intensity, $\tilde{I}$, is defined as follows:

$$\tilde{I} = \frac{IL^2}{\dot{N}dA} \tag{161}$$

Combining Equations 160 and 161 yields in terms of dimensionless speed:

$$\tilde{I} = (2RT_w)^{3/2} \int_0^\infty PS^2 dS \tag{162}$$

From a consideration of the normalization condition given by Equation 2 it can be shown that $\tilde{I}$ is the probability density that a reflected molecule will be in a given direction without regard to speed. Thus $\tilde{I}\, d\omega$ is the probability that a molecule will be reflected within $d\omega$, and therefore enter the detector.

Using Equation 13 for the scattering kernel with the individual kernels given by Equations 38 and 47, Equation 162 becomes, in terms of dimensionless velocities:

$$\tilde{I} = \frac{2A_x^2 A_y^2}{\pi} \int_0^\infty \exp\left\{-\left[(A_x^2-1)^{1/2} S_x' - A_x S \cos\varphi \sin\theta\right]^2 - A_x^2 S^2 \sin^2\varphi - (A_y^2-1) S_y^2 - A_y^2 S^2 \cos^2\varphi \cos^2\theta\right\} I_0\left[2A_y (A_y^2-1)^{1/2} S_y' S \cos\varphi \cos\theta\right] S^3 \cos\varphi \cos\theta\, dS \tag{163}$$

For a given A_x and A_y, $\tilde{I}$ can be evaluated numerically from Equation 163 as a function of φ and θ for various combinations of S_x' and S_y'. (Integration in closed form was not achieved.) The numerical results of Equation 163 for $\alpha_x = 0.5$ and $\alpha_y = 0.8$ are shown in Figure 28, Appendix A, for $\theta_i = -20^\circ$, -50° and -80°. Similar results for $\alpha_x = 0.8$ and $\alpha_y = 0.5$ are shown in Figure 29, Appendix A. The numerical results are presented as a function of θ for $\varphi = 0$, and as a function of φ for $\theta = \theta_m$ where θ_m is the value of θ for which $\tilde{I}$ is a maximum. The results in Figures 28 and 29 are typical for $\alpha_x < \alpha_y$ and $\alpha_y > \alpha_x$, respectively.

For the special case of $A_x = A_y = A(\alpha_x = \alpha_y)$ Equation 163 may be simplified somewhat. For this condition Equation 163 becomes:

$$\tilde{I} = \frac{2}{\pi} \int_0^\infty \exp[-(A^2-1)S'^2 + 2A\sqrt{A^2-1}\, S' \sin\theta_i\, S\cos\varphi -$$

$$A^2S^2]\, I_0[2A\,(A^2-1)^{1/2}S'S\cos\theta_i\cos\varphi\cos\theta] \cdot$$

$$(AS)^3 \cos\varphi\cos\theta\, d(AS) \qquad (164)$$

Equation 164 may be integrated numerically to obtain $\tilde{I}$ as a function of θ_r, θ_i and $\sqrt{A^2-1}\, S'$. The results of Equation 164 for $\varphi = 0$ and $\theta = \theta_m$ are shown as a function of θ, and $\sqrt{A^2-1}\, S'$ for θ_i of -20°, -50° and -80° in Figure 30, Appendix A.

3.2.2 Molecular Density Distribution

The total density of reflected molecules, ρ, is obtained by integrating Equation 158 over all speeds. Thus:

$$\rho = \frac{\dot{N}}{L^2} \int_0^\infty P \, v \, d \, v \tag{165}$$

A dimensionless density, $\tilde{\rho}$, is defined as follows:

$$\tilde{\rho} = \frac{\rho L^2}{\dot{N} \, 2RT_w} \tag{166}$$

Combining Equations 165 and 166 gives for $\tilde{\rho}$ in terms of dimensionless speed:

$$\tilde{\rho} = (2RT_w)^{3/2} \int_0^\infty P \, S \, d \, S \tag{167}$$

The numerical results for $\tilde{\rho}$ are very similar to those for $\tilde{I}$ and therefore will not be presented at this time. However, Equation 167 will be utilized later when comparison of theory to experimental data is made.

3.2.3 Mean Reflected Speed

Mean reflected speed is defined as the average speed of molecules entering the detector; i.e., the average is over the flux of molecules and not over density as is usually the case in the kinetic theory sense. Using Equation 159 for the incremental flux of molecules, the mean velocity becomes:

$$\bar{v} = (\tilde{I}^{-1}) \int_0^\infty P v^3 \, dv \tag{168}$$

or in terms of dimensionless velocity:

$$\bar{S} = (\tilde{I}^{-1})(2RT_w)^{3/2} \int_0^\infty P \, S^3 \, d \, S \tag{169}$$

Using Equations 13, 38 and 47, Equation 169 may be written in a form similar to Equation 163 with $\tilde{I}$ evaluated from Equation 163. Numerical results for $\bar{S}$ for $\alpha_x = 0.5$ and $\alpha_y = 0.8$ are shown in Figure 31, Appendix A, for $\theta_i = -20^\circ$, -50° and -80° for $\varphi = 0$ and $\theta = \theta_m$. Similar results for $\alpha_x = 0.8$ and $\alpha_y = 0.5$ are shown in Figure 32, Appendix A. The results for $\bar{S}$ presented in Figures 31 and 32 are typical for $\alpha_x < \alpha_y$ and $\alpha_y > \alpha_x$, respectively.

For the special case of $A_x = A_y = A$ the number of independent variables in Equation 169 may be reduced to $\theta, \varphi, \theta_i$, and $\sqrt{A^2-1}\, S'$ with $A\bar{S}$ as the dependent variable. Figure 33, Appendix A, gives the numerical results for $A\bar{S}$ with $\theta_i = -20^\circ$, -50° and -80° for $\varphi = 0$ and $\theta = \theta_m$.

3.2.4 Mean Reflected Energy

Mean reflected energy like mean speed is determined by averaging over the flux of molecules. Using Equation 140 the mean energy of molecules reflected in a given direction is:

$$\bar{e} = (\tilde{I}^{-1}) \int_0^\infty \left(\frac{mv^2}{2}\right) P \, v^2 \, dv \tag{170}$$

which is equivalent to:

$$\bar{e} = \frac{m\,\overline{v^2}}{2} \tag{171}$$

or in terms of dimensionless velocities:

$$\bar{e} = \frac{m}{2}\,2RT_w\,\overline{S^2} \tag{172}$$

where:

$$\overline{S^2} = (\tilde{I}^{-1}) \int_0^\infty (2RT_w)^{3/2}\, P\, S^4\, d\, S \tag{173}$$

The numerical results for $\sqrt{\overline{S^2}}$ are very similar to those for $\bar{S}$ and will therefore not be given as such. However, the directional energy accommodation coefficient α_e is often used to describe energy exchange with the surface. It is defined in terms of molecular energy as follows:

$$\alpha_e = \frac{\bar{e} - e_i}{e_w - e_i} \tag{174}$$

where e_i is the molecular incident energy and e_w is the reflected energy if at equilibrium with the surface at T_w. Equation 174 may be rewritten in terms of dimensionless speeds as follows:

$$\alpha_e = \frac{\overline{S^2} - S_i^2}{2 - S_i^2} \tag{175}$$

Use was made of the fact that $e_w = 2mRT_w$.

The local value of α_e is not bounded by zero and unity as one normally expects. From the second law of thermodynamics the total energy accommodation must be within these bounds. However, there are no such restrictions upon the local value. In fact, from Equation 175 it can be seen that for $S_i = \sqrt{2}$, α_e diverges unless $\overline{S^2} = S_i^2$, which occurs only in isolated directions. This uncertainty raises serious questions concerning the usefulness of α_e, however, it is widely used in the literature and it is introduced here for that reason.

3.2.5 Direction of Maximum Molecular Flux

The direction of maximum molecular flux is one of the most widely used parameters in the study of gas-surface interactions. It seems that the test of any gas-surface model or theory is to compare the predicted maximum in reflected flux to experimental data or to other theories (e.g., see the review paper by Trilling [32]).

These maxima in flux for the present theory can be determined for typical values of α_x, α_y and θ_i from the flux distributions as presented in Figures 28, 29 and 30, Appendix A. Numerically differentiating these results, the value of θ for which $\tilde{I}$ is a maximum can be determined, this θ value will be denoted by θ_m. Value of θ_m obtained for the values of α_x, α_y and θ_i given previously are presented in Figures 34, 35 and 36, Appendix A.

The limit of θ_m for large values of S' can be determined in closed form. Recalling that in Sections 2.1.1 and 2.1.2 it was shown that as A_x and A_y increase without limit specular reflection is approached. In a similar manner as S_x' and S_y' increase without limit, the scattering kernels given by Equations 29 and 38 approach the following:

$$\sqrt{2RT_w}\, P_x \longrightarrow \frac{A_x}{S_x'}\, \delta\left(\sqrt{A_x^2-1} - A_x S_x/S_x'\right), \quad S_x' \longrightarrow \infty \tag{176}$$

$$\sqrt{2RT_w}\, P_y \longrightarrow \frac{A_y}{S_y'}\, \delta\left(\sqrt{A_y^2-1} + A_y S_y/S_y'\right), \quad S_y' \longrightarrow \infty \tag{177}$$

Substituting into Equations 128 and 133, $\overline{S_x}$ and $\overline{S_y}$ become:

$$\overline{S_x} = \sqrt{1-\alpha_x}\, S_x', \quad S_x' \longrightarrow \infty \tag{178}$$

$$\overline{S_y} = \sqrt{1-\alpha_y}\, S_y', \quad S_y' \longrightarrow \infty \tag{179}$$

Since for $S' \longrightarrow \infty$ both P_x and P_y approach a delta function the flux of molecules also approaches a delta function, i.e., a spike directed along the direction determined by $\overline{S_x}$ and $\overline{S_y}$. Thus, θ_m is given by:

$$\theta_m = \mathrm{Tan}^{-1}\left(\overline{S_x}/\overline{S_y}\right), \quad S' \longrightarrow \infty \tag{180}$$

or using Equations 178 and 179 and writing in terms of θ_i yields:

$$\theta_m = \text{Tan}^{-1} \left[-\left(\sqrt{1-\alpha_x}/\sqrt{1-\alpha_y}\right) \text{Tan}\ \theta_i \right] , \quad S' \longrightarrow \infty \tag{181}$$

Figure 37, Appendix A, presents the results of Equation 181. Notice that only for the case of $\alpha_x = \alpha_y$ is the specular limit approached as $S' \longrightarrow \infty$ and depending on α_x and α_y the limit can be supra-specular or subspecular.

3.3 REFLECTED VELOCITY DISTRIBUTION FUNCTION

Throughout Section II and thus far in Section III we have considered only the reflected probability of a single incident molecule or the mean reflected properties of an incident monoenergetic molecular beam, i.e., of uniform speed and direction. The special case of a gas with a Maxwellian distribution incident upon a surface will now be considered in each of the three coordinate systems. It is assumed that the velocity distributions of incident molecules is given by:

$$f^- = (2\pi RT^-)^{-3/2} \exp(-v'^2/2RT^-) \tag{182}$$

The velocity distribution function f^- and f^+ were discussed in Section 1.2 and the relation between them and the scattering kernel was given in Equation 3. The determinations of f^+ will be made only for those scattering kernels that have been obtained in closed form, i.e., for $n = 0$. It will be shown that f^+ is Maxwellian in form in each coordinate system, and for equality of accommodation

coefficients thus satisfies the so called "Knudsen's Assumption" discussed in Section 1.1, page 4.

3.3.1 f^+ in Rectangular Coordinates

In rectangular coordinates, using Table I, page 18, and Equations 13, 38, 47 and 182, Equation 3 becomes:

$$f^+ = f_x^+ f_y^+ f_z^+ \tag{183}$$

where:

$$f_x^+ = \frac{A_x}{\pi\sqrt{2RT^-}} \int_{-\infty}^{\infty} \exp[-(\sqrt{A_x^2-1}\, S_x' - A_x S_x)^2 - T_w S_x'^2/T^-]\, dS_x' \tag{184}$$

$$f_y^+ = \frac{2A_y^2}{\sqrt{2\pi RT^-}} \int_{-\infty}^{0} S_y' I_0(-2A_y\sqrt{A_y^2-1}\, S_y' S_y) \exp[-S_y'^2(A_y^2-1 + T_w/T^-) - A_y^2 S_y^2]\, dS_y' \tag{185}$$

and f_z^+ is of exactly the same form as Equation 184 with S_x replaced by S_z.

Integrating Equations 184 and 185 (use of Appendix B was required for the latter) yields:

$$f_x^+ = \frac{A_x(2\pi RT^-)^{-1/2}}{(A_x^2-1 + T_w/T^-)^{1/2}} \exp\left\{-S_x^2 T_w A_x^2/[T^-(A_x^2-1 + T_w/T^-)]\right\} \tag{186}$$

$$f_y^+ = \frac{A_y^2(2\pi RT^-)^{-1/2}}{(A_y^2-1 + T_w/T^-)} \exp\left\{-S_y^2 T_w A_y^2/[T^-(A_y^2-1 + T_w/T^-)]\right\} \tag{187}$$

$$f_z^+ = f_x^+ (S_z) \tag{188}$$

Notice that the reflected velocity distribution is Maxwellian in form with possible differences in temperature in the normal and tangential directions. Defining the remitted temperature in the normal and tangential directions as T_y^+ and T_x^+, respectively, Equations 186, 187 and 188 become:

$$f_x^+ = (2\pi RT_x^+)^{-1/2} \exp(-v_x^2/2RT_x^+) \tag{189}$$

$$f_y^+ = (T_y^-/T_y^+)^{1/2} (2\pi RT_y^+)^{-1/2} \exp(-v_y^2/2RT_y^+) \tag{190}$$

$$f_z^+ = (2\pi RT_x^+)^{-1/2} \exp(-v_z^2/2RT_x^+) \tag{191}$$

Solving for T_x^+ and T_y^+ from Equations 186, 187, 189 and 190 yields:

$$T_x^+ = T^-(A_x^2 - 1 + T_w/T^-)/A_x^2 \tag{192}$$

$$T_y^+ = T^-(A_y^2 - 1 + T_w/T^-)/A_y^2 \tag{193}$$

Writing Equations 192 and 193 in terms of A_x^{-2} and A_y^{-2}, respectively, yields:

$$A_x^{-2} = \frac{T_x^+ - T^-}{T_w - T^-} \tag{194}$$

$$A_y^{-2} = \frac{T_y^+ - T^-}{T_w - T^-} \tag{195}$$

Equations 194 and 195 are the normal definitions of the thermal accommodation coefficients, α_x, α_y, generalized to each coordinate direction. Thus, the relation between the α's and A's is given by:

$$\alpha_x = A_x^{-2} \tag{196}$$

$$\alpha_y = A_y^{-2} \tag{197}$$

These definitions of α_x and α_y were introduced in Section II without proof.

The term $(T_y^-/T_y^+)^{1/2}$ in Equation 190 came about from the conservation of molecules at the surface. Thus, the density of reflected molecules is $(T_y^-/T_y^+)^{1/2}$ times that of the incident density.

For the special case of $A_x = A_y (\alpha_x = \alpha_y = \alpha)$ Equation 183 becomes

$$f^+(\tilde{v}) = (T^-/T^+)^{1/2} \, (2\pi RT^+)^{-3/2} \exp[-\tilde{v}^2/2RT^+] \tag{198}$$

and α is the ordinary thermal accommodation coefficient:

$$\alpha = \frac{T^+ - T^-}{T_w - T^-} \tag{199}$$

3.3.2 f^+ in Cylindrical Coordinates

The reflected velocity distribution function will be evaluated only for n = 0. In cylindrical coordinates, using Table I, page 18, and Equations 51, 62, 47, 63 and 182, Equation 3 becomes:

$$f^+ = f_y^+ \, f_r^+ \tag{200}$$

where f_y^+ is given by Equation 185 and after integration by Equation 190. And:

$$f_r^+ = 2 A_r^2 (2\pi RT^-)^{-1} \int_{-\infty}^{0} S_r' \, I_0(-2A_r\sqrt{A_r^2-1}\, S_r' S_r) \cdot$$

$$\exp[-S_r'^2(A_r^2-1 + T_w/T^-) - A_r^2 S_r^2] \, dS_r' \tag{201}$$

Integrating, using Appendix B yields:

$$f_r^+ = (2\pi RT_r^+)^{-1} \exp(-v^2/2RT_r^+) \tag{202}$$

where:

$$T_r^+ = T^-(A_r^2-1 + T_w/T^-)/A_r^2 \tag{203}$$

or solving for A_r^{-2}:

$$A_r^{-2} = \frac{T_r^+ - T^-}{T_w - T^-}$$

which is again the thermal accommodation coefficient, α_r. Thus:

$$\alpha_r = A_r^{-2} \tag{204}$$

For the special case of $A_r = A_y (\alpha_r = \alpha_y = \alpha)$ Equation 200 becomes identical to Equation 198.

3.3.3 f^+ in Spherical Coordinates

In spherical coordinates for n = 0 and using Table I, page 18, and Equations 64, 83, 124 and 125, Equation 3 becomes, after integrating out the angular parts:

$$f^+ = (2A_\rho^3/S)(A_\rho^2-1)^{-1/2}(2\pi RT^-)^{-3/2} \int_{-\infty}^{0} S'^2 \exp[-(A_\rho^2-1)S'^2 -$$

$$A_\rho^2 S^2 - T_w S'^2/T^-)\,] I_1(-2S'SA_\rho\sqrt{A_\rho^2-1})\, dS' \tag{205}$$

Using Appendix B and integrating yields:

$$f^+(\bar{v}) = (T^-/T_\rho)^{1/2} (2\pi RT_\rho^+)^{-3/2} \exp(-v^2/2RT_\rho^+) \tag{206}$$

where:

$$T_\rho^+ = T^-(A_\rho^2 - 1 + T_w/T^-)\, A_\rho^2 \tag{207}$$

and solving for A_ρ^{-2} gives:

$$A_\rho^{-2} = \frac{T^+ - T^-}{T_w - T^-} \tag{208}$$

which is again the thermal accommodation coefficient, α_ρ.

IV. COMPARISON OF THEORY WITH EXPERIMENT

The purpose of this section is not to define generalized gas-surface interacting parameters, but to show that the theoretical results developed in the first three sections of this paper, indeed are capable of describing real gas surface effects. Experimental reflected flux distributions from a wide range of gases and surfaces indicate that certain scattering characteristics are common to almost all conditions.

4.1 GENERAL CHARACTERISTICS

Stickney [33, page 186] in an excellent article on scattering from solid surfaces, lists eight scattering characteristics which, in terms of present nomenclature, are:

1. $\partial\theta_m/\partial v' \geq 0$
2. $\partial\theta_m/\partial T_w \leq 0$ (This characteristic is invalid if the composition or structure of the surface varies with T_w.)
3. $\partial\theta_m/\partial(-\theta_i) \geq 0$
4. $\partial\theta_m/\partial m < 0$ when $\theta_m < -\theta_i$
   $\partial\theta_m/\partial m > 0$ when $\theta_m > -\theta_i$
   (It is assumed that ΔH, the heat of adsorption, is held constant in these partial derivatives.)
5. The dispersion of the diffuse scattering patterns increases with ΔH and/or with m.

6. Supraspecular patterns (i.e., $\theta_m > -\theta_i$) are most likely to occur when both of the following conditions are met: (a) $S' > 1$ and (b) $-\theta_i \ll 90^\circ$.
7. Nondiffuse scattering is most likely to occur from surfaces that are smooth and free of gross contamination.
8. The dispersion of nondiffuse scattering is greater for the in-plane pattern than for the out-of-plane pattern. (That is, the probability is low that molecules will be scattered out of the plane defined by the incident beam and the target normal.)

Notice that these eight characteristics are concerned with gross surface properties and no mention is made of reflected velocities or energy. This limitation was due to the unavailability of reliable experimental results on these quantities at that time (1967).

The reciprocity condition, in general, places no restriction upon the variations of reflected characteristics with changes in wall or gas properties. Thus, no definite statement can be made concerning characteristics 2, 4, 5 and 7. However, if it is assumed that the wall properties are independent of T_w (say α_x and α_y are constant) then a limited statement may be made concerning characteristic 2. The effect of T_w is manifest in S'. As T_w increases, S' decreases and from an inspection of Figures 34, 35 and 36,

Appendix A, it can be seen that characteristic 2 is satisfied if $\alpha_x \leq \alpha_y$.

Nothing can be said about characteristics 4, 5 and 7 based upon reciprocity since it has been experimentally determined that the accommodations of energy between the gas and surface is a strong function of m (e.g., see [33], Figure 2).

Based upon the results presented in Figures 34, 35 and 36, Appendix A, it can be seen that the present theory satisfies characteristic 1 if $\alpha_x \leq \alpha_y$. Also considering Figure 37, Appendix A, it is seen that characteristic 3 appears to be fulfilled for all α_x and α_y. Likewise, characteristic 6 is valid if $\alpha_x < \alpha_y$ from an investigation of Figure 34, Appendix A. And, finally, characteristic 8 is confirmed for $\alpha_x < \alpha_y$ from a consideration of Figure 28, Appendix A.

Thus, the present gas-surface interaction model is in agreement with general trends as presented in characteristics 1, 2, 3, 6 and 8 if $\alpha_x < \alpha_y$ and is not in disagreement with characteristics 4, 5 and 7.

4.2 DETAILED COMPARISON WITH EXPERIMENTAL RESULTS

4.2.1 Comparison with Data of Moran [34]

In order to adequately check the theoretical results, it is desirable to have experimental measurements on several reflected molecular properties from a given surface for various incident angles and velocities. The most complete experimental investigation of the interaction between a

monatomic gas and an isotropic surface is that done by Moran [34] for argon on platinum. He measured the reflected time of flight signal as a function of reflected angle for two incident energies at several incident angles from which several reflected properties are determined. His results are presented in Figures 38 through 44, Appendix A, for reflected relative flux, speed ratio, and mean speed, from a heated platinum surface.

The reflected speed ratio, S_r, is a measure of the thermal spread in the reemitted molecular velocity distribution. Moran defines S_r in terms of $\bar{v}$ and $\overline{v^2}$ as follows:

$$S_r = (\overline{v^2}/\bar{v}^2 - 1)^{1/2} \tag{209}$$

Notice that any consistent error in the scale of the velocities tends to cancel out in this definition of S_r.

As has been pointed out previously in this work, the solution for n = 0 in rectangular coordinators (Equations 13, 38 and 47) seems to be adequate to describe most experimental results. Values of α_x and α_y were chosen so as to best fit the reflected flux distributions in a least squares sense. Moran, like most other experimentalists, presents flux in only relative terms, i.e., arbitrary units. This is due to the difficult problem of the absolute calibration of a molecular flux instrument. The relative molecular flux, I', is calculated from $\tilde{I}$ by introducing an aribtrary multiplication factor so that the mean value of I' from experiment and from theory is identical.

The values of α_x and α_y determined for the best fit was 0.147 and 0.710, respectively. Using these values, I', $\overline{v}$ and $\overline{v^2}$ can be determined by the numerical integrations as discussed in Section 3.2, and S_r obtained from Equation 209. These theoretical results are shown as the curves in Figures 38 through 44, Appendix A.

4.2.2 Comparison with Data of Romney [35]

The data of Moran was limited to low incident velocity (S' = 0.742 and 1.313). However, Romney, using a seeded beam technique, wherein the argon was accelerated using a light carrier gas, obtains reflected density distributions of high velocity argon (S' = 1.14 to 9.38) reflected from a crystalline silver surface. The silver surface he used was vapor deposited in situ during the scattering measurements so as to ensure an uncontaminated surface.

Using the same method as described in the previous section, α_x and α_y were determined to be 0.77 and 0.85, respectively. The theoretical results for the relative reflected density distribution for an incident argon beam with energy of 2.56 ev is compared to the experimental result in Figure 45-a, Appendix A.

Romney also determines the variation of the position of maximum reflected density with incident energy for various angles of incident. This maximum density, for the conditions of Romney's test, is indistinguishable from the position of maximum reflected flux, θ_m, therefore his results will be

assumed to be equal to θ_m. Figure 46, Appendix A, presents these experimental values of θ_m for incident angles of 35°, 50° and 65° and the theoretical results obtained using the previously determined values of α_x and α_y.

One of the major disadvantages of the seeded beam techniques, as used by Romney, is that the molecular flux of the species of interest is drastically reduced for the higher energies, thereby making the measurement of reflected velocities very difficult. At the present there are no known data available on the velocity of reflected molecules under high energy conditions.

4.2.3 Comparison with Data of Bishara [26, 36]

Bishara [29, 36] has obtained data on the flux and mean velocity of argon scattered from a crystalline silver surface. These results for an incident energy of 0.64 ev and a surface temperature of 550°K are shown in Figures 46, 47 and 48, Appendix A, for incident angles of -40°, -50° and -60°, respectively. He made measurements not only in the principal plane ($\varphi = 0$) but at two transverse planes ($\theta = 0$ and $\theta = \theta_m$). While both Romney [35] and Bishara used silver surfaces, Bishara did not deposit silver in situ as did Romney but polished and etched the surface in the atmosphere prior to testing. Data, in fact, indicated that the scattering pattern varied during the period of testing.

Using the technique previously described whereby α_x and α_y were determined to best fit the experimental data,

values of 0.92 and 1.0 were obtained, respectively, from Bishara's results. However, the theoretical results did not adequately explain the experimentally observed reflected flux distributions. Near the specular direction the data were more peaked while further away the data seemed to be more diffuse. This characteristic is similar to that observed by Saltsburg and Smith [37] for a clean silver surface purposely contaminated by exposure to the atmosphere. This explanation is consistent with the higher α's obtained from the Bishara [29] data than the Romney [35] data.

For any real surface, especially a contaminated one, there are variations in properties over the surface, i.e., the surface is not homogeneous. Recalling that the reciprocity relation is linear, the scattering kernel could be made up of several kernels each of which would correspond to a micro-surface and have an α_x and α_y associate with it.

In regard to contaminated surfaces, recent experimental results from Dawbarn et al [38] for nitrogen on contaminated aluminum indicate that the scattering is toward the backscatter direction (i.e., Equation 5 is applicable to the scattering kernel).

In an attempt to better describe theoretically the results of Bishara [29, 36] it was assumed that the scattering kernel was a linear combination of two kernels each of which could be reflected according to Equation 5. The best fit to the reflected flux distribution, both in the principal

plane and in the transverse planes, was obtained for the following kernel.

$$P(\bar{v}',\bar{v}) = 0.755\ P_1' + 0.245\ P_2 \qquad (210)$$

where:

P_1' is a backscattered kernel with $\alpha_x = 0.99$ and $\alpha_y = 0.99$

P_2 is a scattering kernel with $\alpha_x = 0.53$ and $\alpha_y = 1.0$

Using Equation 210 the mean reflected velocity can also be obtained by numerical integration, these results for $\bar{v}$ and I' are compared with the experimental data in Figures 46 through 48, Appendix A.

V. SUMMARY AND CONCLUSIONS

In the paper by Kuscer et al [7] the statement is made, "It is surprisingly difficult to construct non-trivial mathematical models for $P(\bar{v}',\bar{v})$ satisfying all three requirements," (Equations 1, 2 and 4). In the present work, by assuming a product solution for $P(\bar{v}',\bar{v})$ in each of three coordinate systems, several solutions are found that satisfy Equations 1, 2 and 4. It is shown that one particular solution, as given by Equations 38 and 47, agrees with experimental results in regard to reflected flux distributions, mean velocities, and speed ratio. This is the first time that any theoretical result has been compared to all these detailed reflected quantities. The theoretical results for the position of the maximum reflected flux are also shown to be in agreement with experimental data, and, for typical surfaces with high incident velocity, the reflected lobe is supraspecular.

A more general scattering kernel can be obtained by a linear combination of several, or in the limit an infinite number of individual scattering kernels. In the limit the infinite sum becomes an integral and the following can be obtained in rectangular coordinates:

$$P(\bar{v}',\bar{v}) = \int_0^1 \int_0^1 \int_0^1 F(\alpha_x,\alpha_y,\alpha_z)\ P_x(v_x',v_x,\alpha_x)\ P_y(v_y',v_y,\alpha_y)\cdot$$

$$P_z(v_z',v_z,\alpha_z)\ d\alpha_x\ d\alpha_y\ d\alpha_z \qquad (211)$$

where F is an arbitrary function subject to:

$$\int_0^1 \int_0^1 \int_0^1 F(\alpha_x, \alpha_y, \alpha_z)\, d\alpha_x\, d\alpha_y\, d\alpha_z = 1 \tag{212}$$

and such that $P(\bar{v}', \bar{v})$ is non-negative. Notice that this scattering kernel is not, in general, of a product form unless F is assumed to be a product. The scattering kernel given by Equation 211 is so general that is is not very helpful for the description of a practical gas-surface interaction. A result analogous to Equation 211 can be obtained in cylindrical and spherical coordinates, and the scattering kernel can be further generalized by a linear combination of the results in various coordinate systems.

Thus, the results obtained in this paper when combined, using the linearity and reflectivity (Equation 5) property, permit an almost unlimited generalization. However, reciprocity places restrictions upon the variation of the scattering kernel with incident gas conditions, e.g., F in Equation 211 cannot be a function of incident gas energy or direction.

The primary usefulness of the results obtained herein is not the "curve fittings" of existing data per se, but the determination of gas-surface effects under conditions where experimental data are not available. In other words, reciprocity helps us extrapolate. Thus, surface parameters such as α_x and α_y obtained under moderate incident energy conditions, can be used to obtain gas-surface interaction

parameters under high energy conditions.

In regard to future experimental investigations, it is desirable that investigators publish more detailed results on the reflected molecular distribution. At present, reflected mean molecular quantities are determined by means of a numerical integration, with appropriate weighting factors, of the time of flight signal, which is related to $P(\bar{v}', \bar{v})$. Much of the details of the gas-surface interaction are thus lost in this integration. Experimental results, e.g., [34, 35, 36], in the past have usually been presented as mean reflected quantities mainly because of the unavailability of theories which could be compared to the more detailed results. Therefore, in order to better confirm the present theory it would be desirable to compare direct with the experimental scattering kernel determined from the time of flight signal of the reflected molecules.

As more experimental data are obtained under more extreme conditions of gas and surface, it would be necessary to substantiate the applicability of Equations 38 and 47. It may be that under some conditions that other scattering kernels, developed in the present work, are necessary to completely describe the gas-surface interactions.

LISTS OF REFERENCES

1. Kundt, A. and Warburg, E. "Uber Reibung und Wärmeleitung Verdunnter Gase," Poggendarff's Annalen der Physik, 155:337, 1875.

2. Reynolds, Osborne. "On Certain Dimensional Properties of Matter in the Gaseous State," Royal Society of London, Philosophical Transactions, 170:727-845, 1879.

3. Maxwell, J. Clerk. "On Stresses in Rarefied Gases Arising from Irregularities of Temperature," Royal Society of London, Philosophical Transactions, 170: 231-256, 1879.

4. Maxwell, J. Clerk. The Scientific Papers of James Clerk Maxwell. Vol. 2. London and New York: Cambridge University Press. 1890.

5. Smolnchowski, M. S. "On the Conduction of Heat by Rarefied Gases," Philosophical Magazine, 46:192-206, 1898.

6. Knudsen, Martin. "Die Molekulare Wärmeleitung der Gase und der Akkommodationskoeffizient," Annalen Der Physik, 34:593-656, 1911.

7. Kuscer, I., J. Mozina, and F. Krizanic. "The Knudsen Model of Thermal Accommodation," Proceedings of the Seventh International Symposium on Rarefied Gas Dynamics, Dino Dini, editor, Vol. 1. New York and London: Academic Press, Inc., (to be published).

8. Soddy, F. and A. J. Berry. "Conduction of Heat Through Rarefied Gases," Proceedings of the Royal Society. A83:254-264, 1910.

9. Blodgett, K. B. and I. Langmuir. "The Accommodation Coefficient of Hydrogen: A Sensitive Detector of Surface Films," Physical Review. 40:78-104, 1932.

10. Baule, B. "Theoretische Behandlung Der Erscheinungen In Verdunnters Gases," Annalen Der Physik, 44:145-176, 1914.

11. Estermann, I. and O. Stern. "Bengung Von Molekularstrahlen," Zeitschrift Für Physik, 61:95-125, 1930.

12. Estermann, I., R. Frisch and O. Stern. "Monochromasierung der de Broghi Wellen von Molecularstrahlen," Zeitschrift Für Physik, 73(5-6):348-365, 1931.

13. Kantrowitz, Arthur and Jerry Grey. "A High Intensity Source for the Molecular Beam," Review of Scientific Instruments, 22:328-332, May 1951.

14. Oman, R. A., A. Bogan, C. H. Weiser and C. H. Li. "Interaction of Gas Molecules with an Ideal Crystal Surface," AIAA Journal, 2:1722-1730, October 1964.

15. Logan, R. M. and R. E. Stickney. "Simple Classical Model for the Scattering of Gas Atoms from a Solid Surface," The Journal of Chemical Physics, 44:195-201, January 1966.

16. Logan, R. M. and J. C. Keck. "Classical Theory for the Interaction of Gas Atoms with Solid Surfaces," Fluid Mechanics Laboratory Publication No. 67-8, Department of Mechanical Engineering, Massachusetts Institute of Technology, October 1967.

17. Goodman, Frank O. "Review of the Theory of the Scattering of Gas Atoms by Solid Surfaces," Surface Science, 26:327-362, 1971.

18. Busby, Michael R. "Interactions of a Monoenergetic Argon Molecular Beam with a Solid Argon Surface." Ph.D. dissertation, The University of Tennessee, Knoxville, 1970.

19. Nocilla, Silvio. "Stream-Body Interaction in Free-Molecule Flow," Rarefied Gas Dynamics, L. Talbot, editor. New York and London: Academic Press, Inc., 1961, Pp. 169-208.

20. Nocilla, Silvio. "The Surface Re-Emission Law in Free Molecule Flow." Rarefied Gas Dynamics, J. A. Laurmann, editor. New York and London: Academic Press, Inc., 1963, Pp. 327-346.

21. Hurlbut, F. C. and F. S. Sherman. "Application of the Nocilla Wall Reflection Model to Free-Molecule Kinetic Theory," The Physics of Fluids, 11:486-496, March 1968.

22. Epstein, Melvin. "A Model of the Wall Boundary Condition in Kinetic Theory," AIAA Journal, 5:1797-1800, October 1967.

23. Shidlovskiy, V. P. Introduction to the Dynamics of of Rarefied Gases. Translation from the Russian edited by J. A. Laurmann. New York: American Elsevier Publishing Company, Inc., 1967.

24. Cercignani, Carlo. Mathematical Methods in Kinetic Theory. New York: Plenum Press, 1969.

25. Kuscer, I. and G. C. Summerfield, "Symmetrics in Scattering of Slow Neutrons." Physical Review, 188:1445-1449, December 1969.

26. Kuscer, Ivan. "Reciprocity in Scattering of Gas Molecules by Surfaces," Surface Science, 25:225-237, 1971.

27. Berman, Abraham S. and Wendel J. Maegley. "Internal Rarefied Gas Flows with Backscattering," The Physics of Fluids, 15.772-779, May 1972.

28. Gaede, W. "Die aupere Reibung der Gase," Annalen der Physik, 41:289-336, 1913.

29. Bishara, Michael N. "An Experimental Investigation of Intensity and Velocity Distributions of Thermal-Energy Argon Atoms Scattered by a Monocrystalline Silver Surface." Ph.D. dissertation, The University of Virginia, Charlottesville, 1969.

30. Abramowitz, M., and I. A. Stegun (editors). Handbook of Mathematical Functions. National Bureau of Standards, United States Department of Commerce. Washington: Government Printing Office, 1967.

31. Korn, Granino A., and Theresa M. Korn. Mathematical Handbook for Scientists and Engineers. New York: McGraw-Hill Book Company, Inc., 1968.

32. Trilling, Leon. "The Scattering of Inert Gases on Solid Surfaces," Proceedings of the Seventh International Symposium on Rarefied Gas Dynamics, Dino Dini, editor, Vol. 1. New York and London: Academic Press, Inc., (to be published).

33. Stickney, Robert E. "Atomic and Molecular Scattering from Solid Surfaces," Advances in Atomic and Molecular Physics, D. R. Bates and I. Estermann, editors, Vol. 3. New York: Academic Press, Inc., 1967. Pp. 143-204.

34. Moran, James P. "Experiments on Scattering of Mono-Energetic Argon Beams of Heated Platinum." Ph.D. dissertation, Massachusetts Institute of Technology, Cambridge, 1968.

35. Romney, Michael John. "Molecular Beam Scattering of Argon from the (111) Plane of Silver at Hyperthermal Energies." Ph.D. dissertation, Princeton University, Princeton, N. J., 1969.

36. Bishara, N. M., and S. S. Fisher. "Observed Intensity and Speed Distribution of Thermal-Energy Argon Atoms Scattered from the (111) Face of Silver," The Journal of Chemical Physics, 52:5661-5675, 1970.

37. Saltsburg, Howard, and Joe N. Smith, Jr. "Molecular-Beam Scattering from the (111) Plane of Silver," The Journal of Chemical Physics, 45:2175-2183, September 1966.

38. Dawbarn, R., M. R. Busby, and M. Kinslow. "Studies of High-Energy Gases Impinging on Various Cryosurfaces," Arnold Engineering Development Center TR-72-33, Arnold Air Force Station, Tennessee, April 1972.

39. Gradshteyn, I. S. and I. M. Ryzhik. Table of Integrals, Series, and Products. Fourth edition. Translation from the Russian edited by Alan Jeffrey. New York: Academic Press, Inc., 1965.

APPENDIXES

A. ILLUSTRATIONS

B. EVALUATION OF CERTAIN INTEGRALS OF EXPONENTIALS AND BESSEL FUNCTIONS

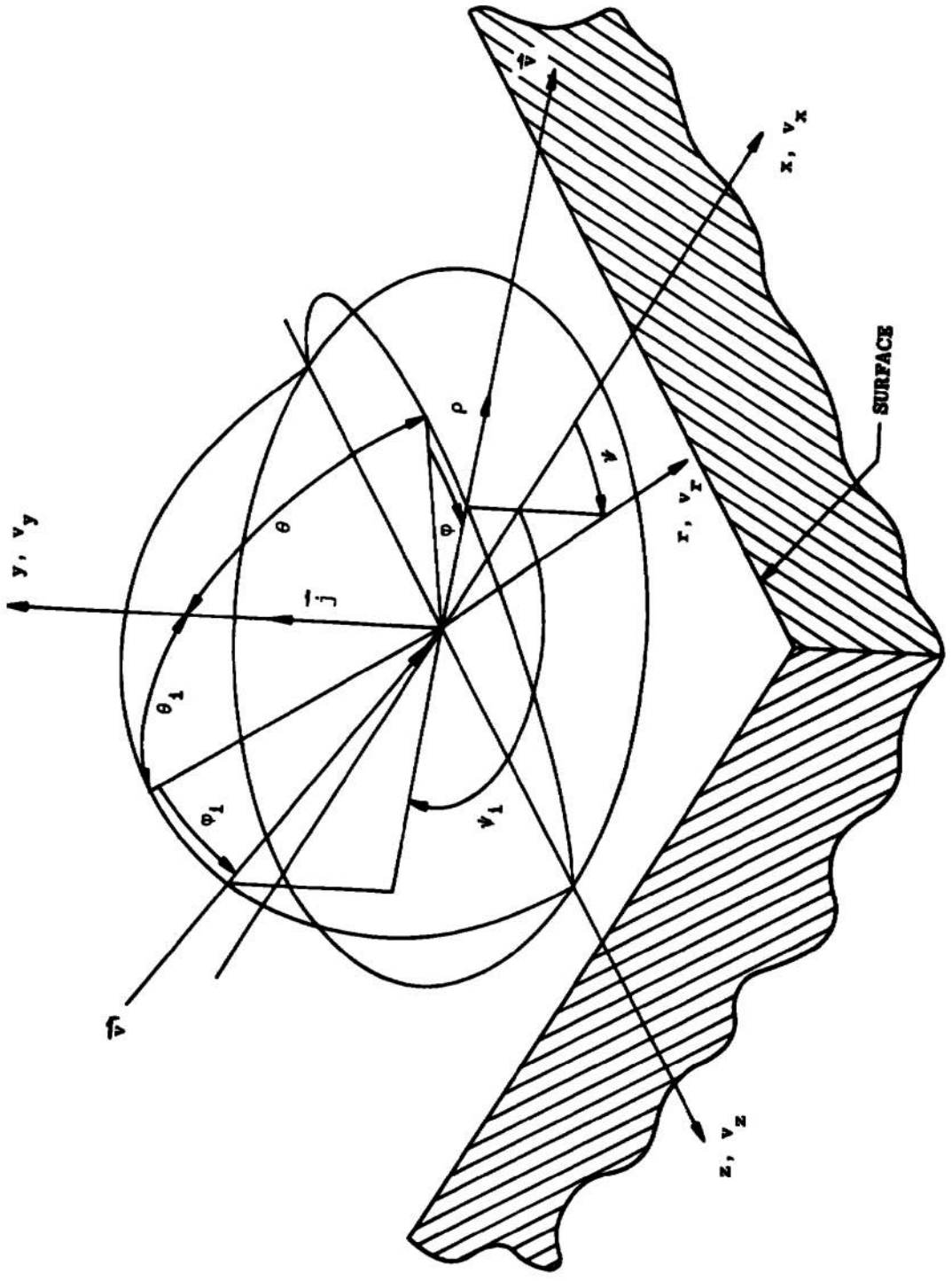

Figure 1. Coordinate Systems.

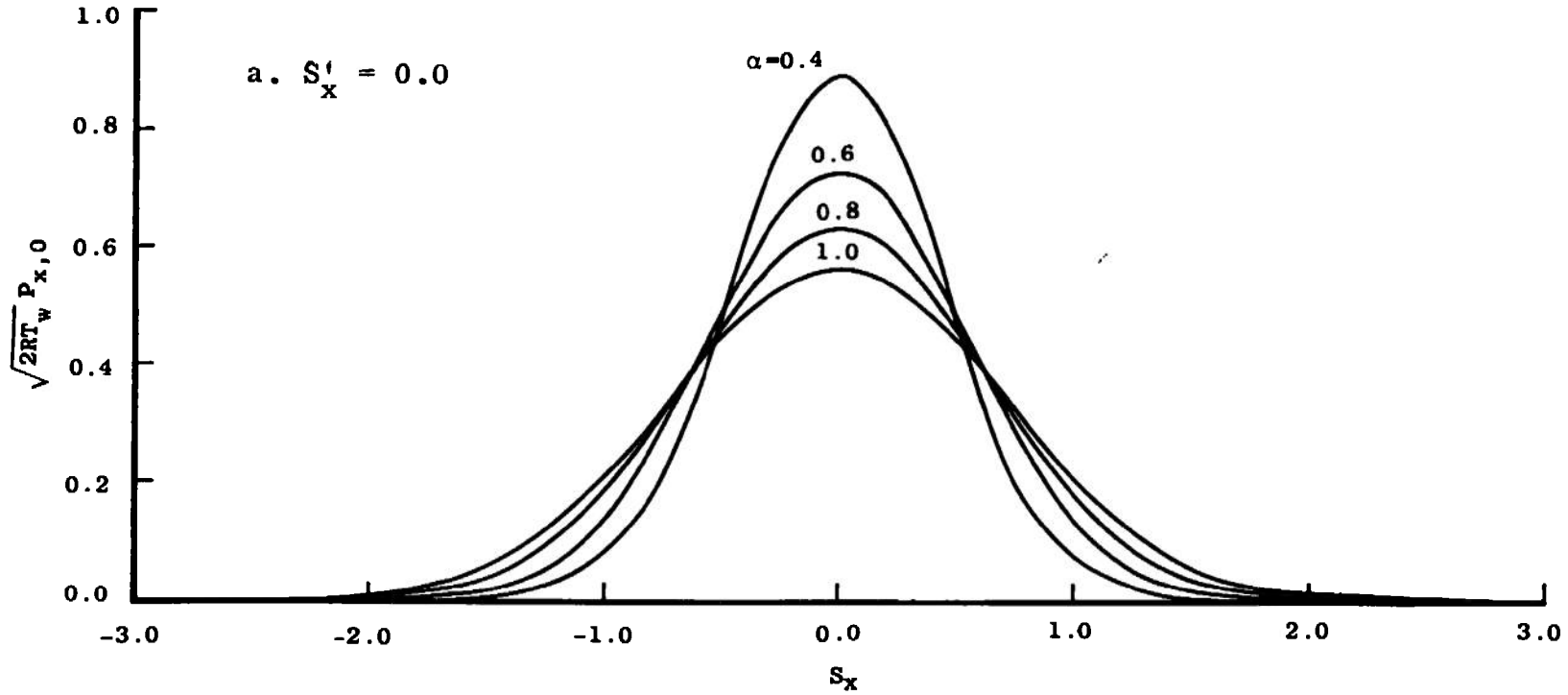

Figure 2. Plot of $\sqrt{2RT_w}\ P_{x,0}$.

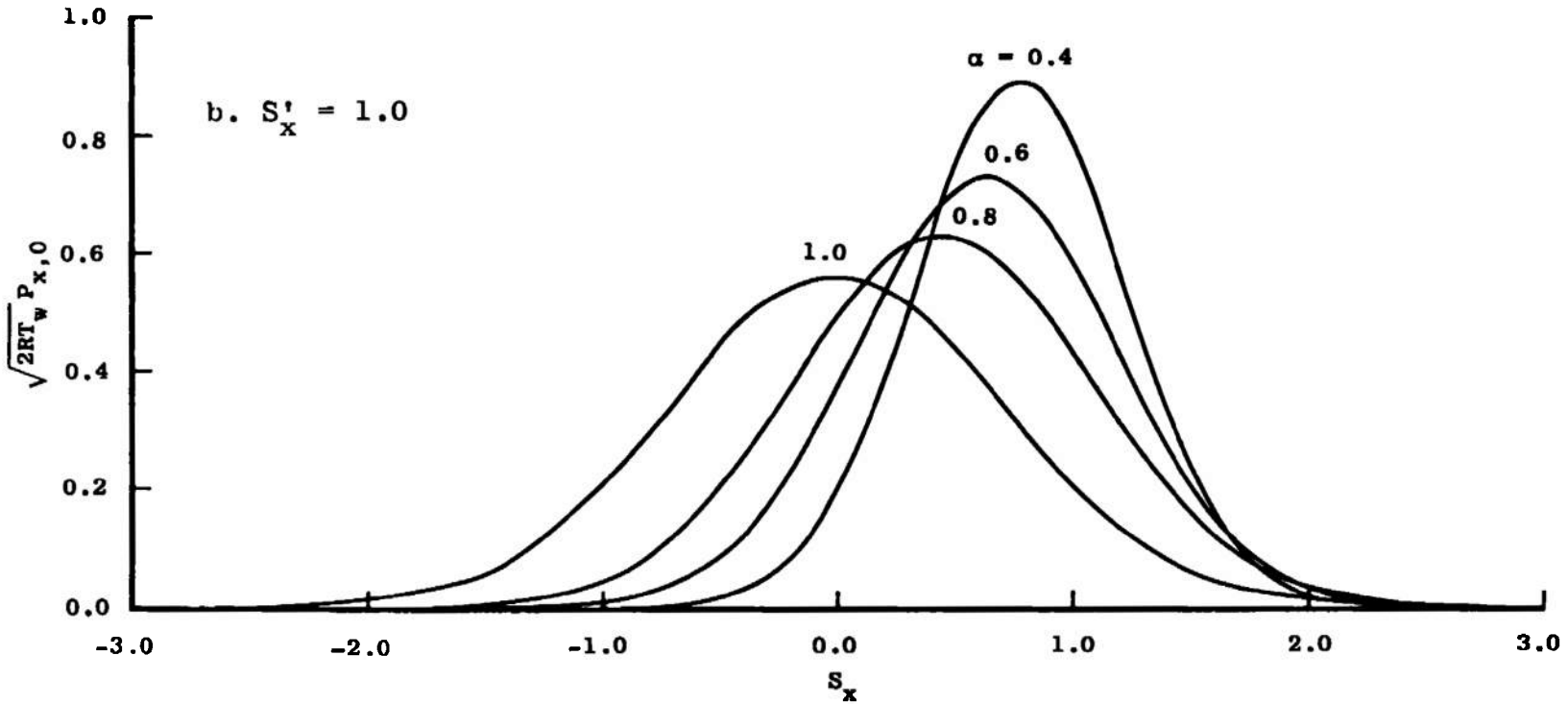

Figure 2. (Continued).

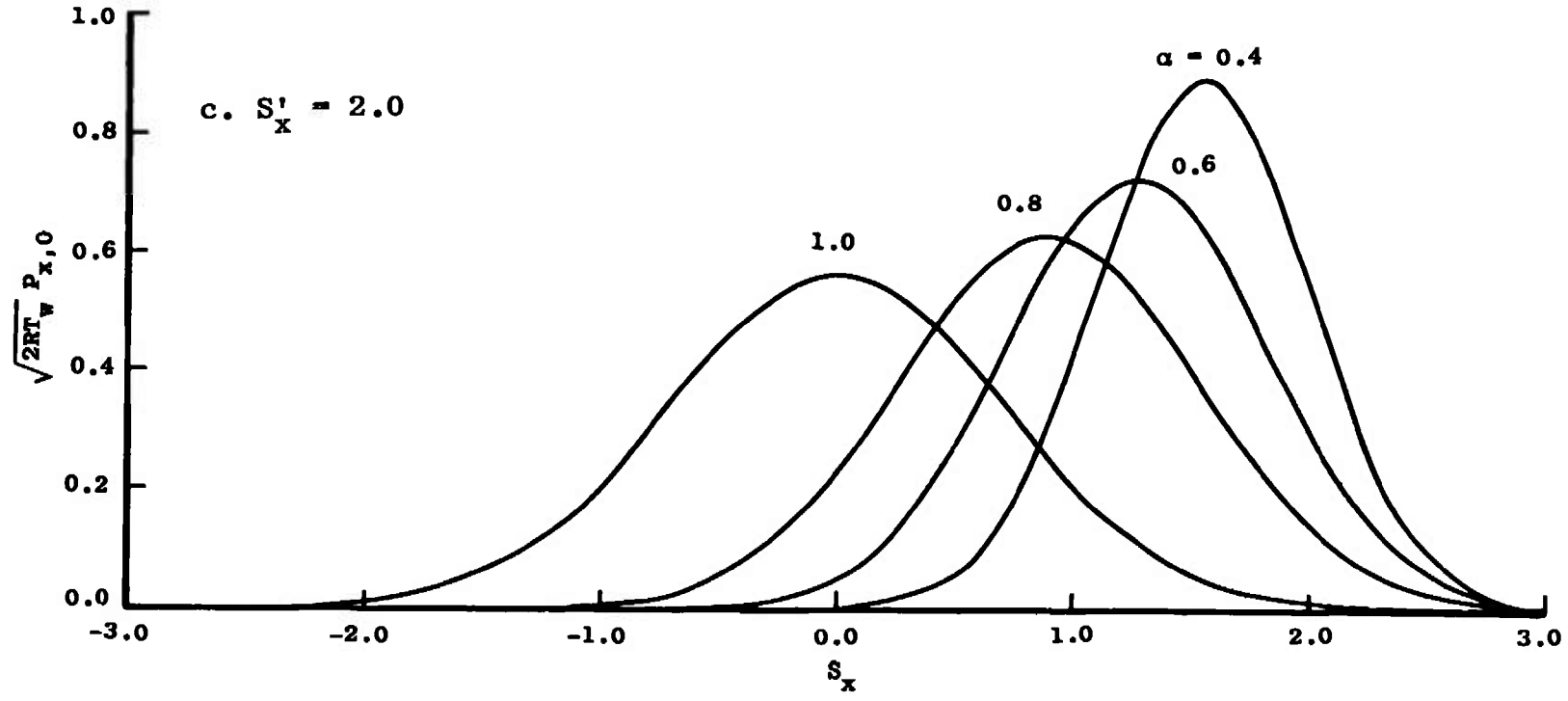

Figure 2. (Continued).

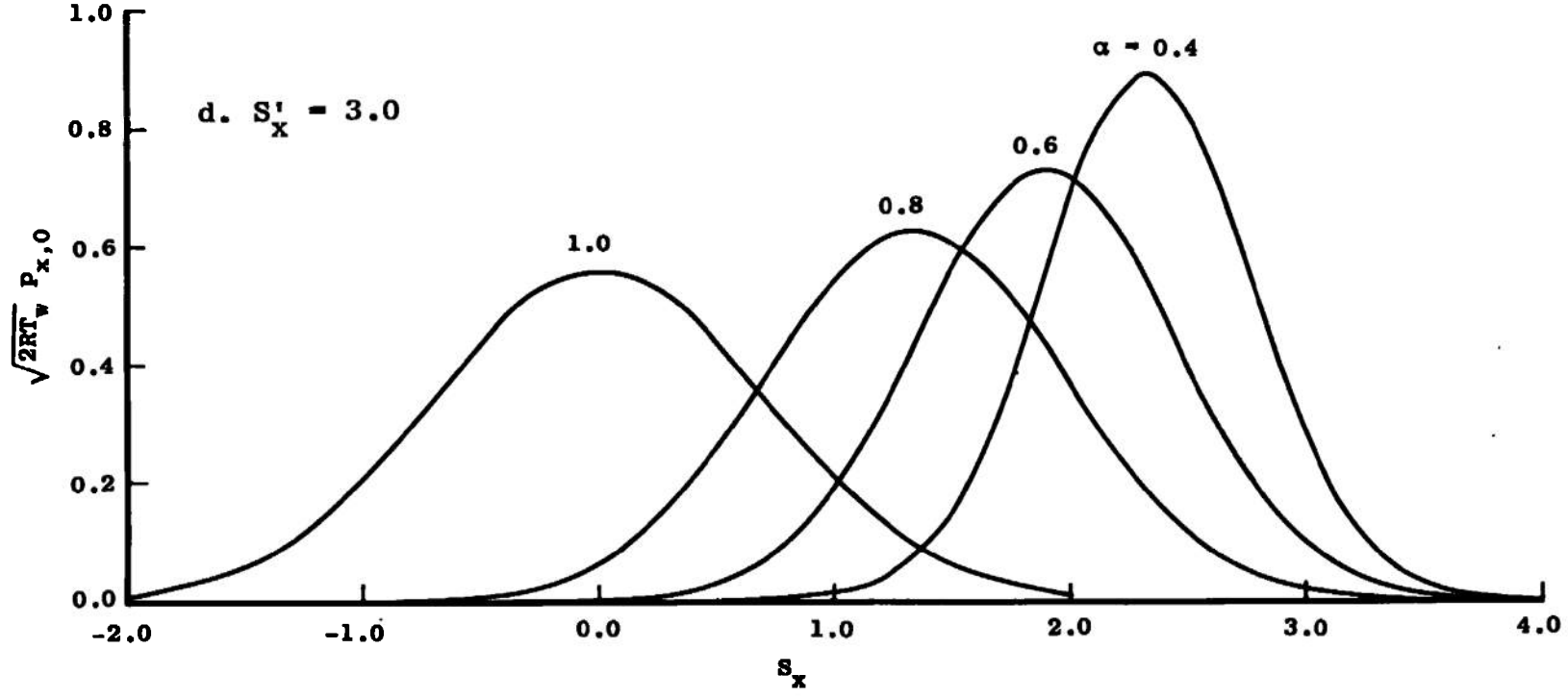

Figure 2. (Continued).

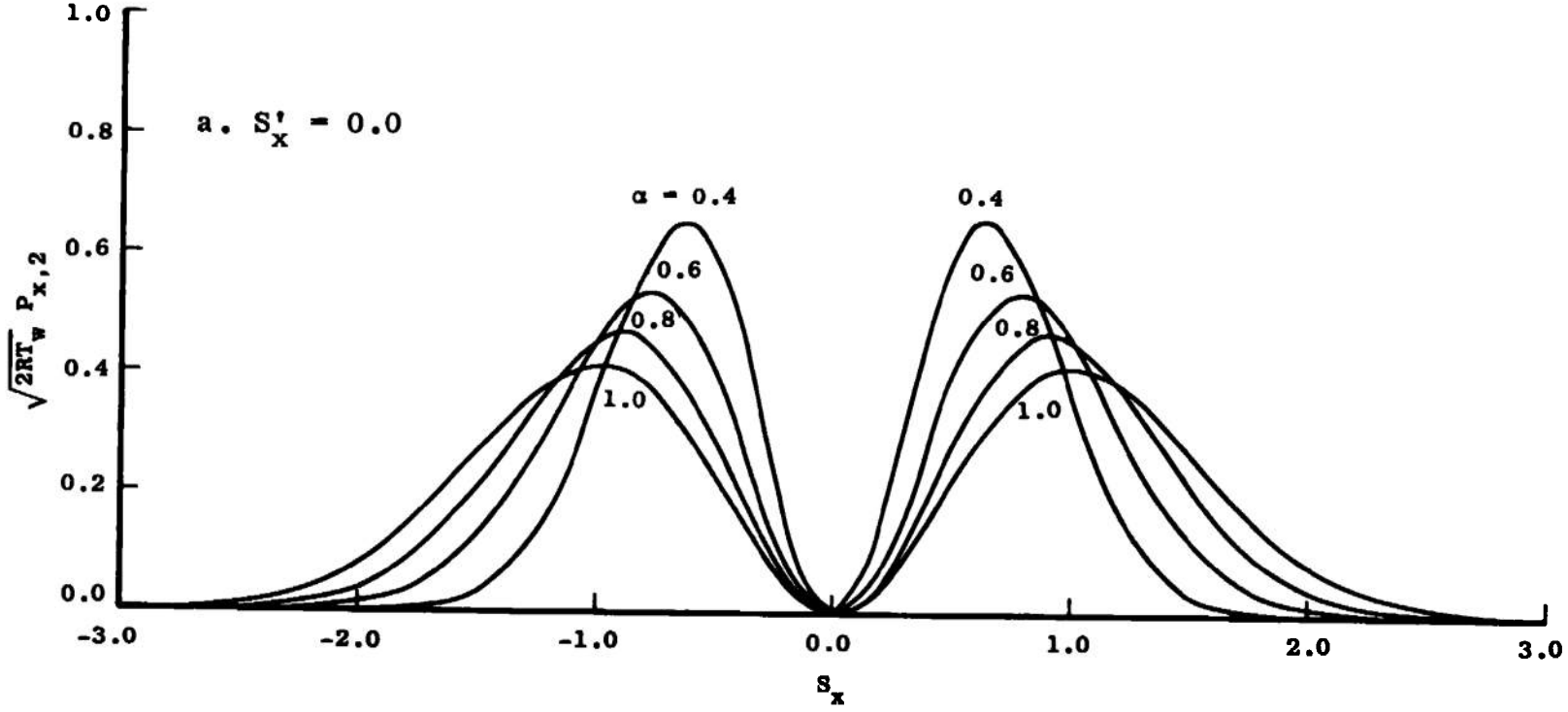

Figure 3. Plot of $\sqrt{2RT_w}\ P_{x,2}$.

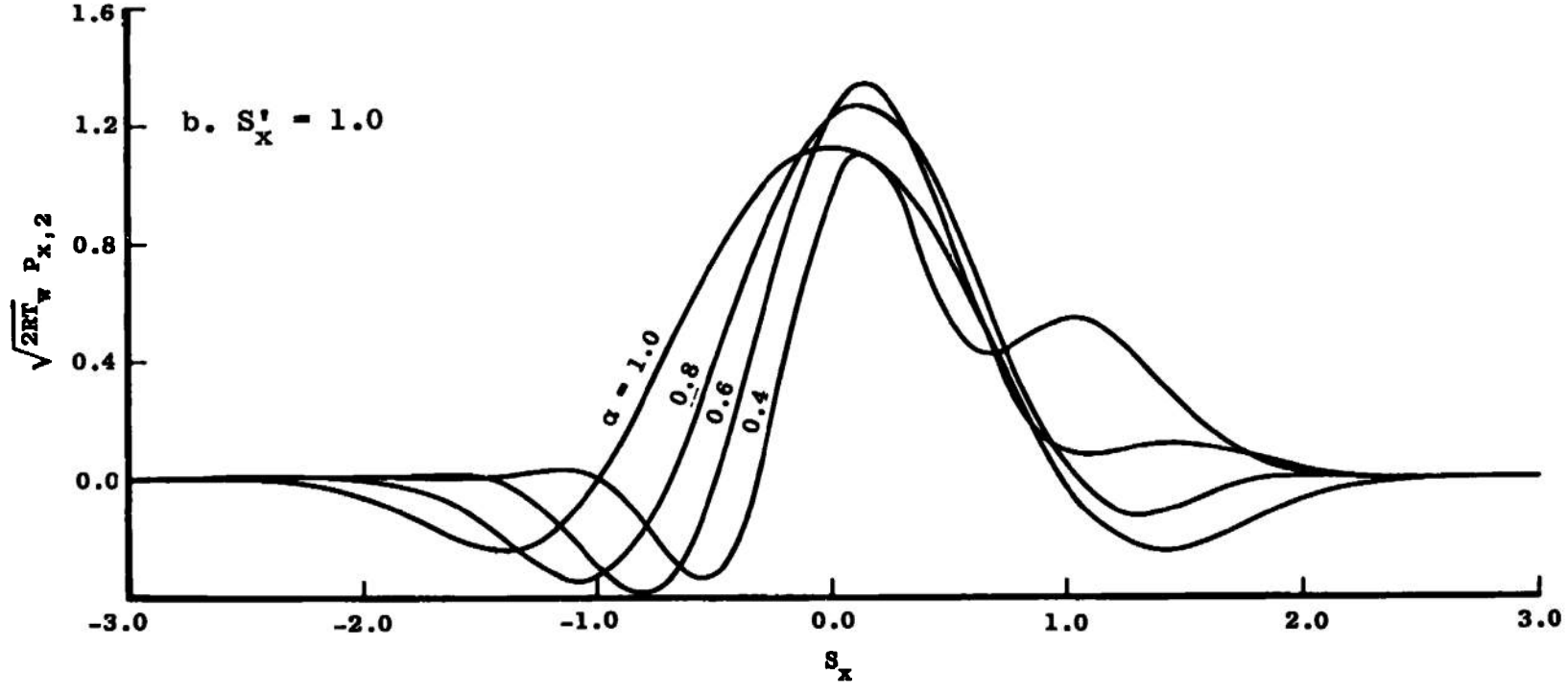

Figure 3. (Continued).

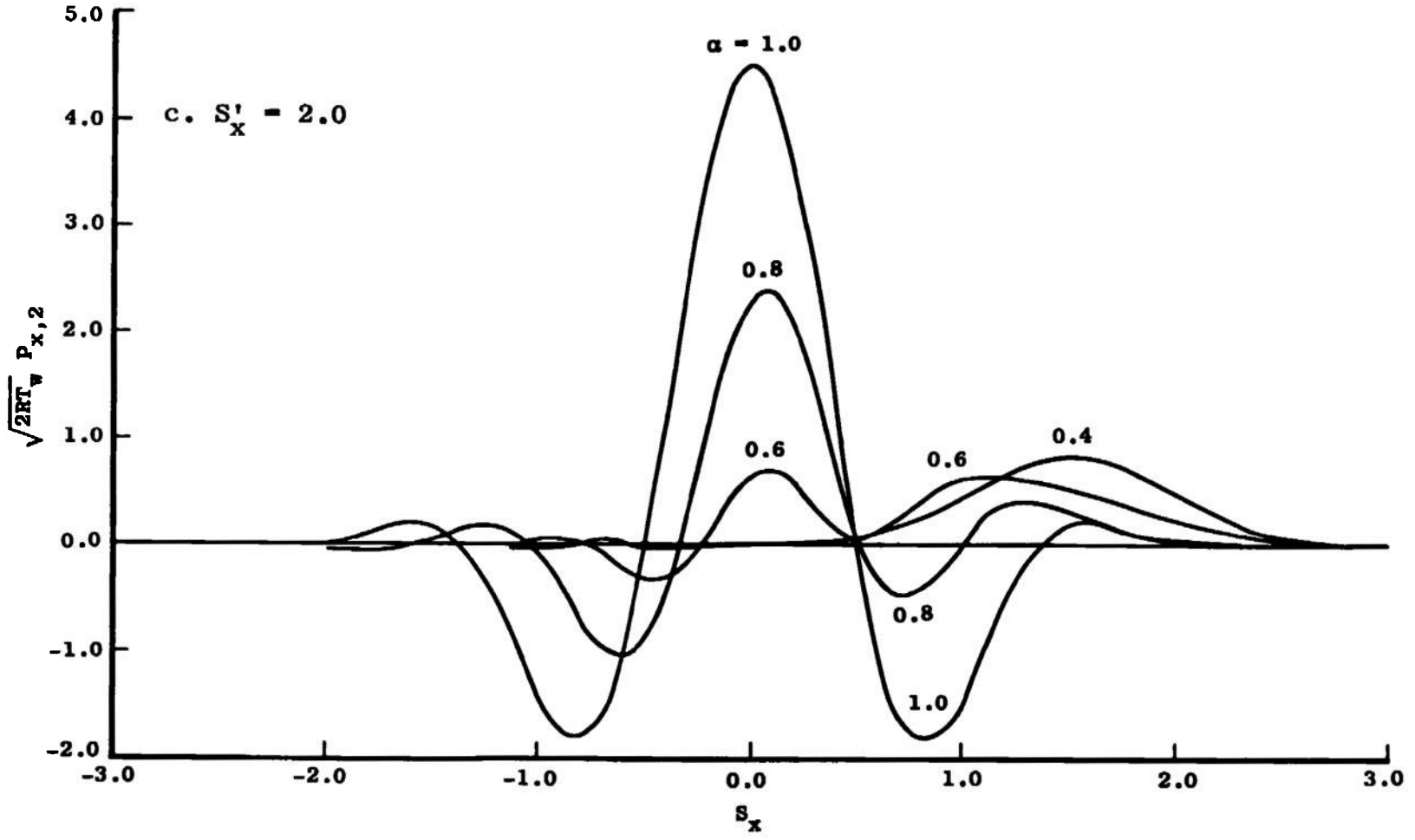

Figure 3. (Continued).

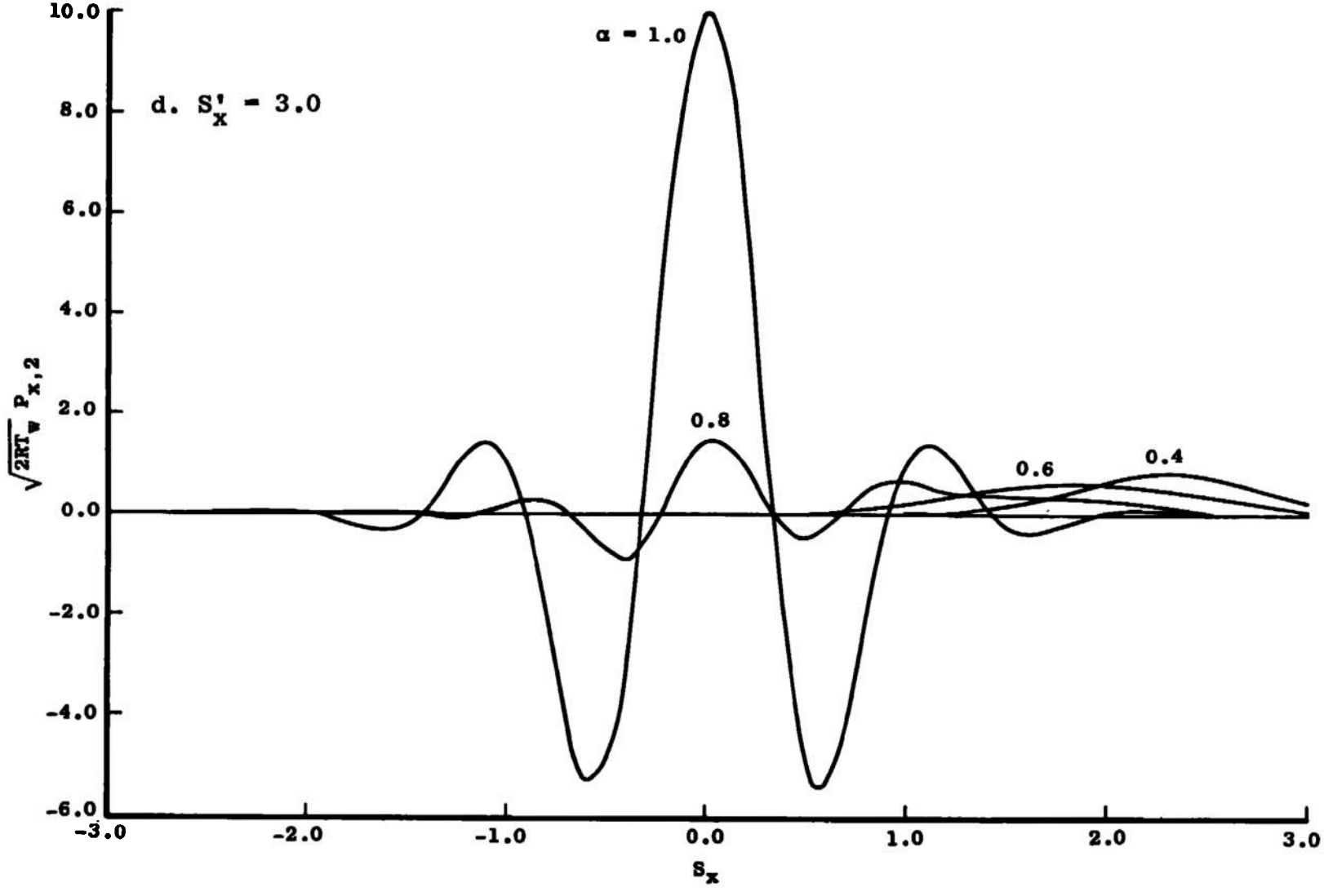

Figure 3. (Continued).

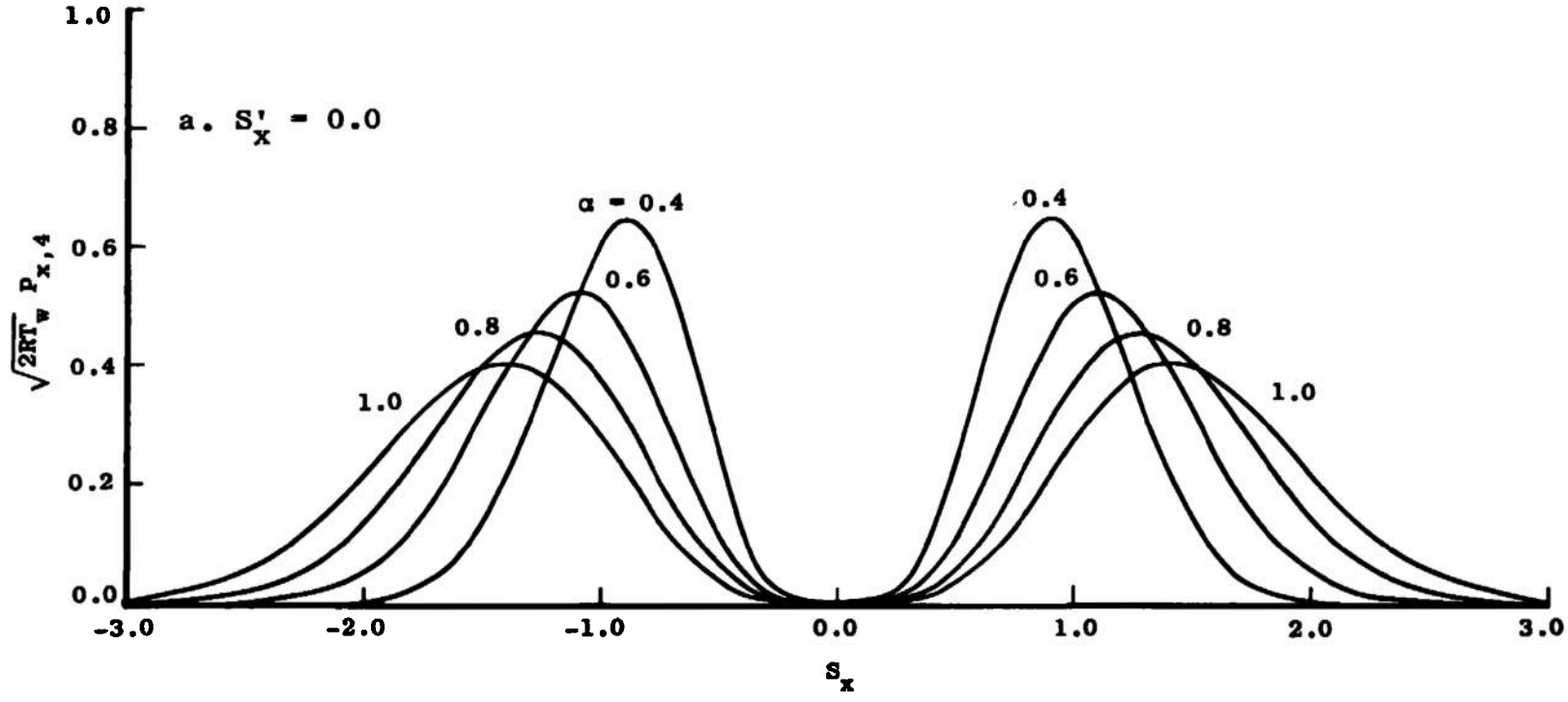

Figure 4. Plot of $\sqrt{2RT_w}\ P_{x,4}$.

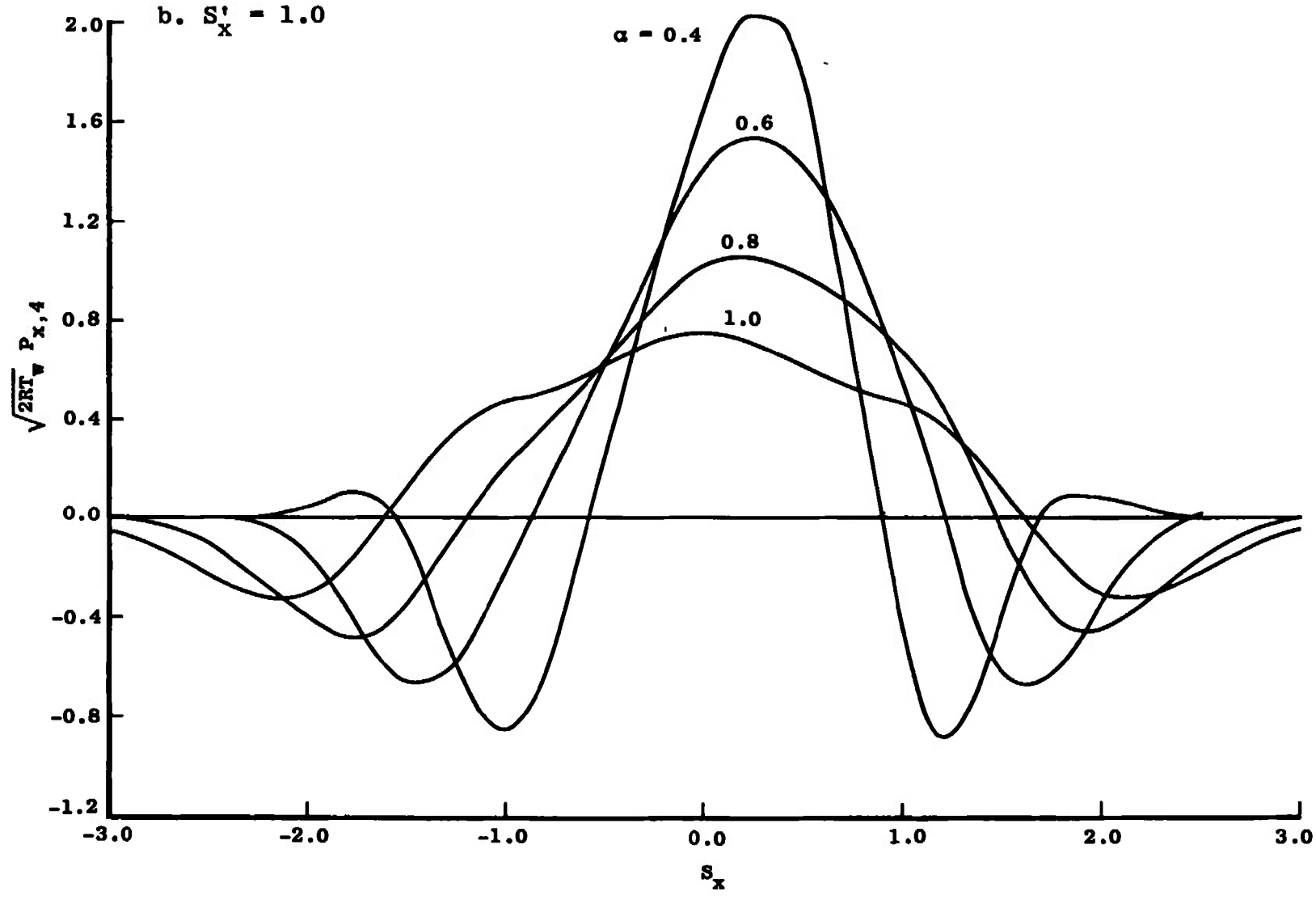

Figure 4. (Continued).

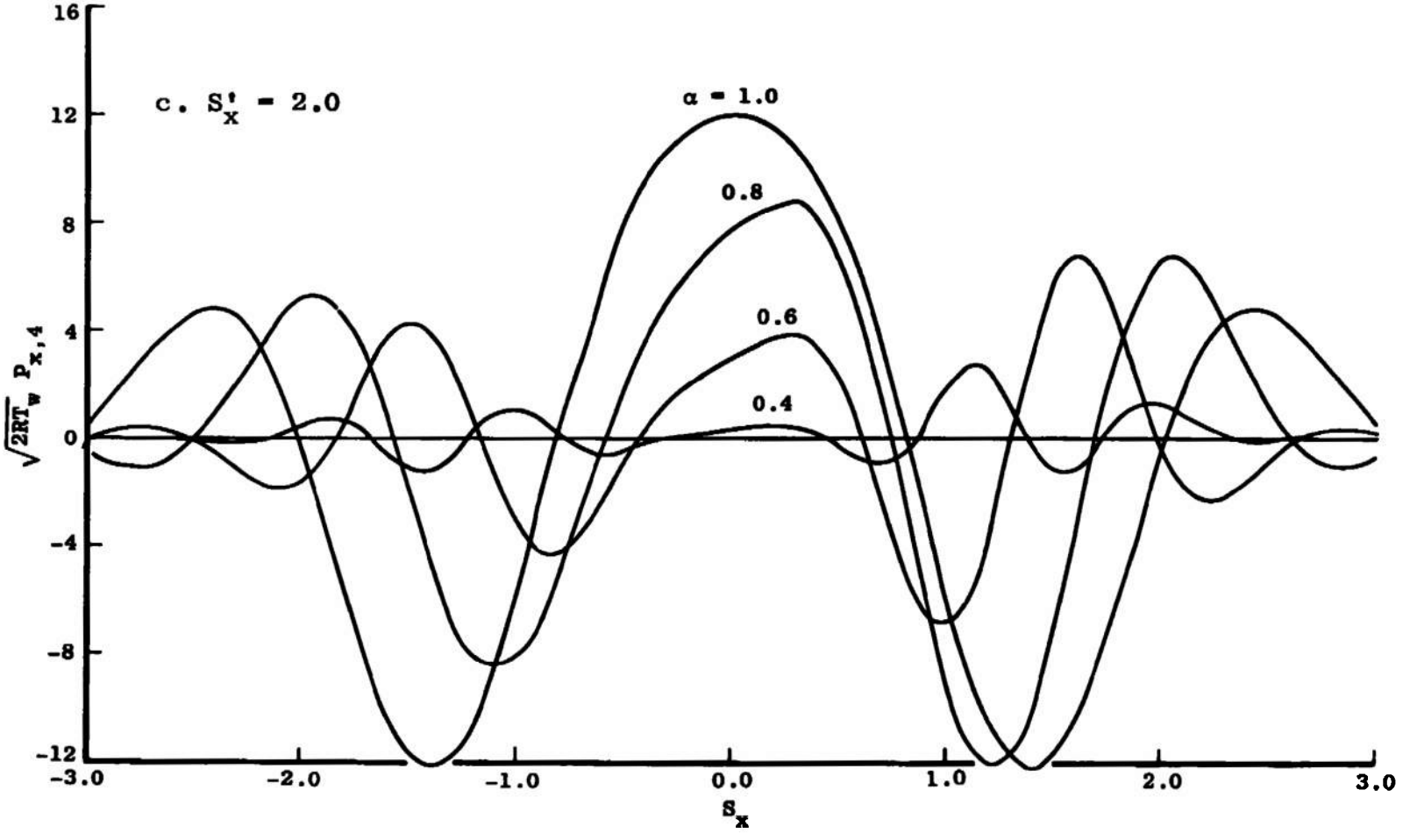

Figure 4. (Continued).

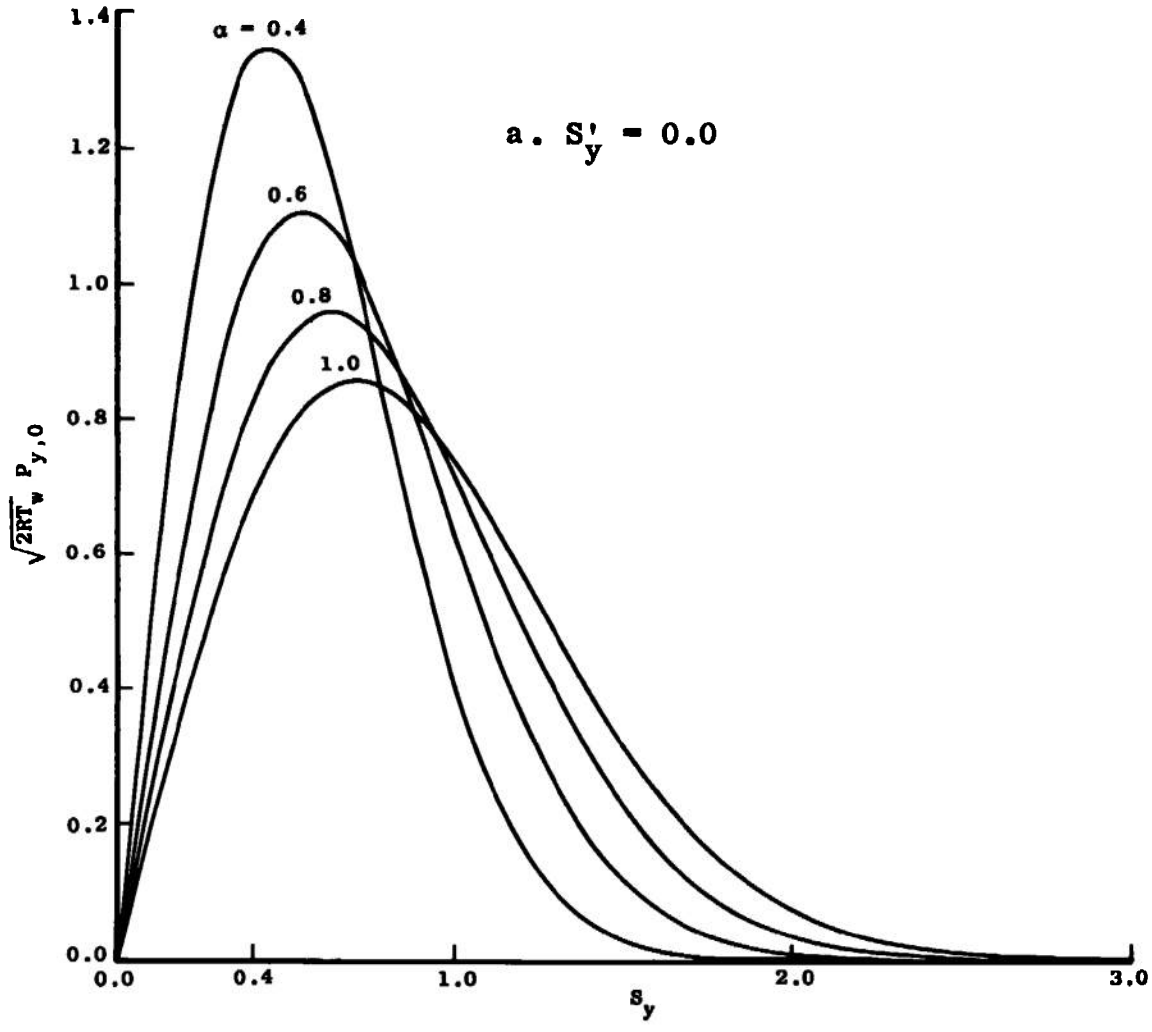

Figure 5. Plot of $\sqrt{2RT_w}\ P_{y,0}$.

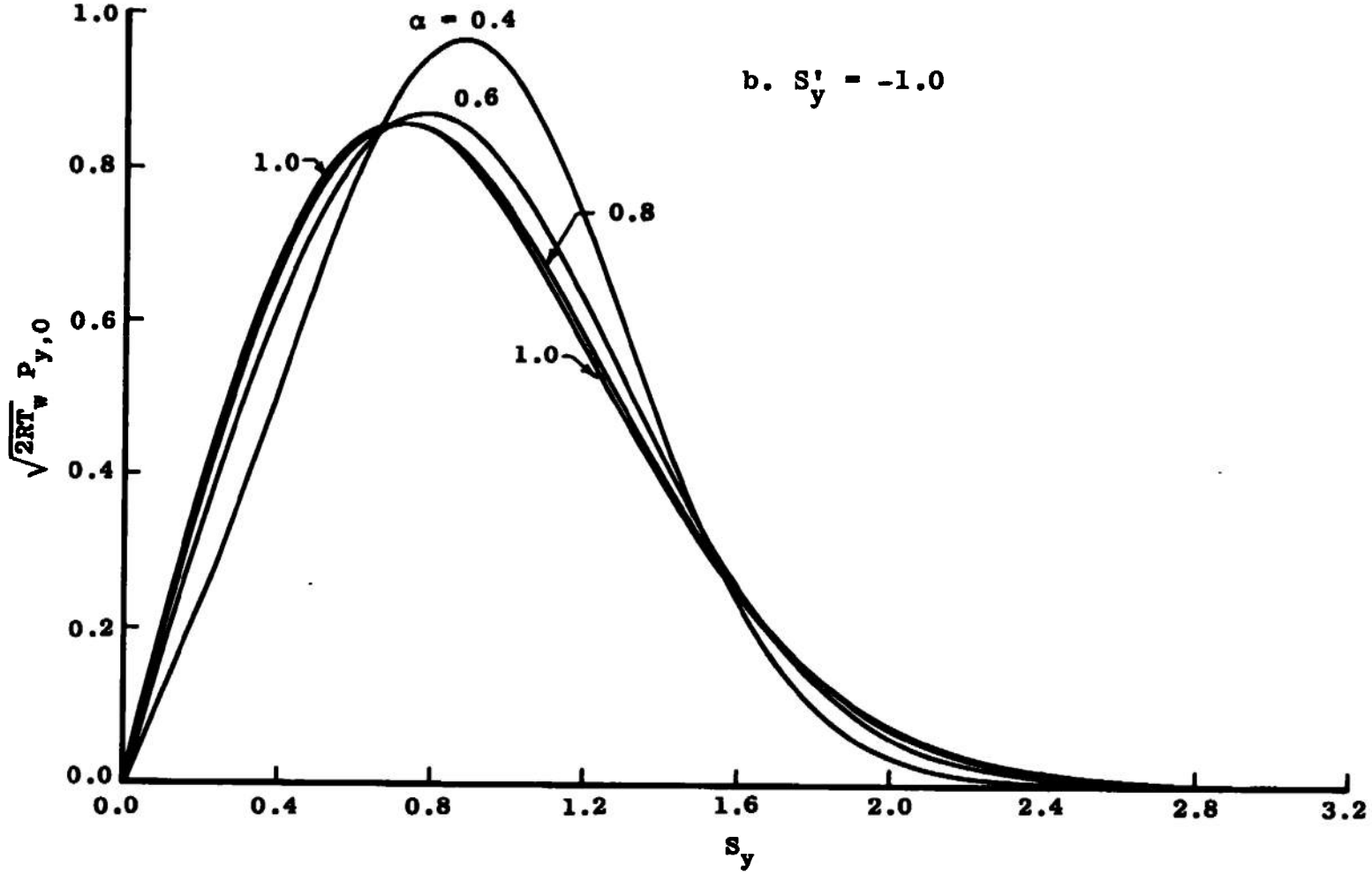

Figure 5. (Continued).

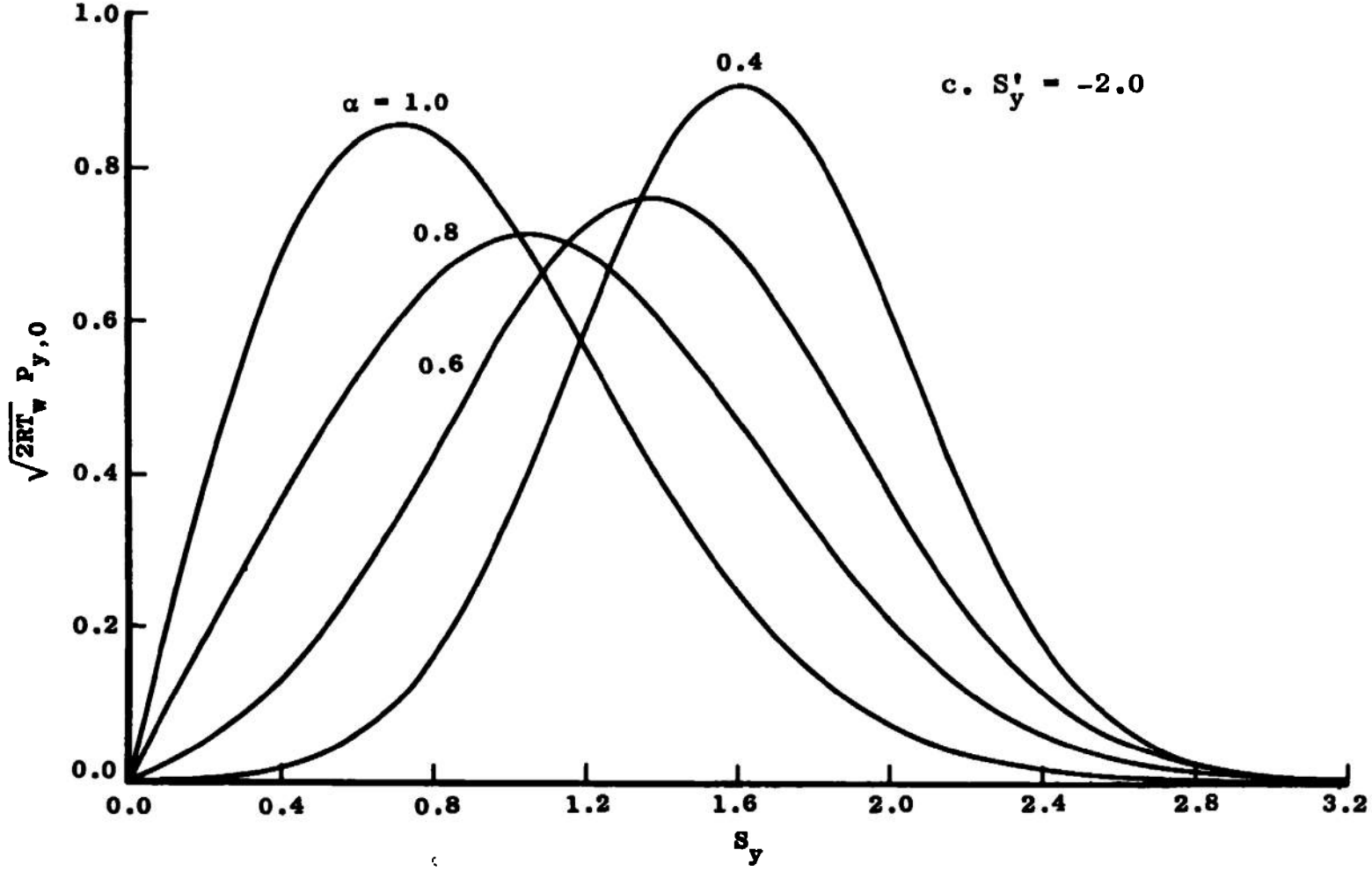

Figure 5. (Continued).

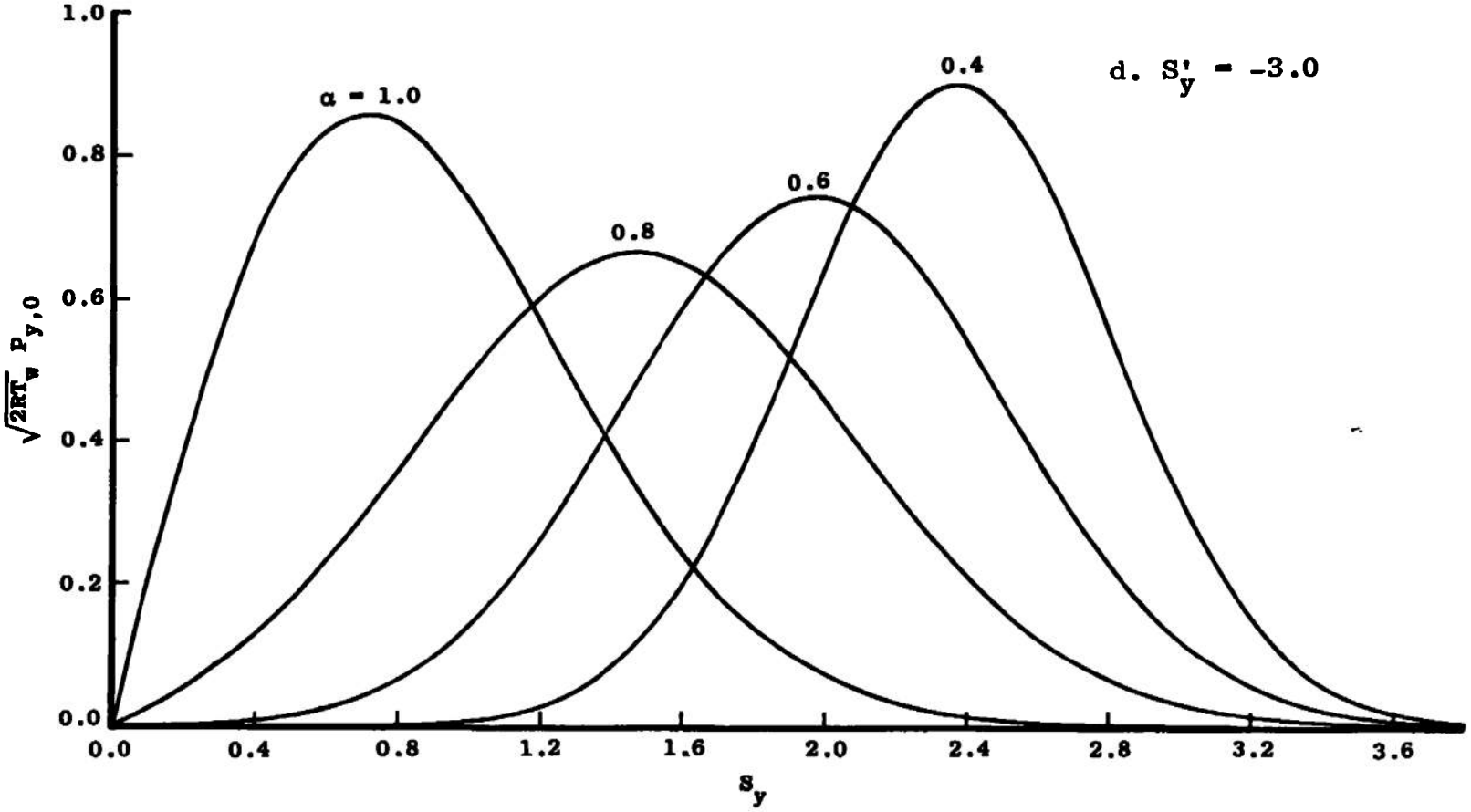

Figure 5. (Continued).

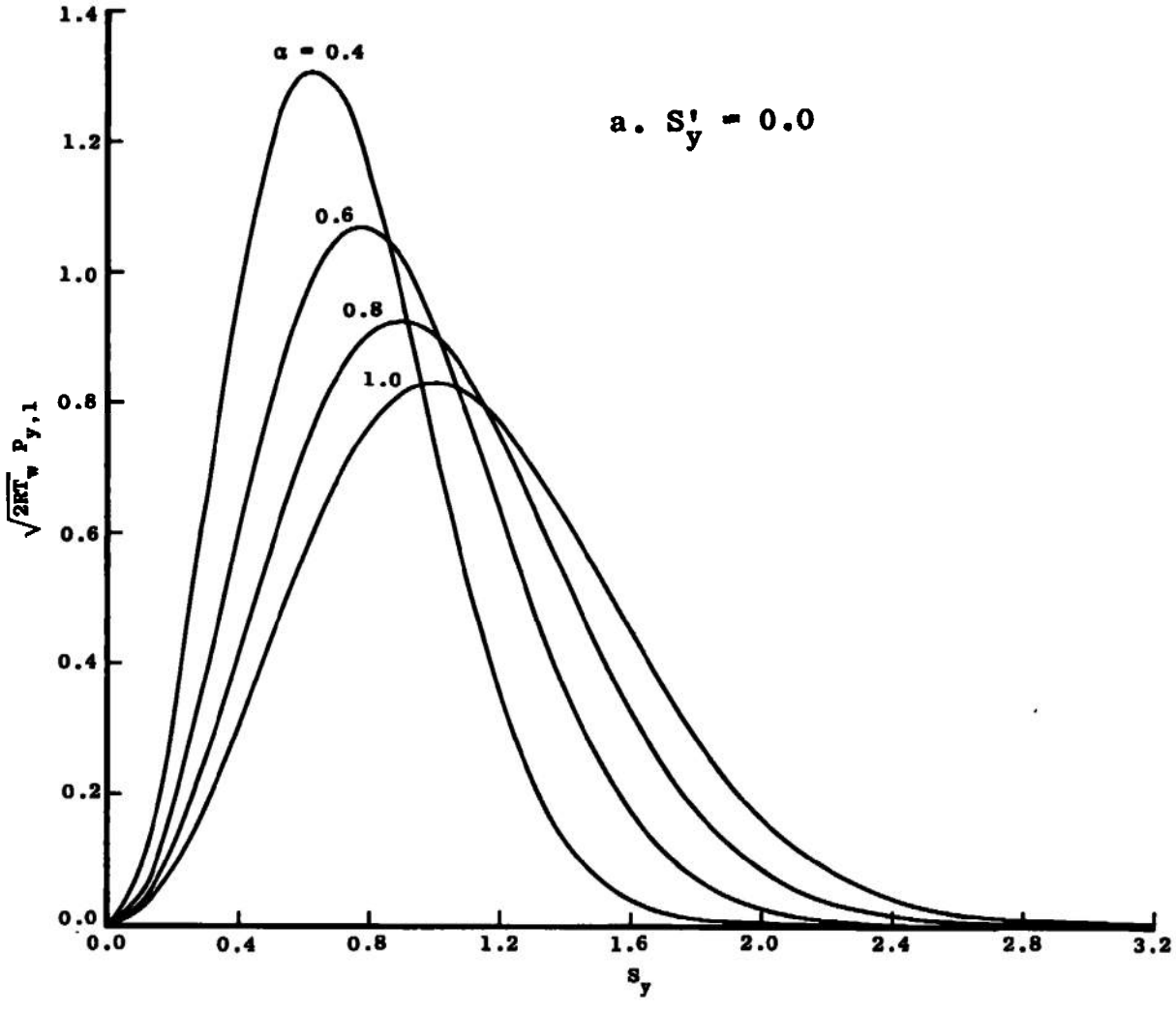

Figure 6. Plot of $\sqrt{2RT_w}\ P_{y,1}$.

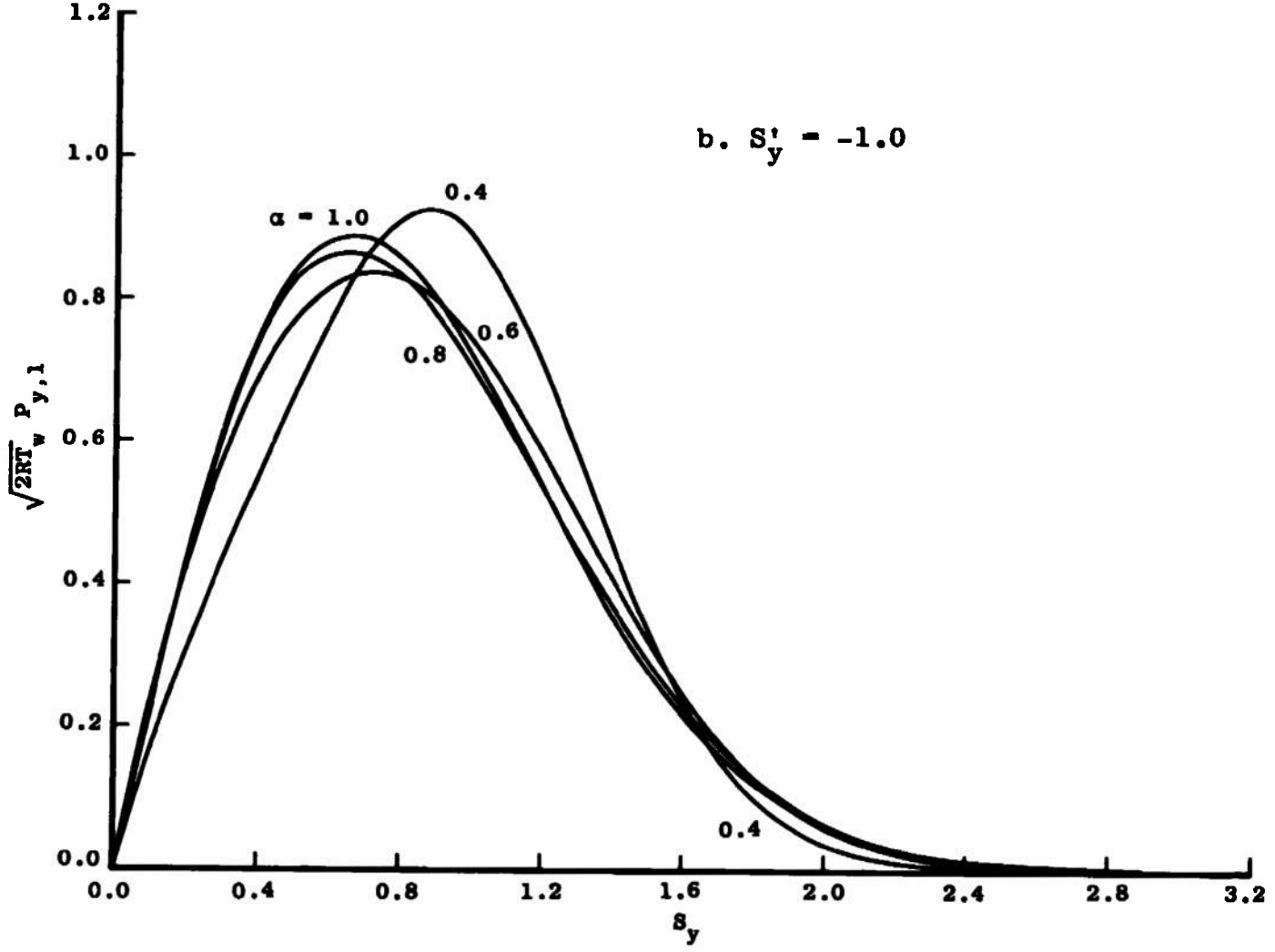

Figure 6. (Continued).

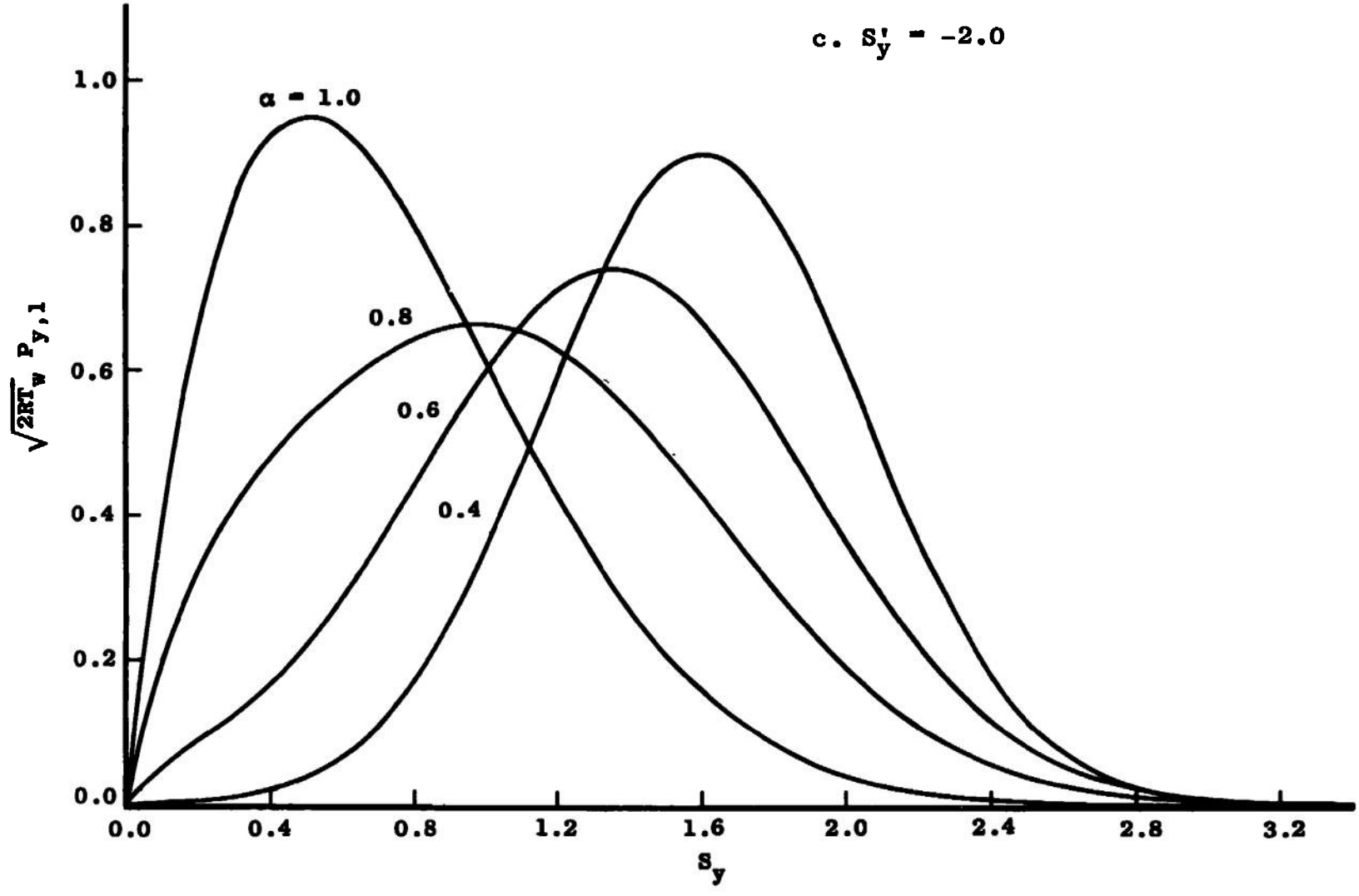

Figure 6. (Continued).

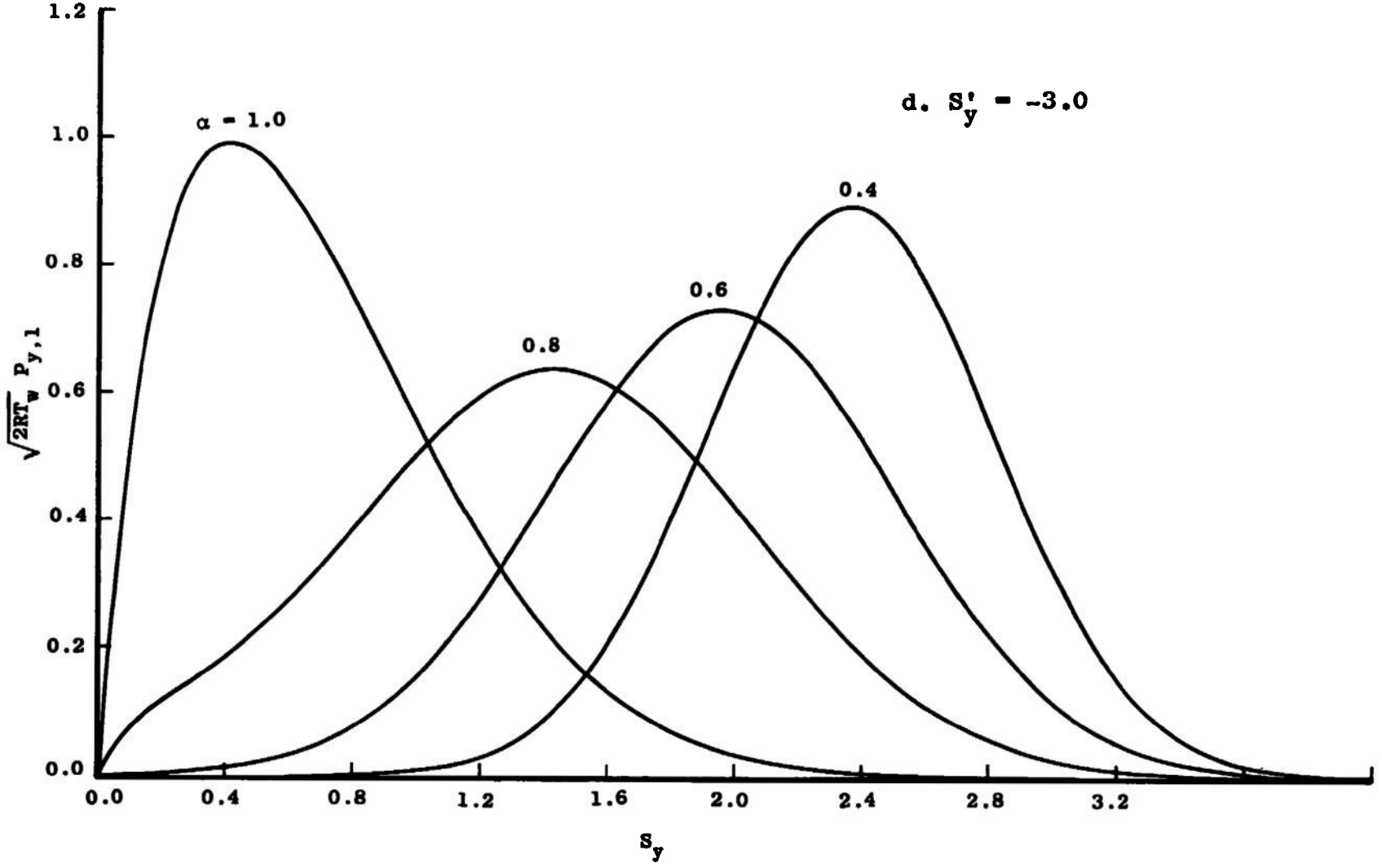

Figure 6. (Continued).

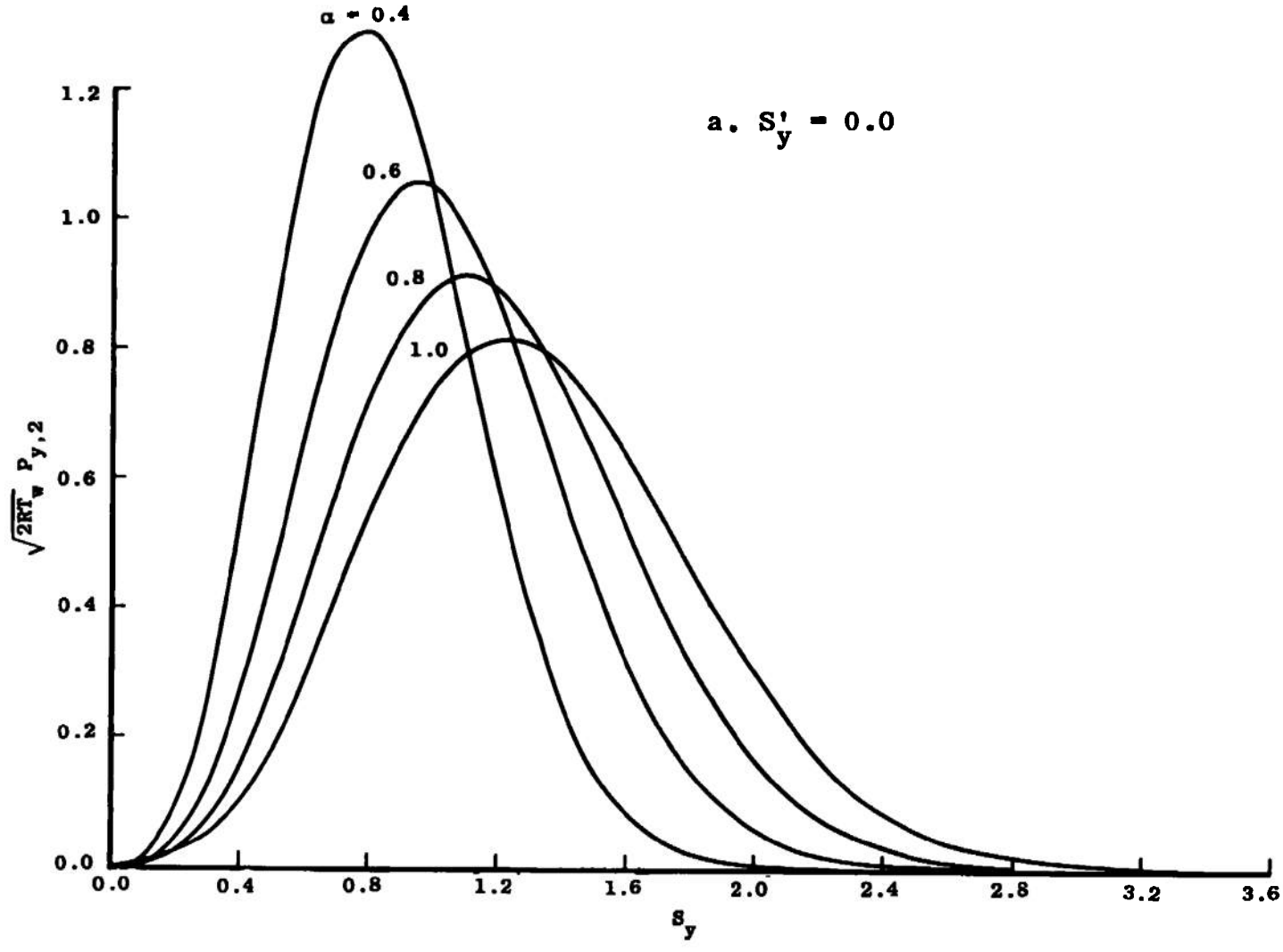

Figure 7. Plot of $\sqrt{2RT_w}\ P_{y,2}$.

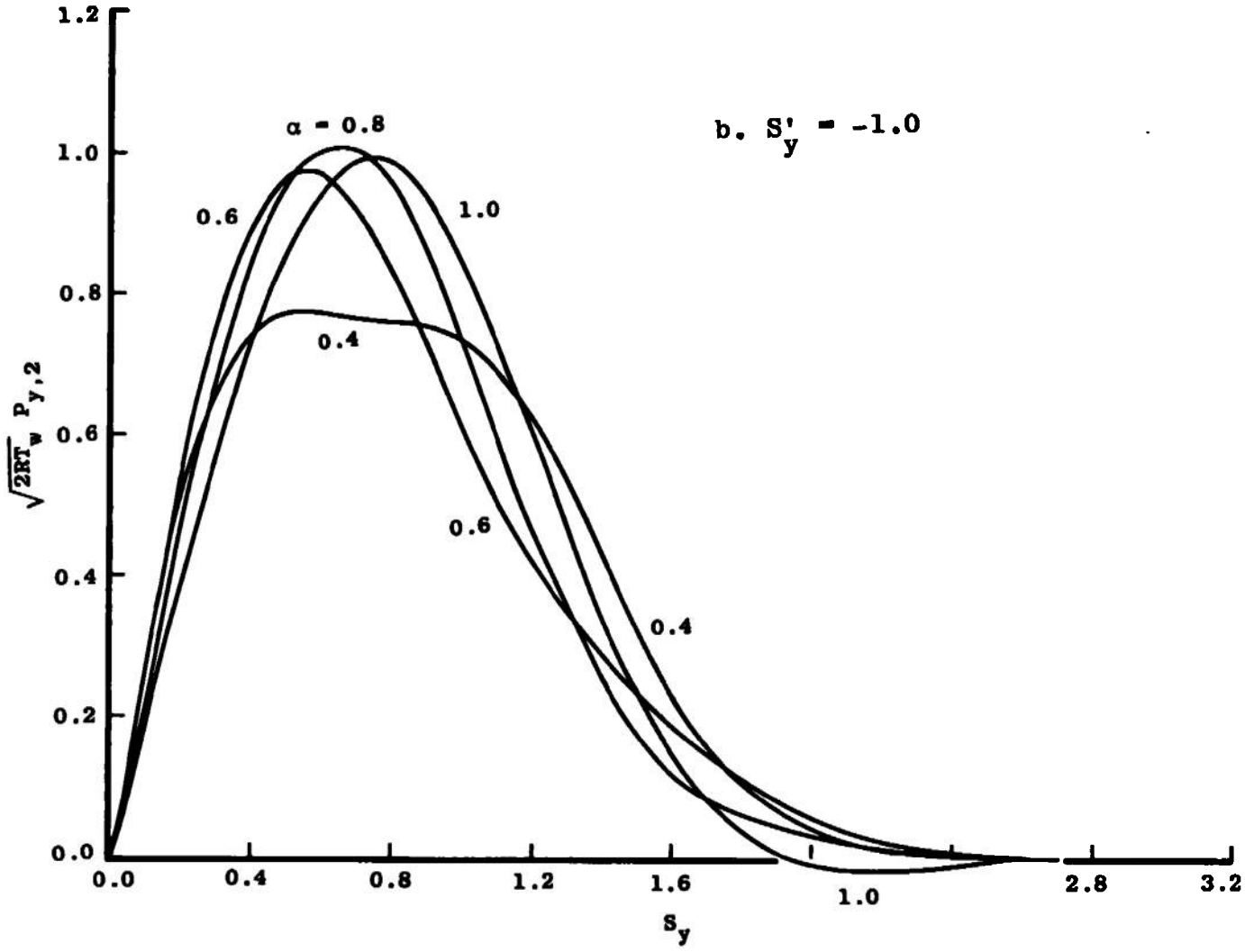

Figure 7. (Continued).

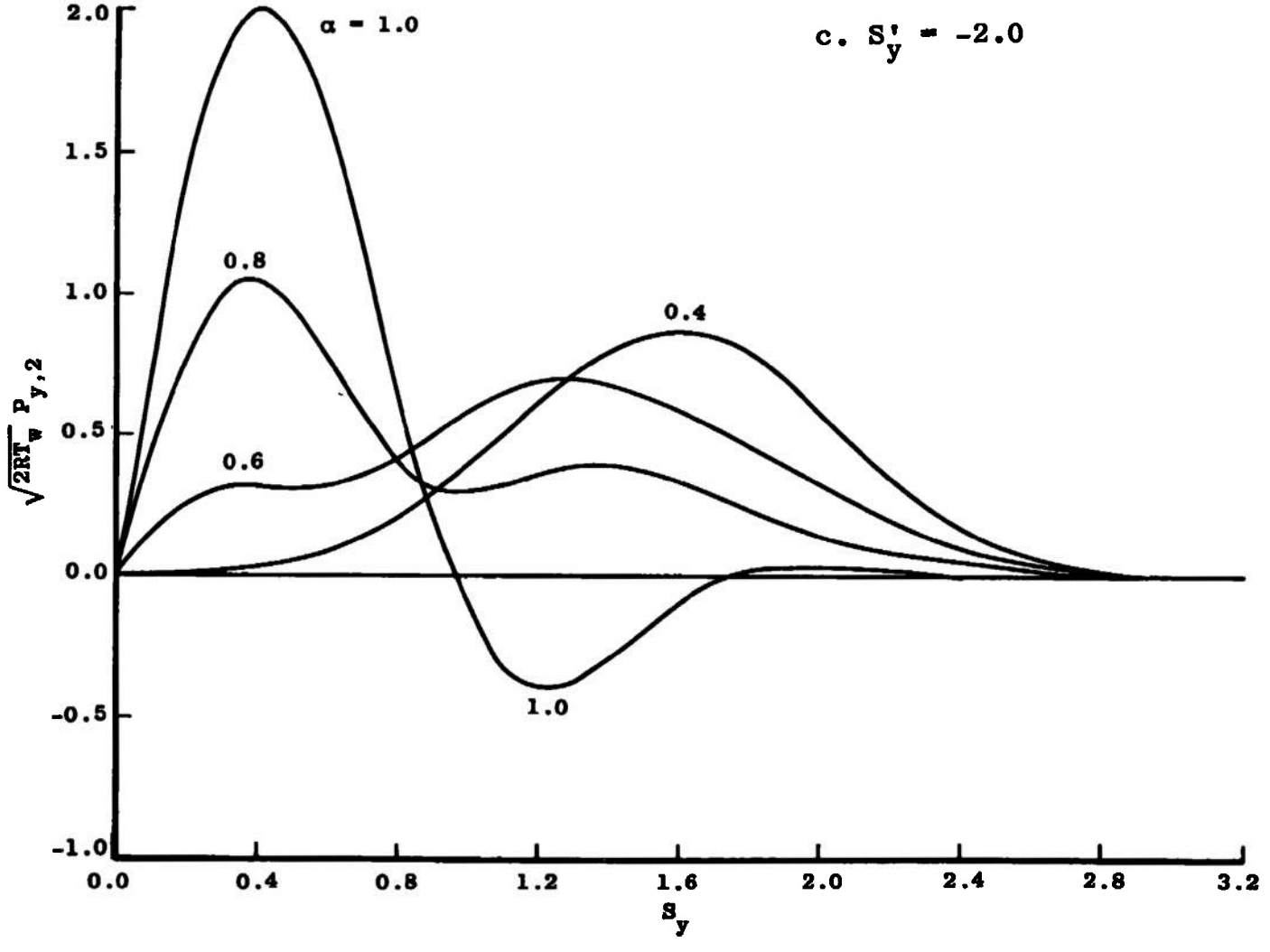

Figure 7. (Continued).

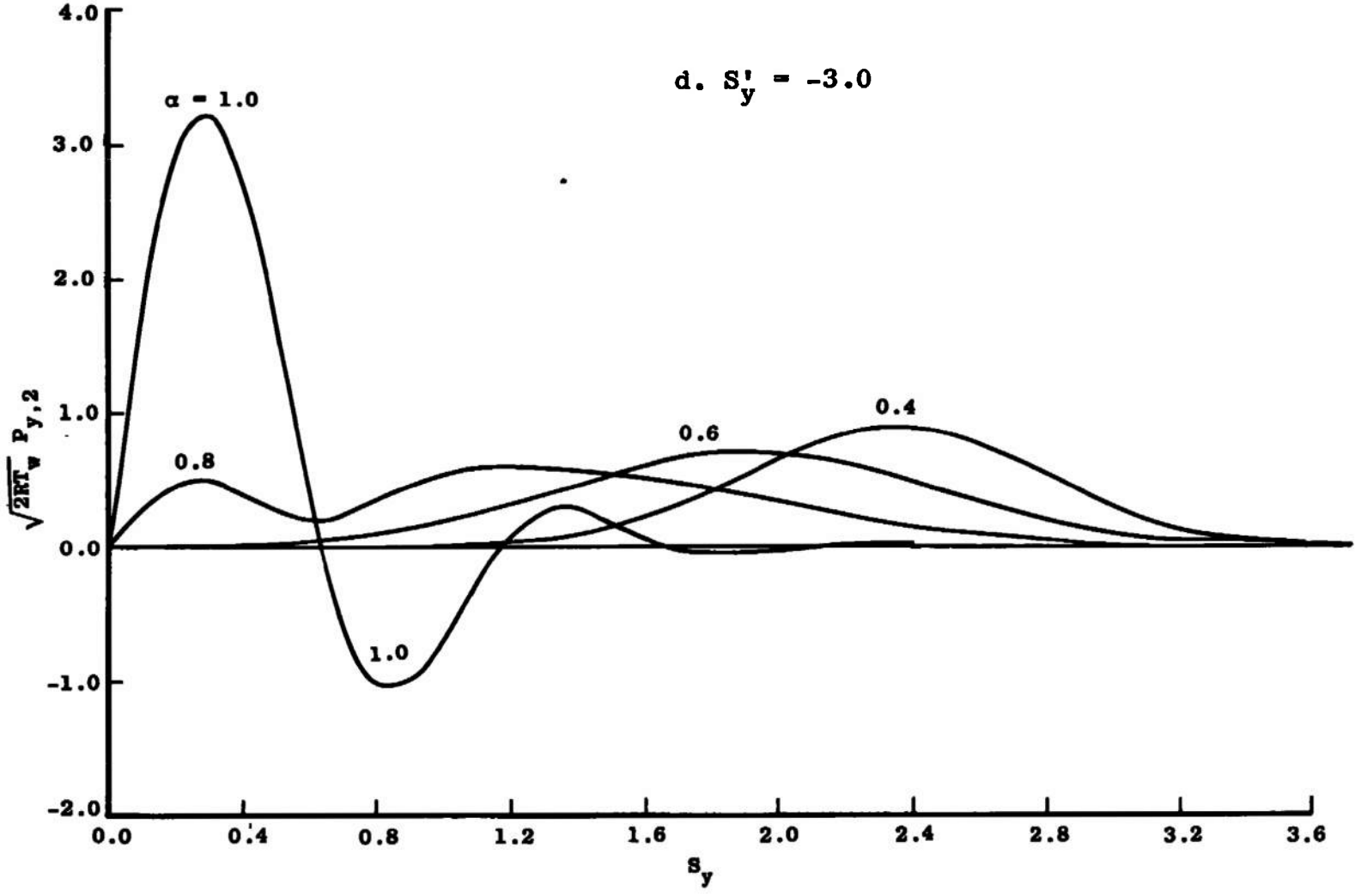

Figure 7. (Continued).

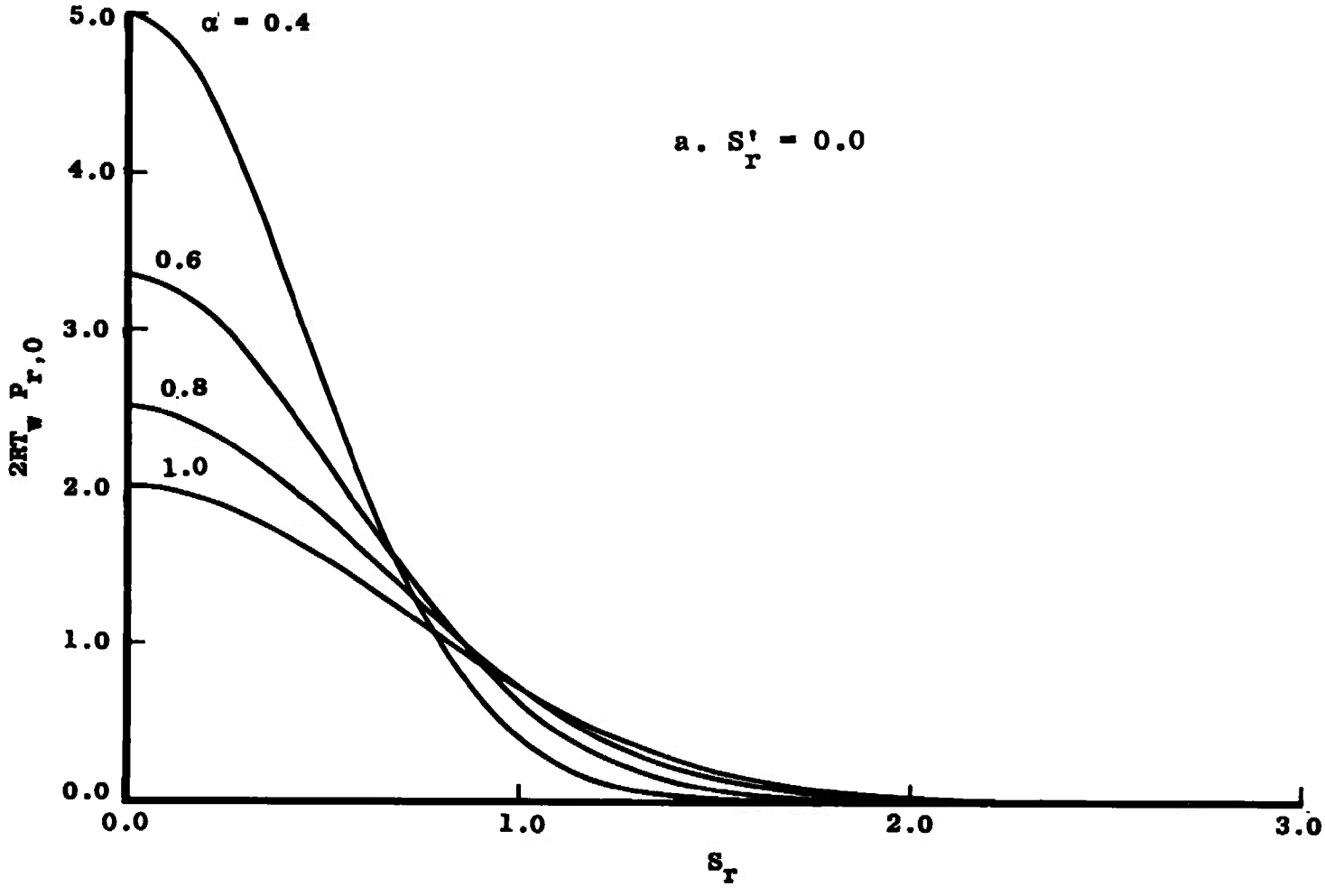

Figure 8. Plot of $2RT_w P_{r,0}$.

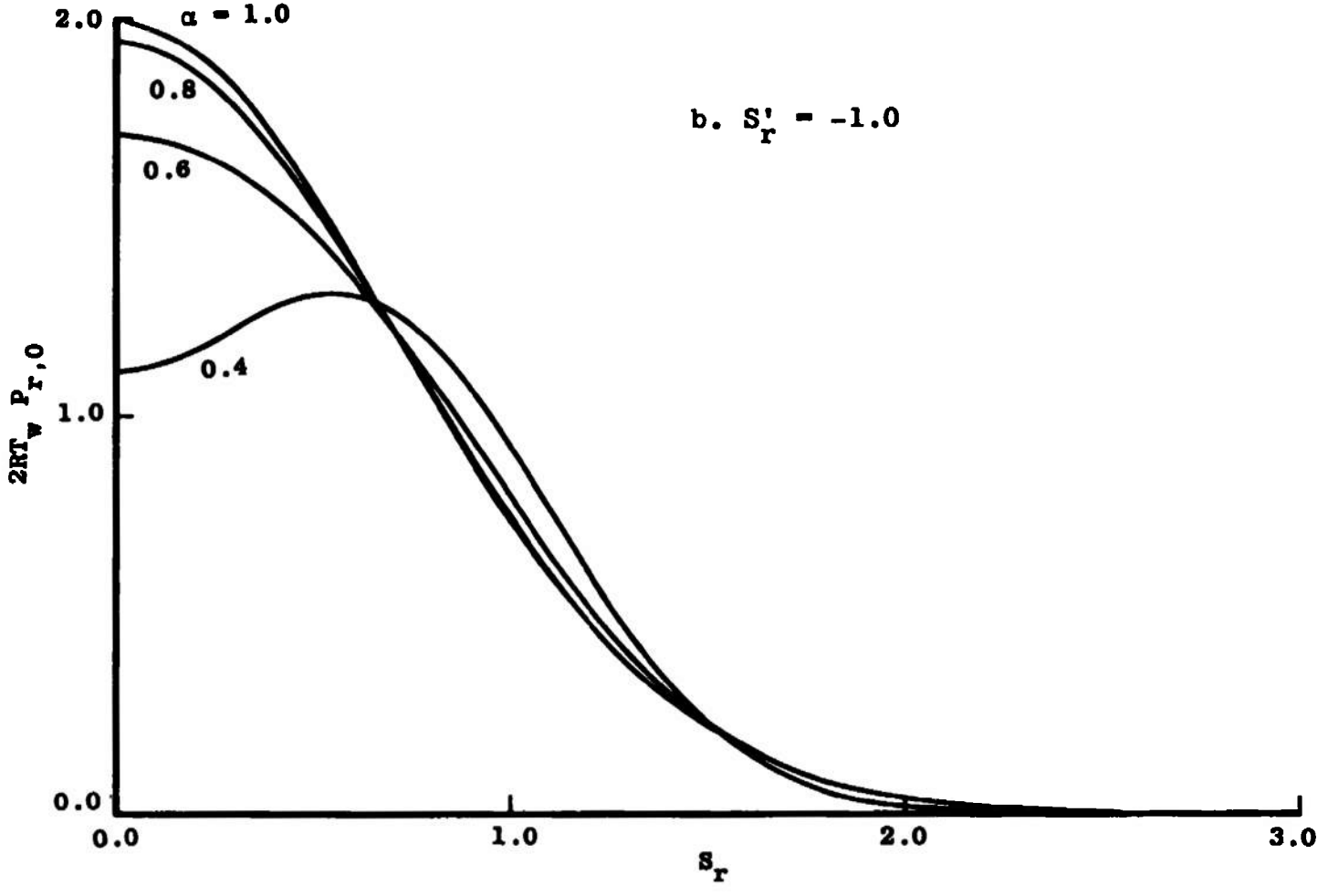

Figure 8. (Continued).

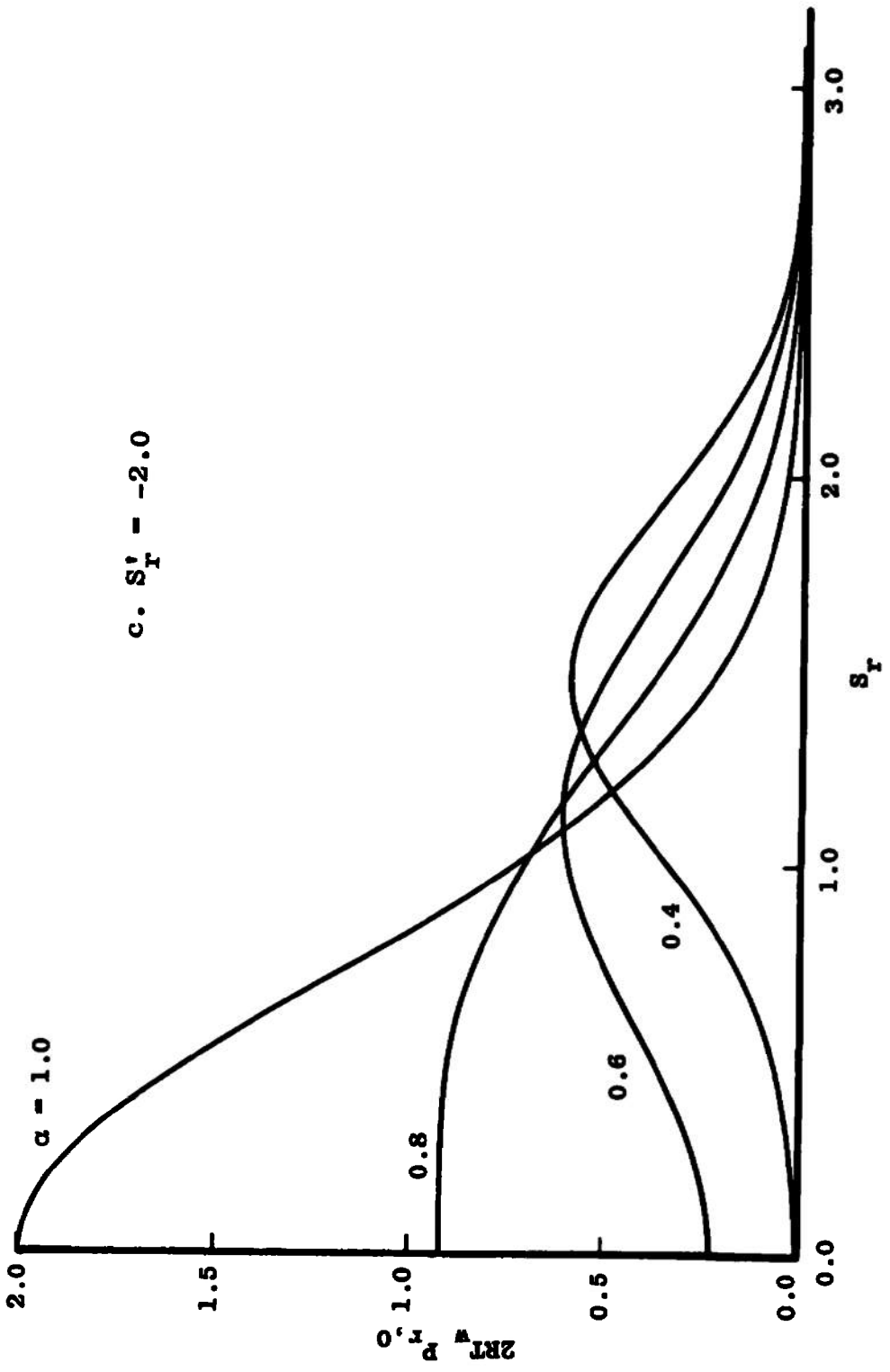

Figure 8. (Continued).

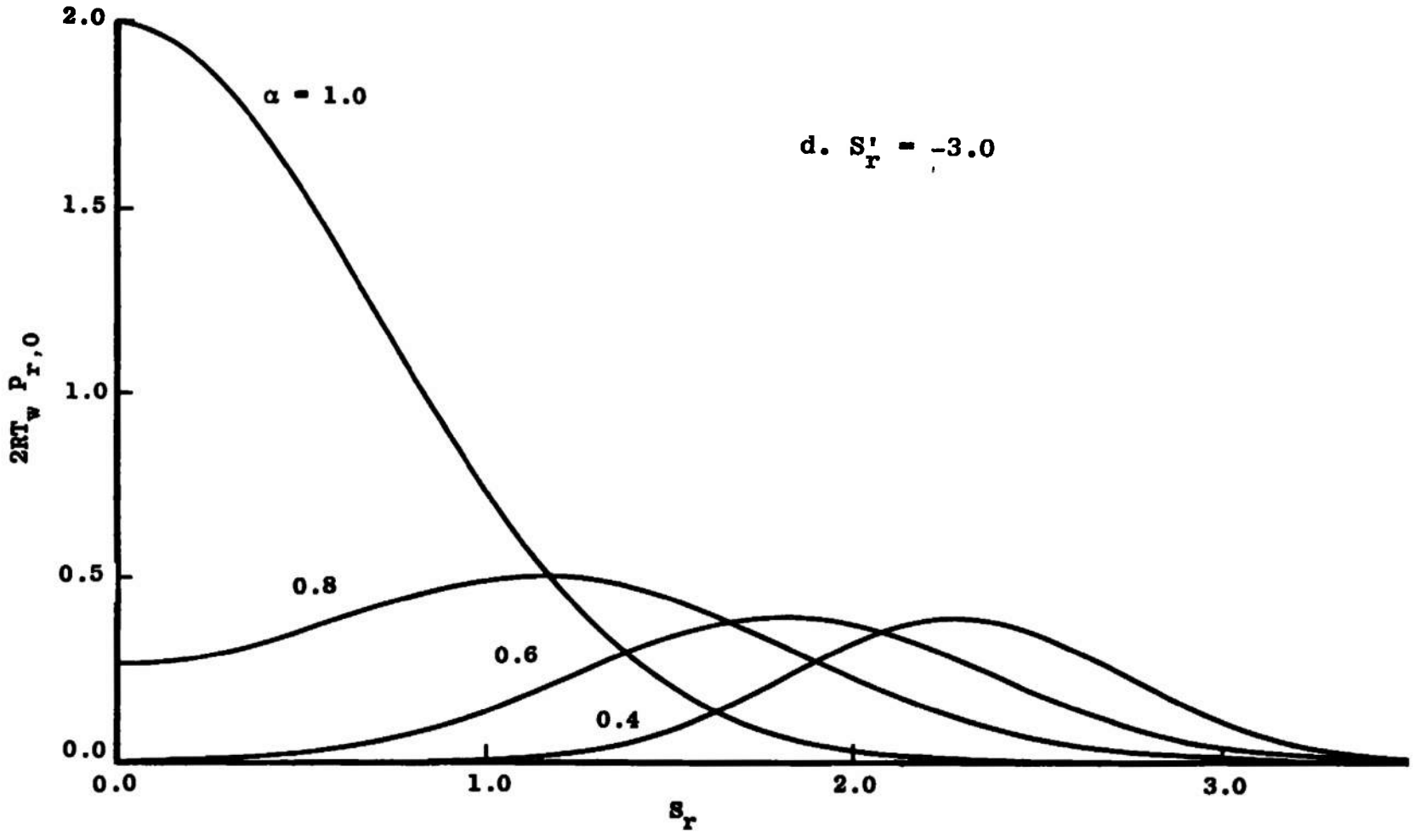

Figure 8. (Continued).

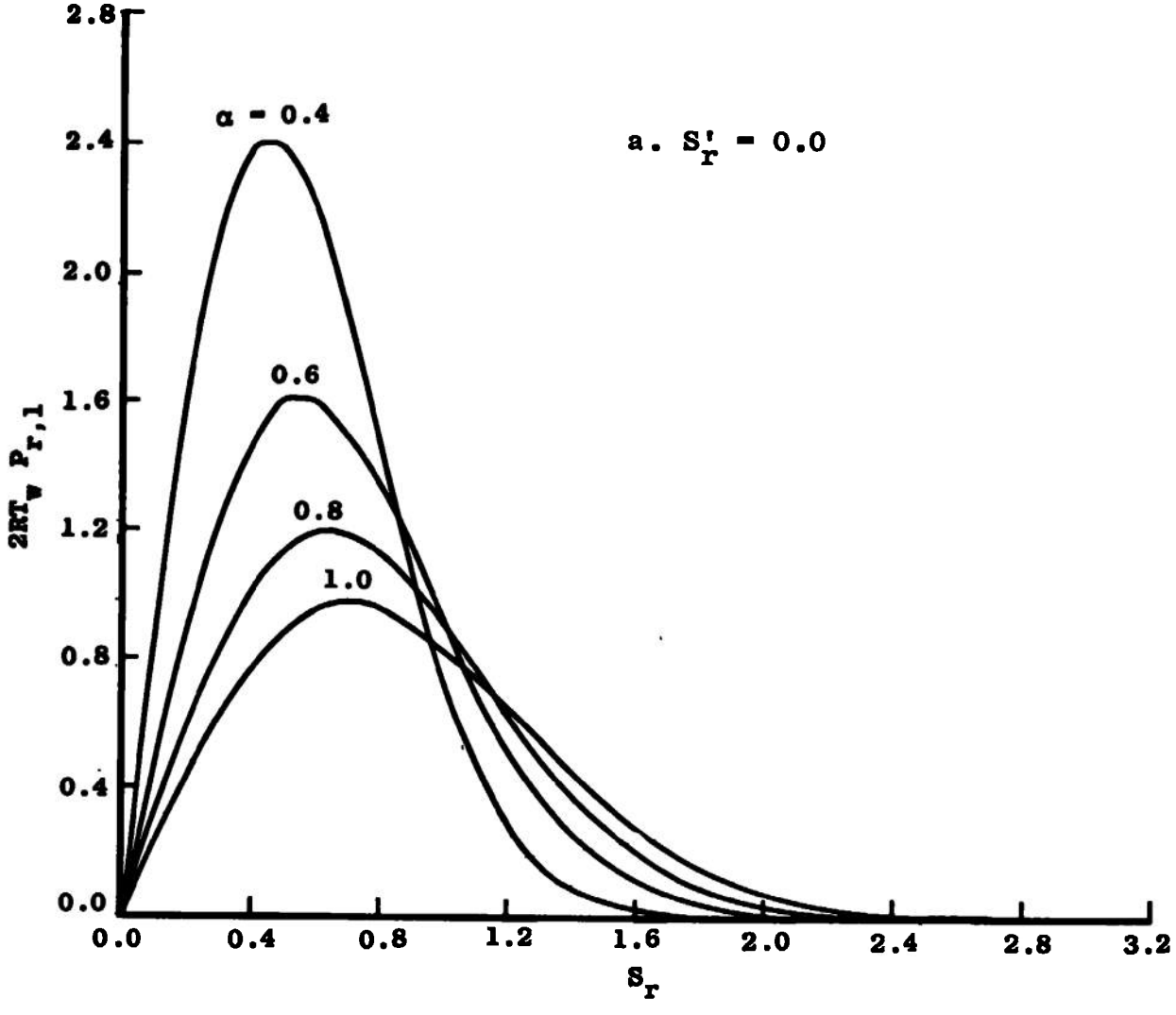

Figure 9. Plot of $2RT_w P_{r,1}$.

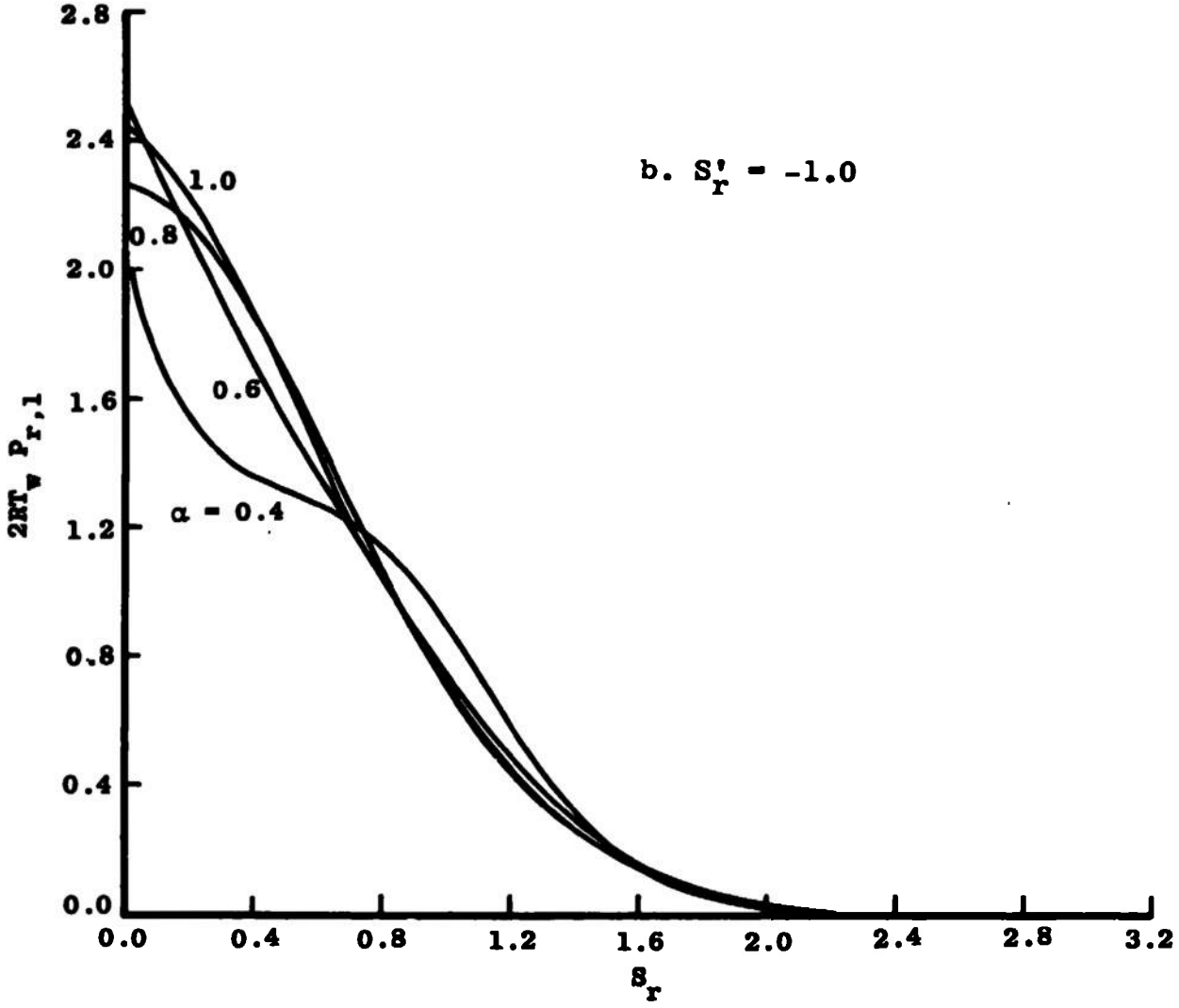

Figure 9. (Continued).

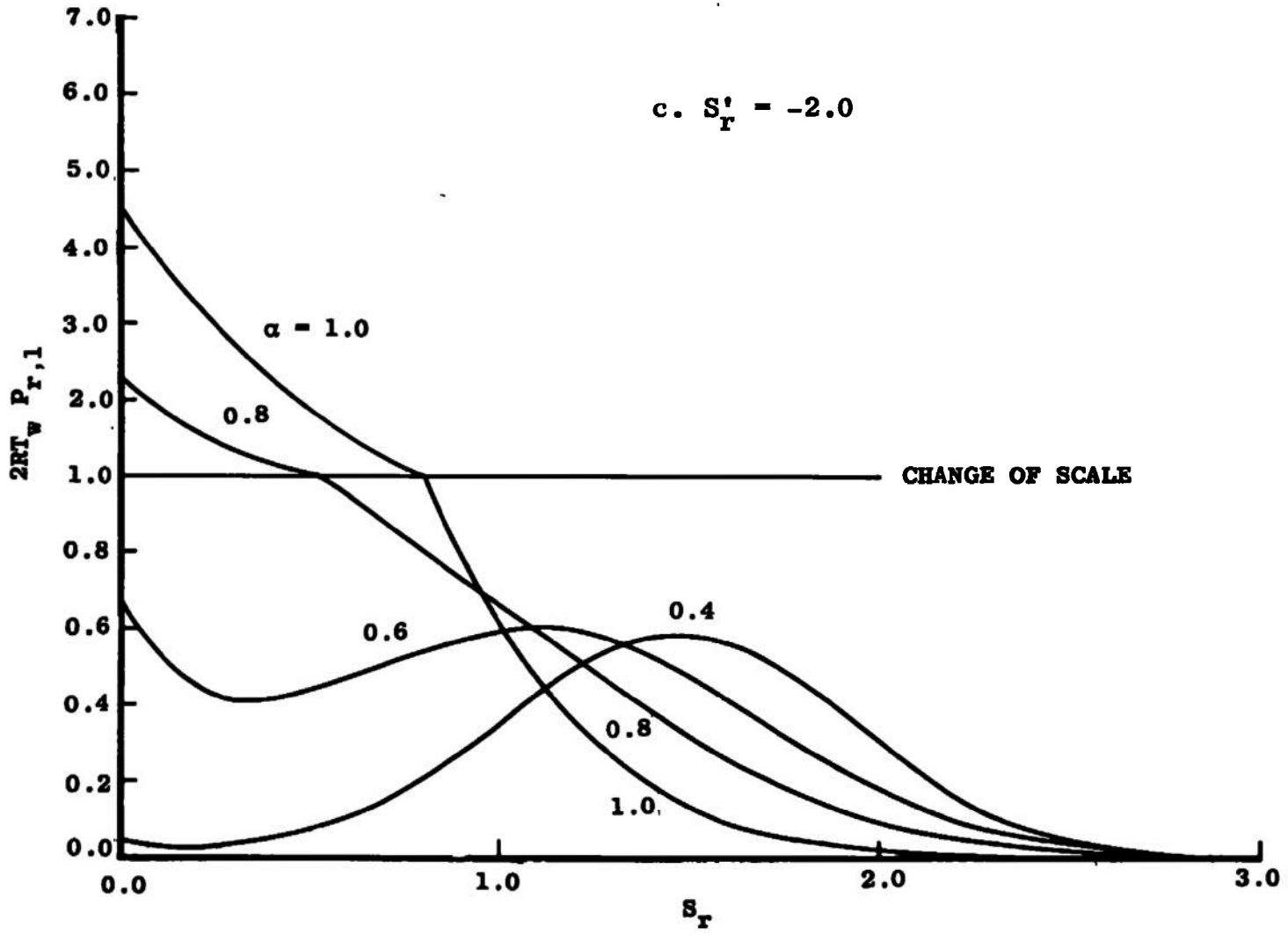

Figure 9. (Continued).

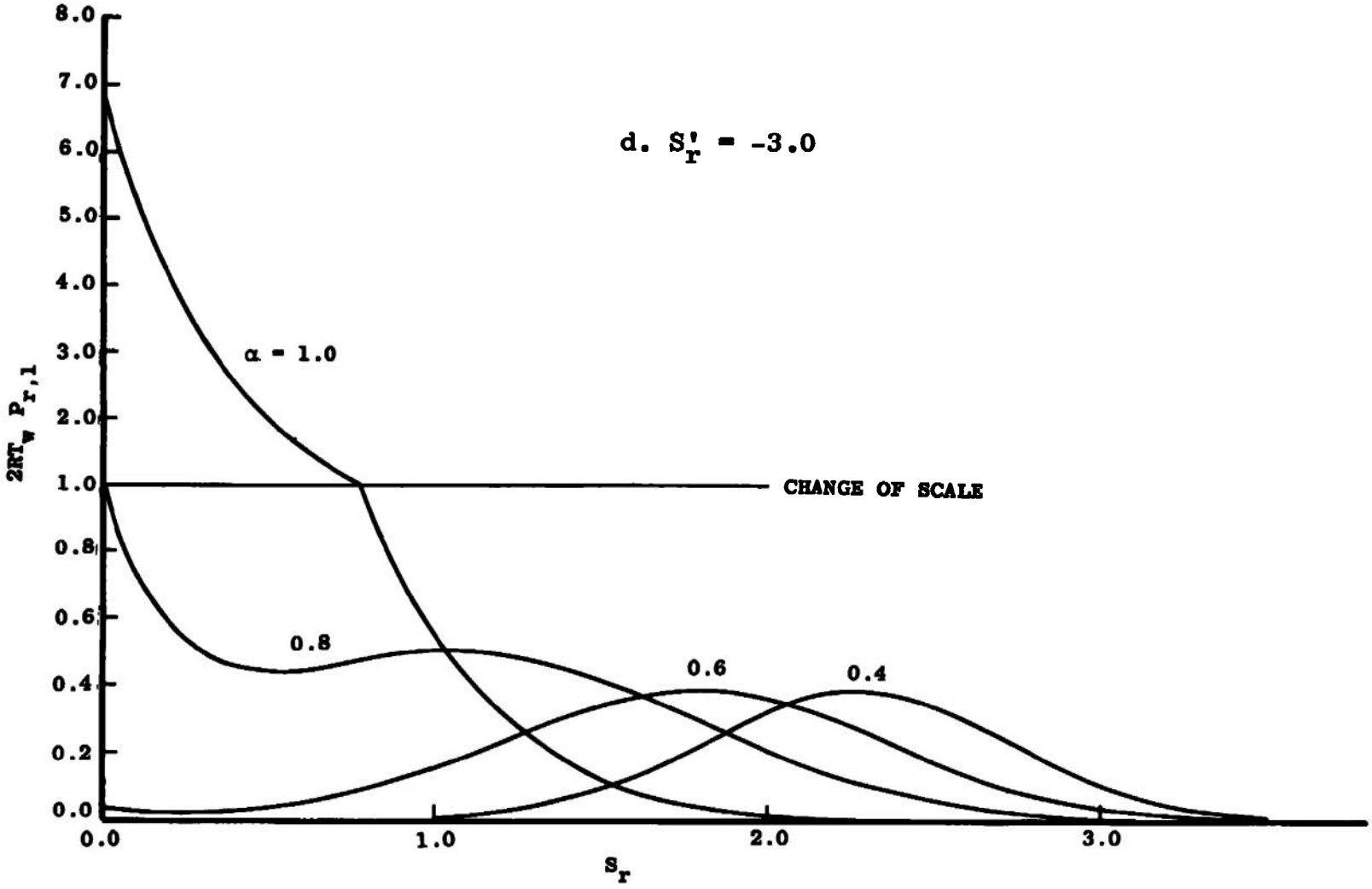

Figure 9. (Continued).

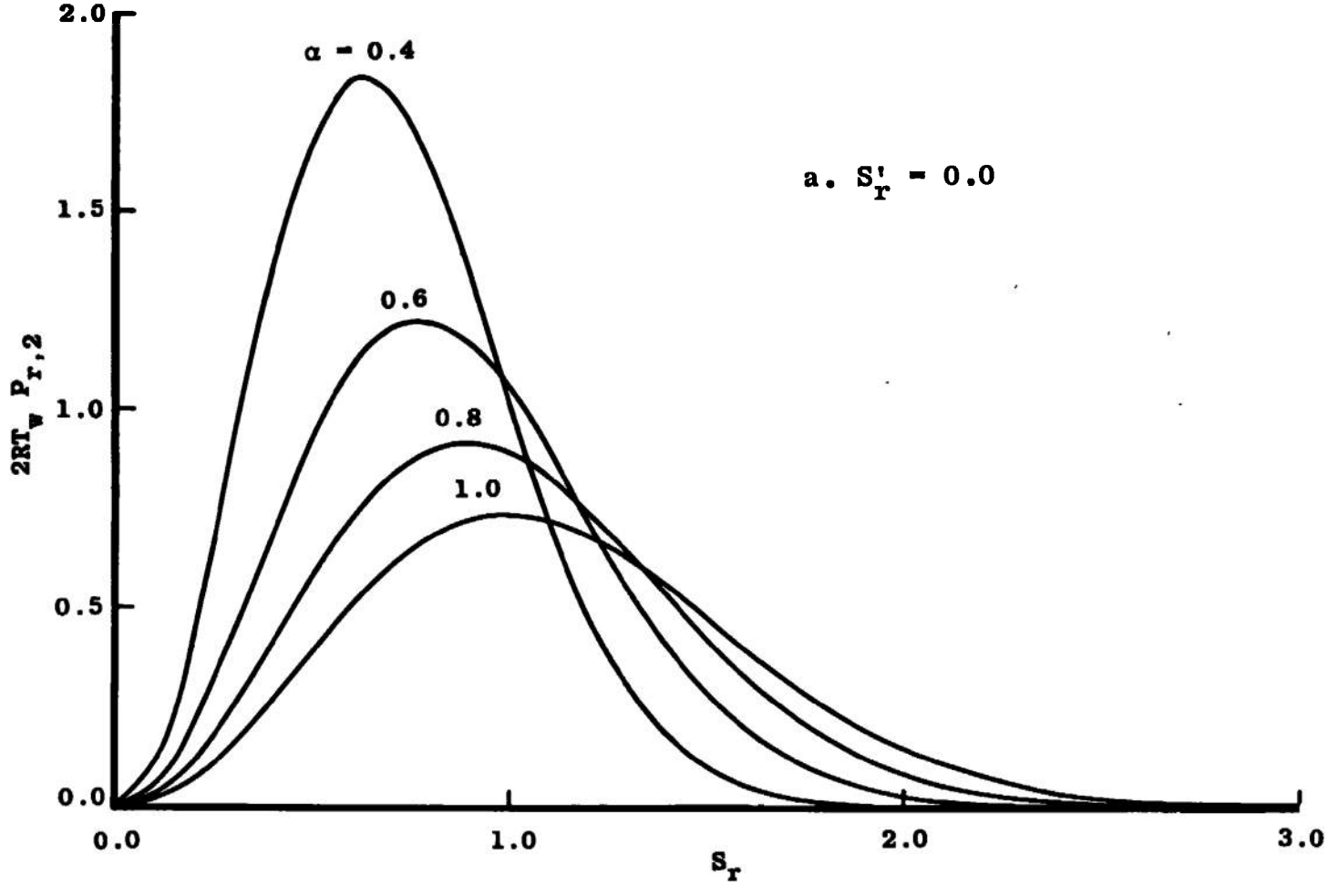

Figure 10. Plot of $2RT_w P_{r,2}$.

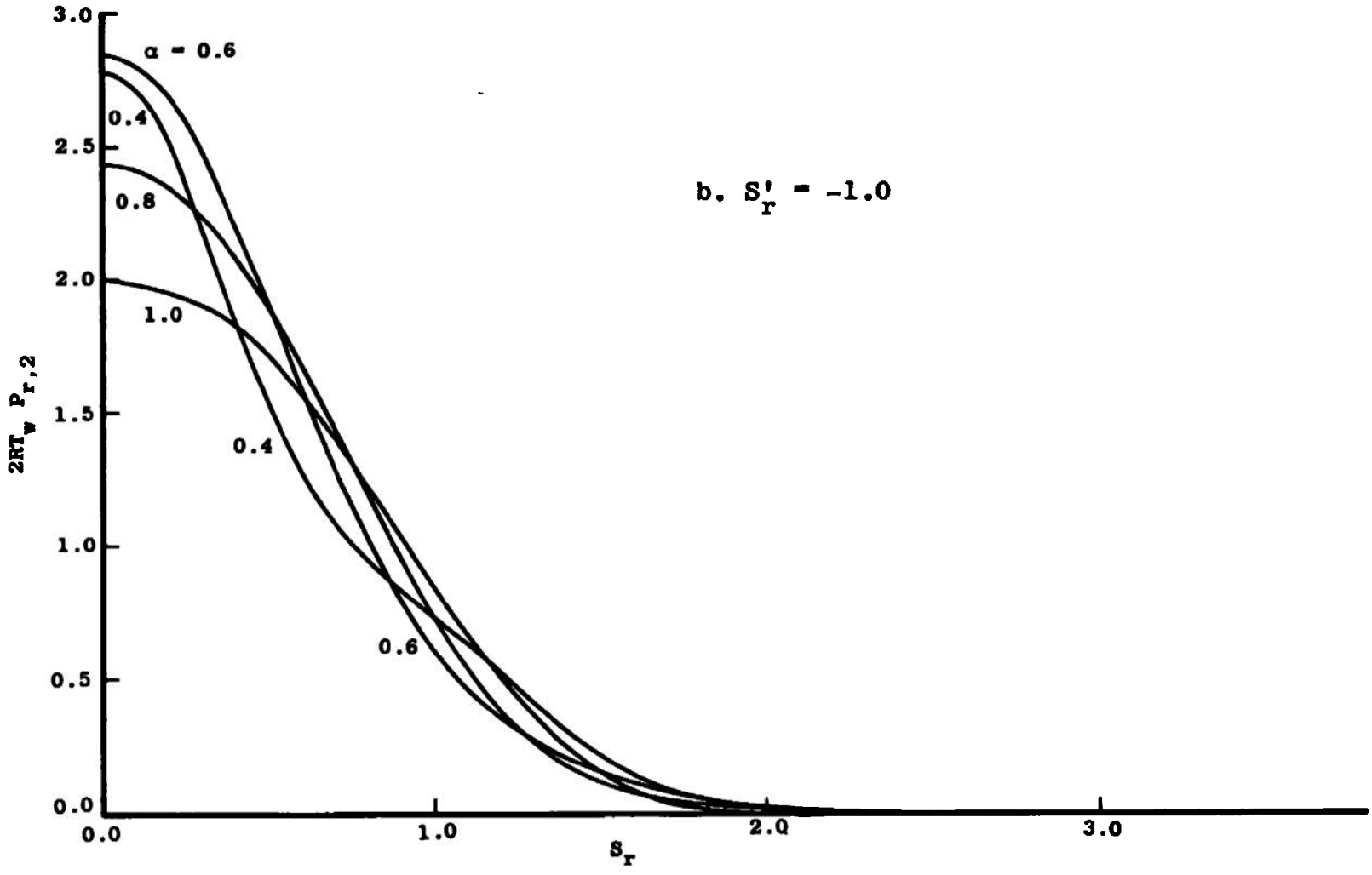

Figure 10. (Continued)

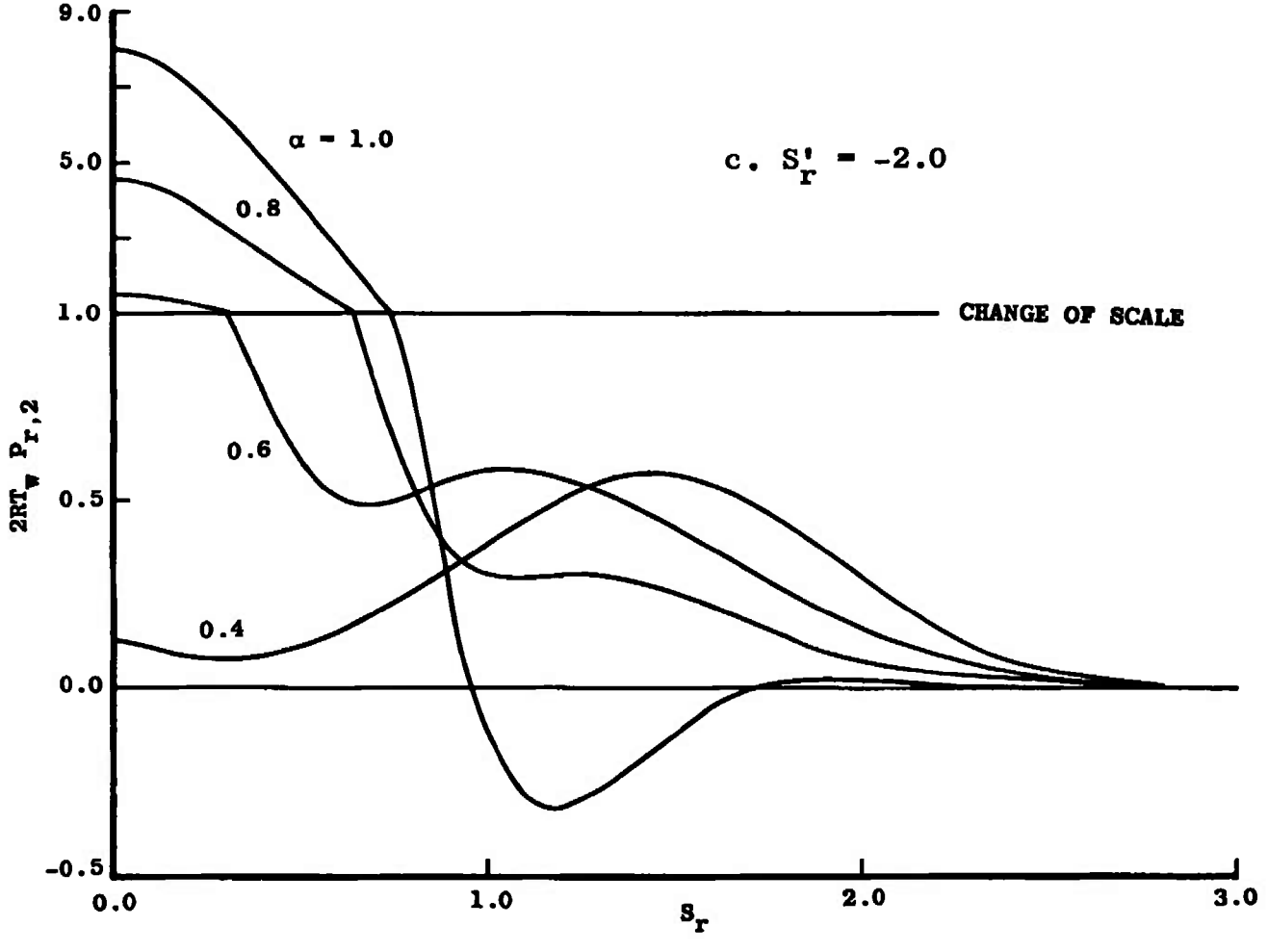

Figure 10. (Continued)

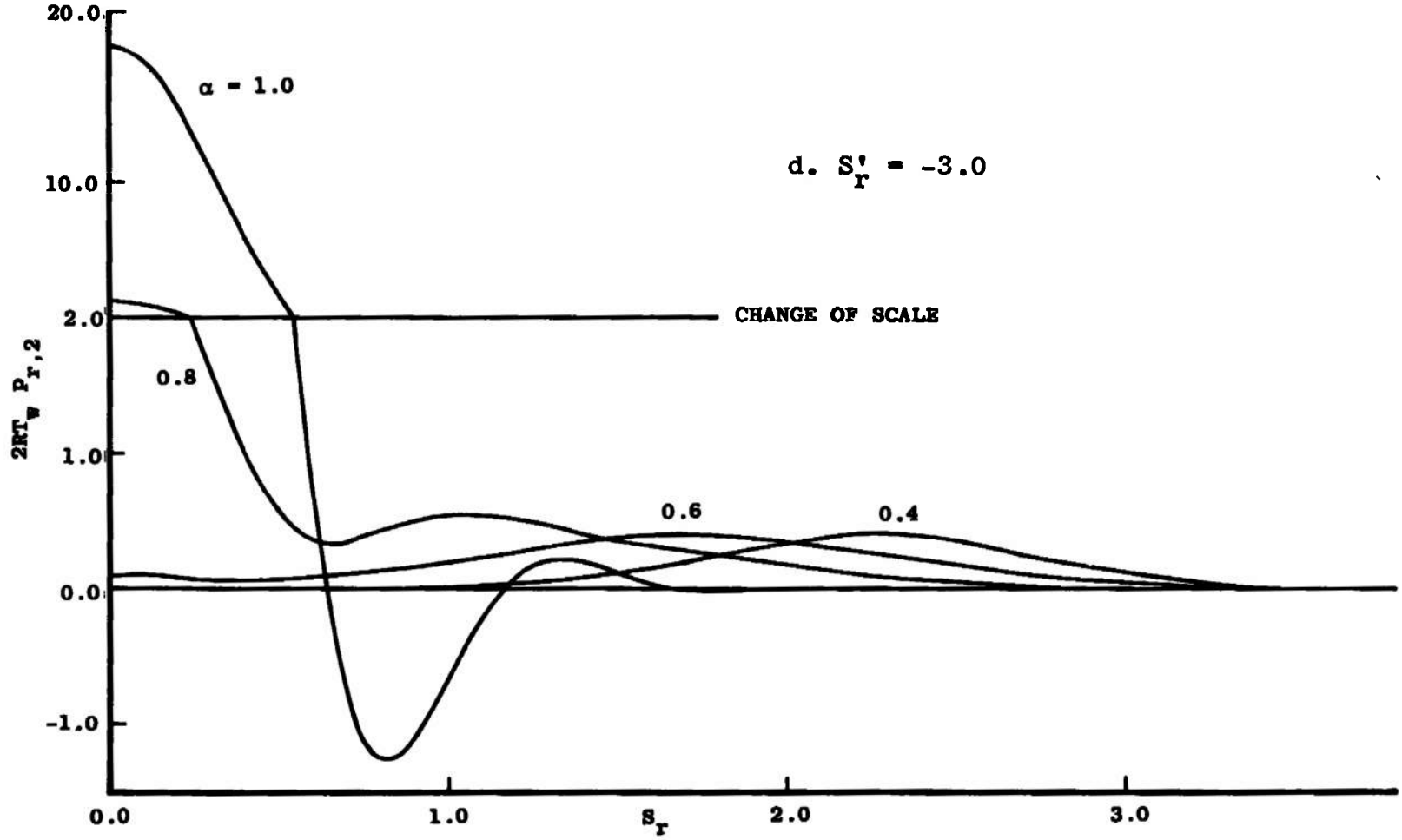

Figure 10. (Continued)

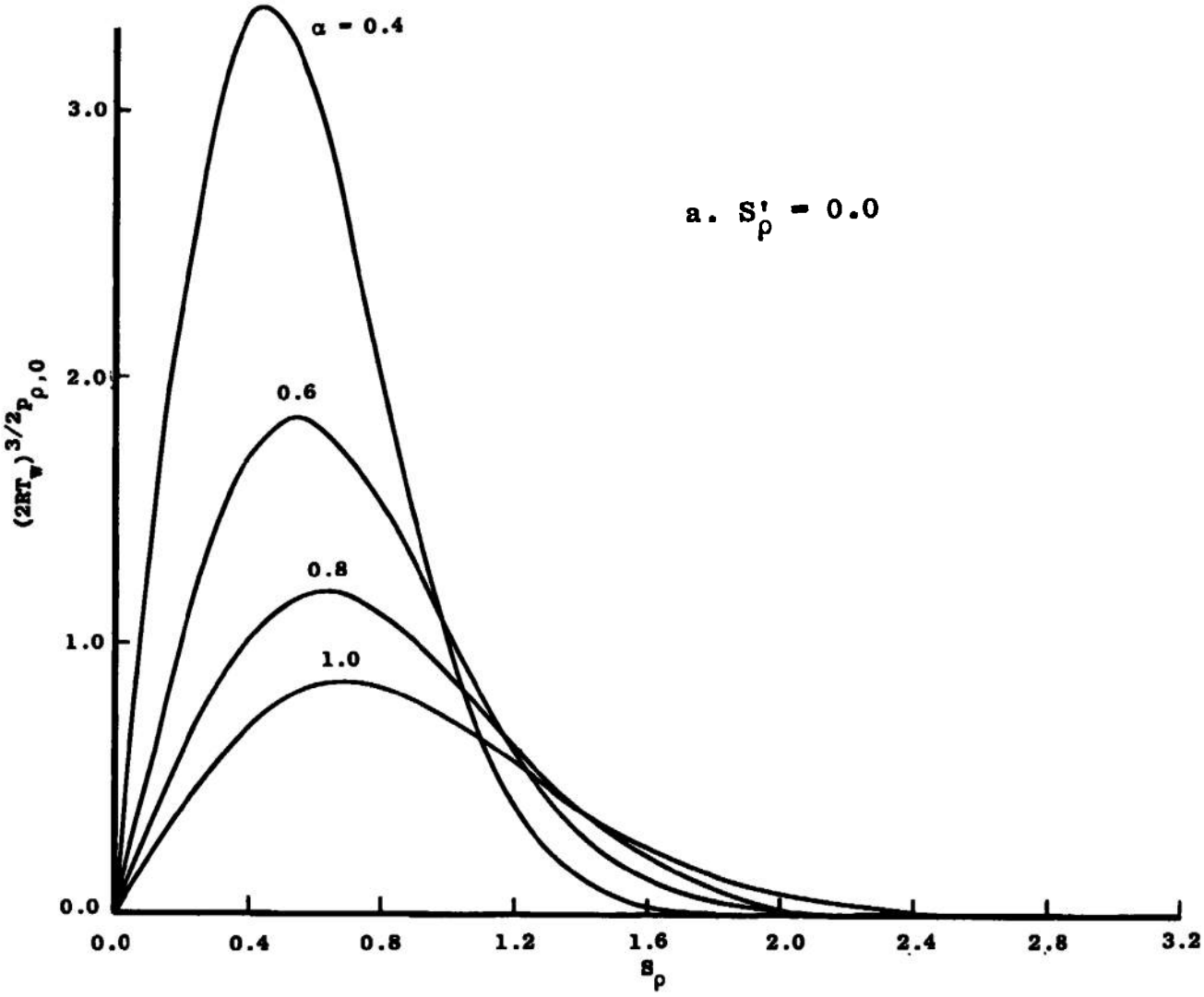

Figure 11. Plot of $(2RT_w)^{3/2}\ P_{\rho,0}$.

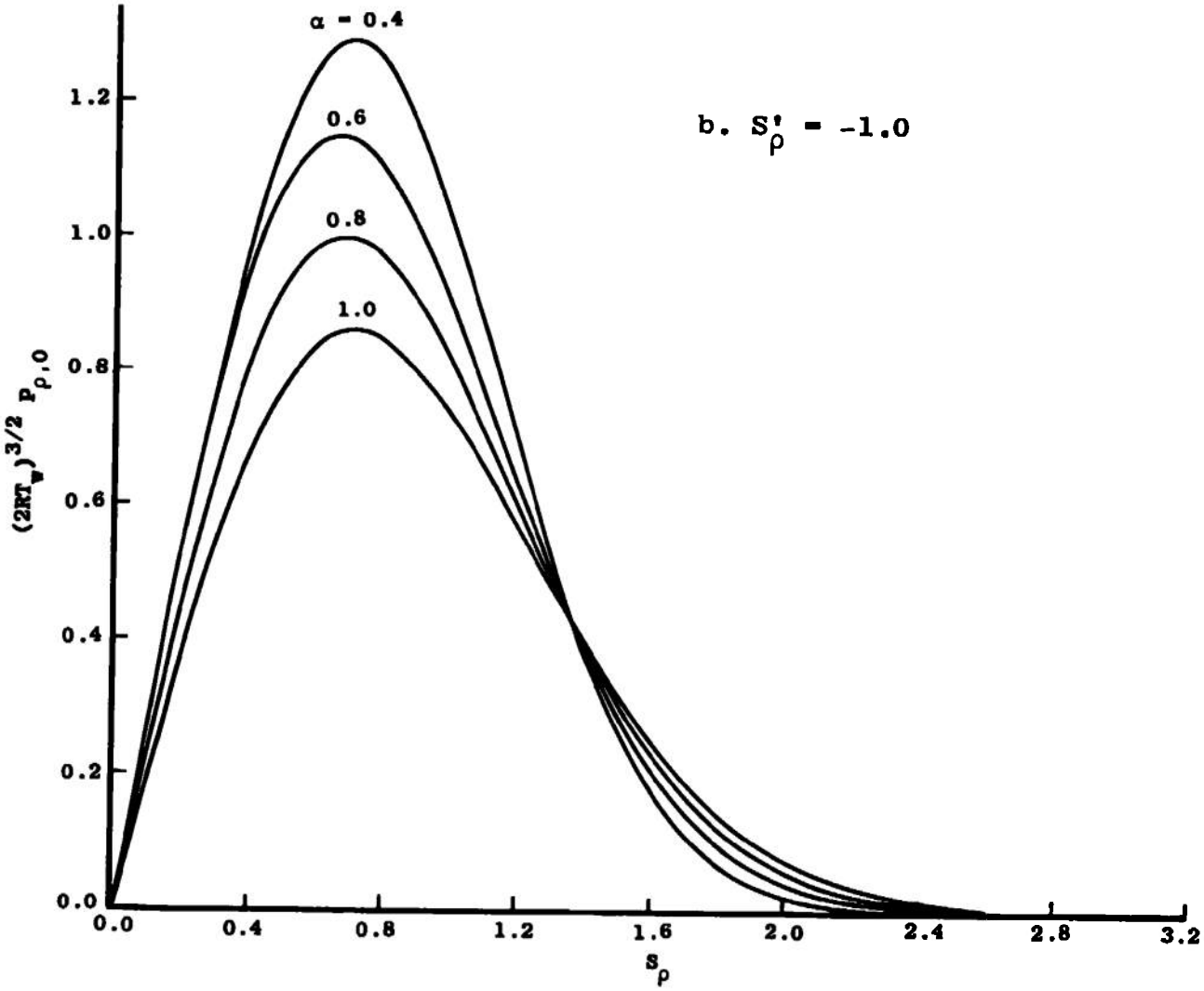

Figure 11. (Continued).

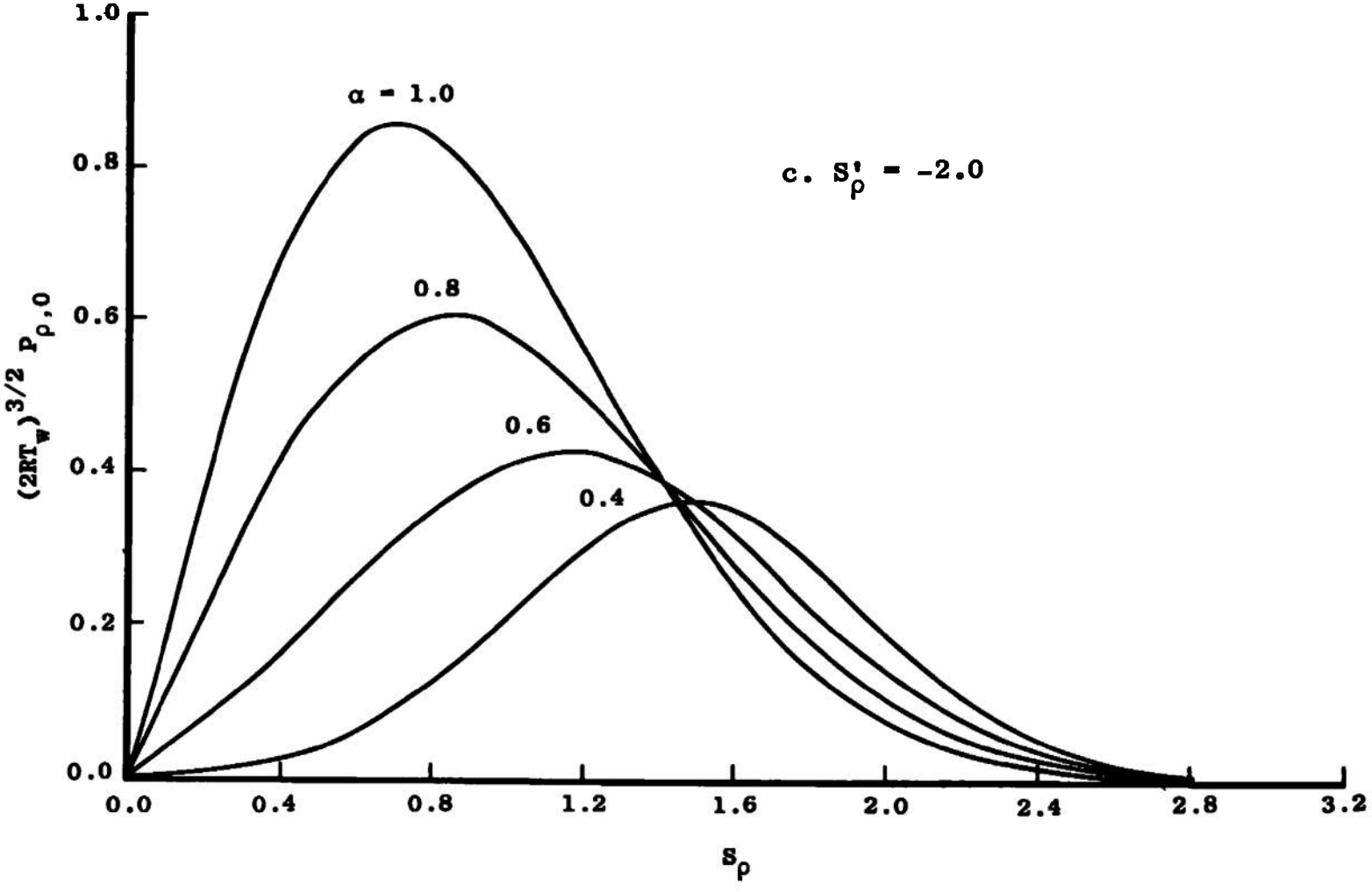

Figure 11. (Continued).

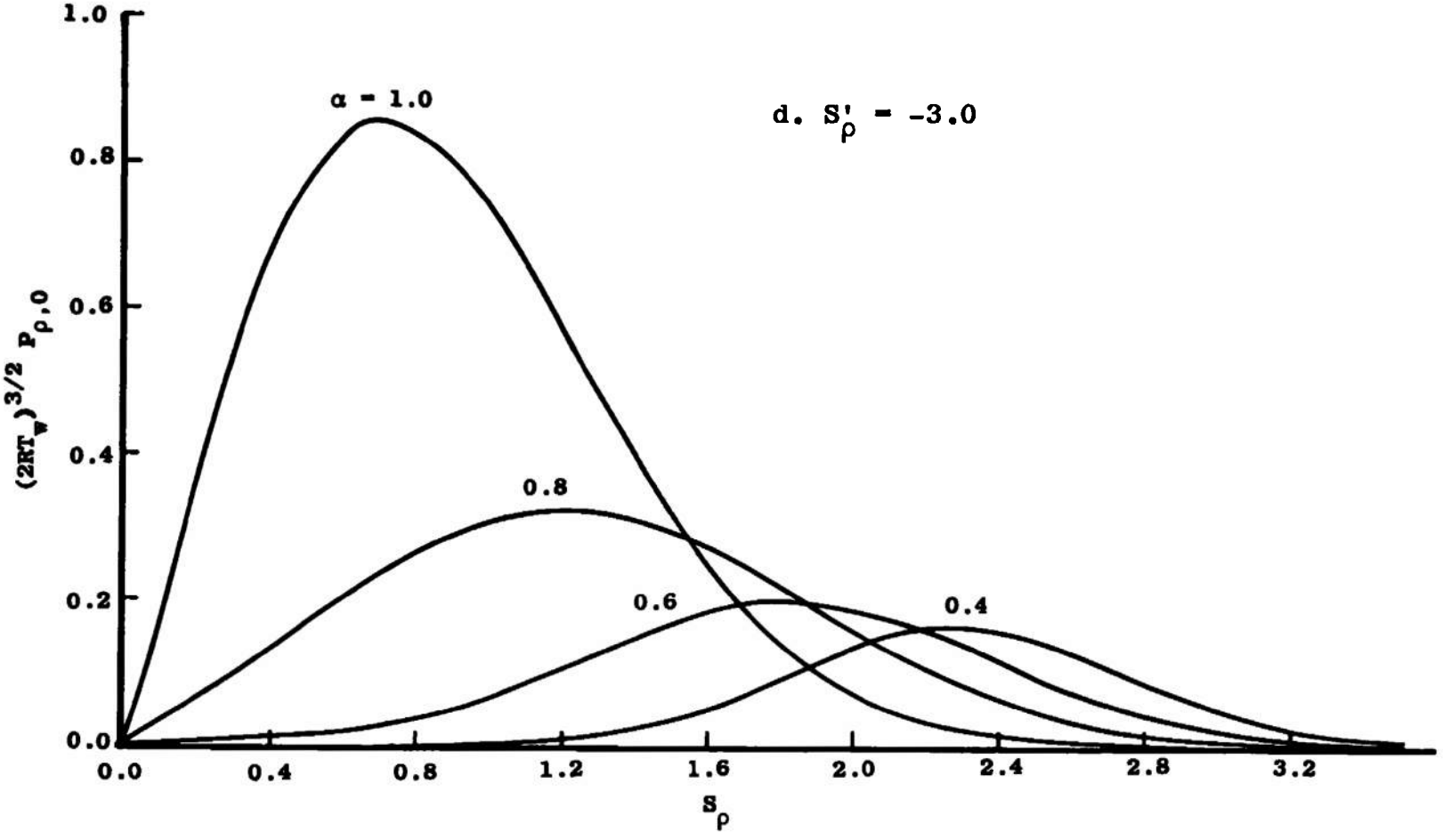

Figure 11. (Continued).

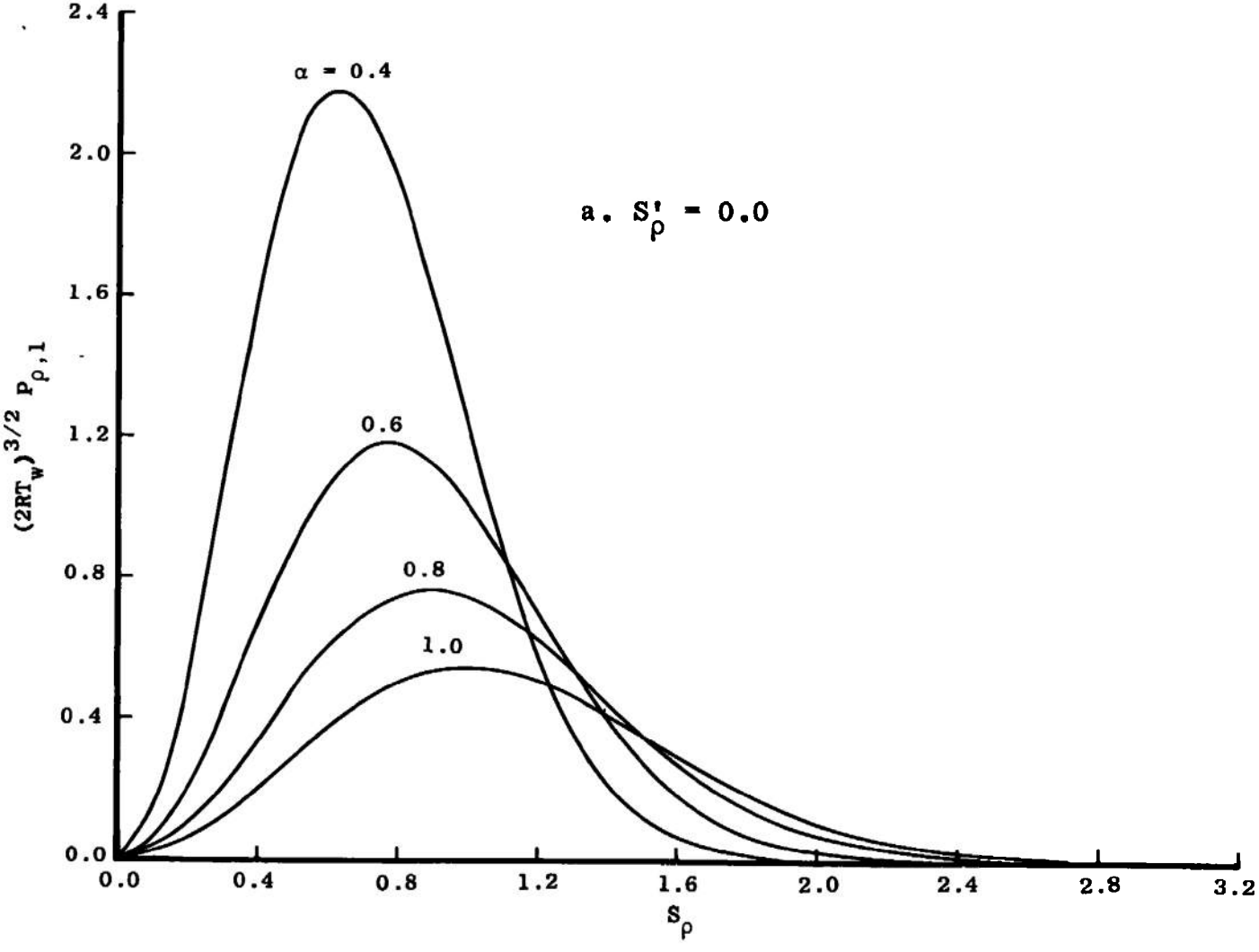

Figure 12. Plot of $(2RT_w)^{3/2}\ P_{\rho,1}$.

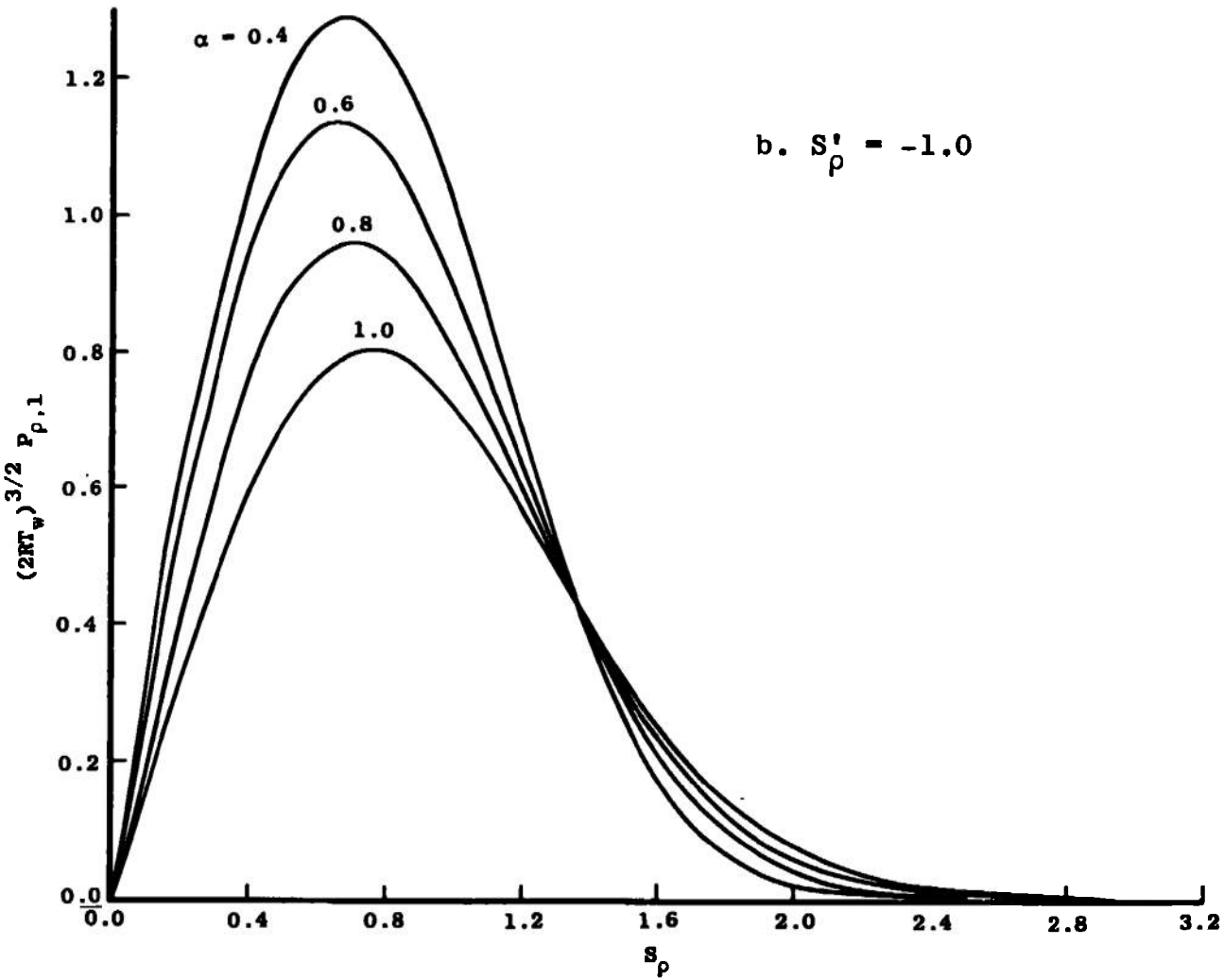

Figure 12. (Continued).

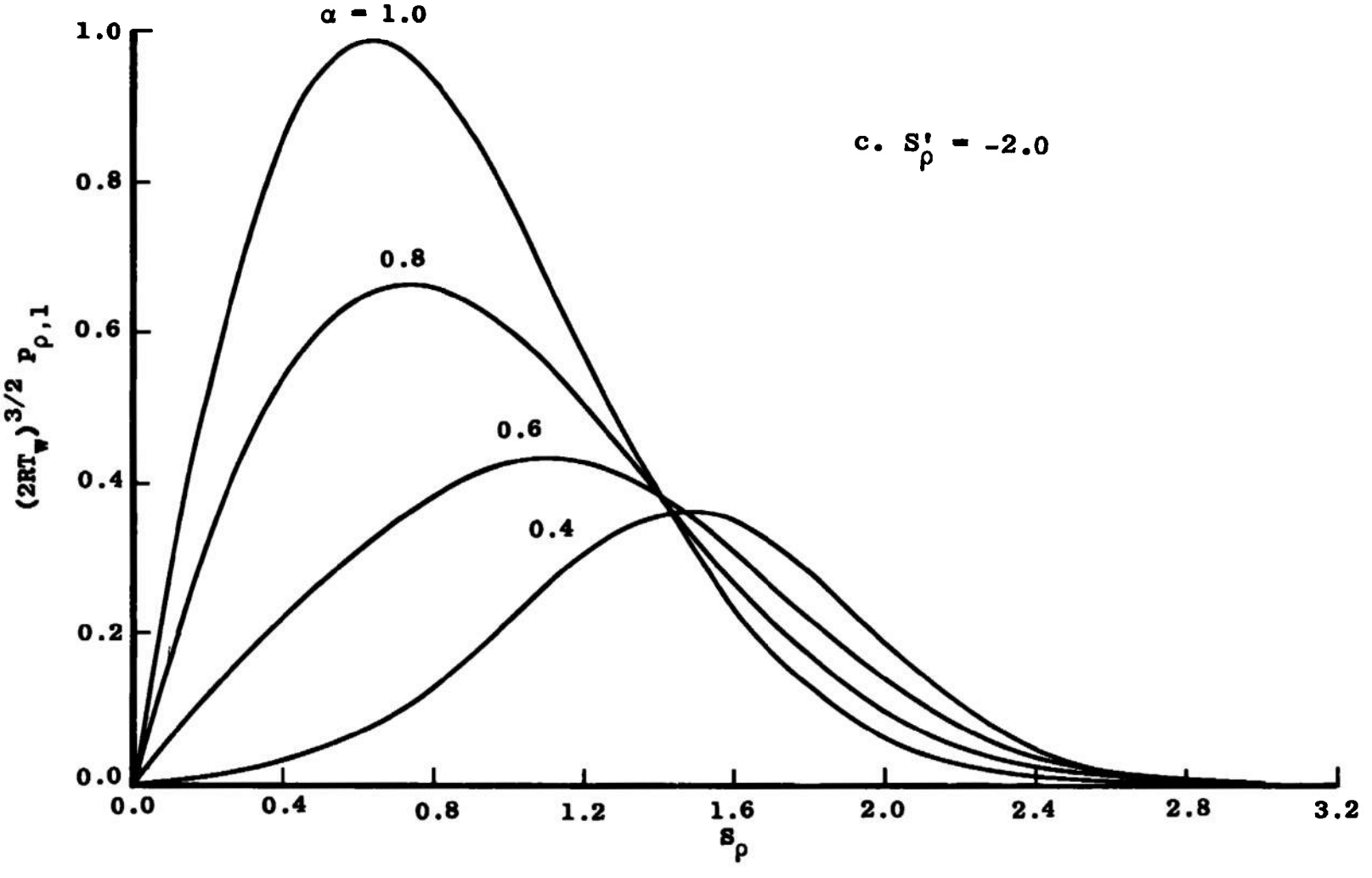

Figure 12. (Continued).

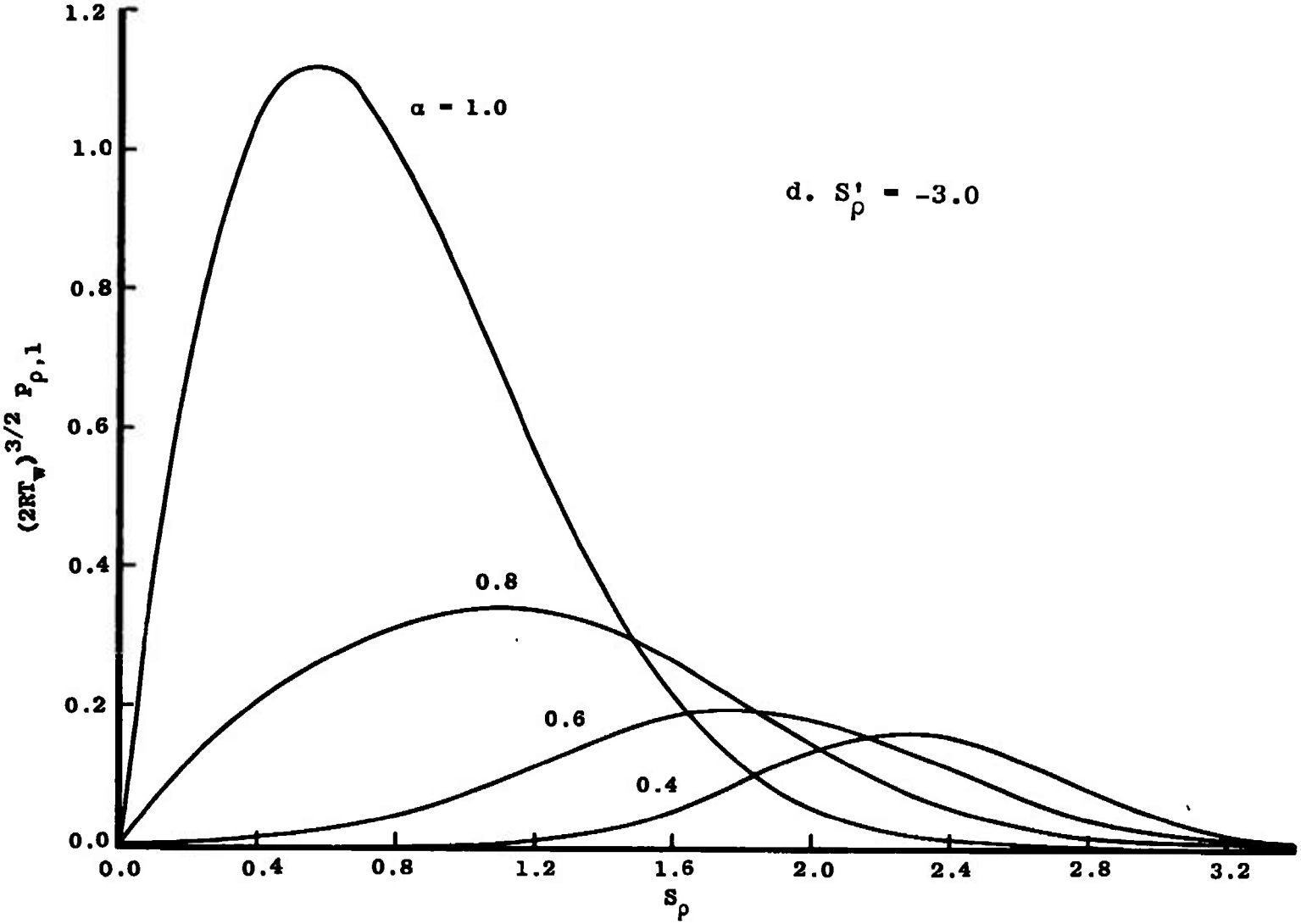

Figure 12. (Continued).

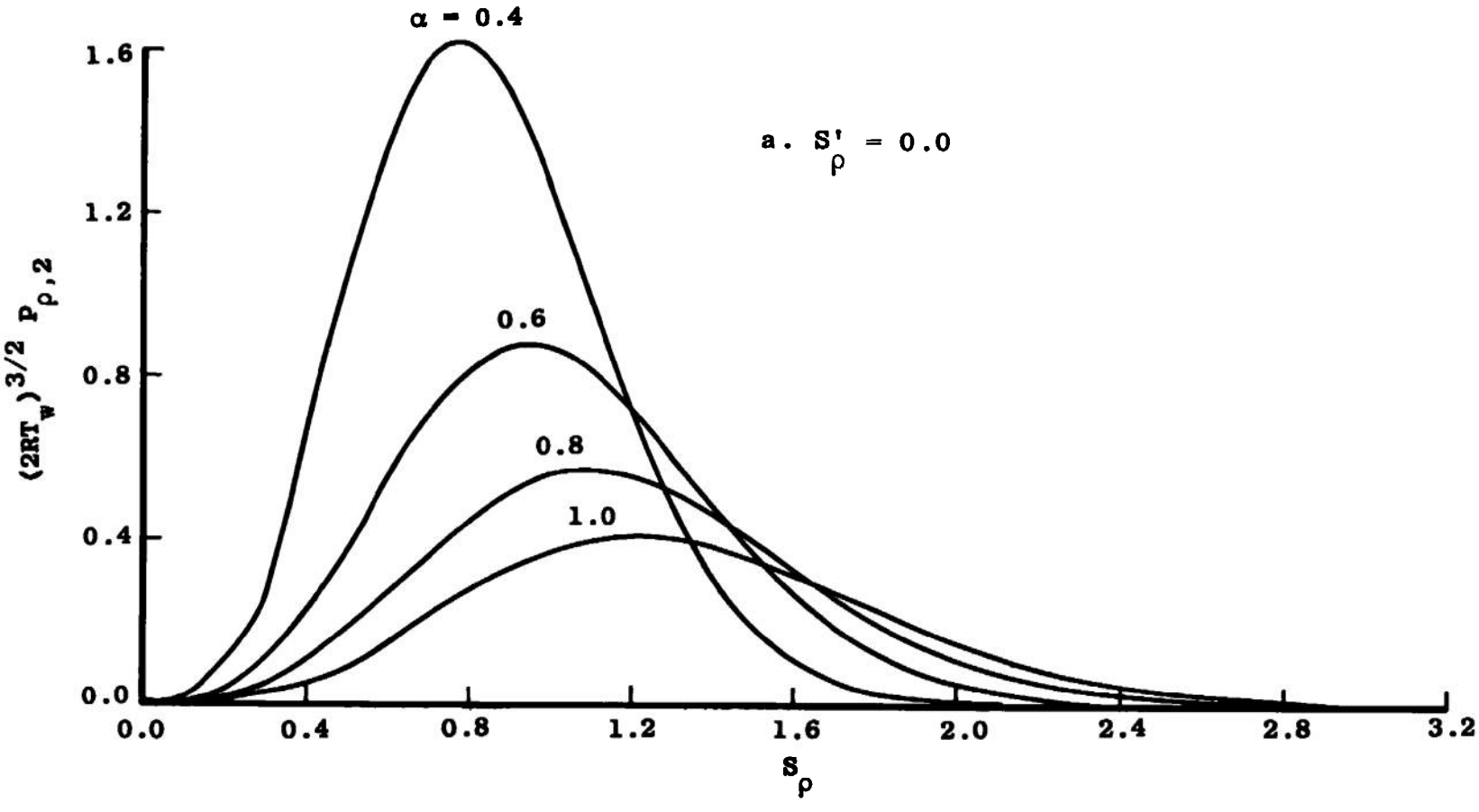

Figure 13. Plot of $(2RT_w)^{3/2} P_{\rho,2}$.

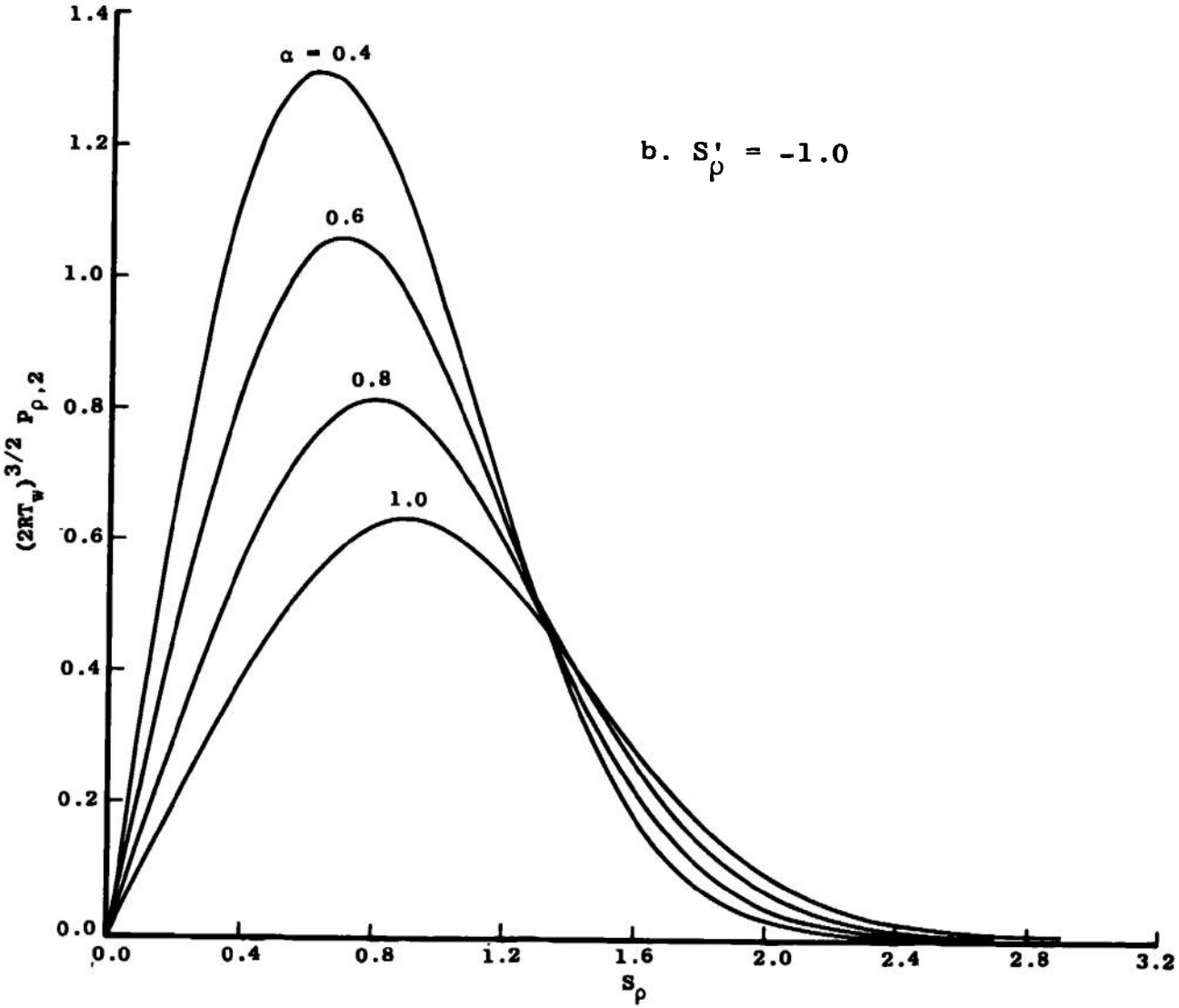

Figure 13. (Continued).

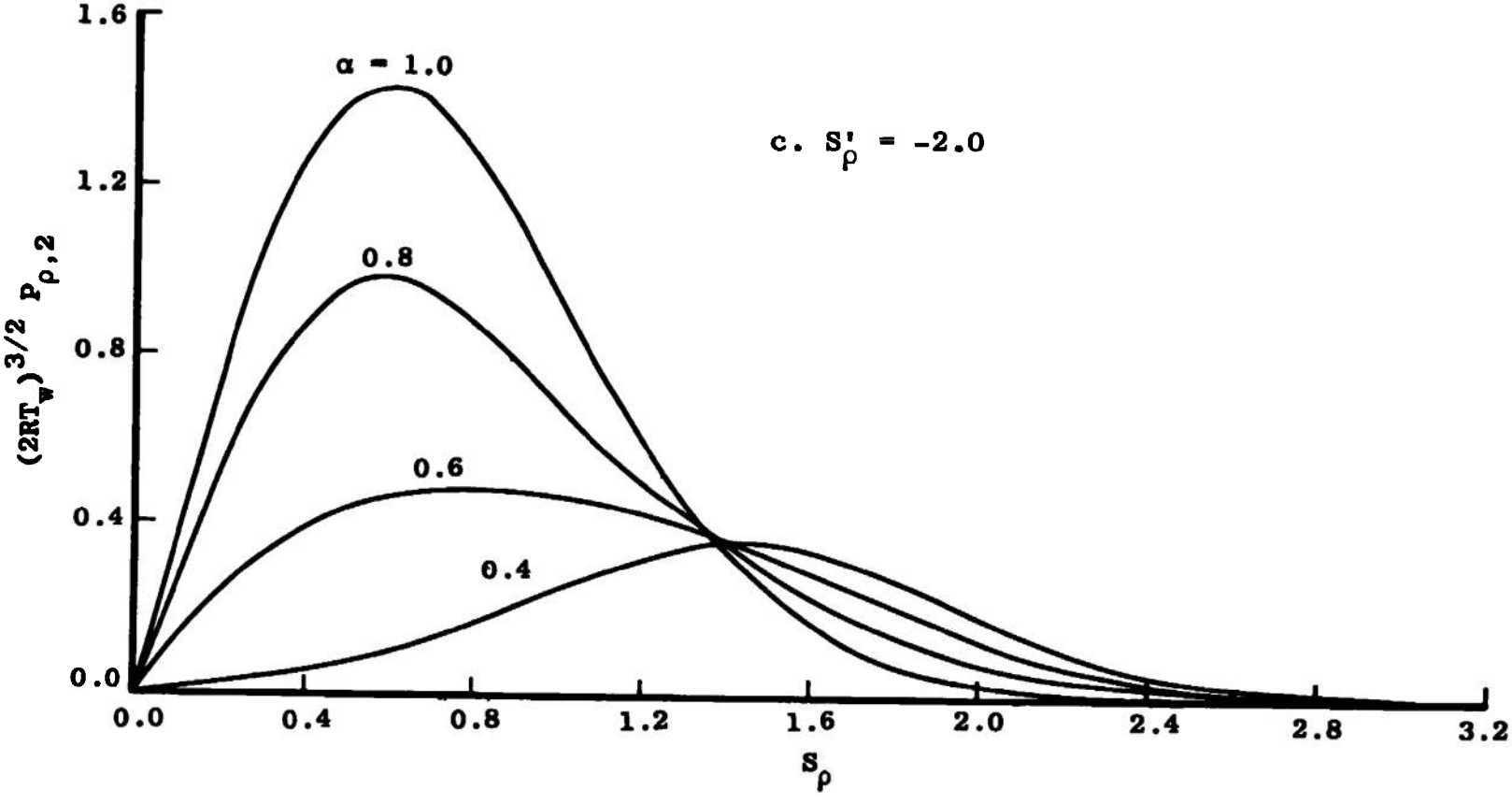

Figure 13. (Continued).

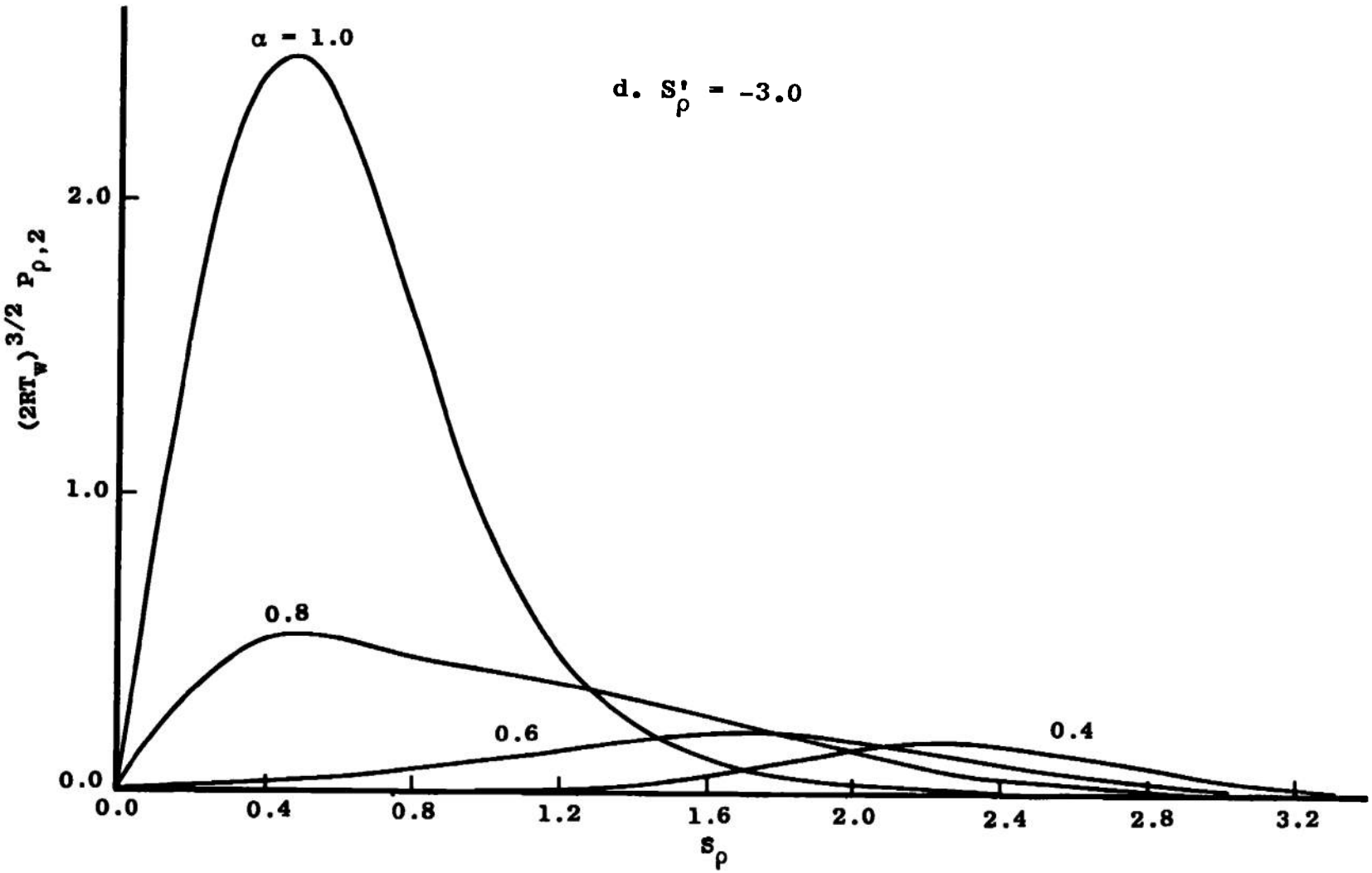

Figure 13. (Continued).

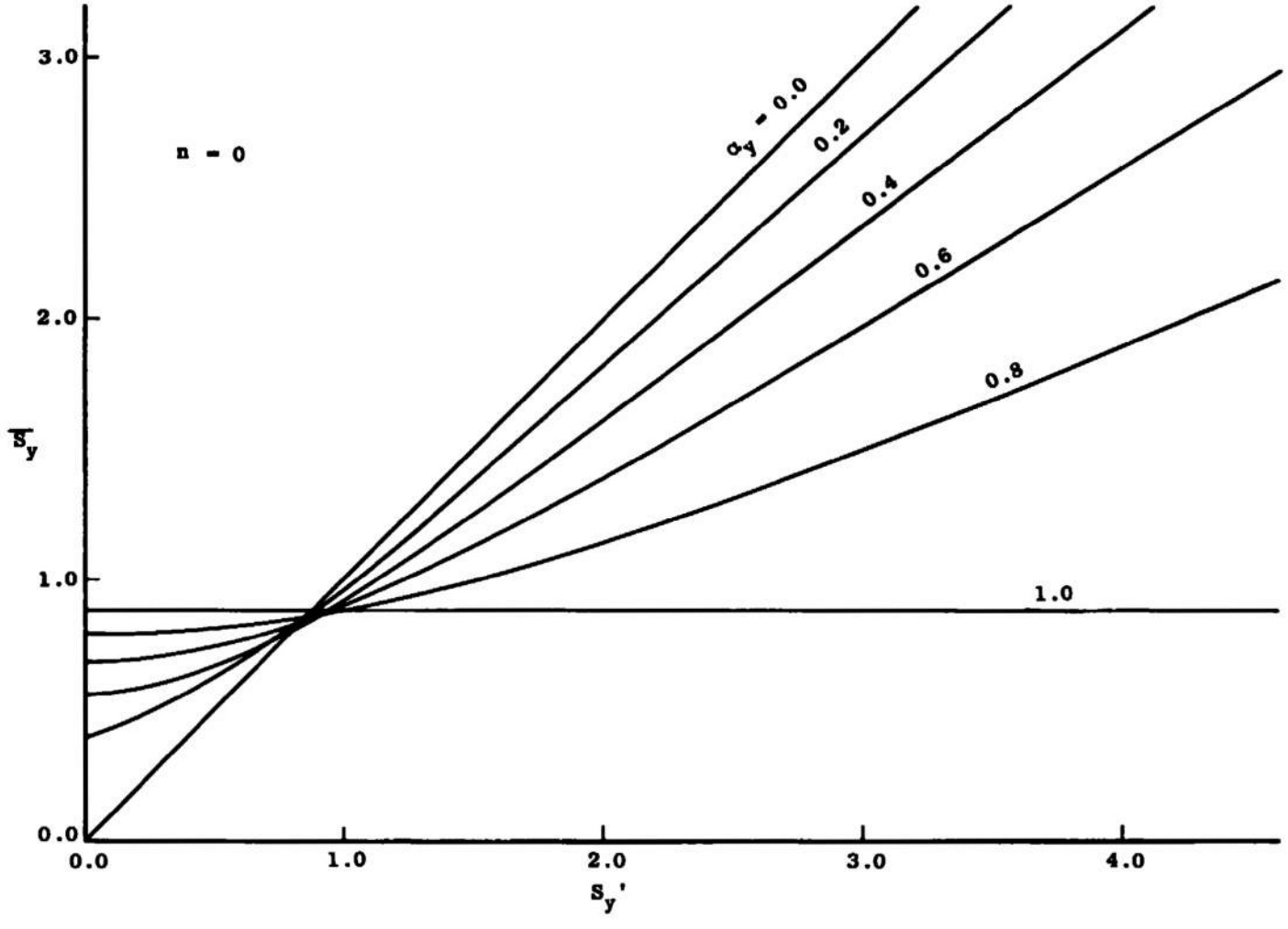

Figure 14. $\bar{S}_y$ for n = 0 in Rectangular and Cylindrical Coordinates.

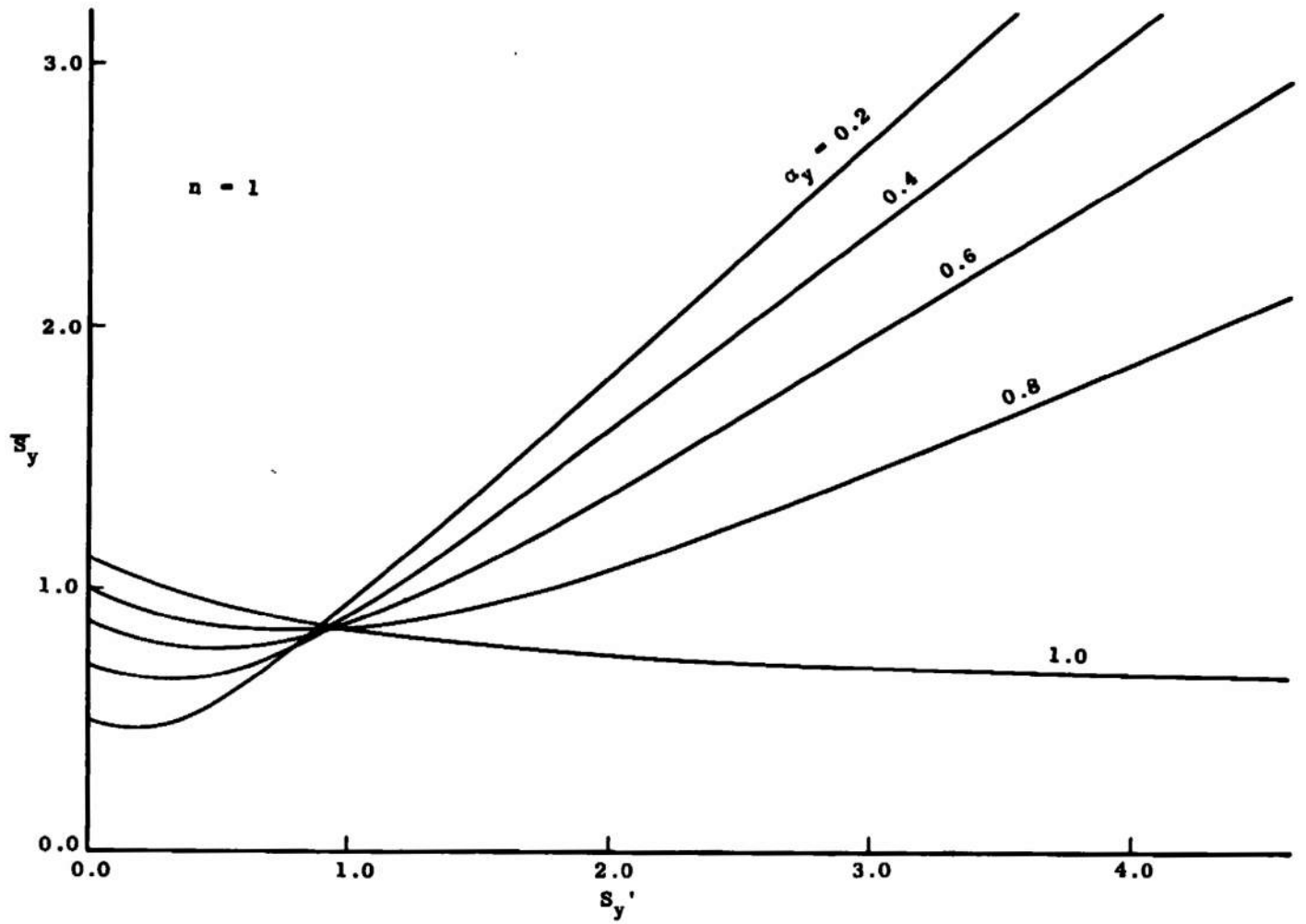

Figure 15. $\bar{S}_y$ for n = 1 in Rectangular and Cylindrical Coordinates.

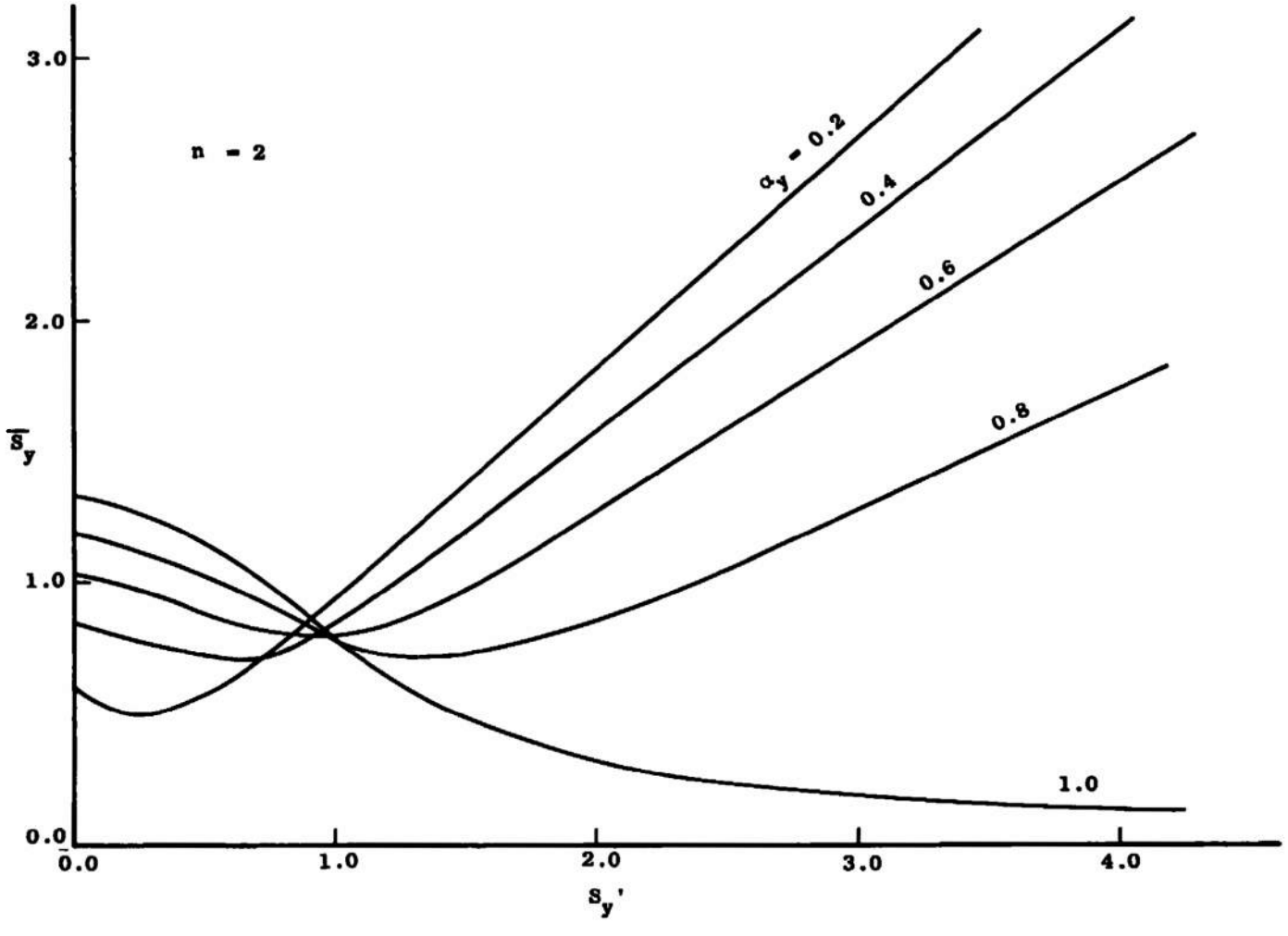

Figure 16. $\bar{S}_y$ for n = 2 in Rectangular and Cylindrical Coordinates.

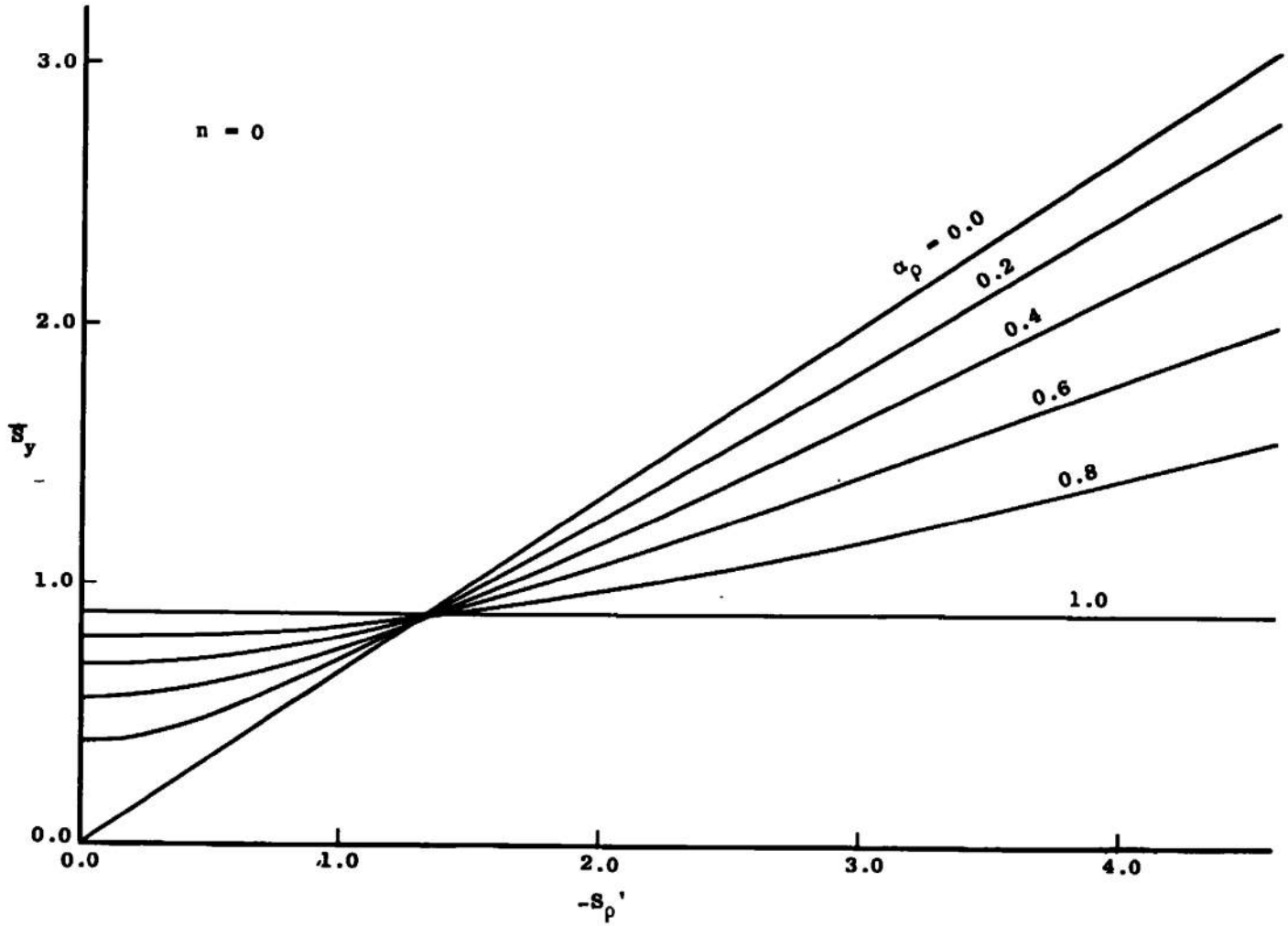

Figure 17. $\bar{S}_y$ for n = 0 in Spherical Coordinates.

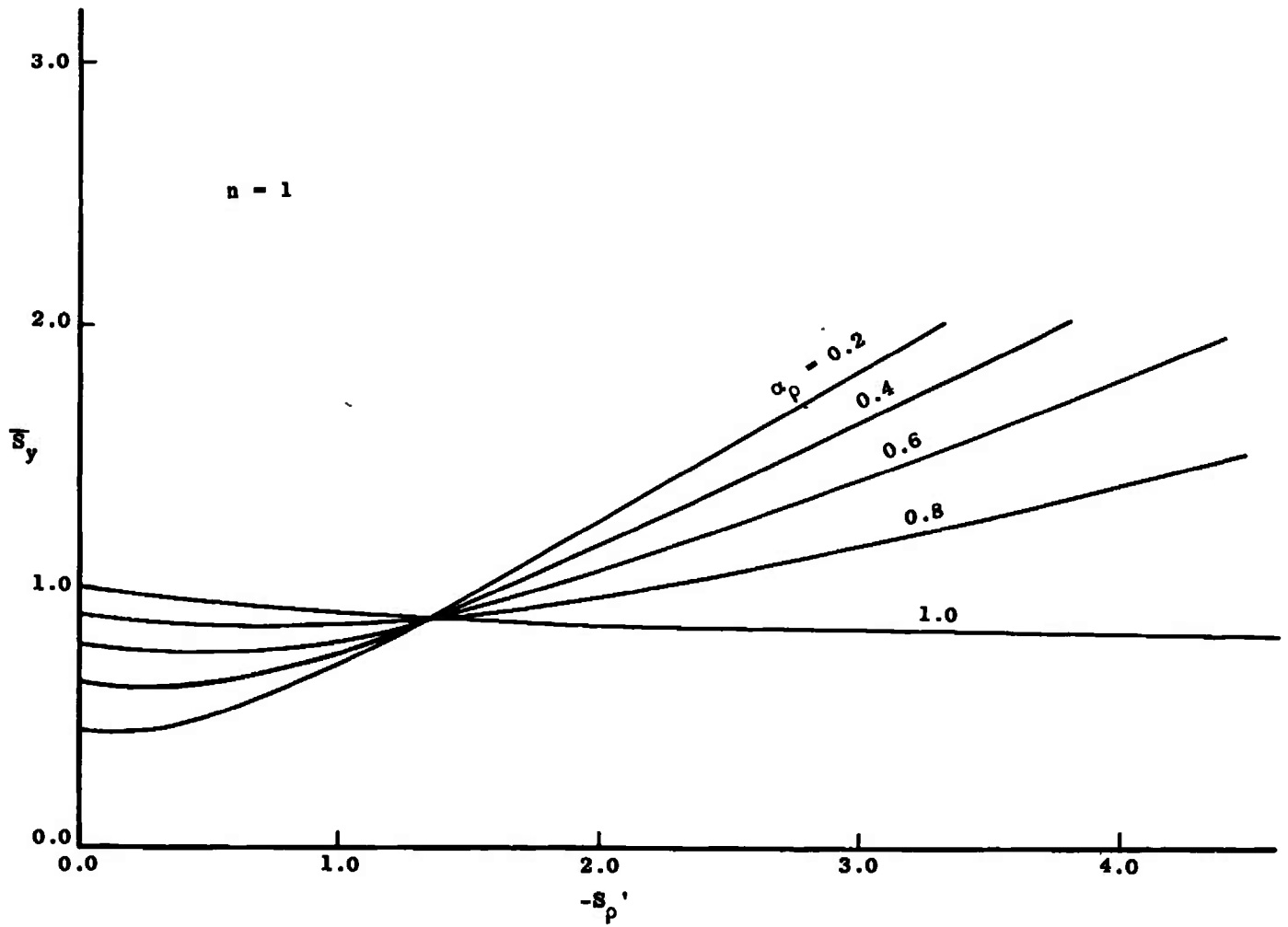

Figure 18. $\tilde{S}_y$ for n = 1 in Spherical Coordinates.

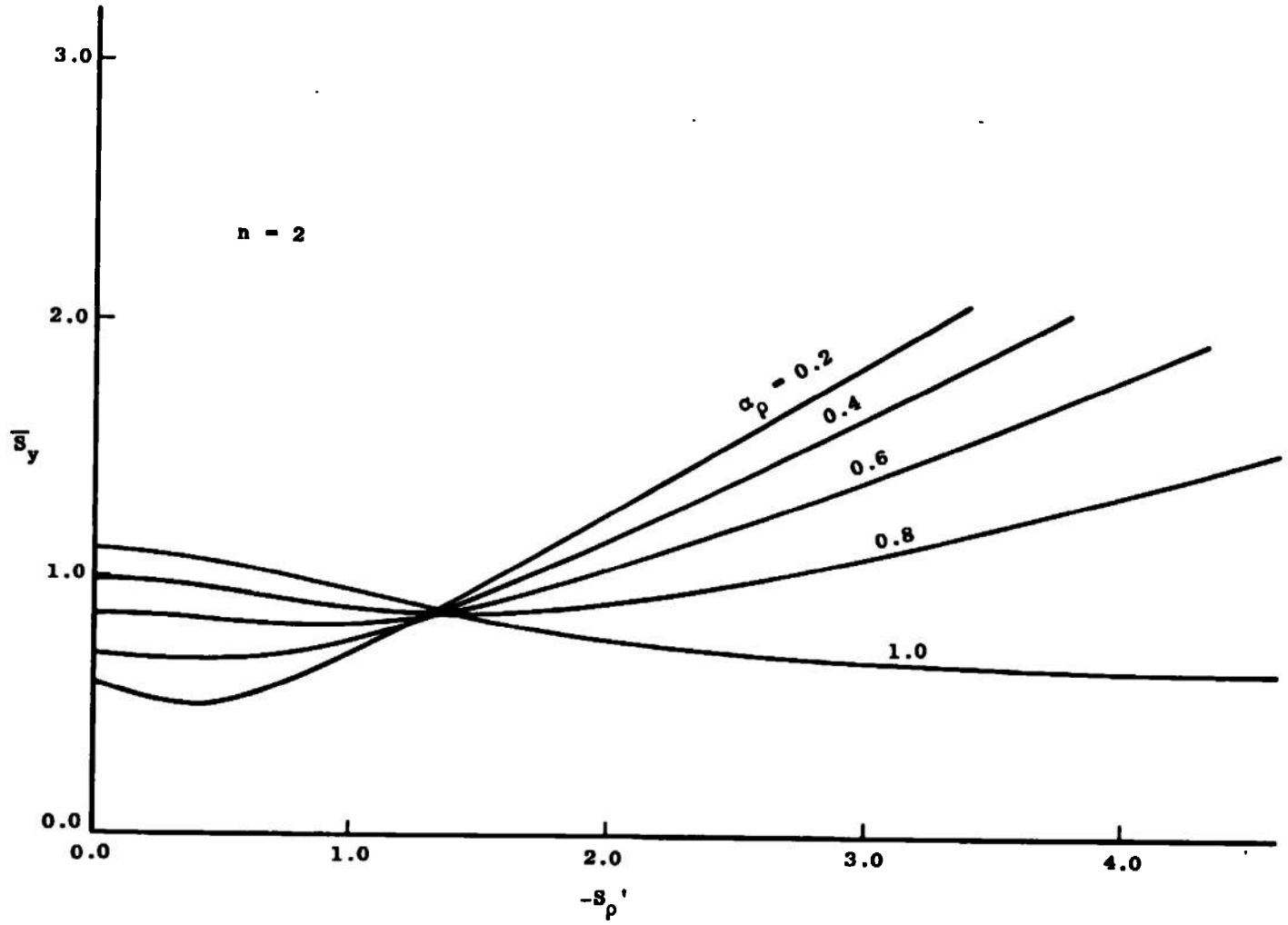

Figure 19. $\overline{S}_y$ for n = 2 in Spherical Coordinates.

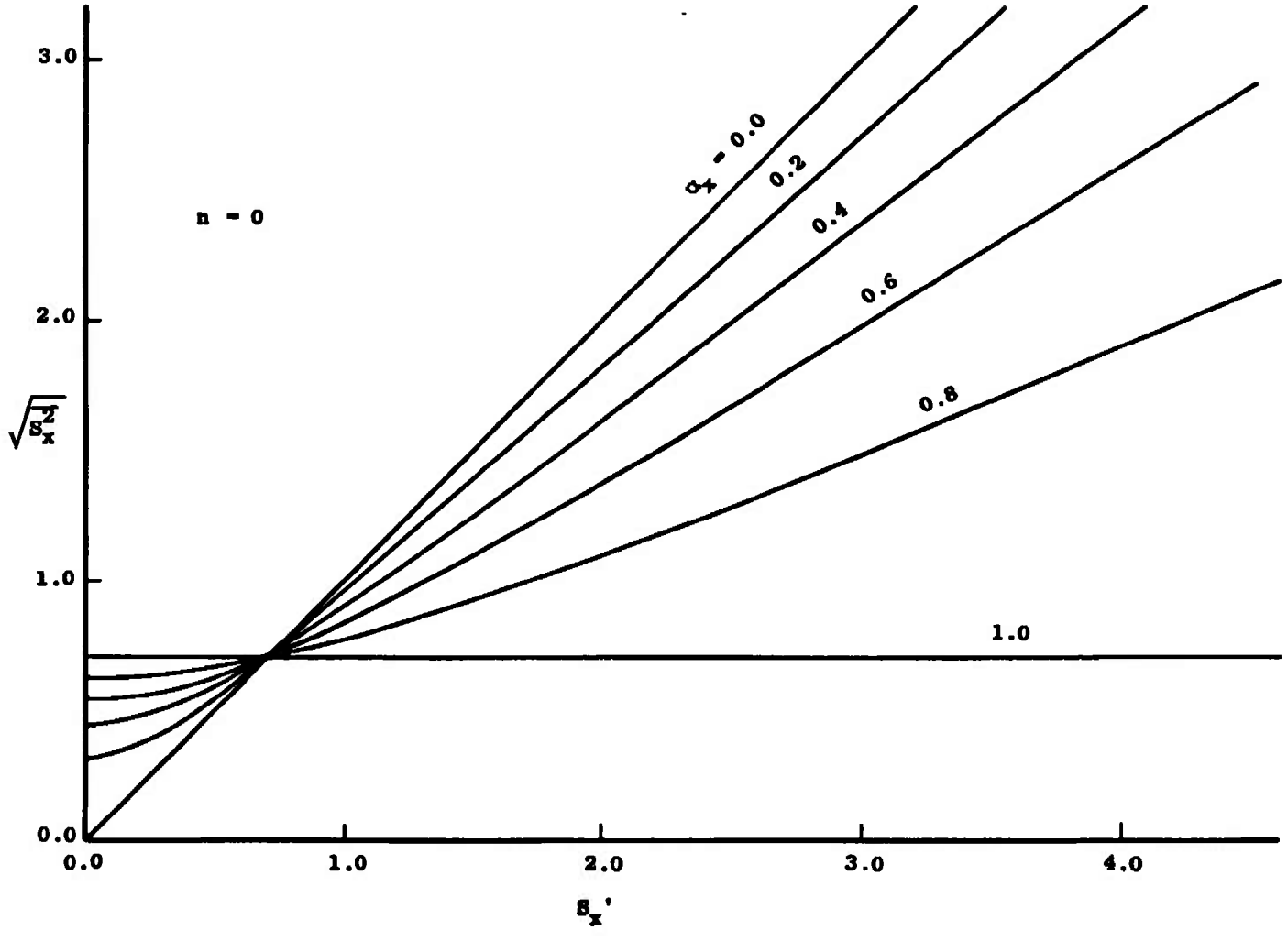

Figure 20. $\sqrt{S_x^2}$ for n = 0 in Rectangular Coordinates.

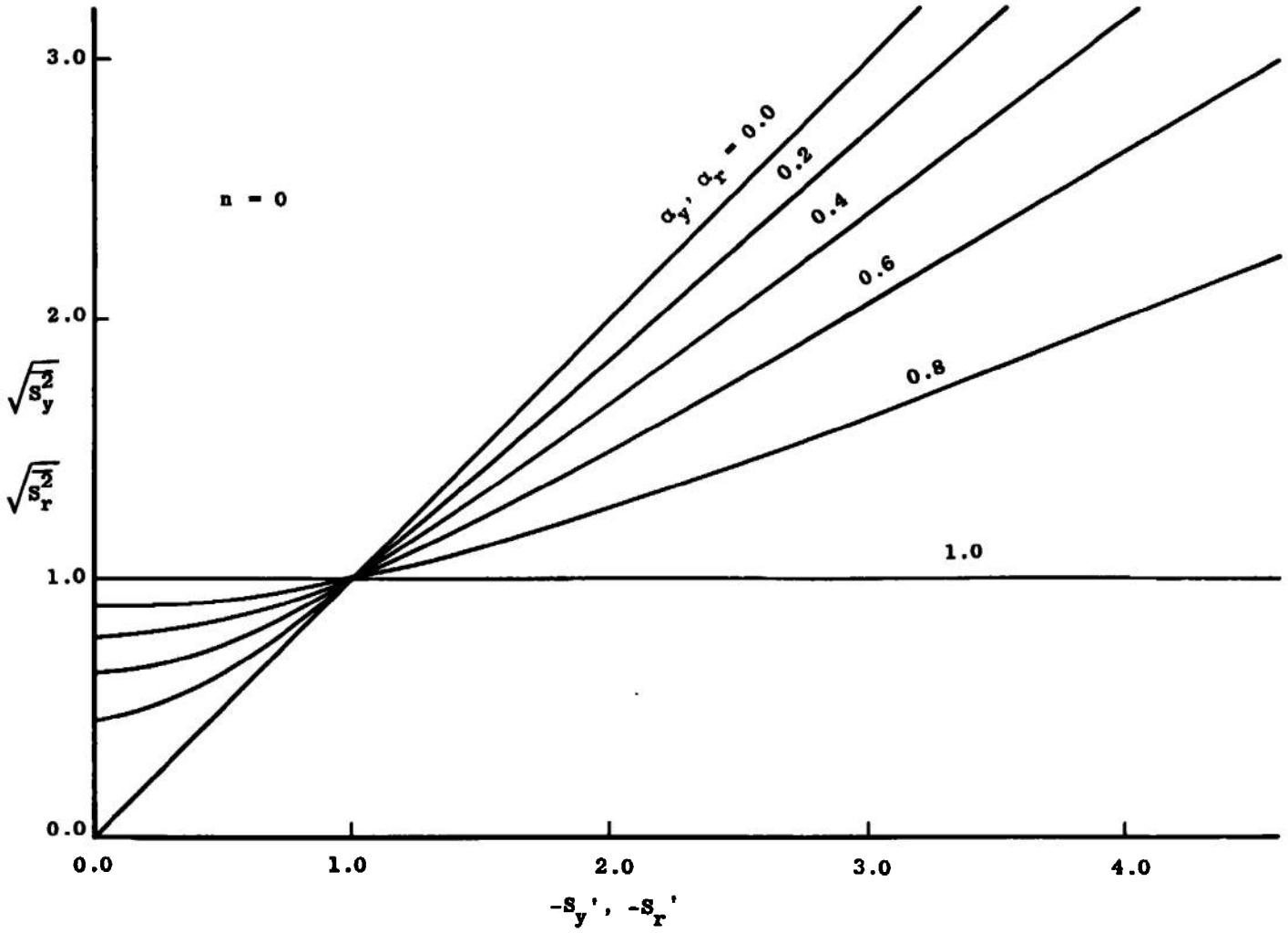

Figure 21. $\sqrt{S_y^2}$ and $\sqrt{S_r^2}$ for n = 0 in Rectangular and Cylindrical Coordinates.

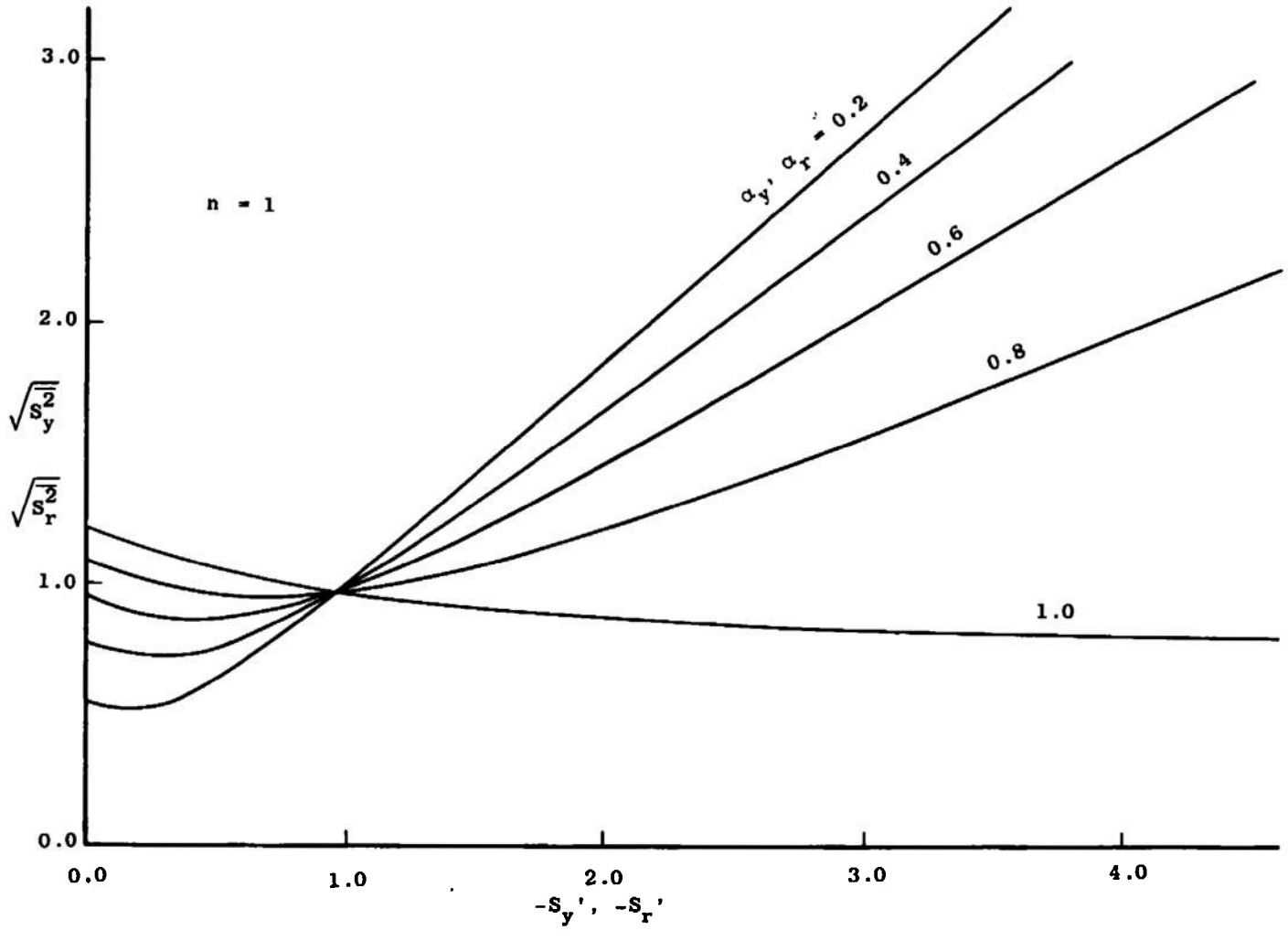

Figure 22. $\sqrt{S_y^2}$ and $\sqrt{S_r^2}$ for n = 1 in Rectangular and Cylindrical Coordinates.

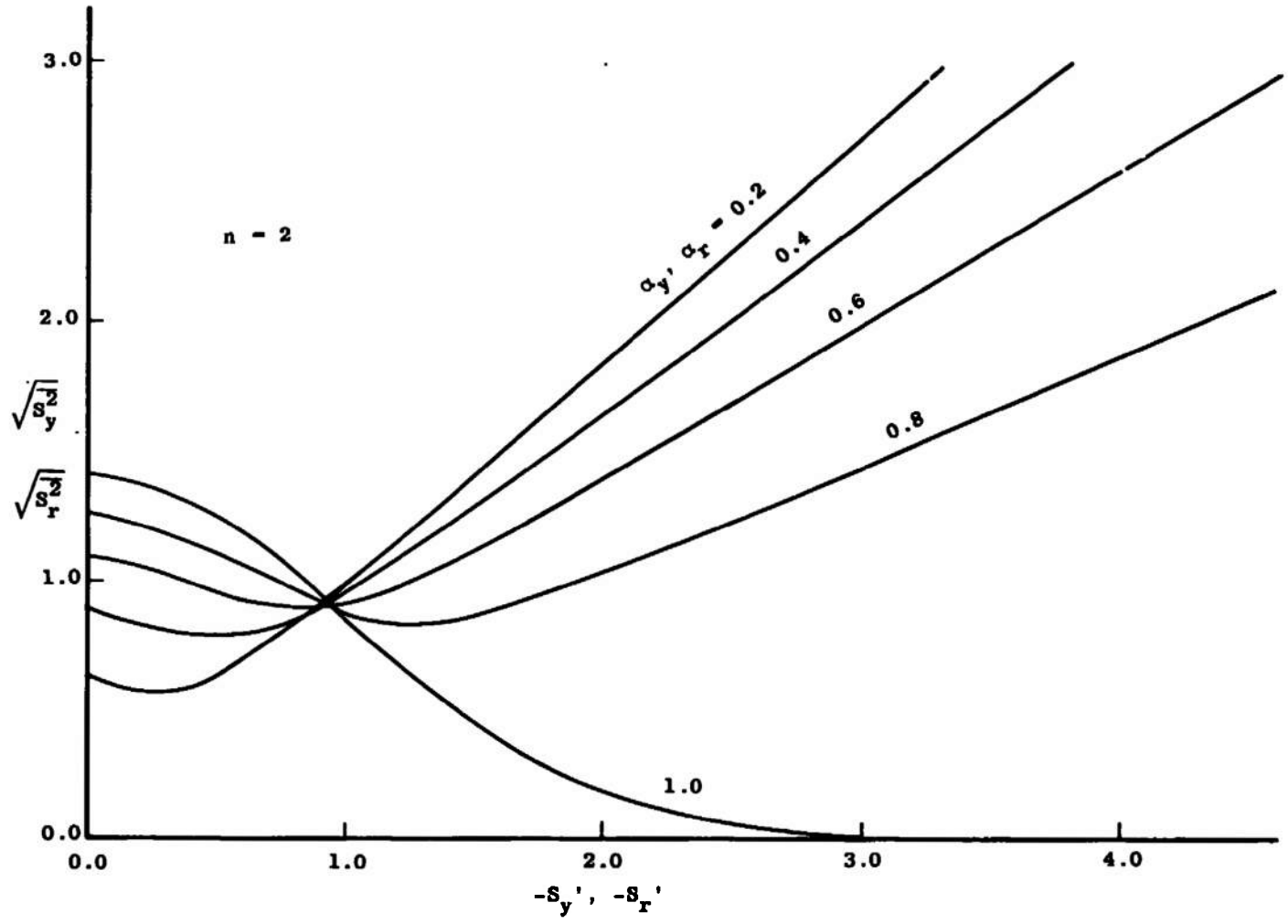

Figure 23. $\sqrt{\overline{S_y^2}}$ and $\sqrt{\overline{S_r^2}}$ for n = 2 in Rectangular and Cylindrical Coordinates.

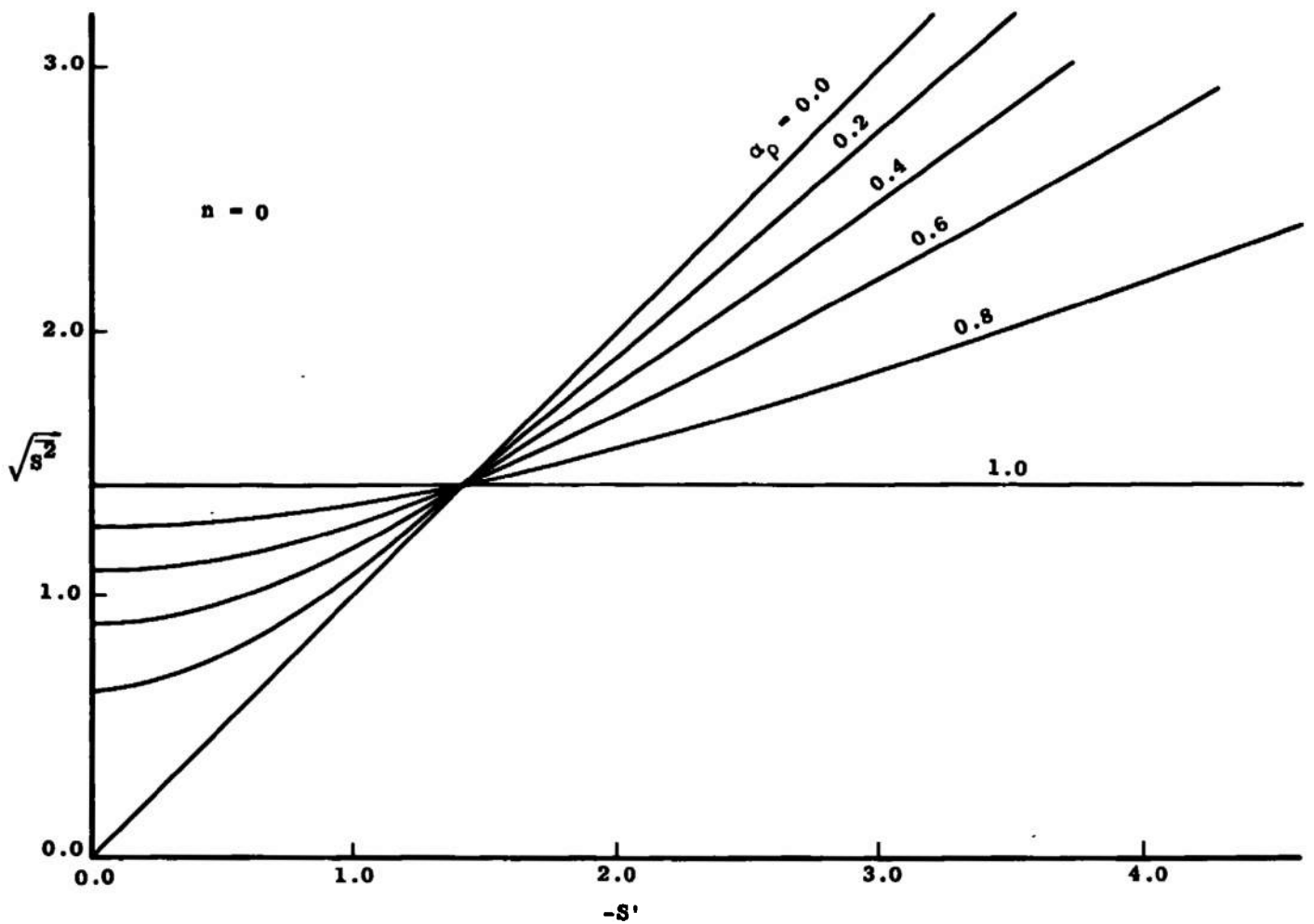

Figure 24. $\sqrt{\overline{S^2}}$ for n = 0 in Spherical Coordinates.

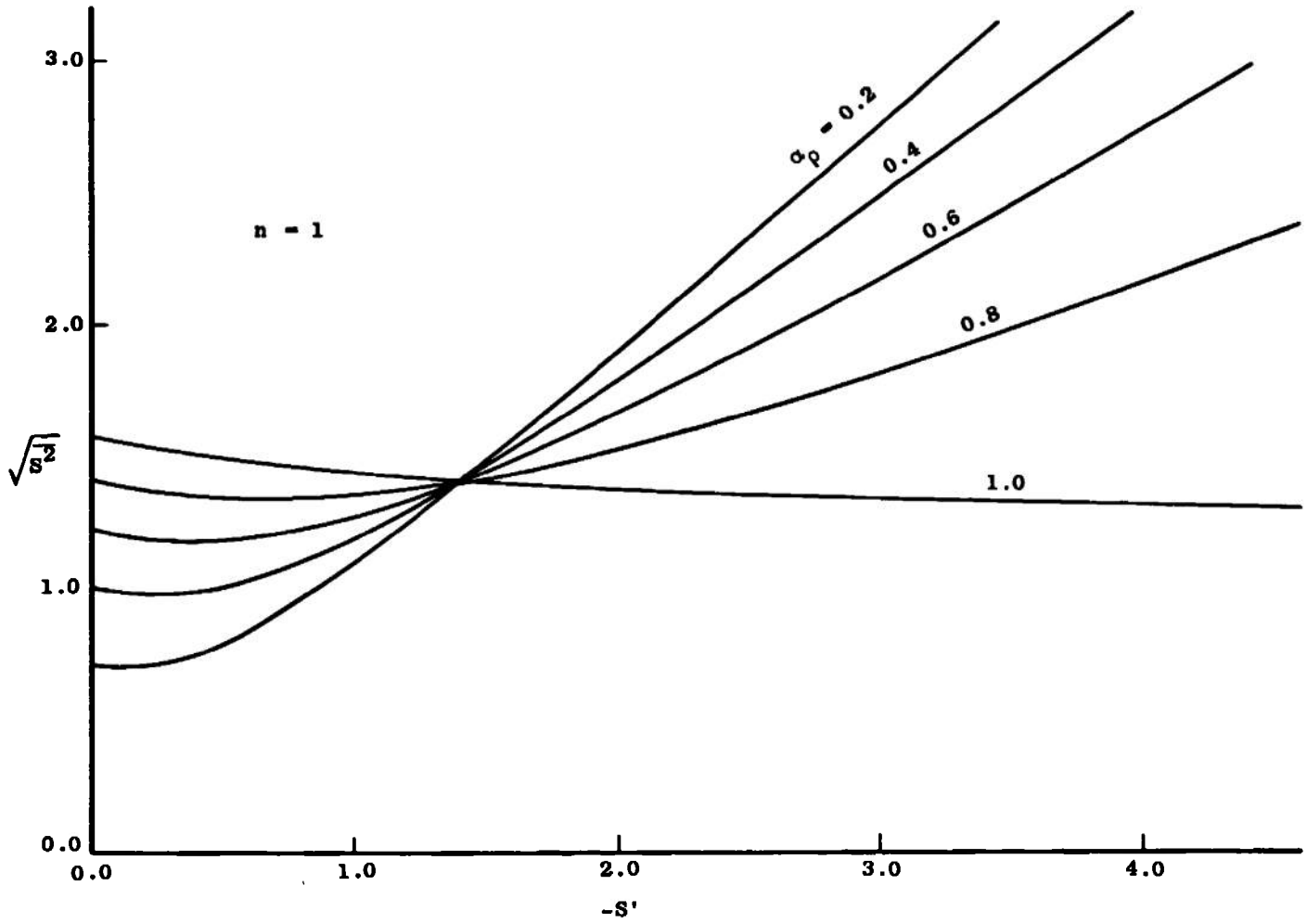

Figure 25. $\sqrt{\bar{S}^2}$ for n = 1 in Spherical Coordinates.

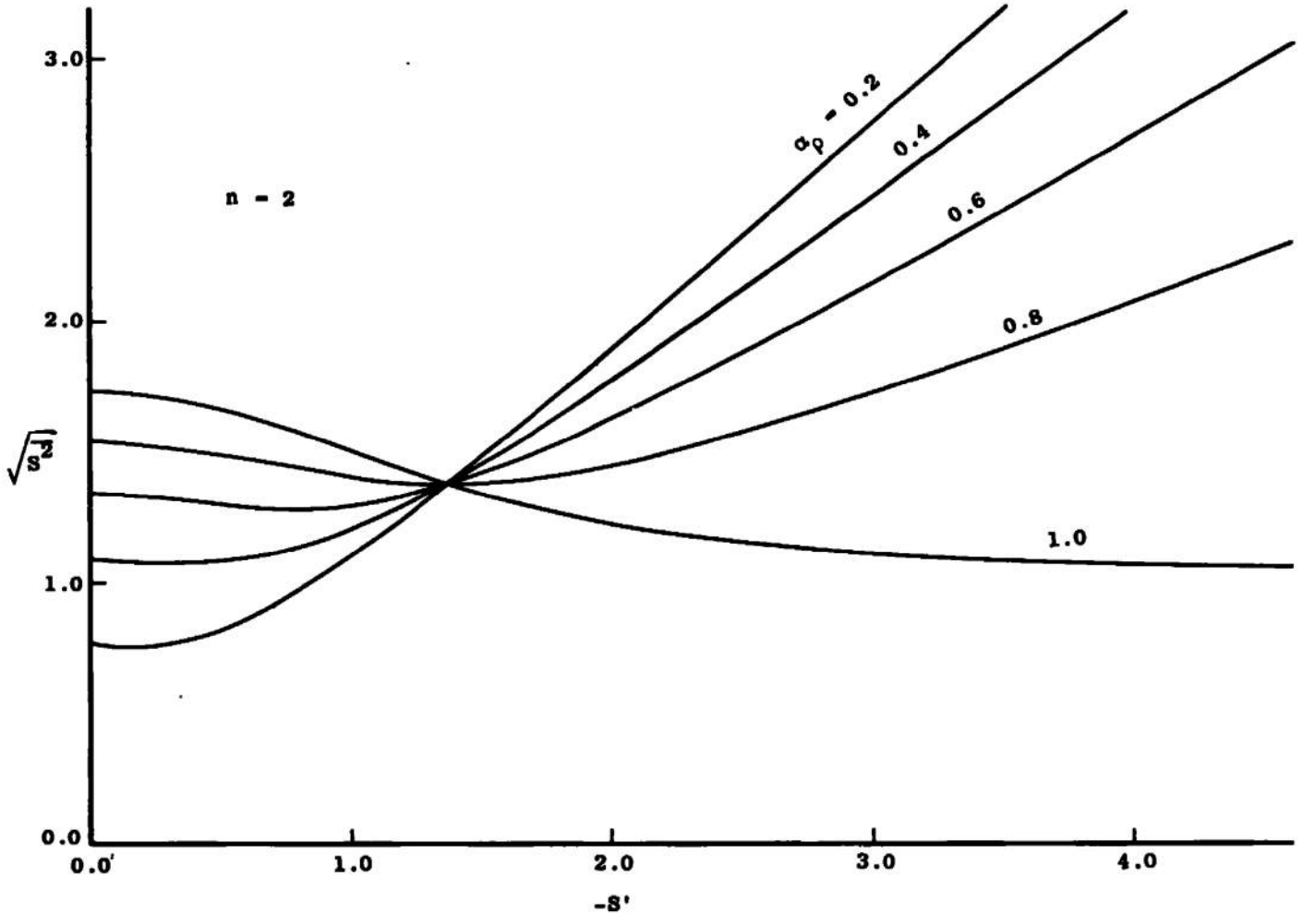

Figure 26. $\sqrt{S^2}$ for n = 2 in Spherical Coordinates.

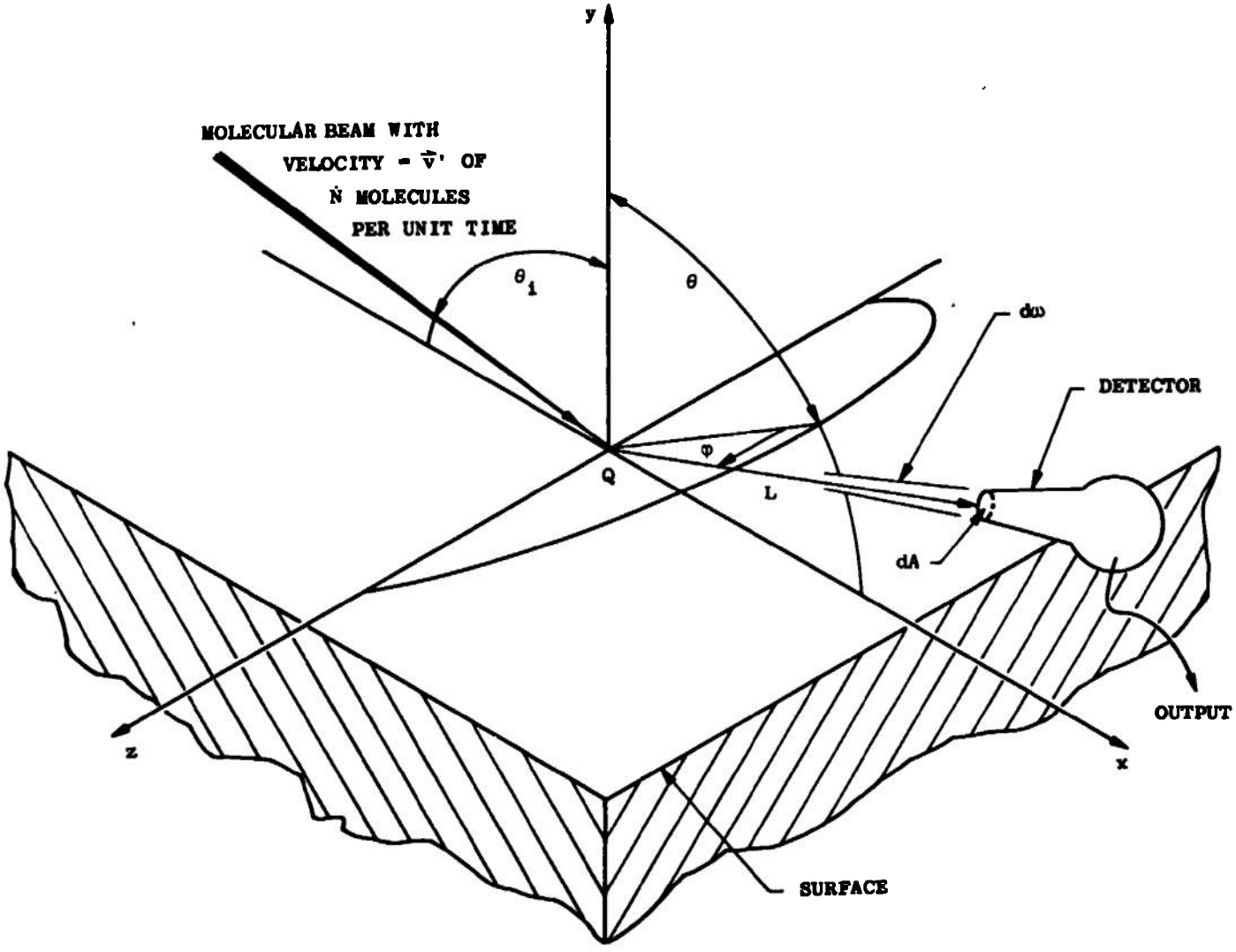

Figure 27. Molecular Beam and Detector Geometry.

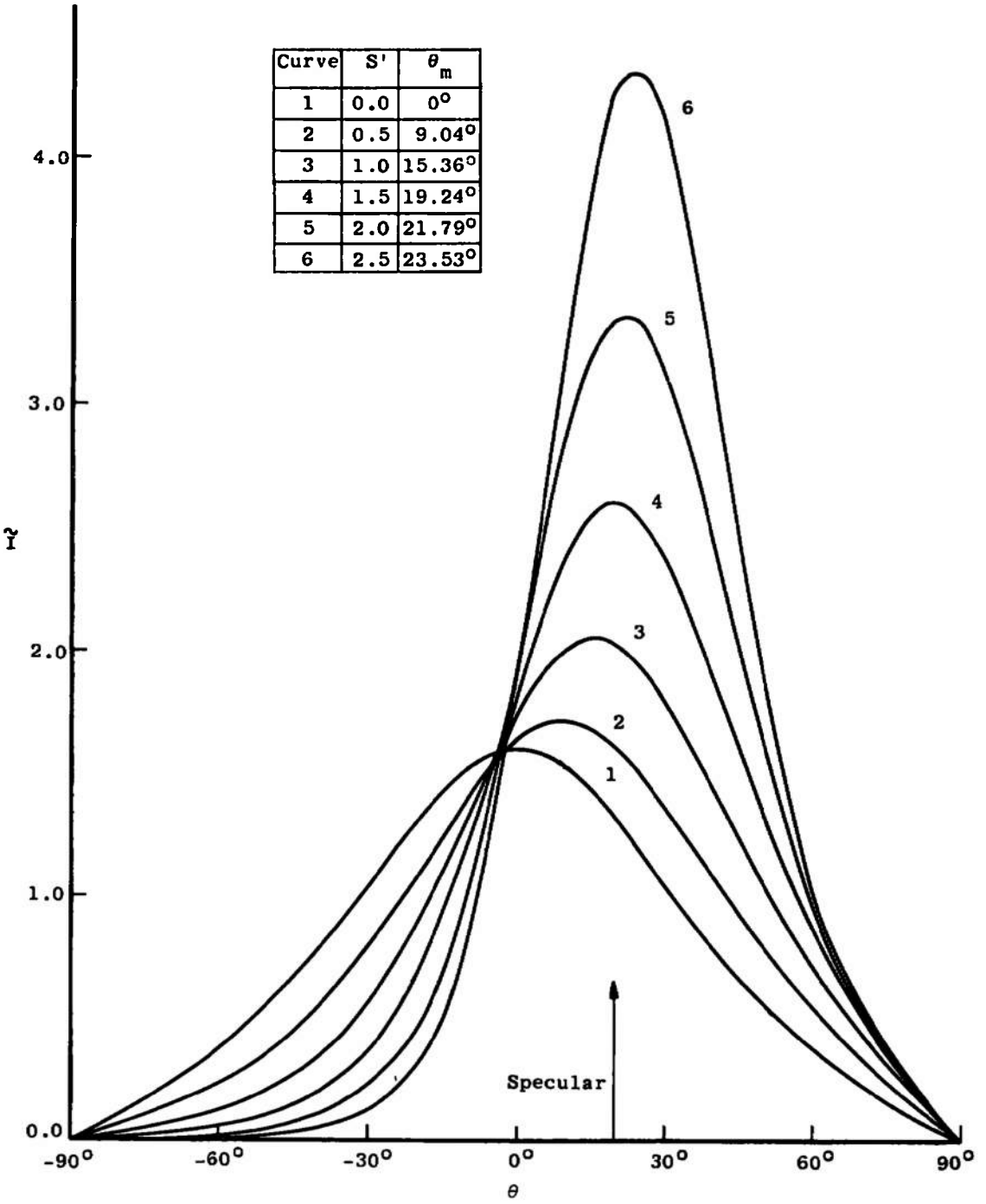

a. $\phi = 0$, $\theta_i = -20°$

Figure 28. Reflected Molecular Intensity ($a_x = 0.5$, $a_y = 0.8$).

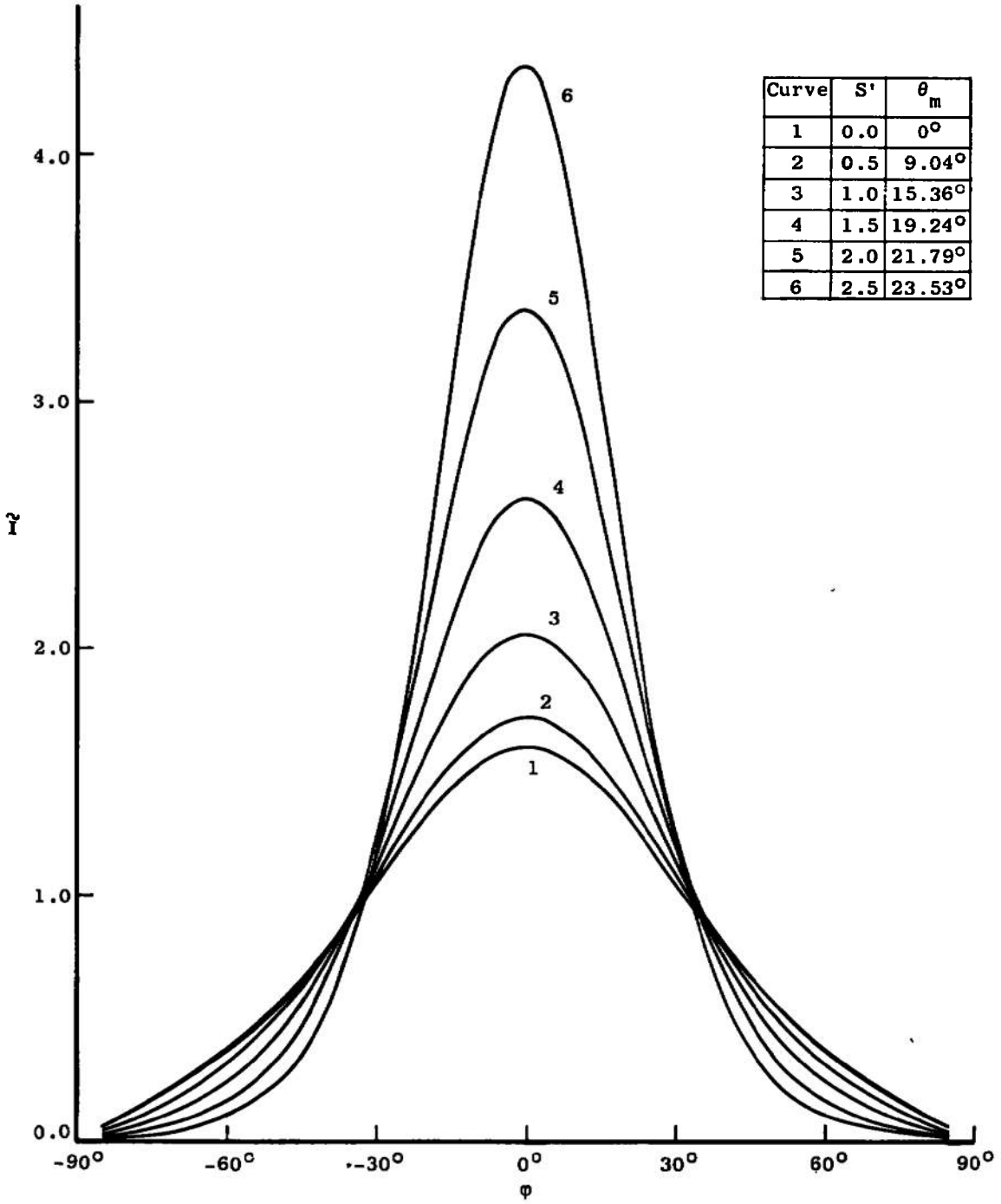

b. $\theta = \theta_m$, θ_i = -20°

Figure 28. (Continued).

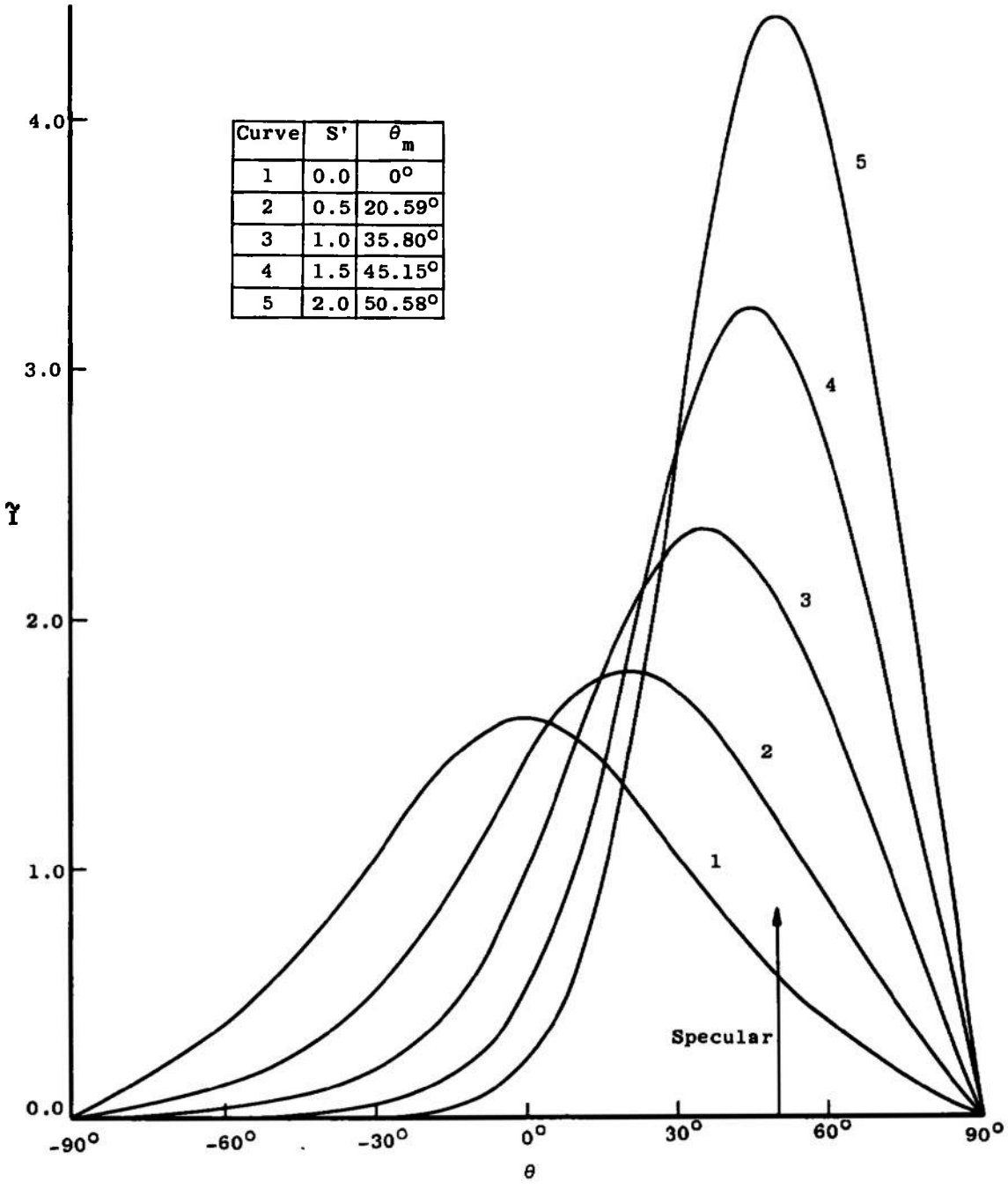

c. ϕ = 0, θ = -50°.
Figure 28. (Continued).

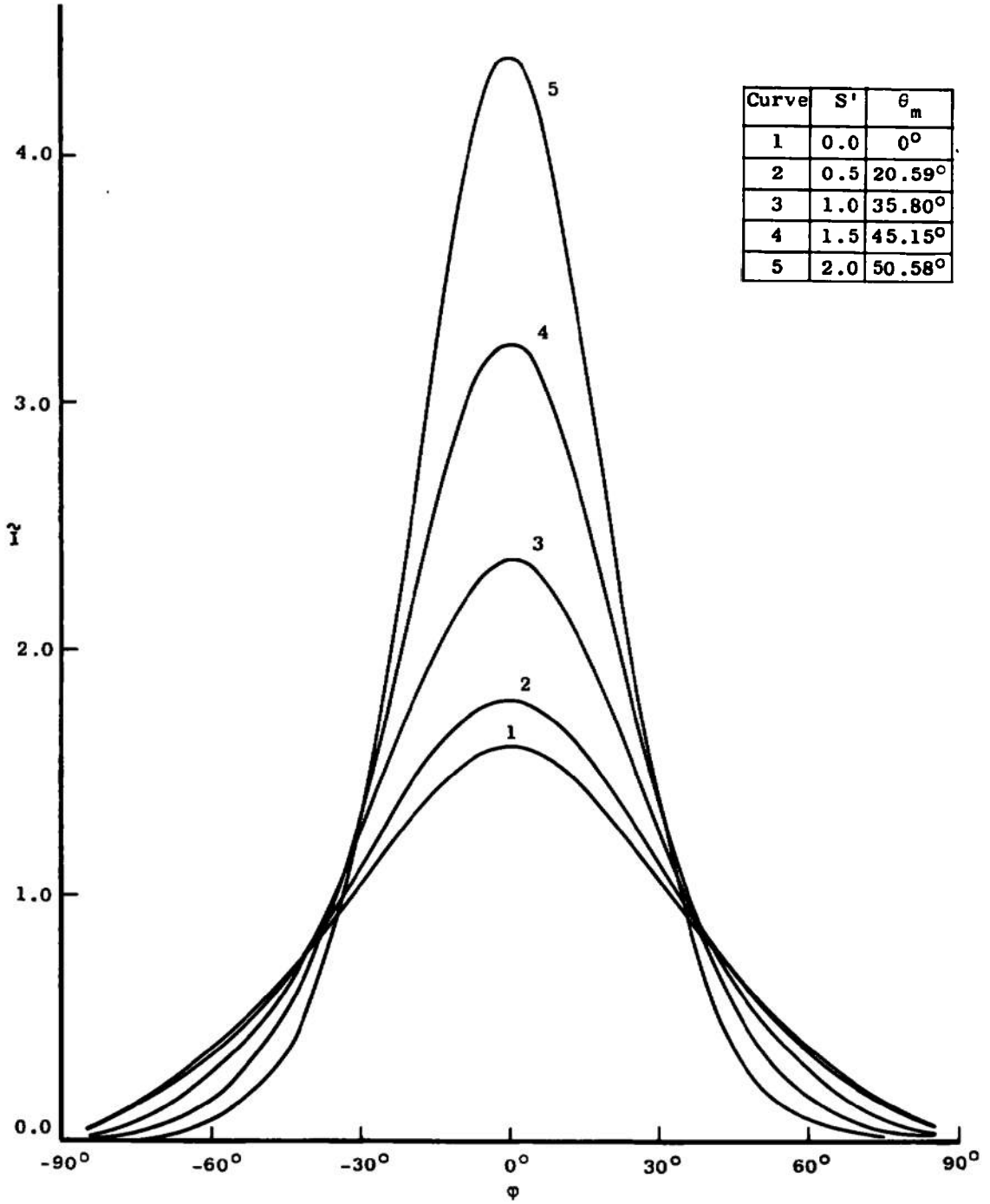

d. $\theta = \theta_m$, θ_i = -50°.
Figure 28. (Continued).

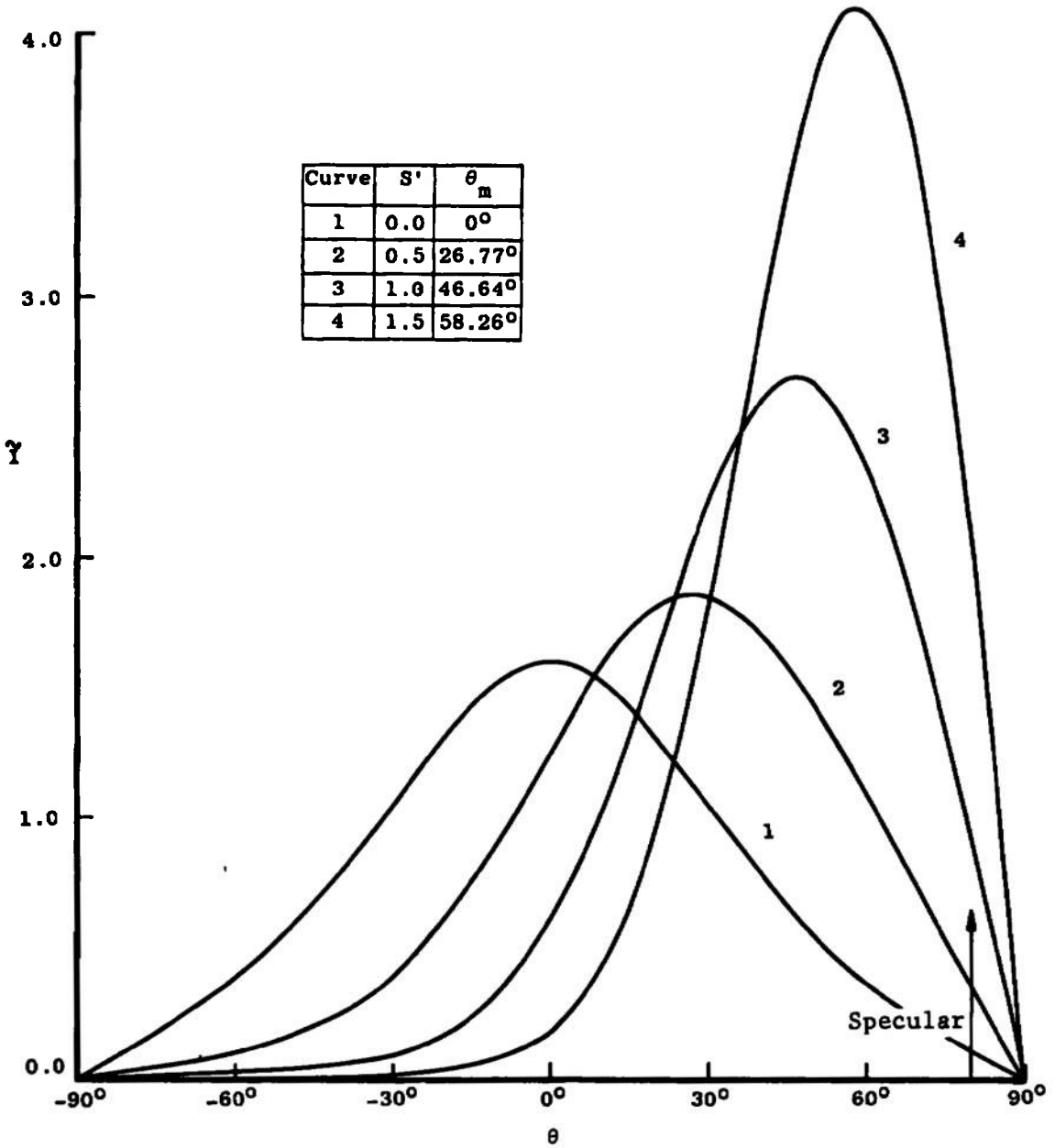

e. $\phi = 0$, $\theta_i = -80°$.
Figure 28. (Continued).

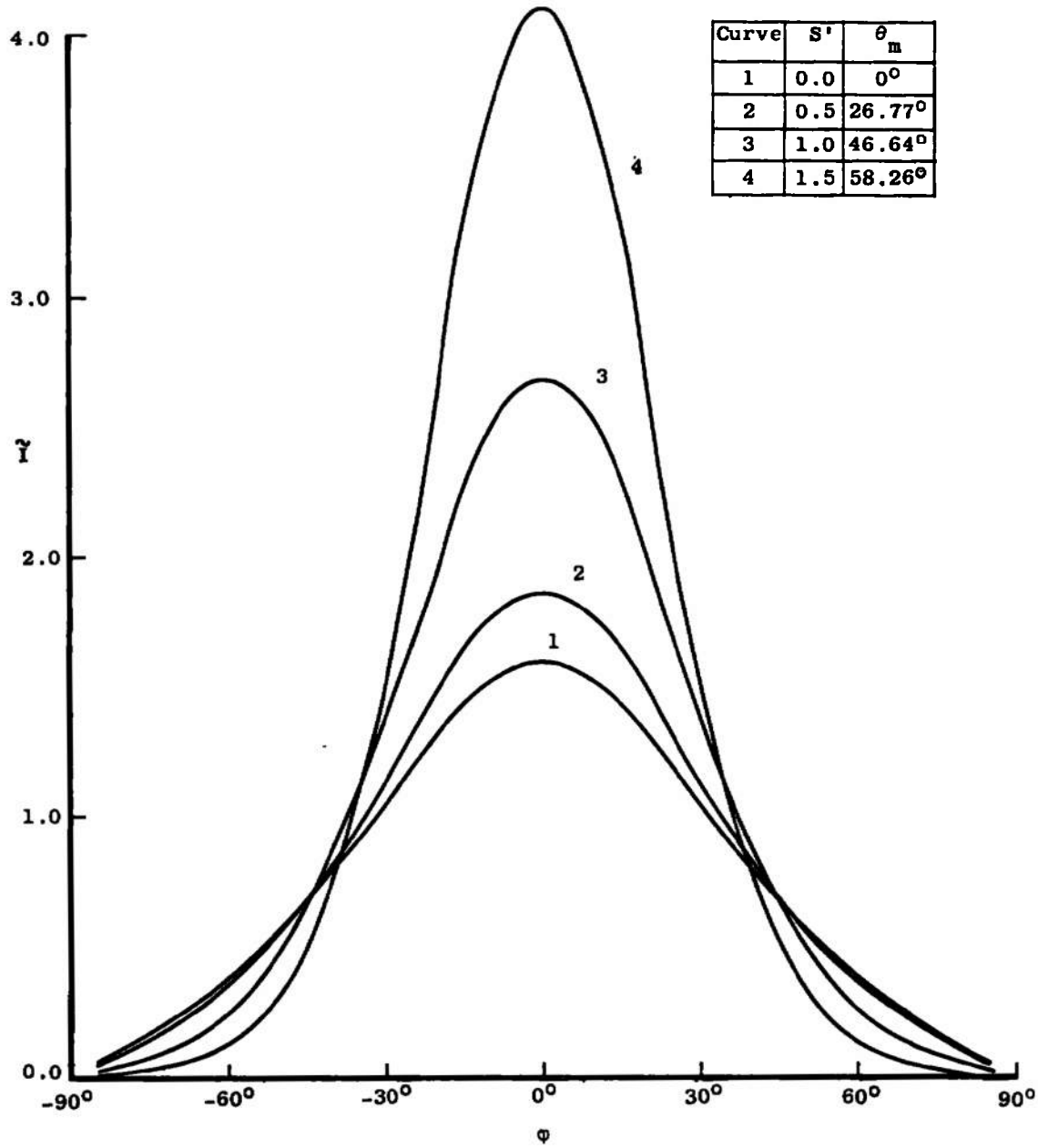

f. $\theta = \theta_m$, θ_i = -80°.
Figure 28. (Continued).

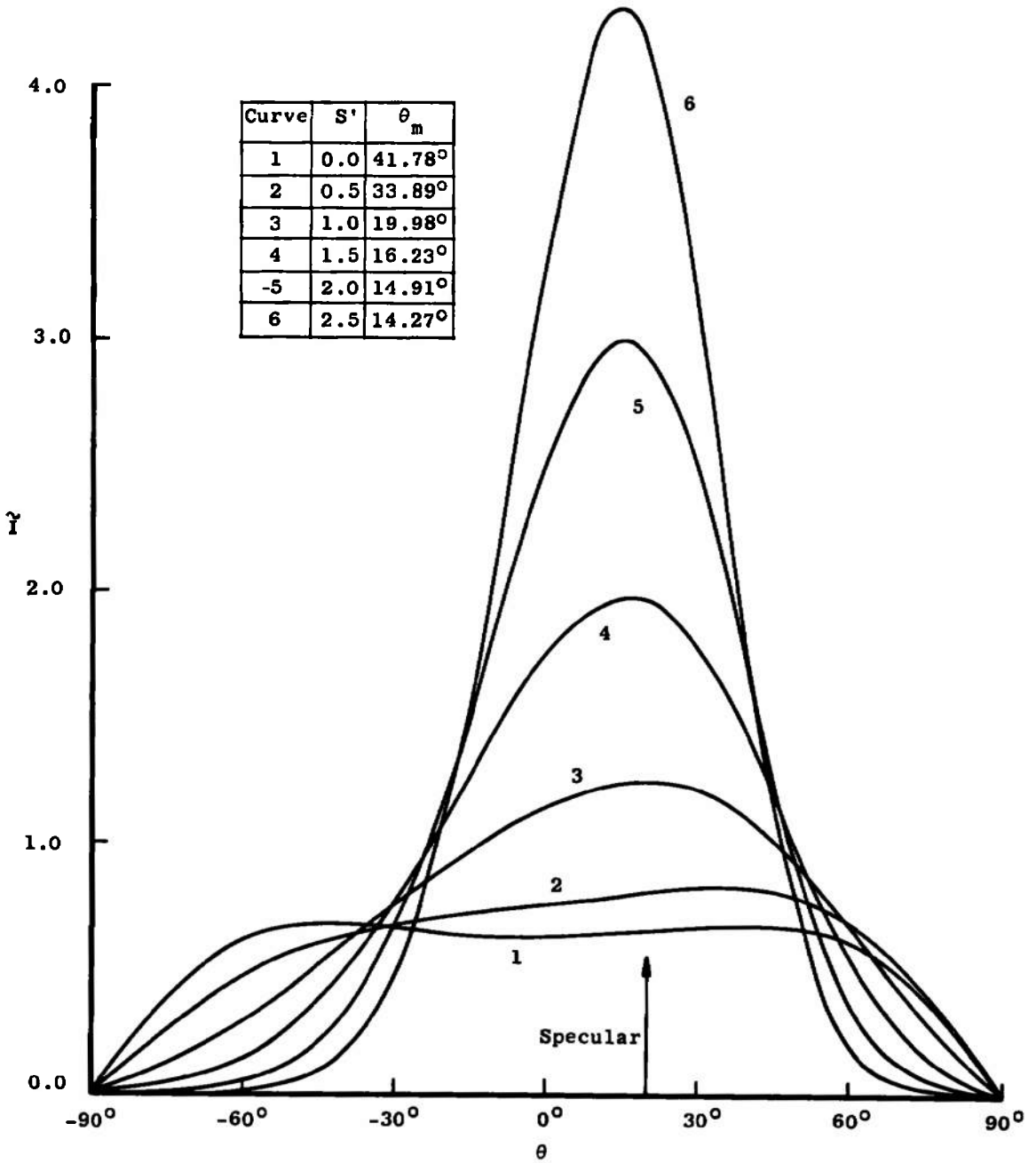

a. $\phi = 0$, $\theta_i = -20°$.

Figure 29. Reflected Molecular Intensity ($a_x = 0.8$, $a_y = 0.5$).

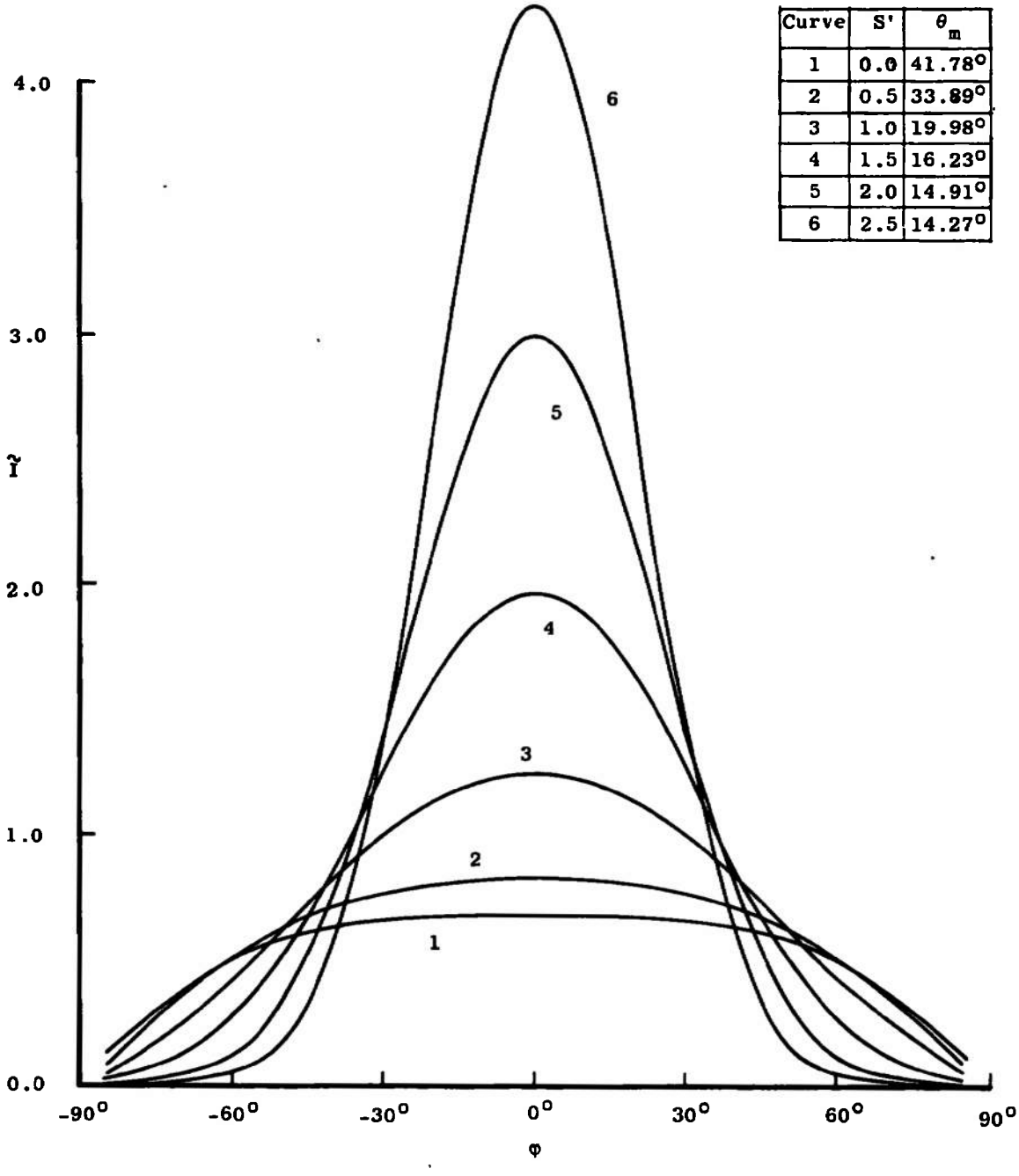

b. $\theta = \theta_m$, $\theta_i = -20°$.
Figure 29. (Continued).

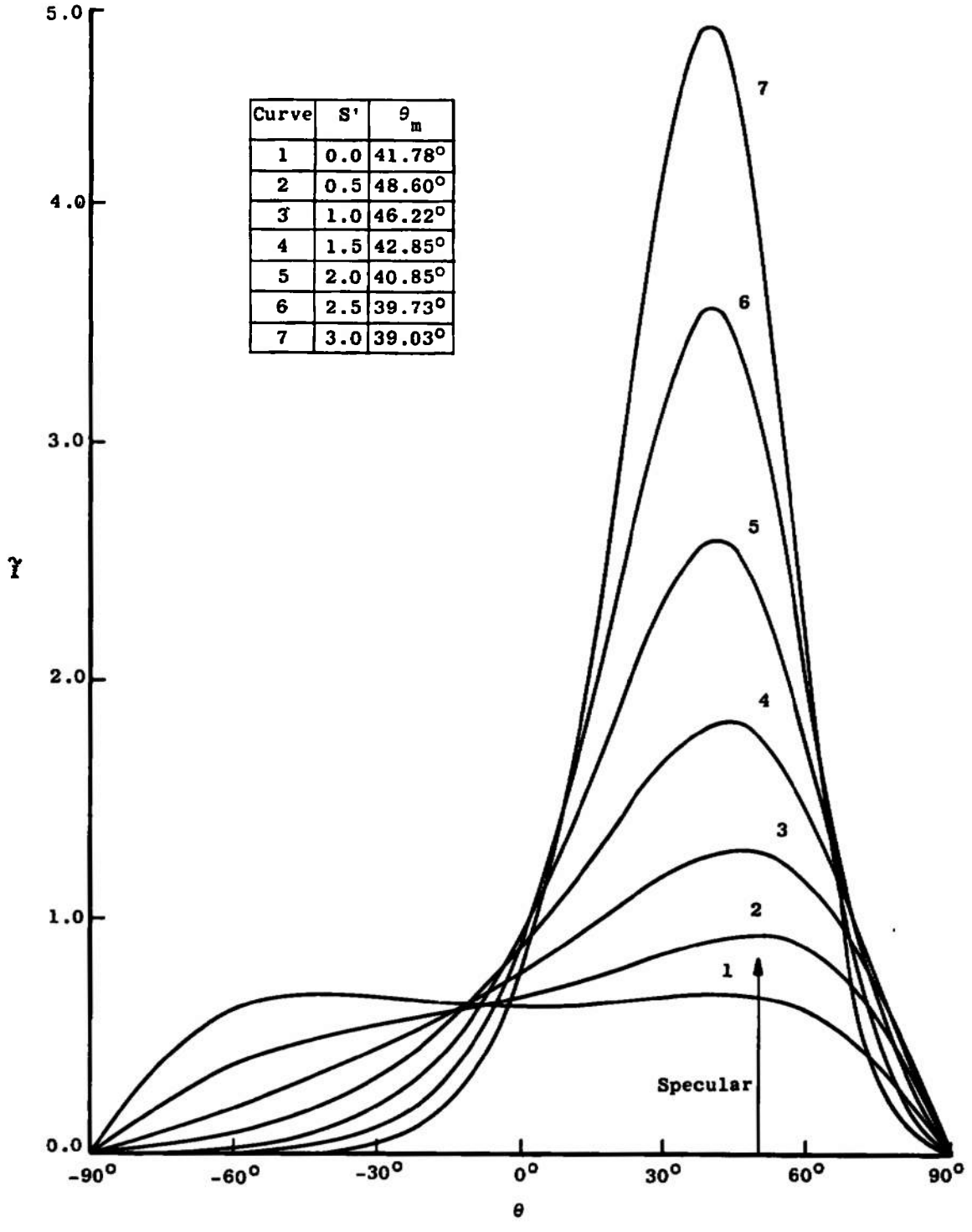

c. $\phi = 0, \theta = -50°$.

Figure 29. (Continued).

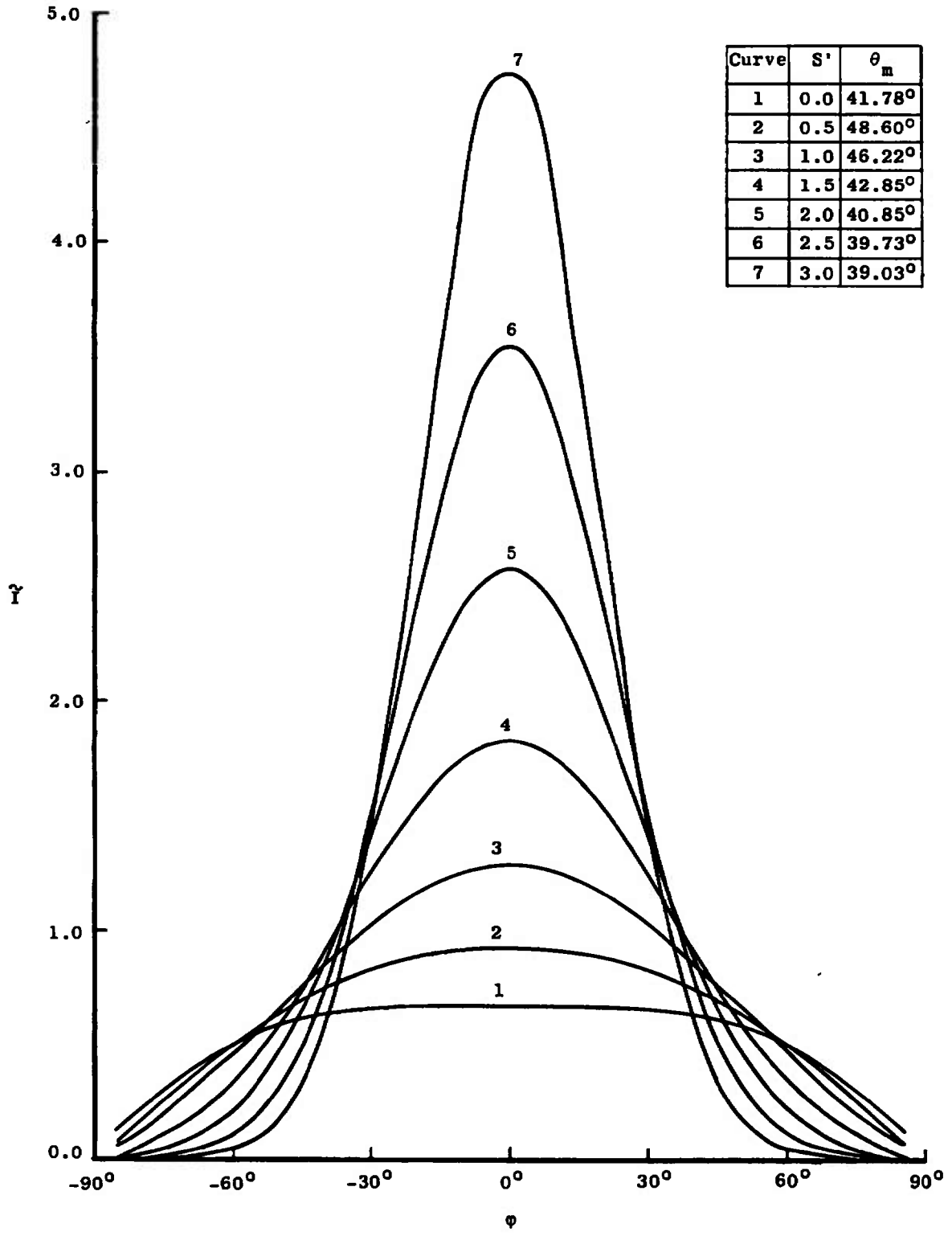

Curve	S'	θ_m
1	0.0	41.78°
2	0.5	48.60°
3	1.0	46.22°
4	1.5	42.85°
5	2.0	40.85°
6	2.5	39.73°
7	3.0	39.03°

d. $\theta = \theta_m$, θ_i = -50°.
Figure 29. (Continued).

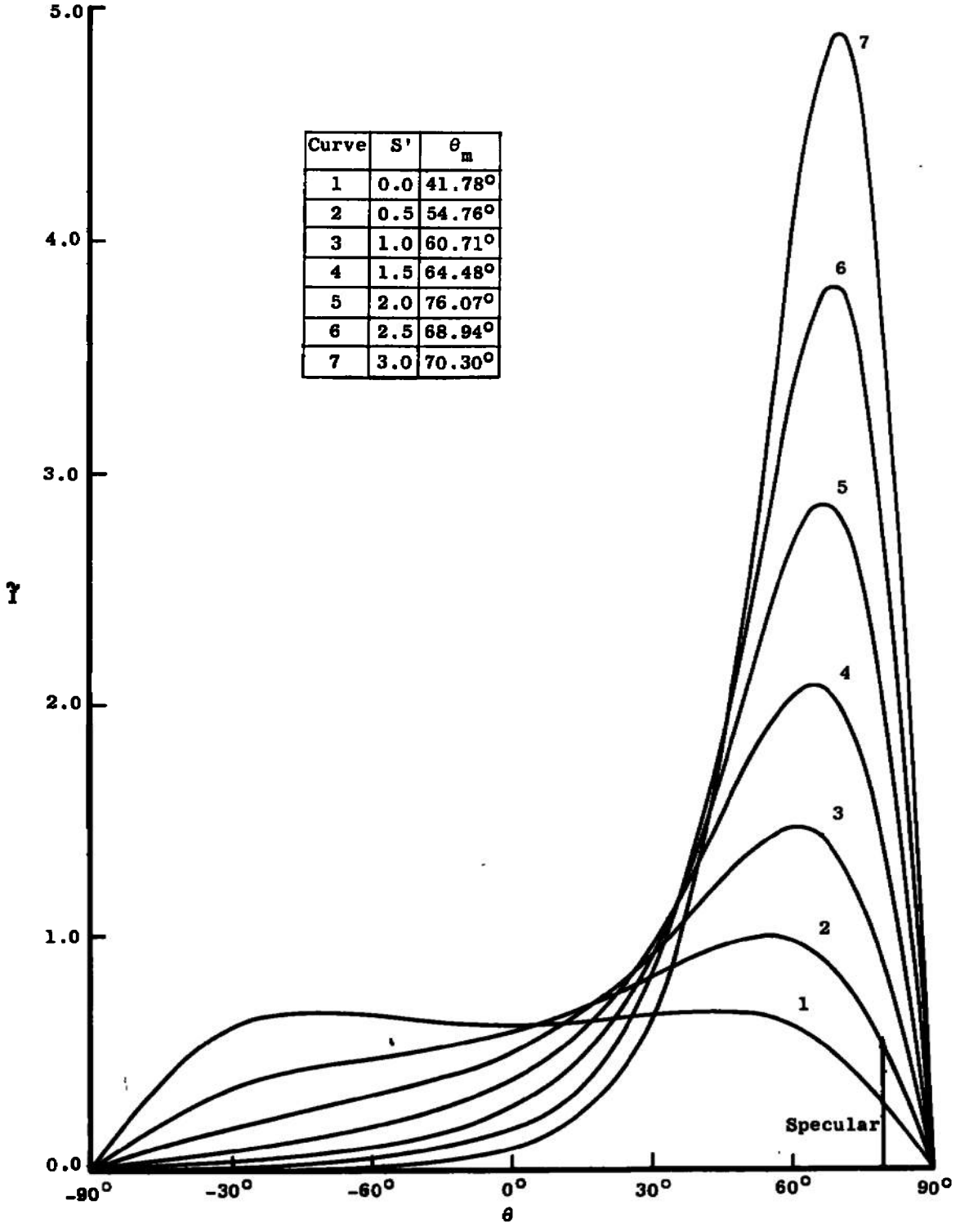

Curve	S'	θ_m
1	0.0	41.78°
2	0.5	54.76°
3	1.0	60.71°
4	1.5	64.48°
5	2.0	76.07°
6	2.5	68.94°
7	3.0	70.30°

e. $\phi = 0$, $\theta_i = -80°$.

Figure 29. (Continued).

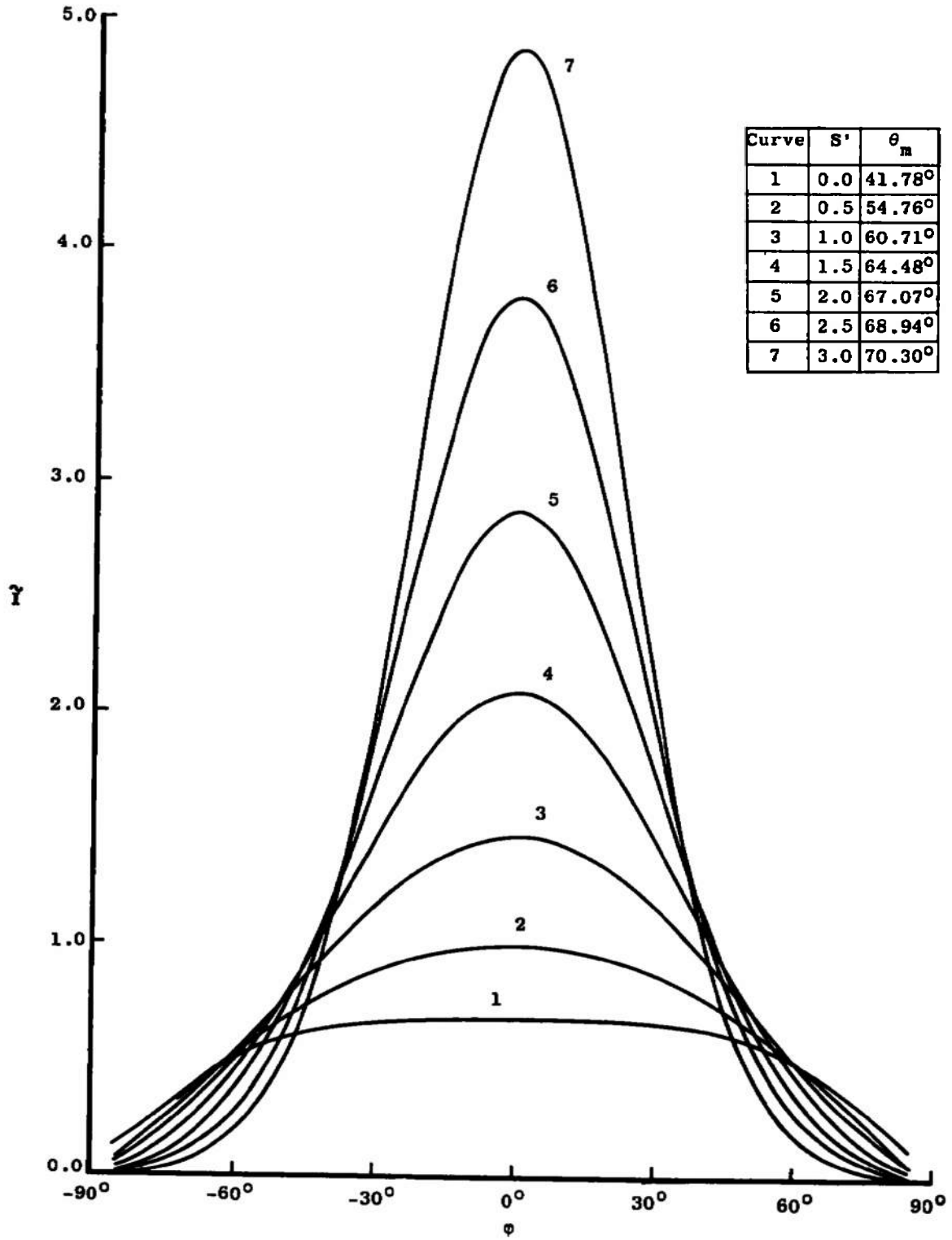

Curve	S'	θ_m
1	0.0	41.78°
2	0.5	54.76°
3	1.0	60.71°
4	1.5	64.48°
5	2.0	67.07°
6	2.5	68.94°
7	3.0	70.30°

f. $\theta = \theta_m$, $\theta_i = -80°$.

Figure 29. (Continued).

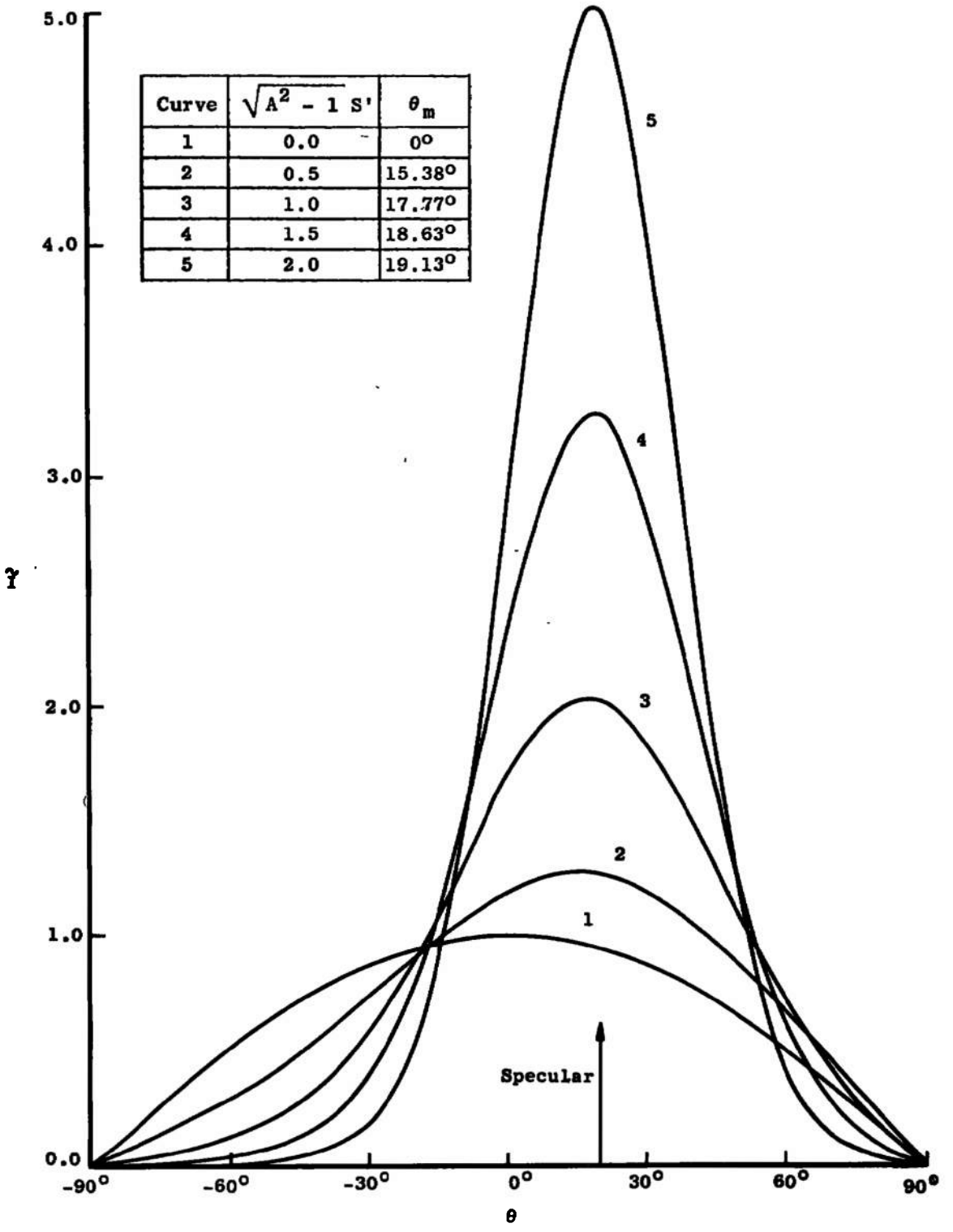

a. $\phi = 0$, $\theta_i = -20°$.

Figure 30. Reflected Molecular Intensity ($a_x = a_y = A^{-2}$).

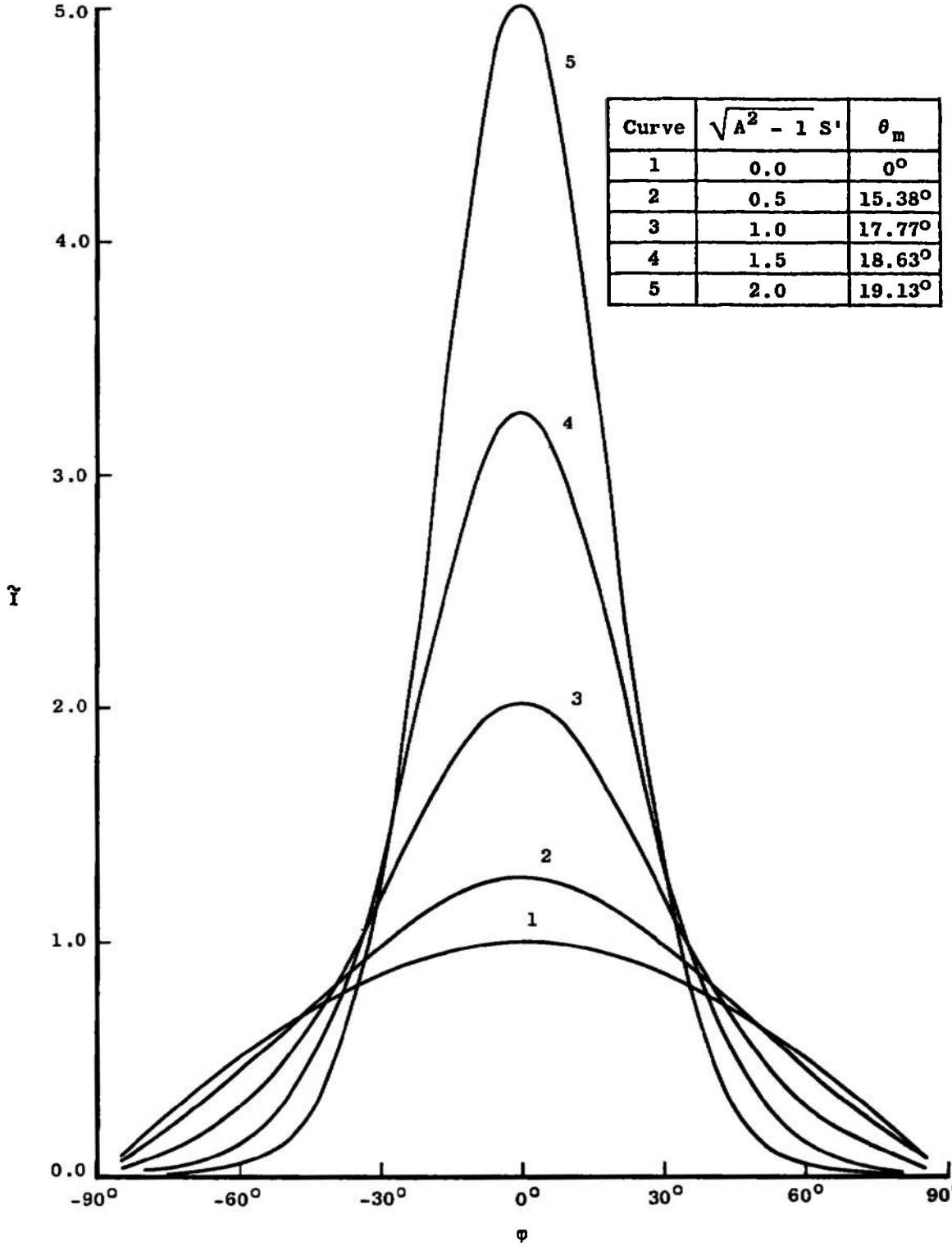

Curve	$\sqrt{A^2 - 1}\, S'$	θ_m
1	0.0	0°
2	0.5	15.38°
3	1.0	17.77°
4	1.5	18.63°
5	2.0	19.13°

b. $\theta = \theta_m$, θ_i = -20°.
Figure 30. (Continued).

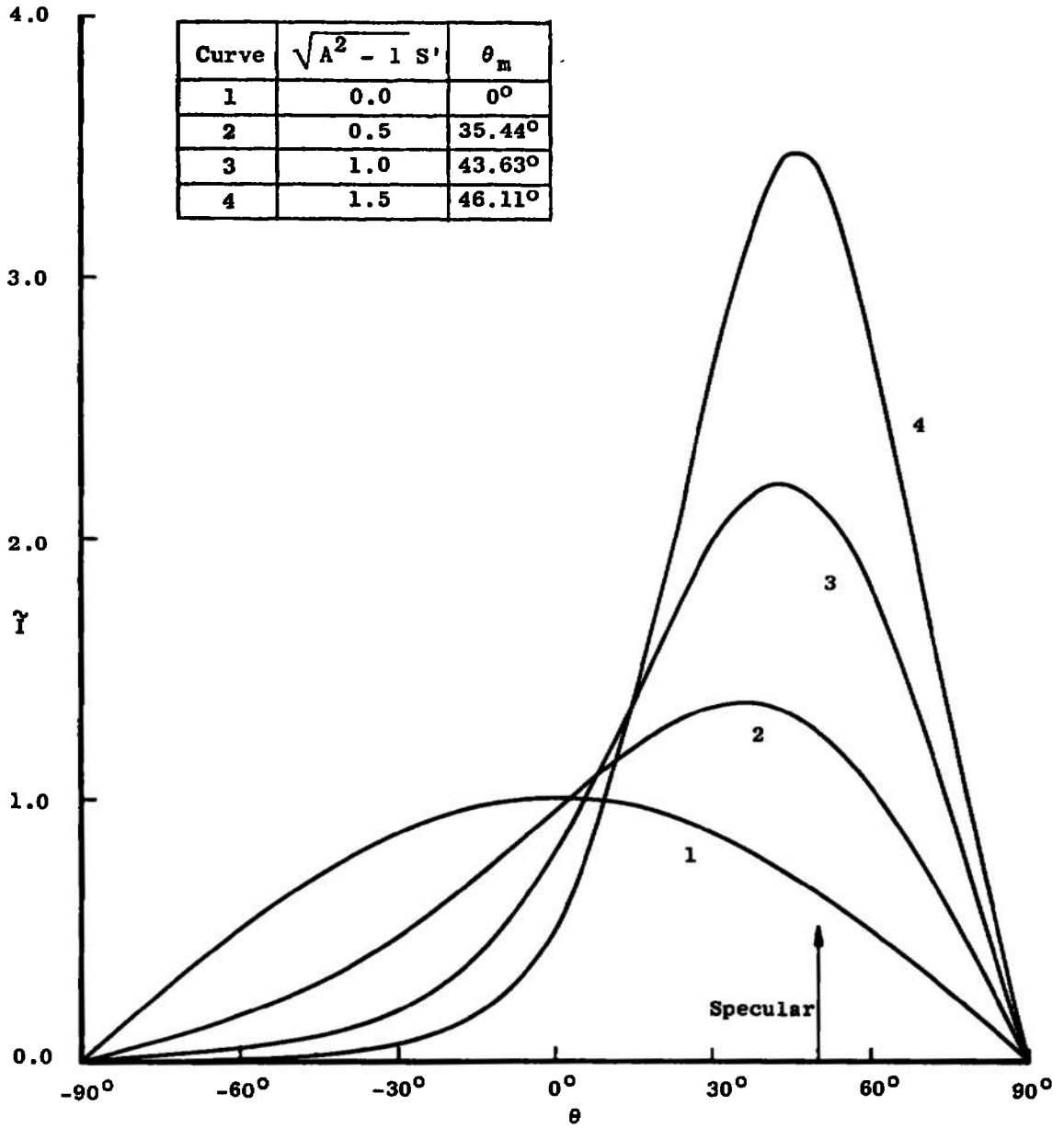

Curve	$\sqrt{A^2 - 1}\ S'$	θ_m
1	0.0	0°
2	0.5	35.44°
3	1.0	43.63°
4	1.5	46.11°

c. $\phi = 0, \theta = -50°$.

Figure 30. (Continued).

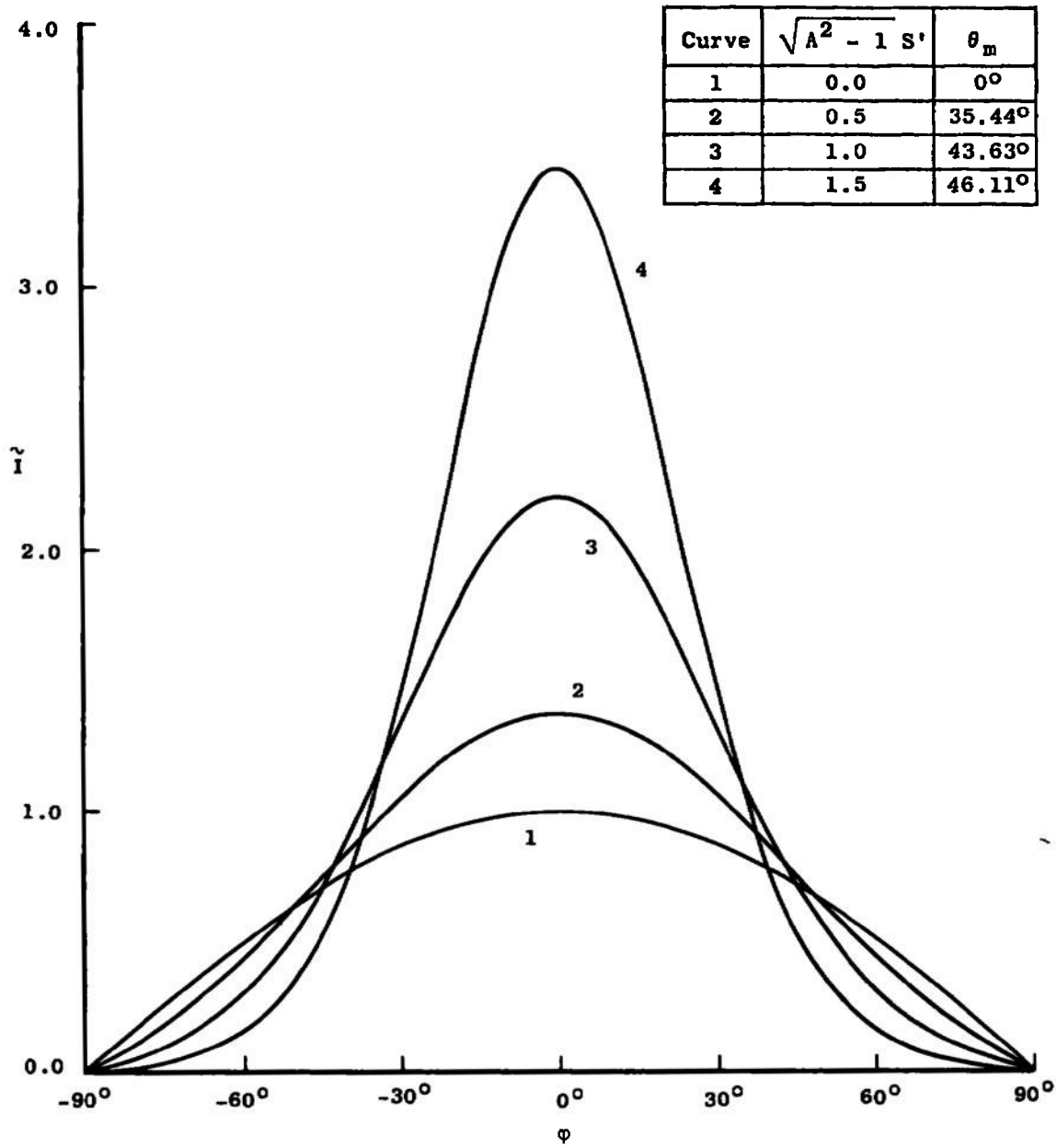

d. $\theta = \theta_m$, $\theta_i = -50°$.

Figure 30. (Continued).

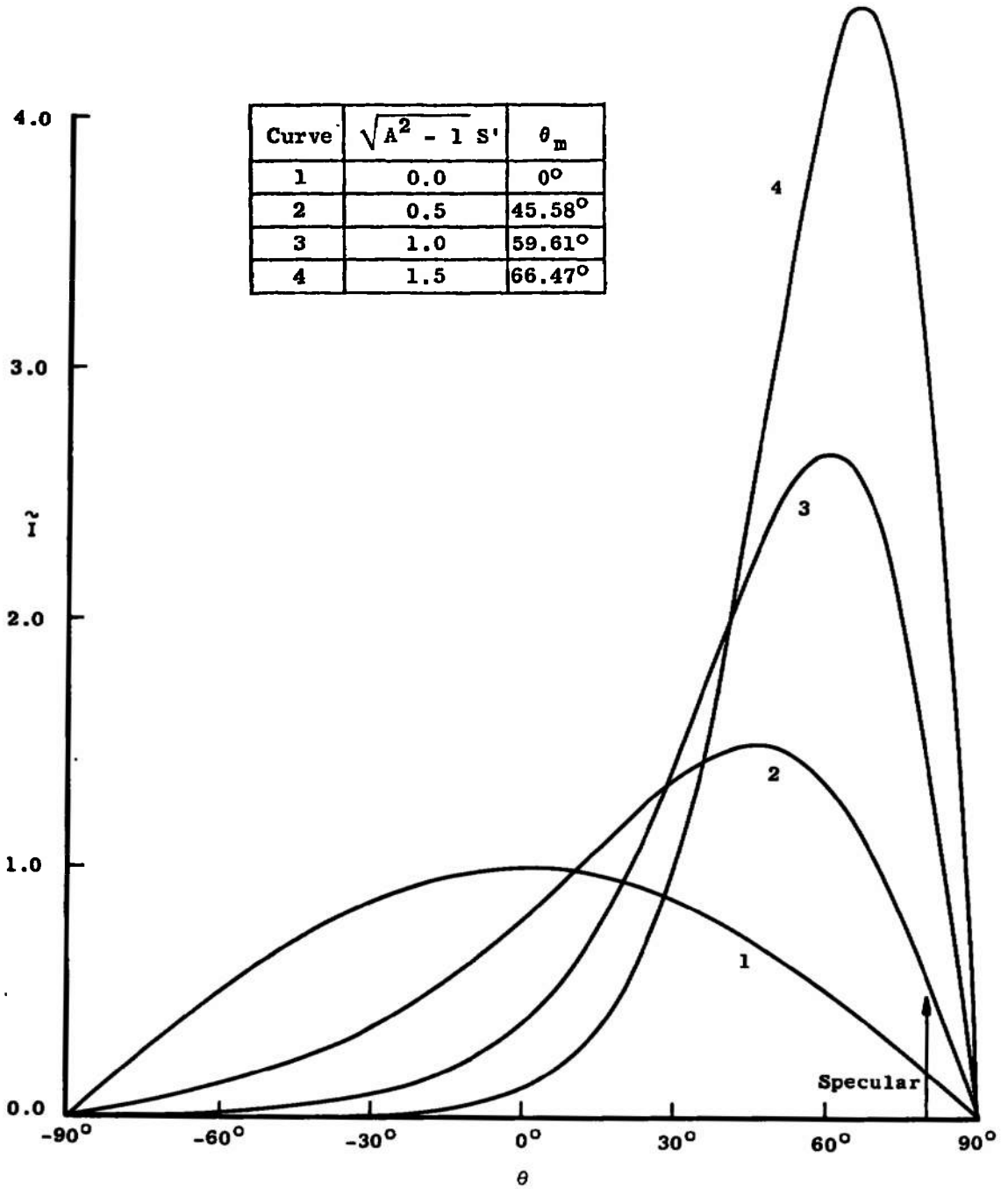

e. $\phi = 0$, $\theta_i = -80°$.

Figure 30. (Continued).

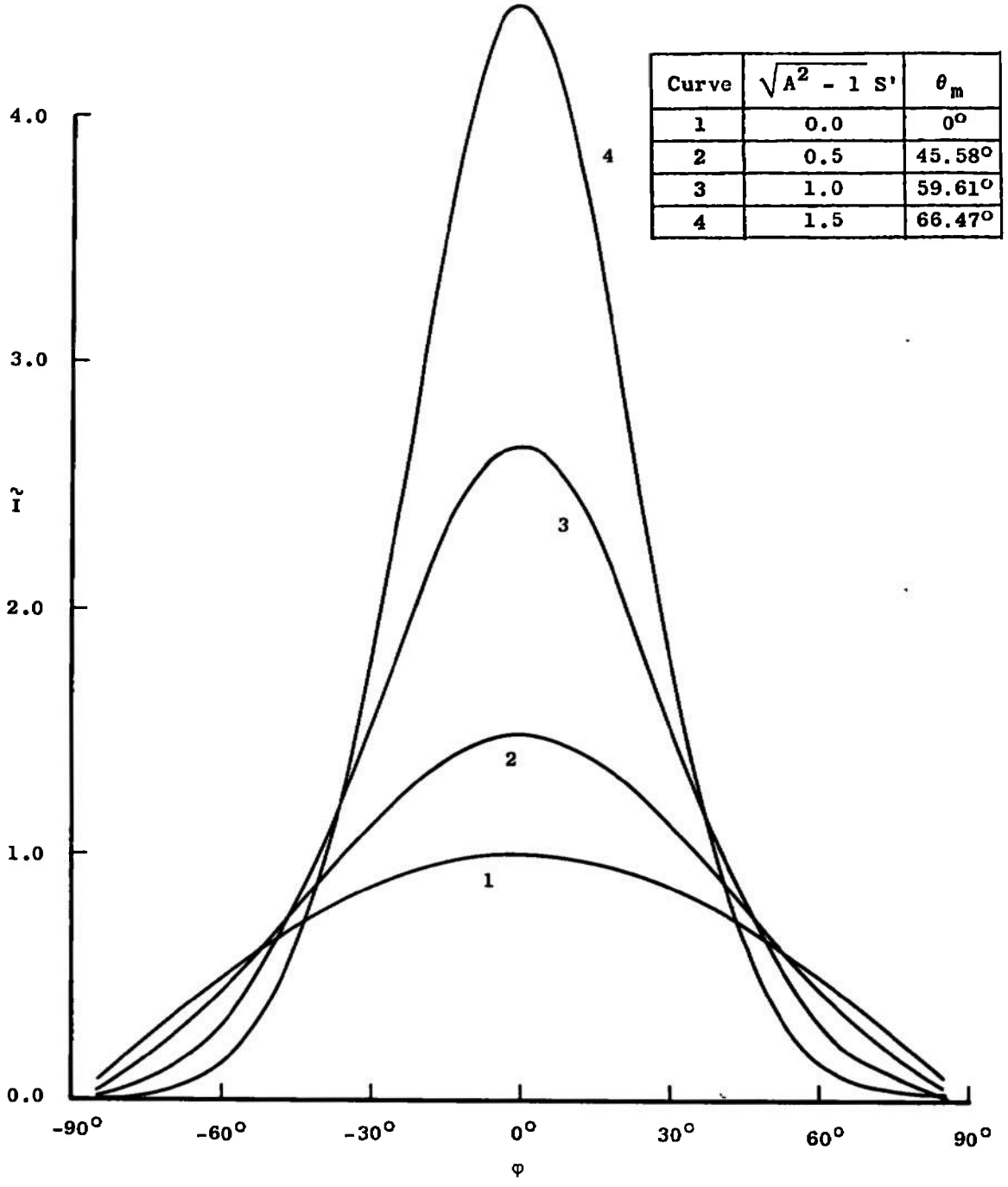

f. $\theta = \theta_m$, θ_i = -80°.

Figure 30. (Continued).

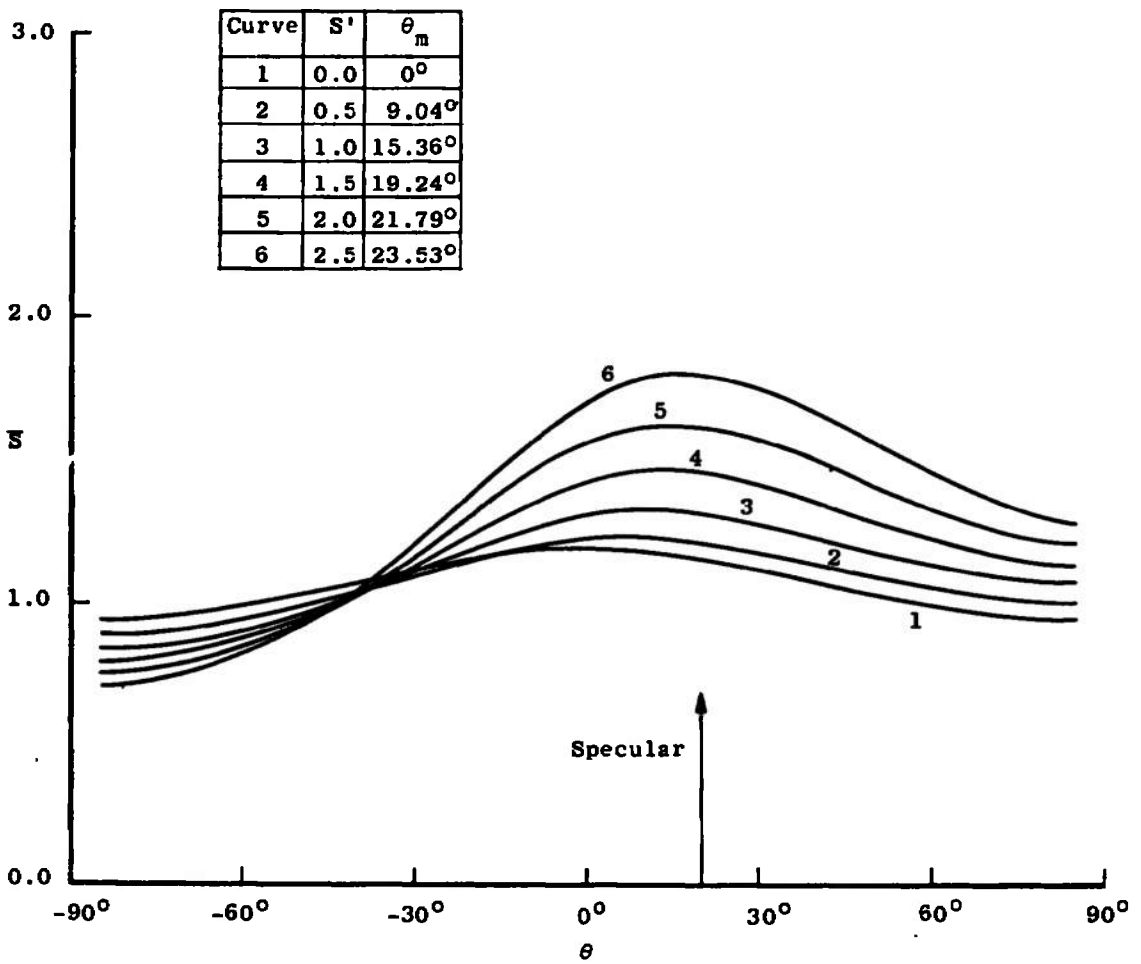

a. $\phi = 0$, $\theta_i = -20°$.

Figure 31. Mean Reflected Dimensionless Speed ($a_x = 0.5$, $a_y = 0.8$).

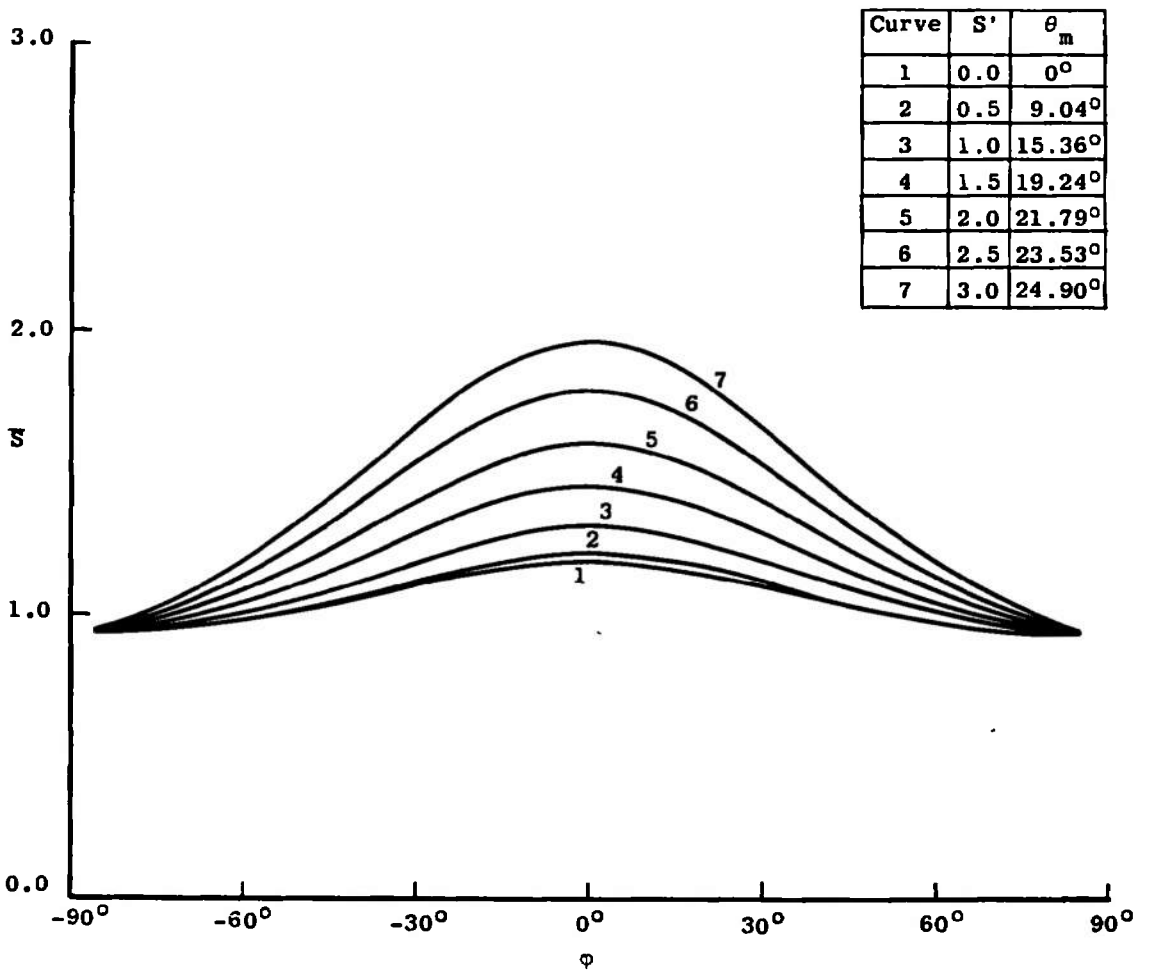

b. $\theta = \theta_m$, θ_i = -20°.

Figure 31. (Continued).

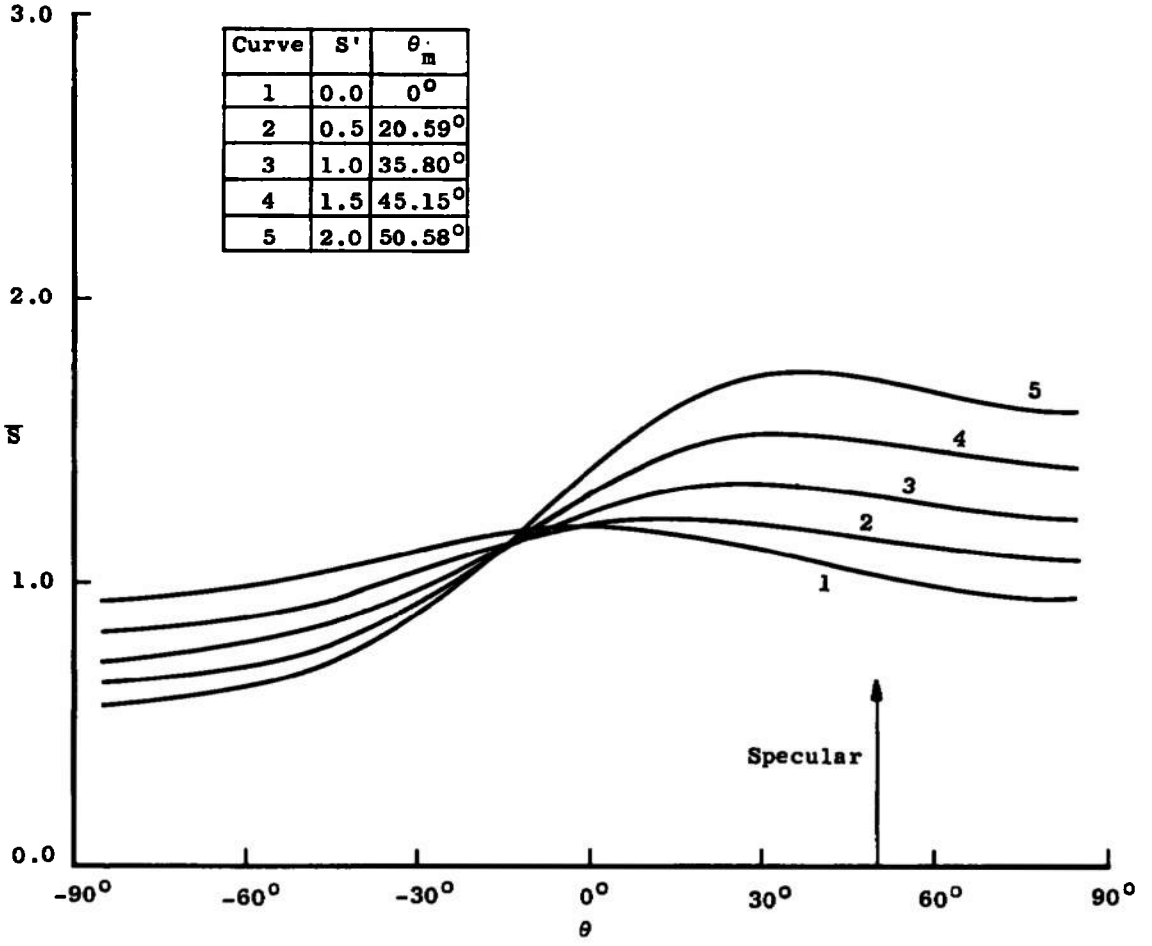

c. $\phi = 0$, $v_i = -50°$.

Figure 31. (Continued).

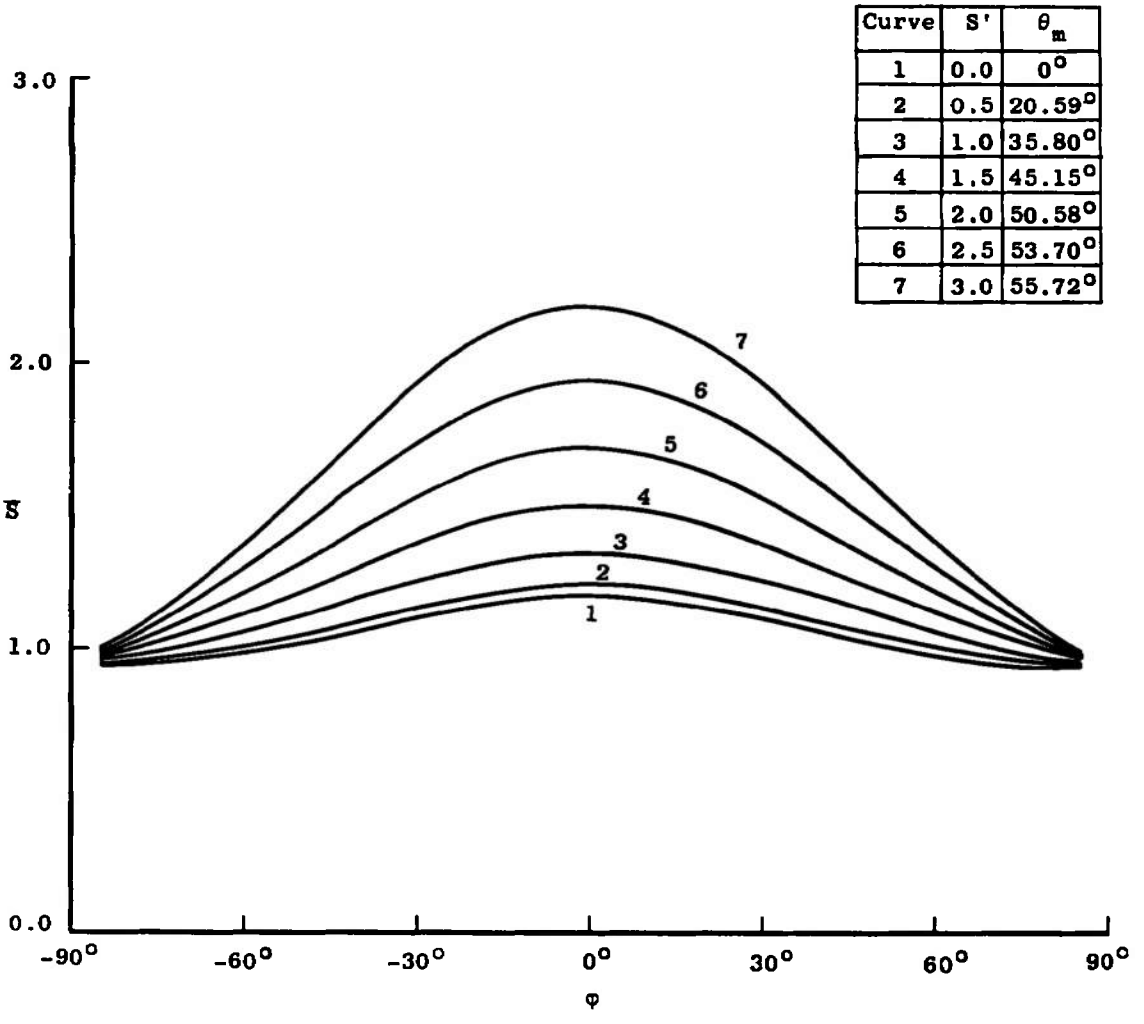

d. $\theta = \theta_m$, θ_i = -50°.

Figure 31. (Continued).

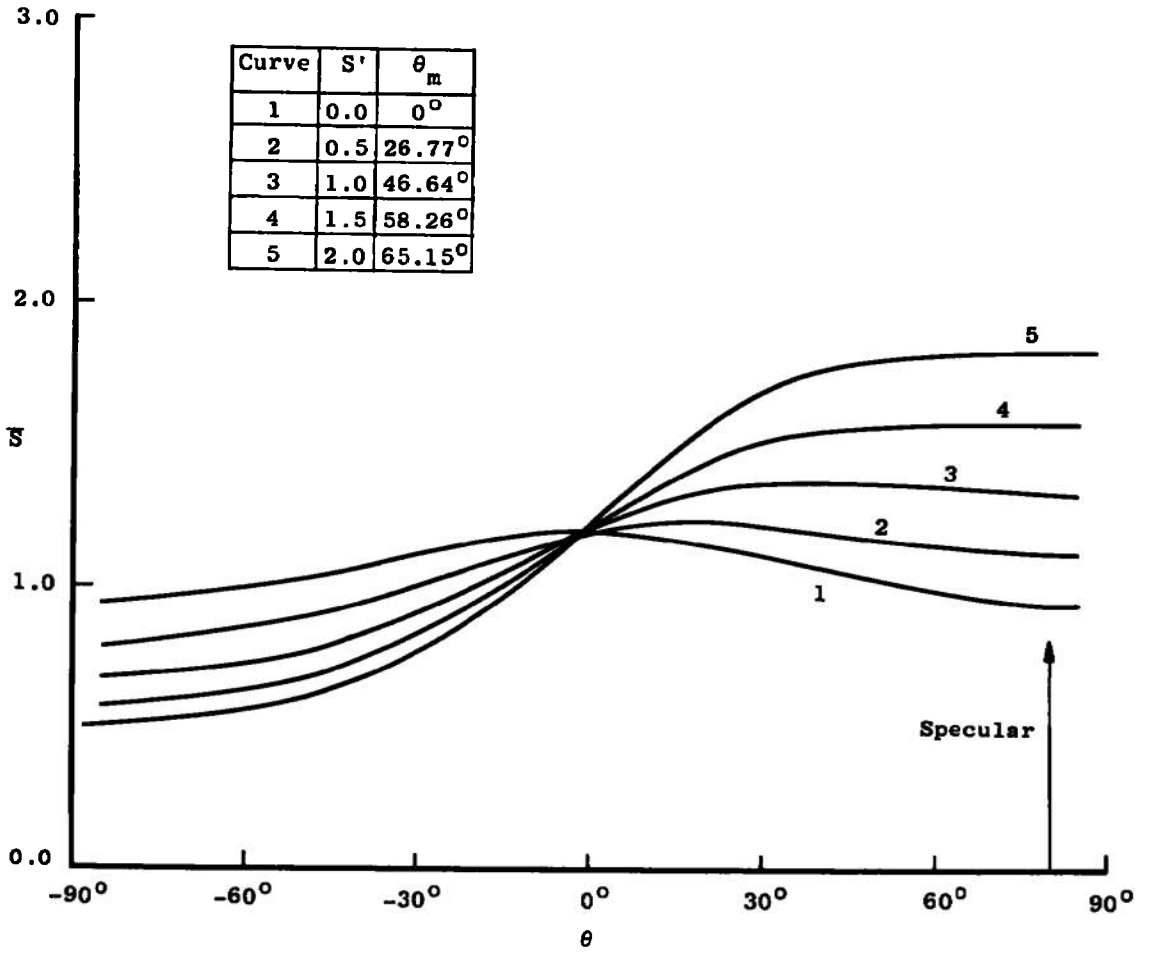

e. $\phi = 0$, $\theta_i = -80°$.

Figure 31. (Continued).

Curve	S'	θ_m
1	0.0	0°
2	0.5	26.77°
3	1.0	46.64°
4	1.5	58.26°
5	2.0	65.15°
6	2.5	69.55°
7	3.0	72.54°

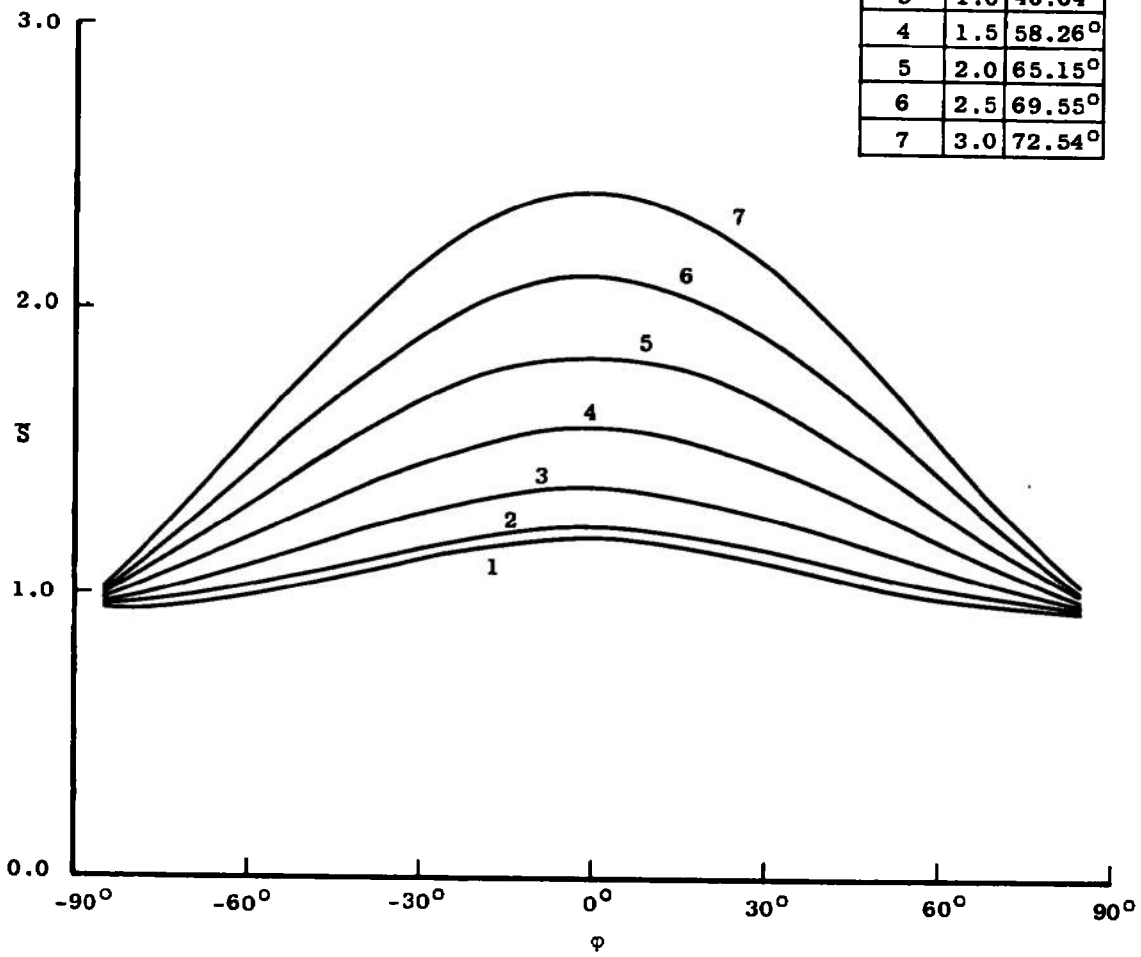

f. $\theta = \theta_m$, θ_i = -80°.
Figure 31. (Continued).

Curve	S'	θ_m
1	0.0	41.78°
2	0.5	33.89°
3	1.0	19.98°
4	1.5	16.23°
5	2.0	14.91°
6	2.5	14.27°

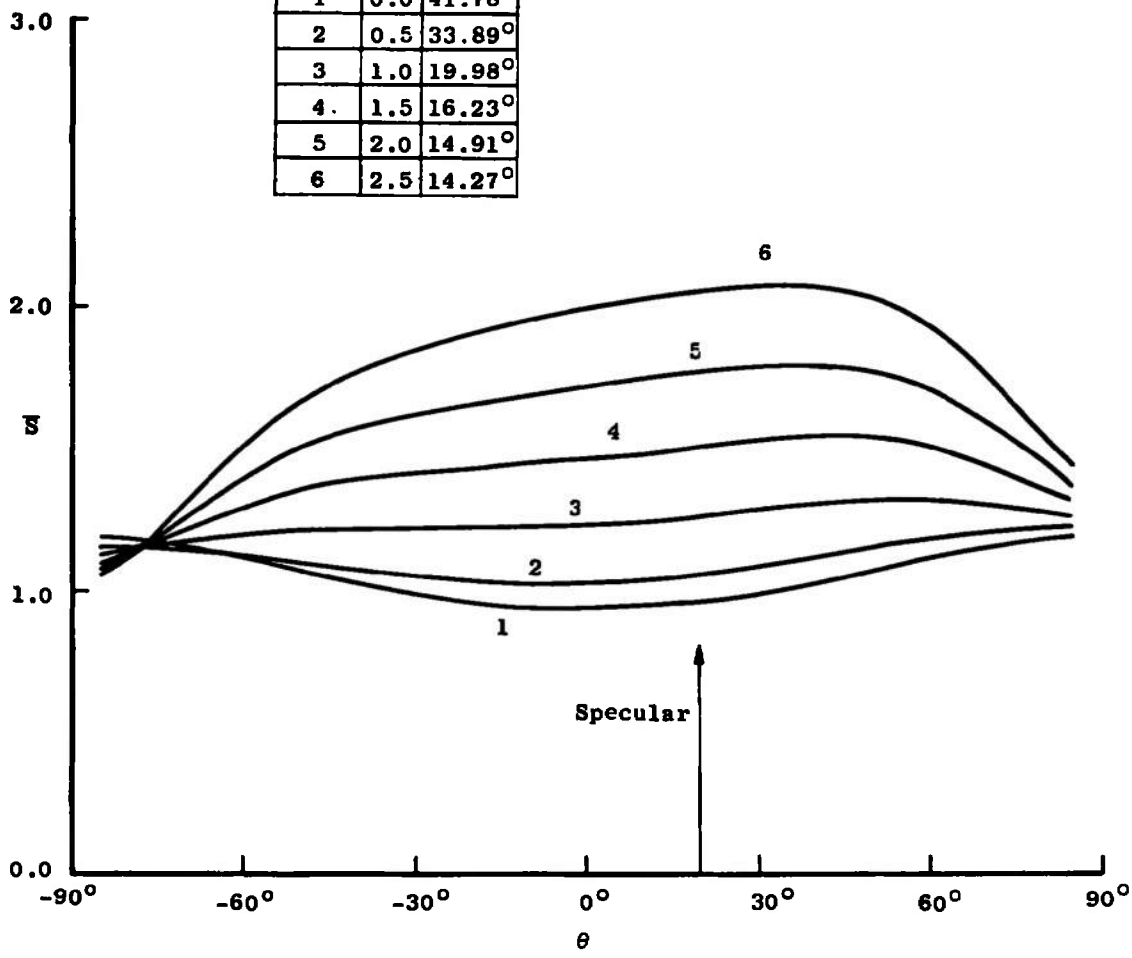

a. $\phi = 0$, $\theta_i = -20°$.

Figure 32. Mean Reflected Dimensionless Speed ($a_x = 0.8$, $a_y = 0.5$).

Curve	S'	θ_m
1	0.0	41.78°
2	0.5	33.89°
3	1.0	19.98°
4	1.5	16.23°
5	2.0	14.91°
6	2.5	14.27°
7	3.0	13.92°

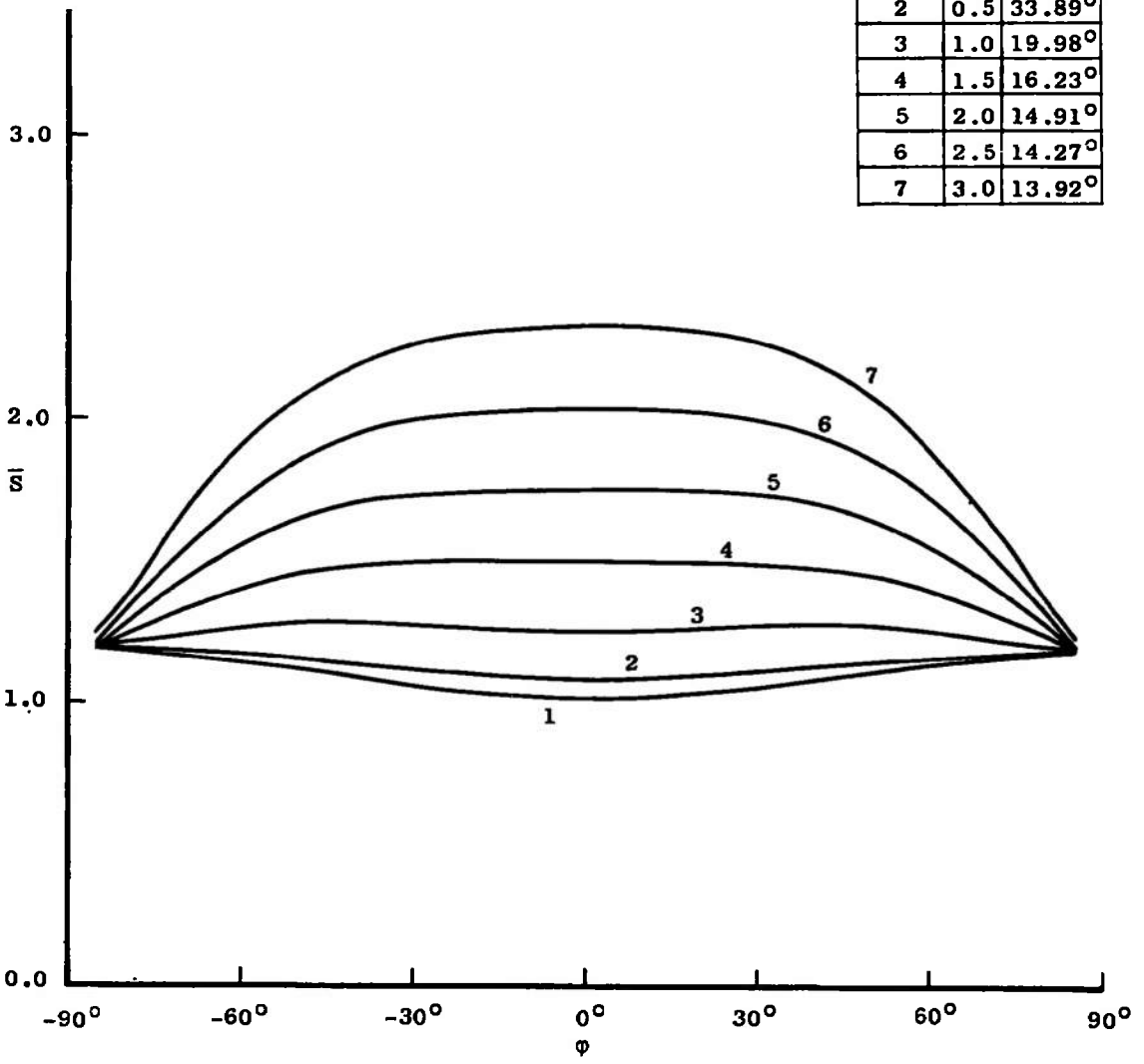

b. $\theta = \theta_m$, θ_i = -20°.

Figure 32. (Continued).

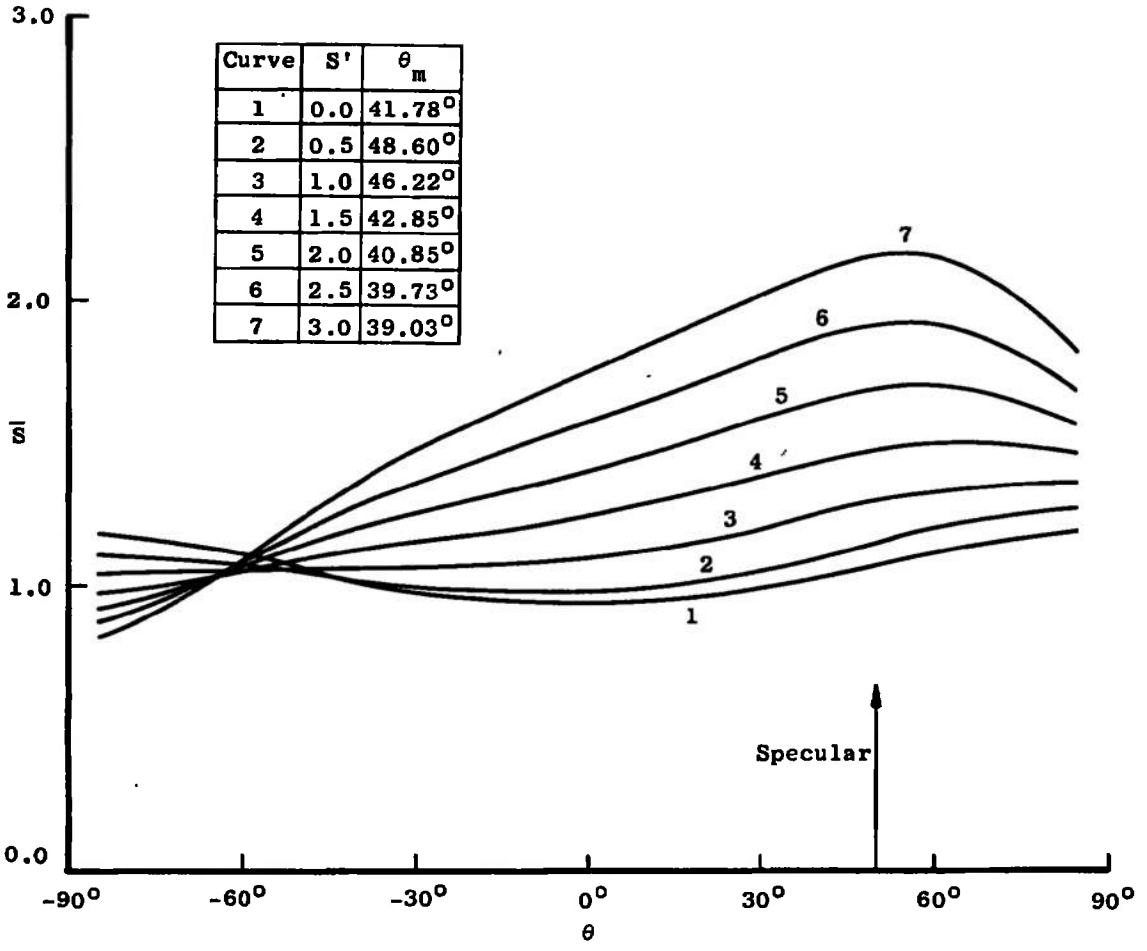

c. $\phi = 0$, $\theta_i = -50°$.

Figure 32. (Continued).

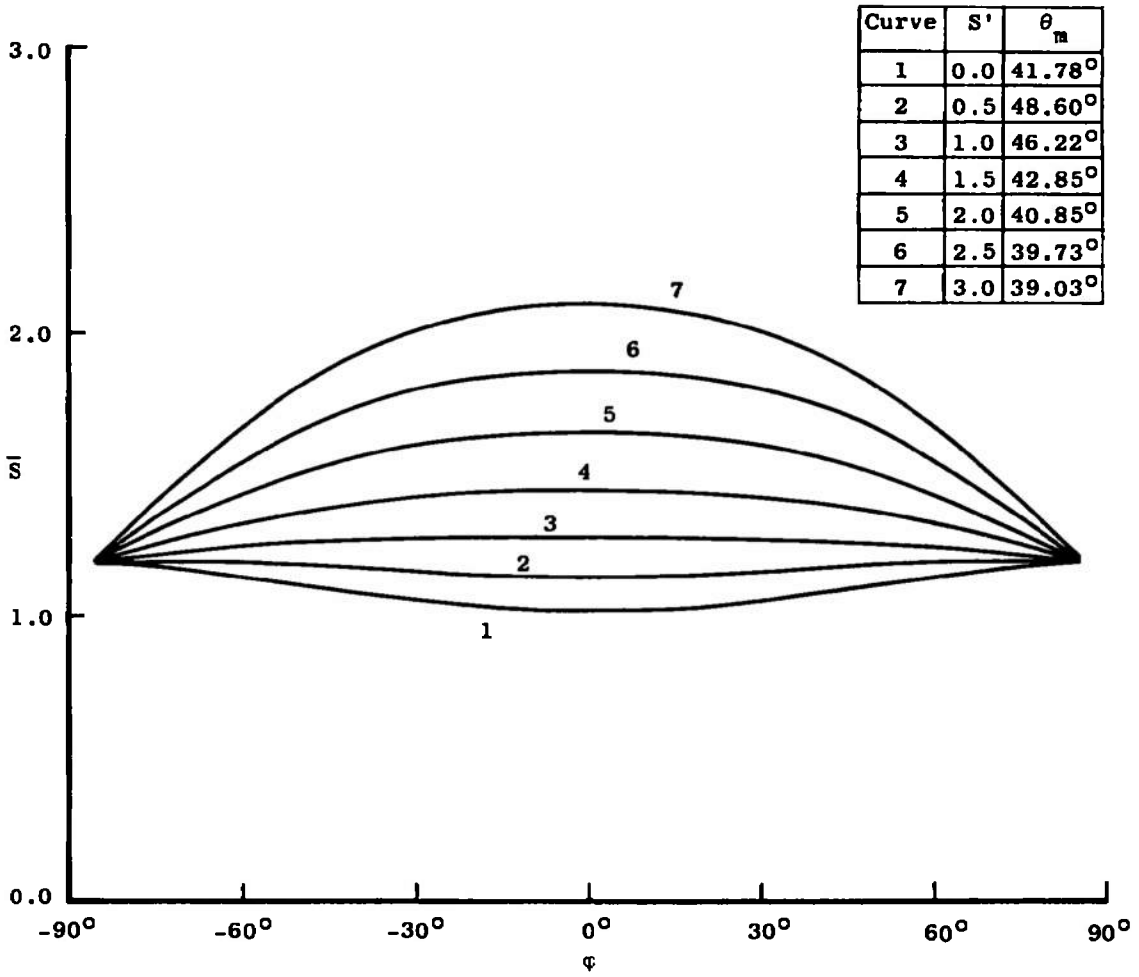

d. $\theta = \theta_m$, $\theta_1 = -50°$.

Figure 32. (Continued).

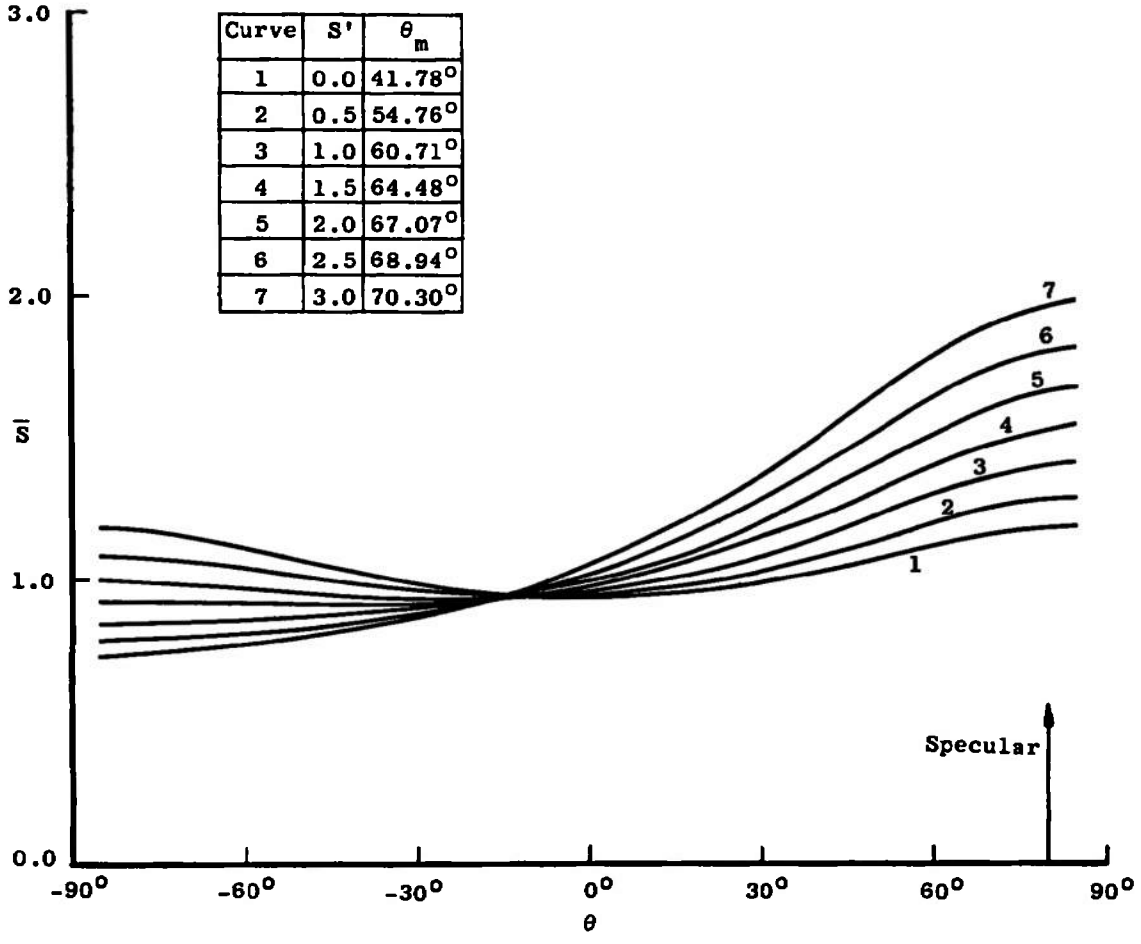

e. $\phi = 0$, $\theta_i = -80°$.

Figure 32. (Continued).

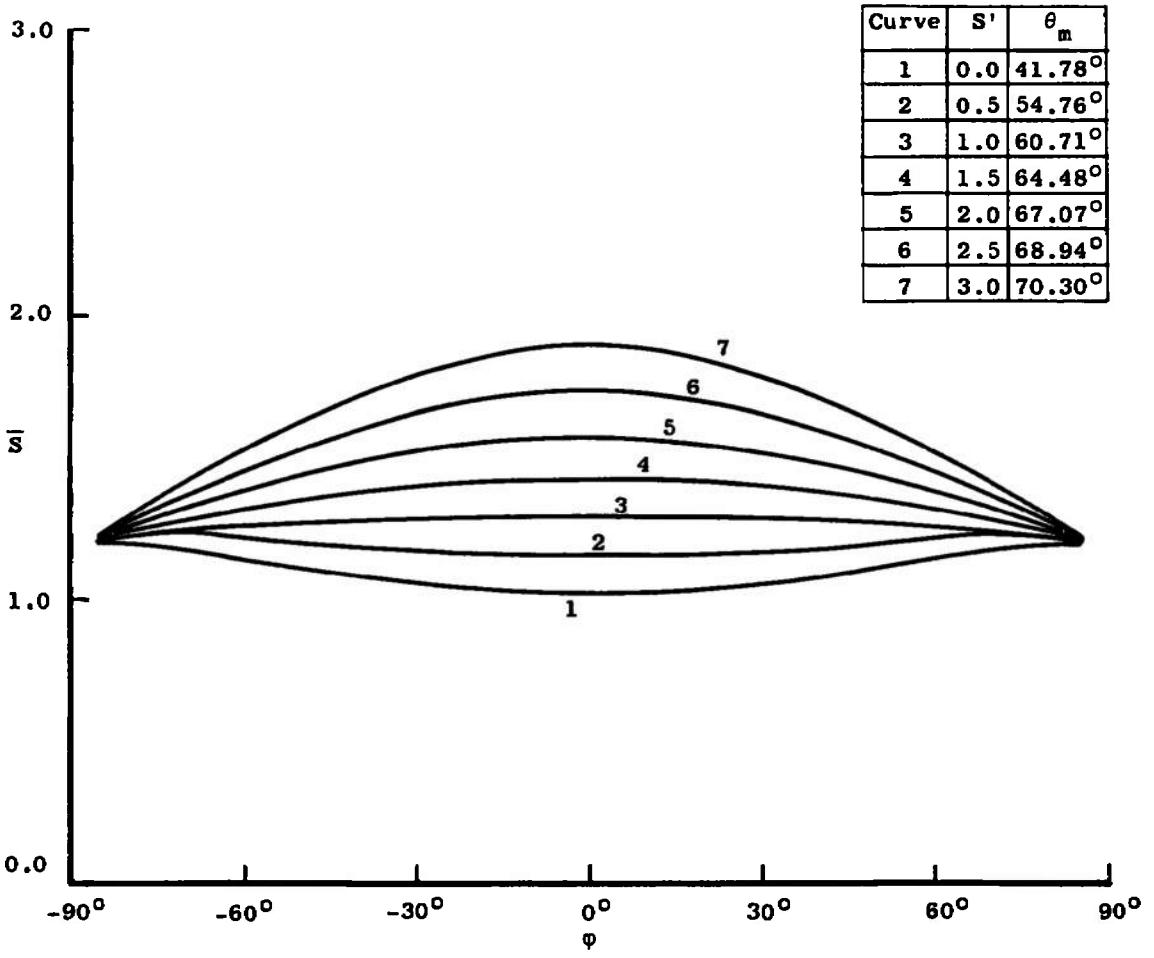

f. $\theta = \theta_m$, $\theta_i = -80°$.

Figure 32. (Continued).

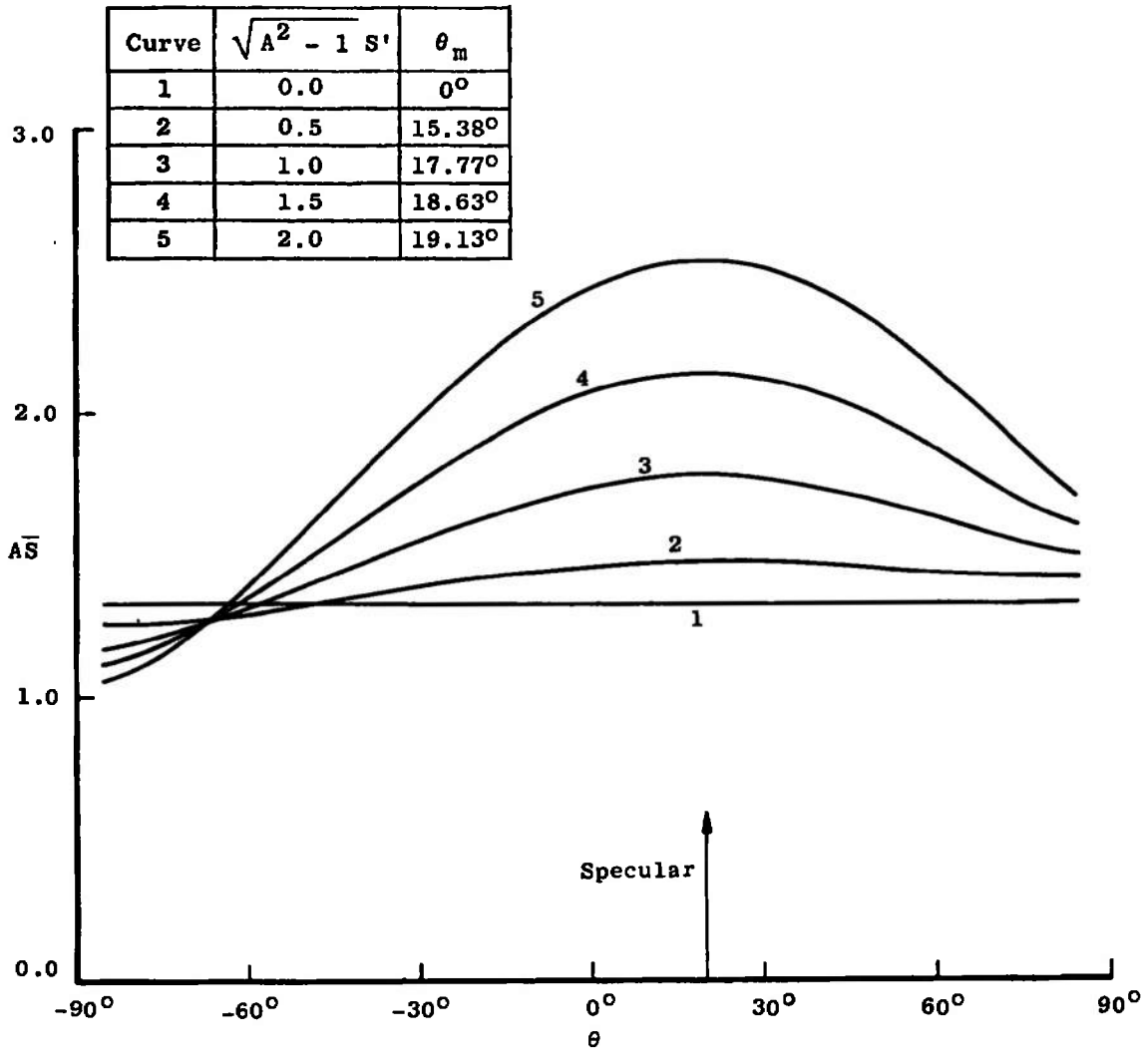

a. $\phi = 0, \theta_i = -20°$.

Figure 33. Reflected Value of $A\bar{S}$ ($a_x = a_y = A^{-2}$).

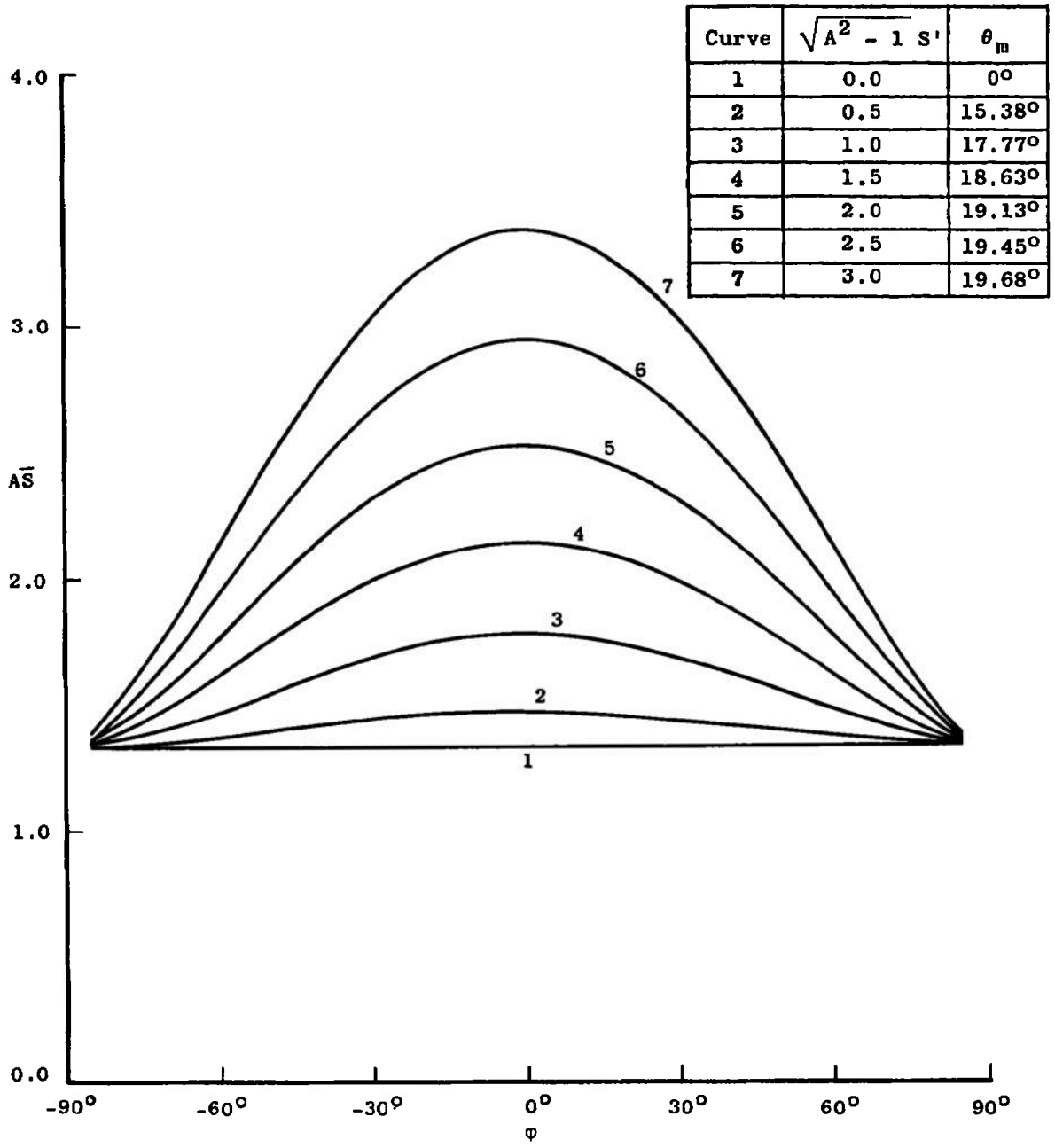

b. $\theta = \theta_m$, $\theta_i = -20°$.

Figure 33. (Continued).

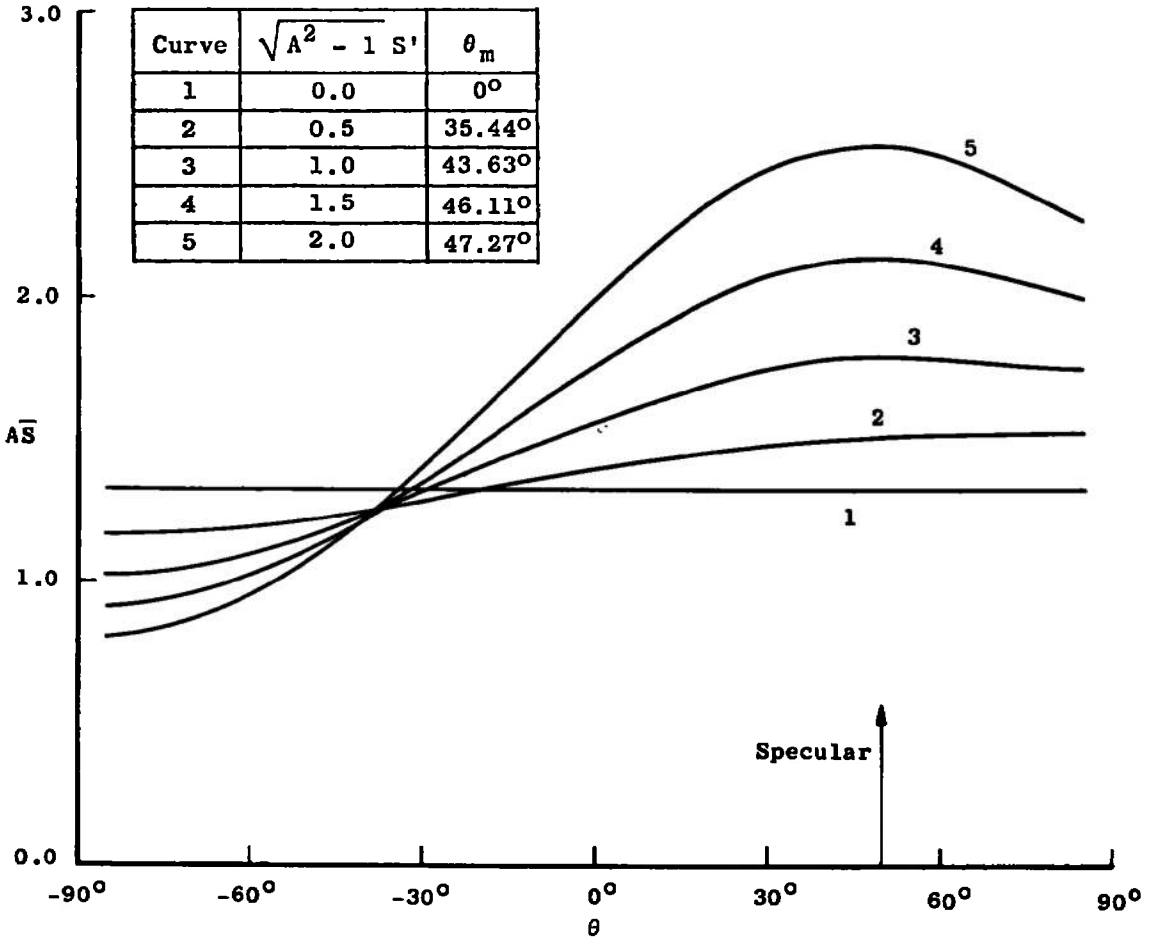

c. $\phi = 0, \theta_i = -50°$.

Figure 33. (Continued).

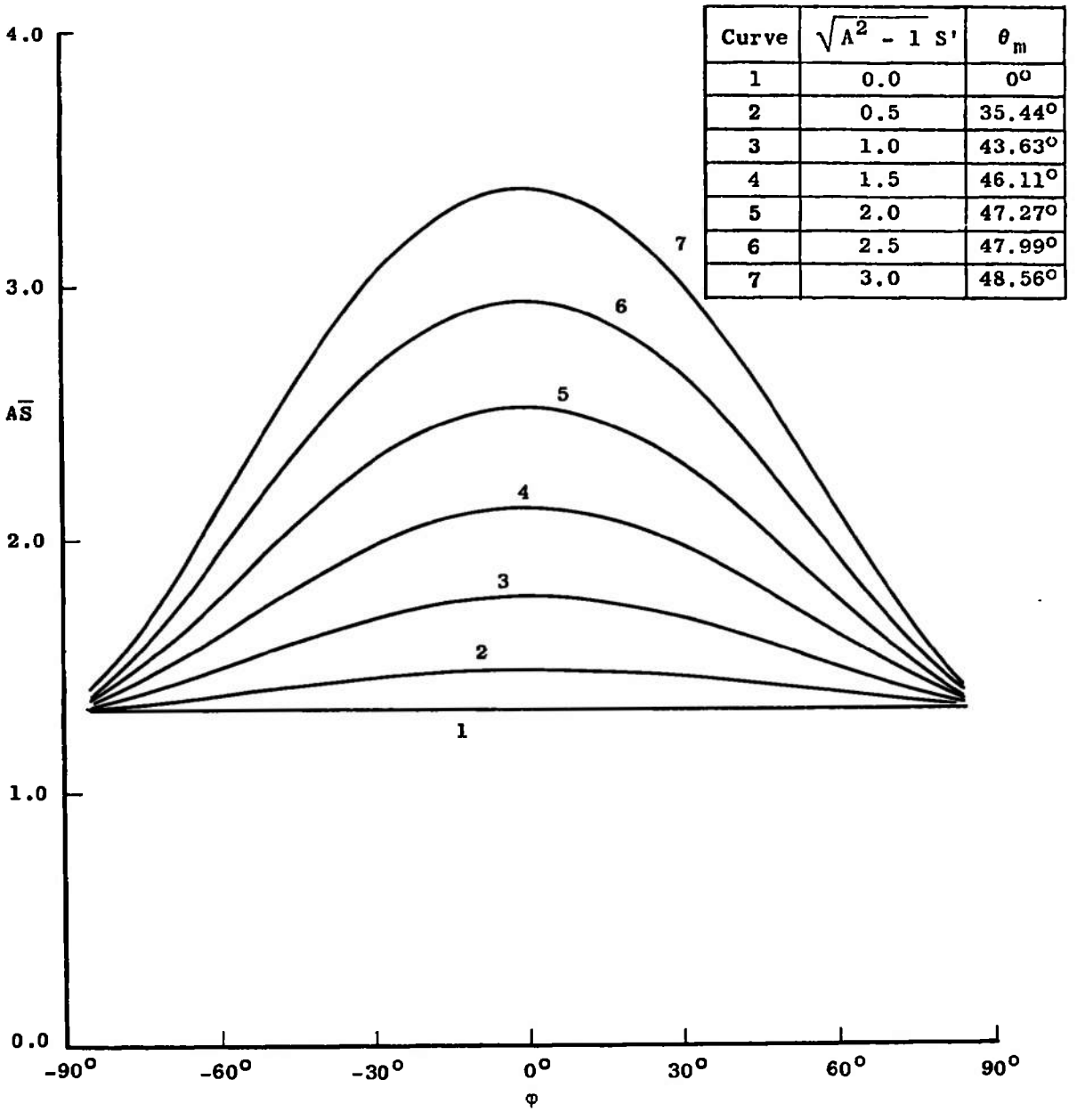

Curve	$\sqrt{A^2 - 1}\ S'$	θ_m
1	0.0	0°
2	0.5	35.44°
3	1.0	43.63°
4	1.5	46.11°
5	2.0	47.27°
6	2.5	47.99°
7	3.0	48.56°

d. $\theta = \theta_m$, $\theta_i = -50°$.
Figure 33. (Continued).

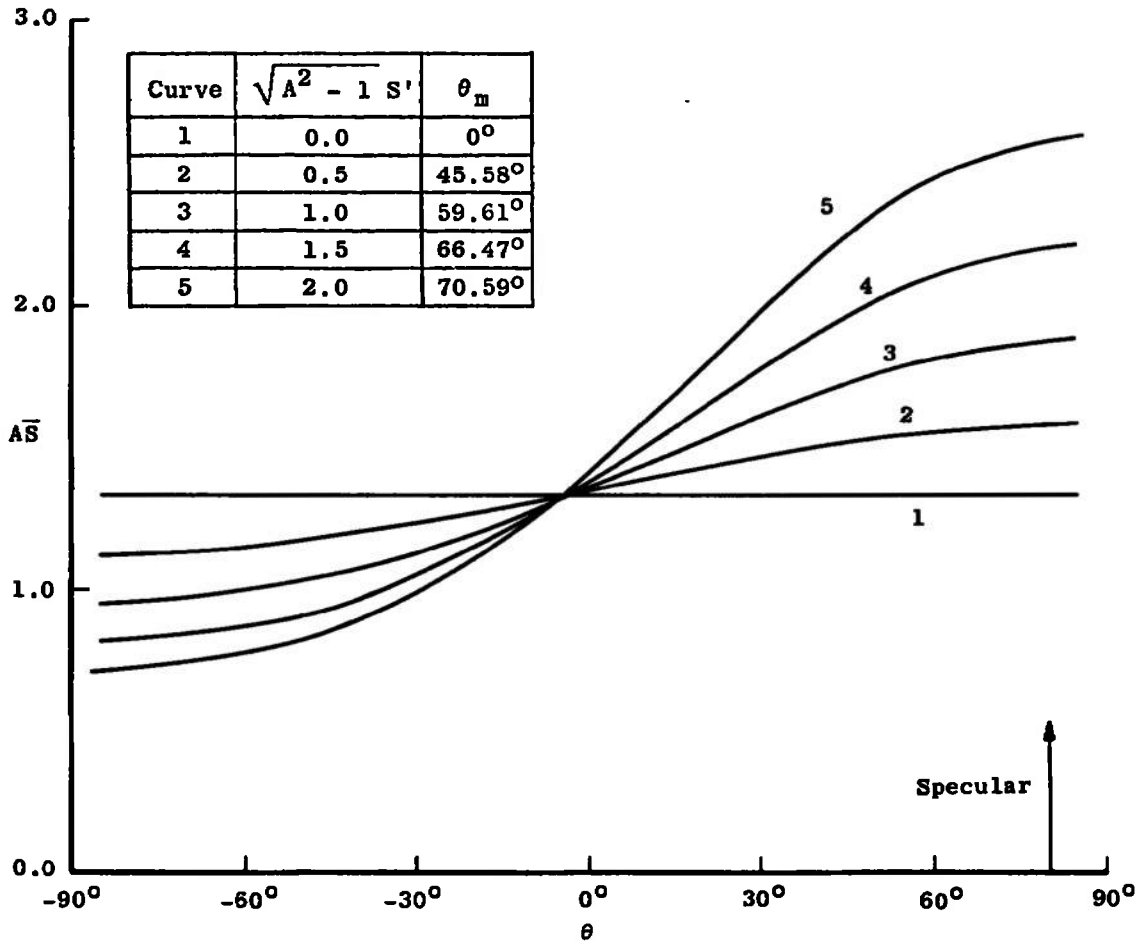

e. $\phi = 0$, $\theta_i = -80°$.

Figure 33. (Continued).

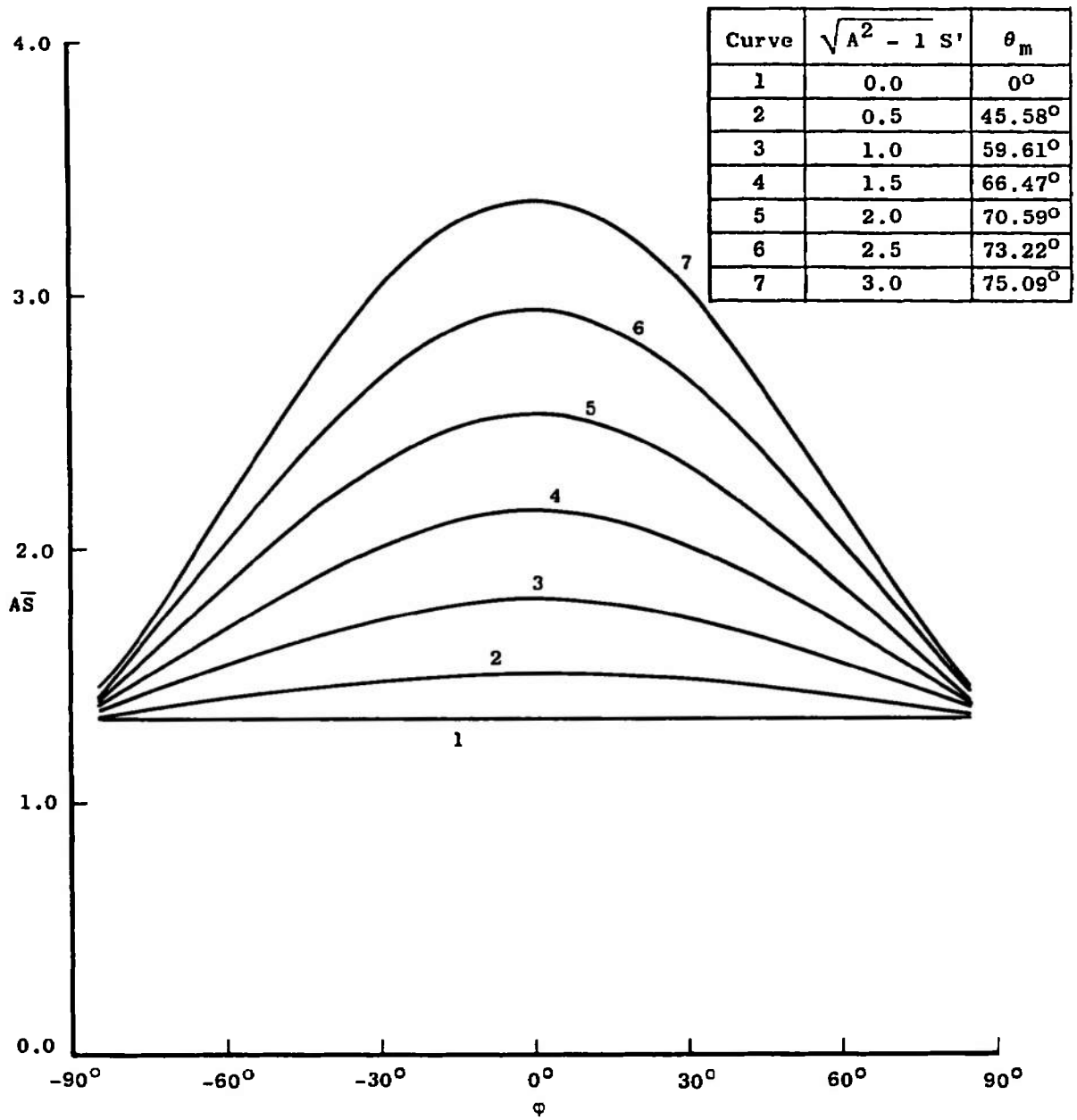

f. $\theta = \theta_m$, θ_i = -80°.
Figure 33. (Continued).

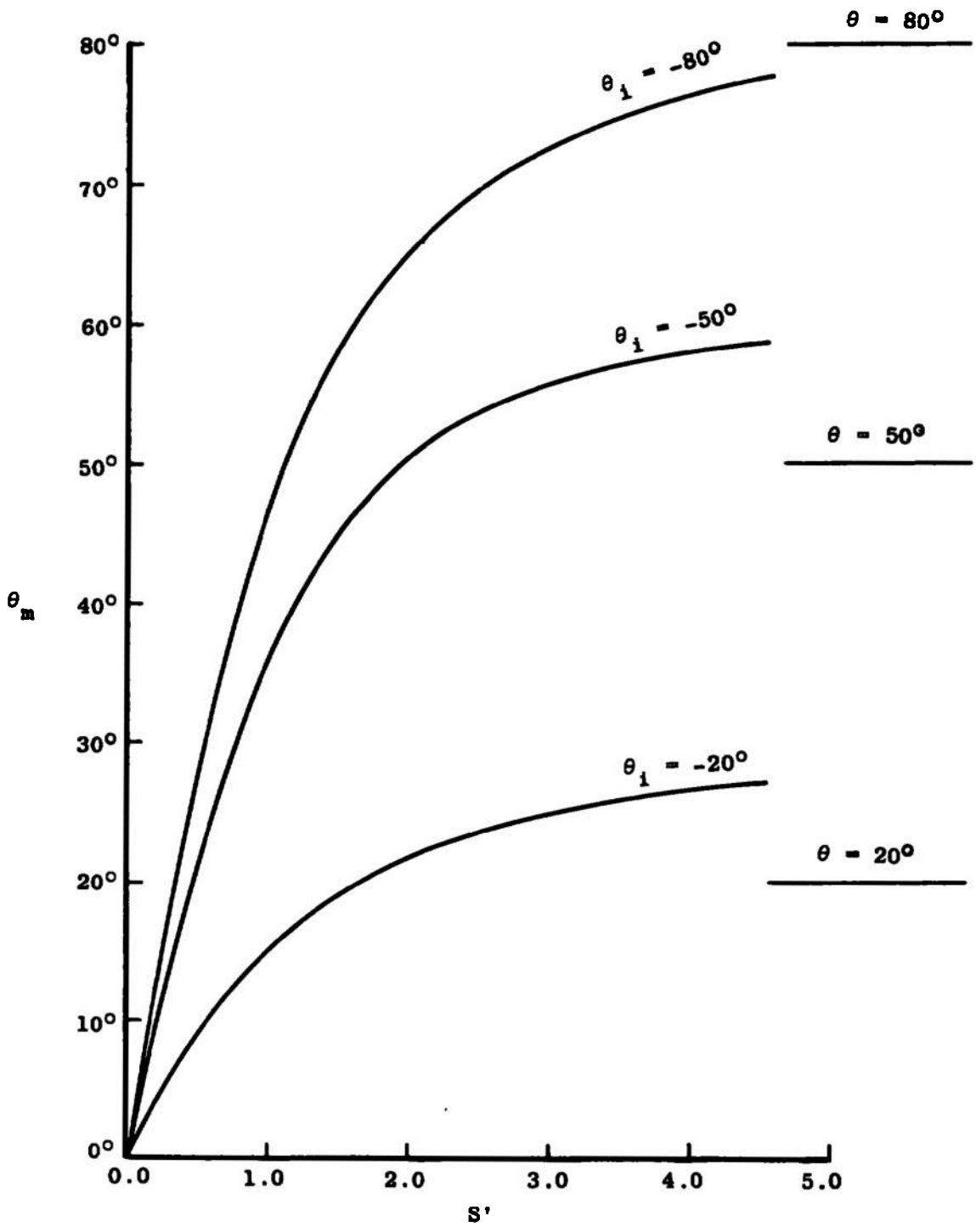

Figure 34. Position of Maximum Intensity (a_y = 0.5, a_y = 0.8).

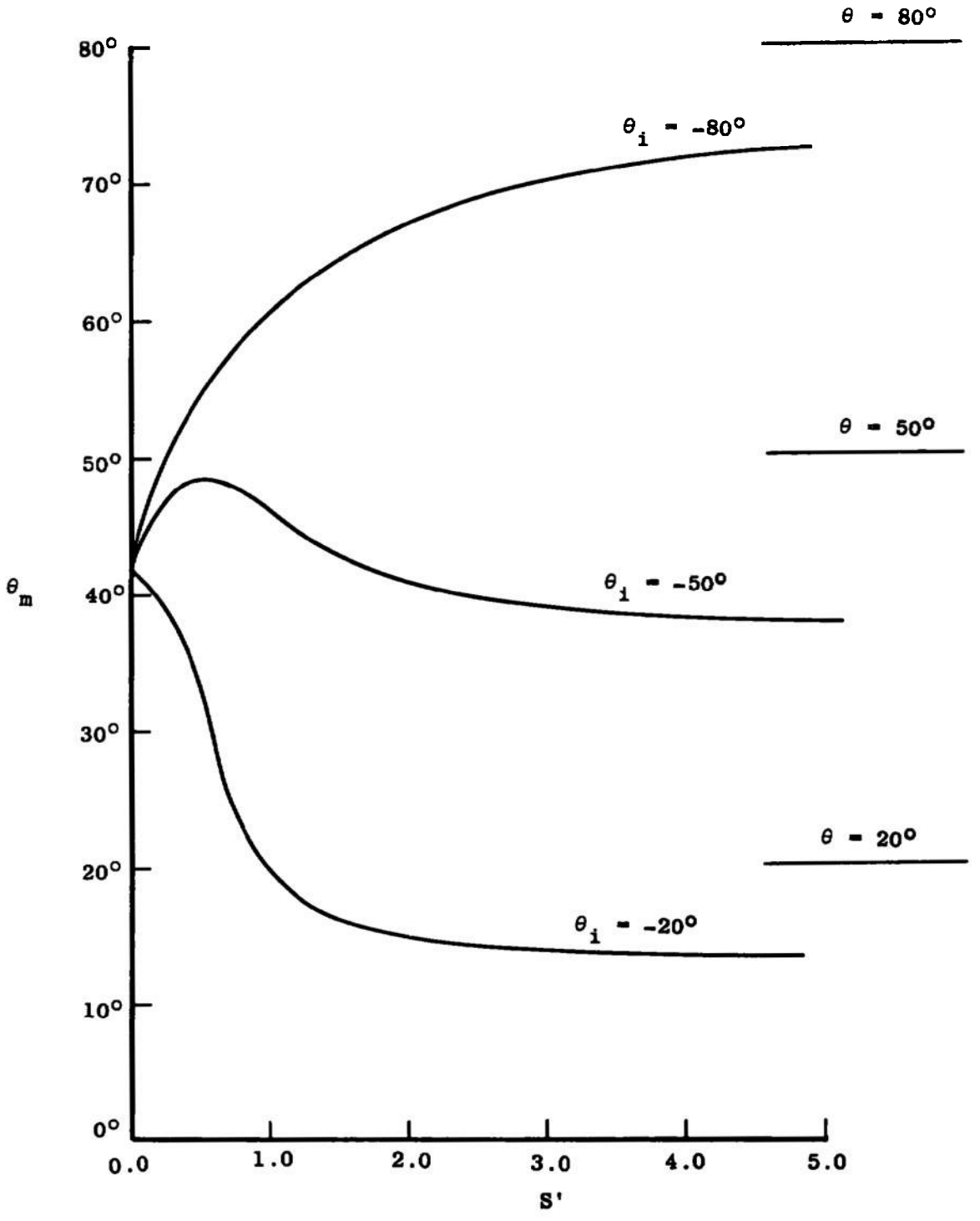

Figure 35. Position of Maximum Intensity (a_x = 0.8, a_y = 0.5).

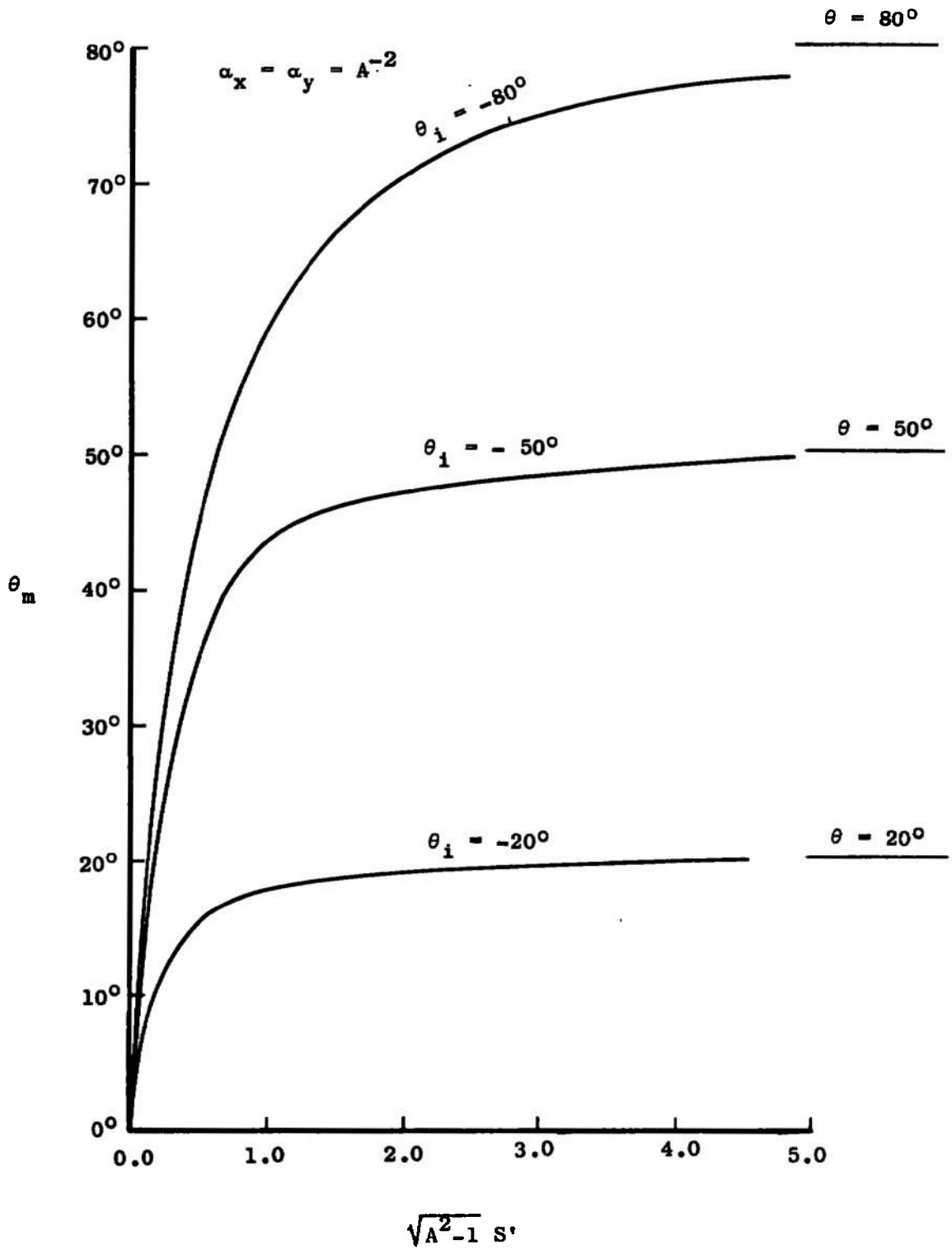

Figure 36. Position of Maximum Intensity ($a_x = a_y = A^{-2}$).

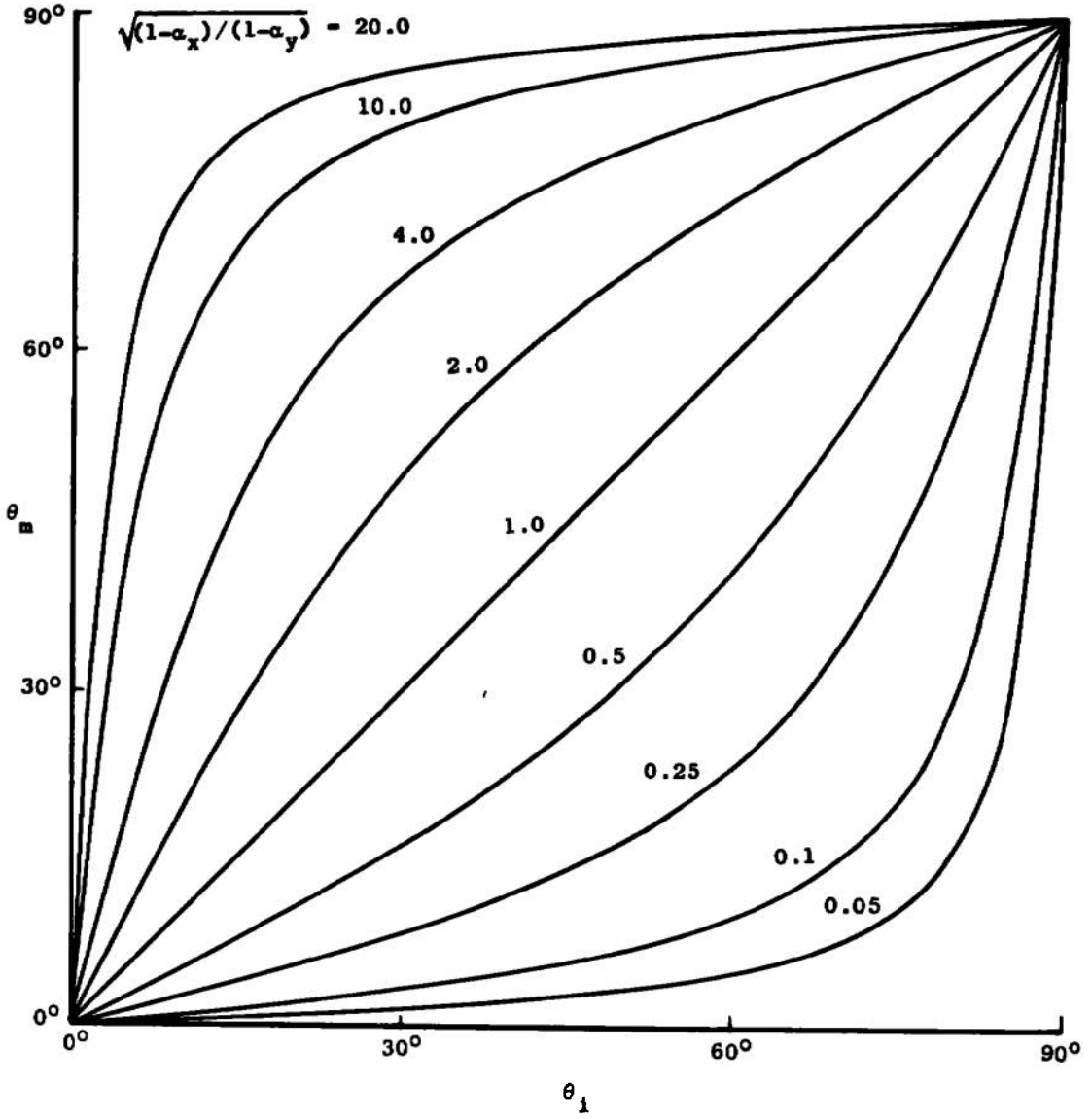

Figure 37. Limit of θ_m for S' ≈ ∞.

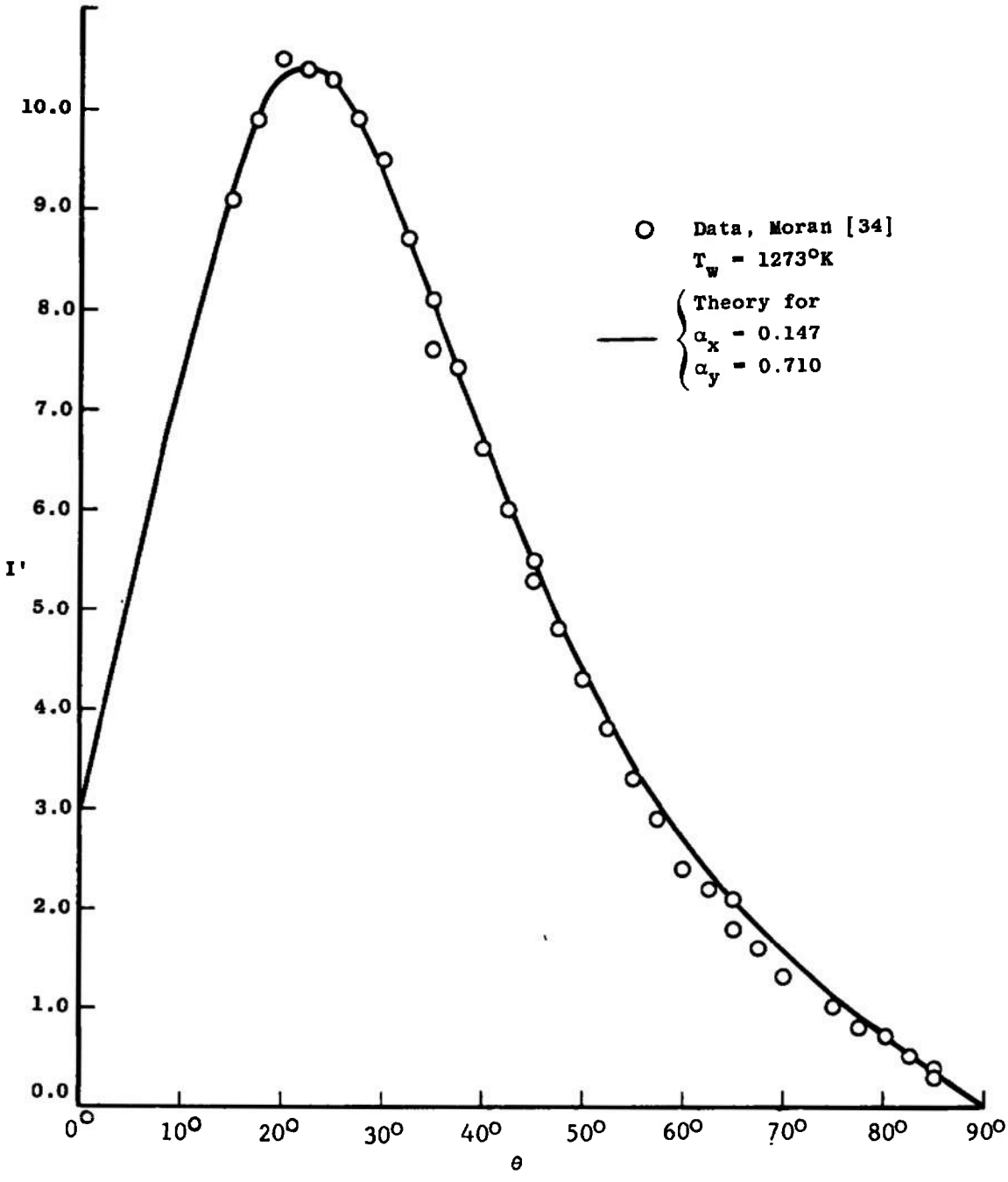

a. Relative Flux.

Figure 38. Comparison of Theory and Data for Argon Scattered from Platinum, θ_i = -40°, v' = 5.4 x 10^4 cm/sec.

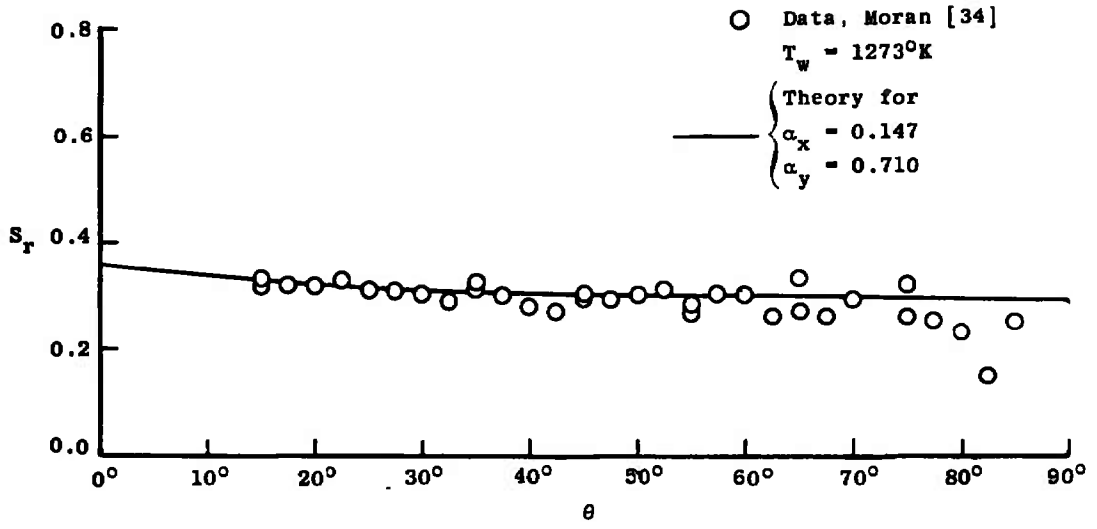

b. Speed Ratio.

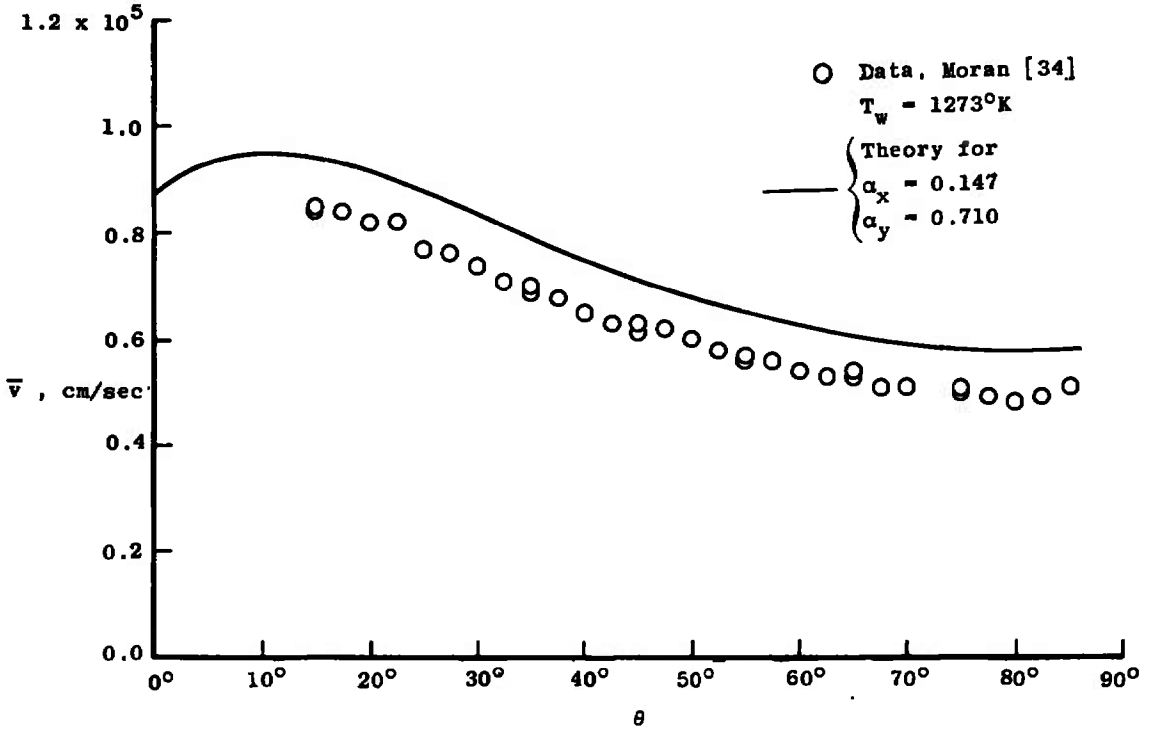

c. Mean Speed.

Figure 38. (Continued).

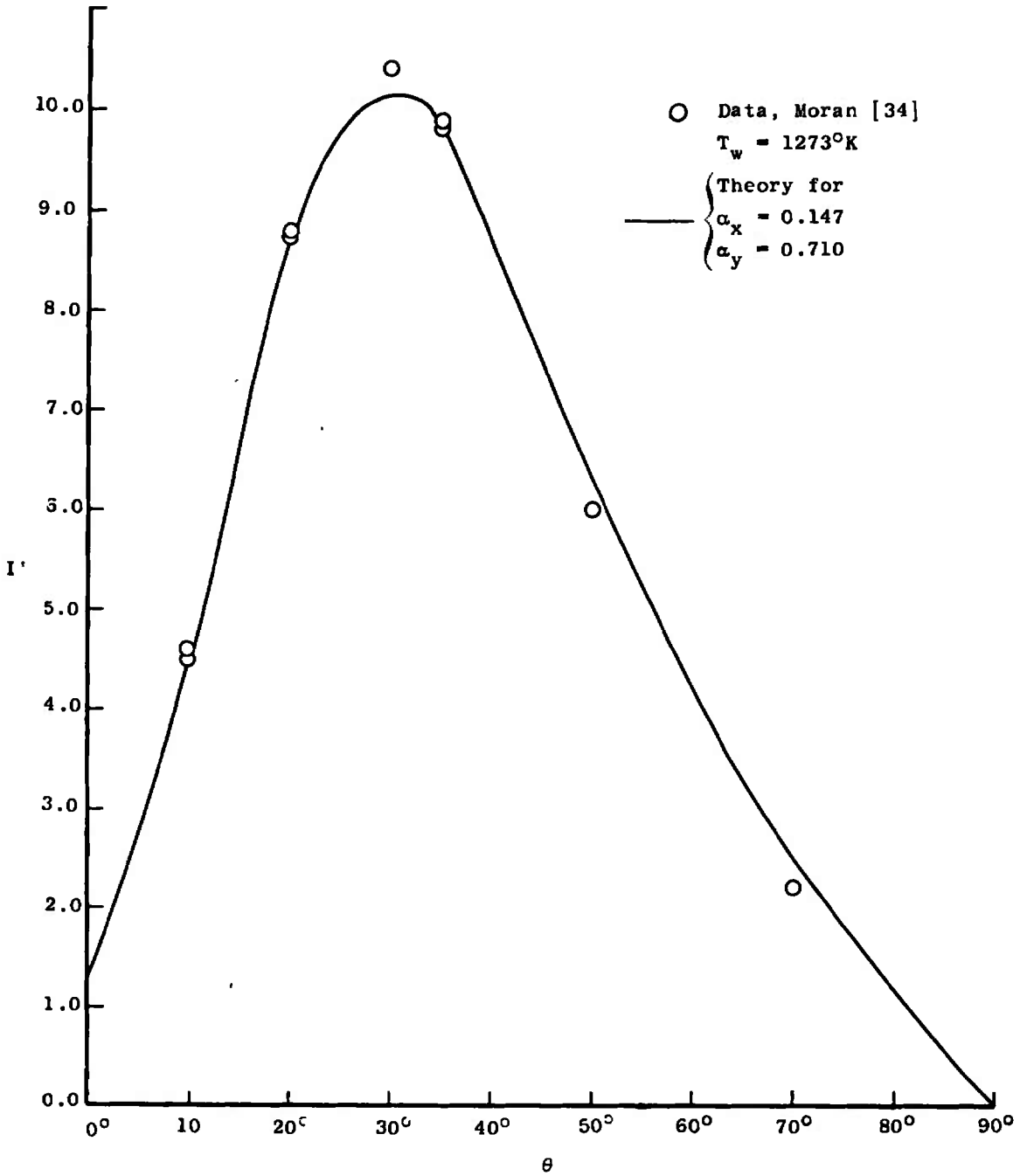

a. Relative Flux.

Figure 39. Comparison of Theory and Data for Argon Scattered from Platinum, θ_i = -55°, v' = 5.4 x 10^4 cm/sec.

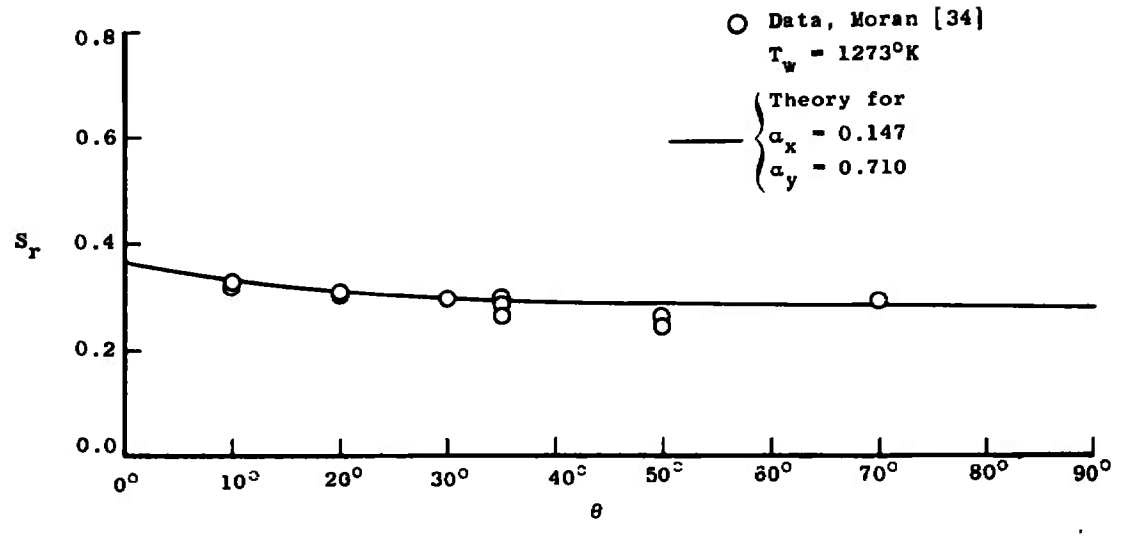

d. Speed Ratio.

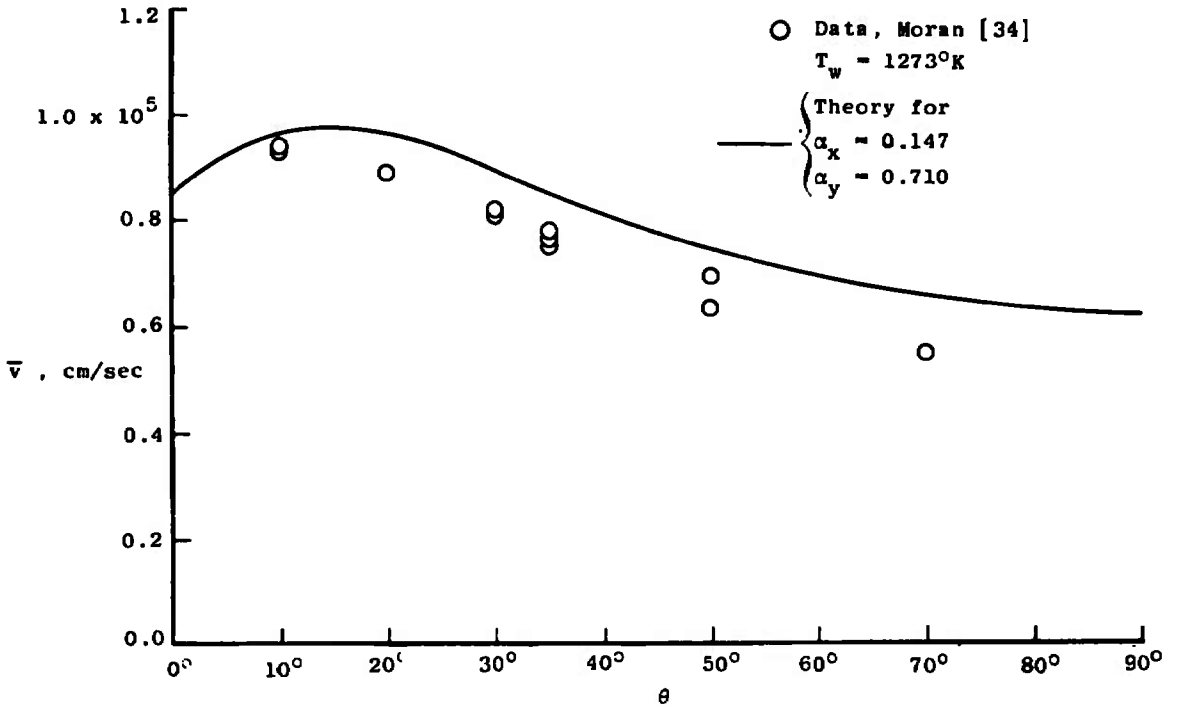

c. Mean Speed.

Figure 39. (Continued).

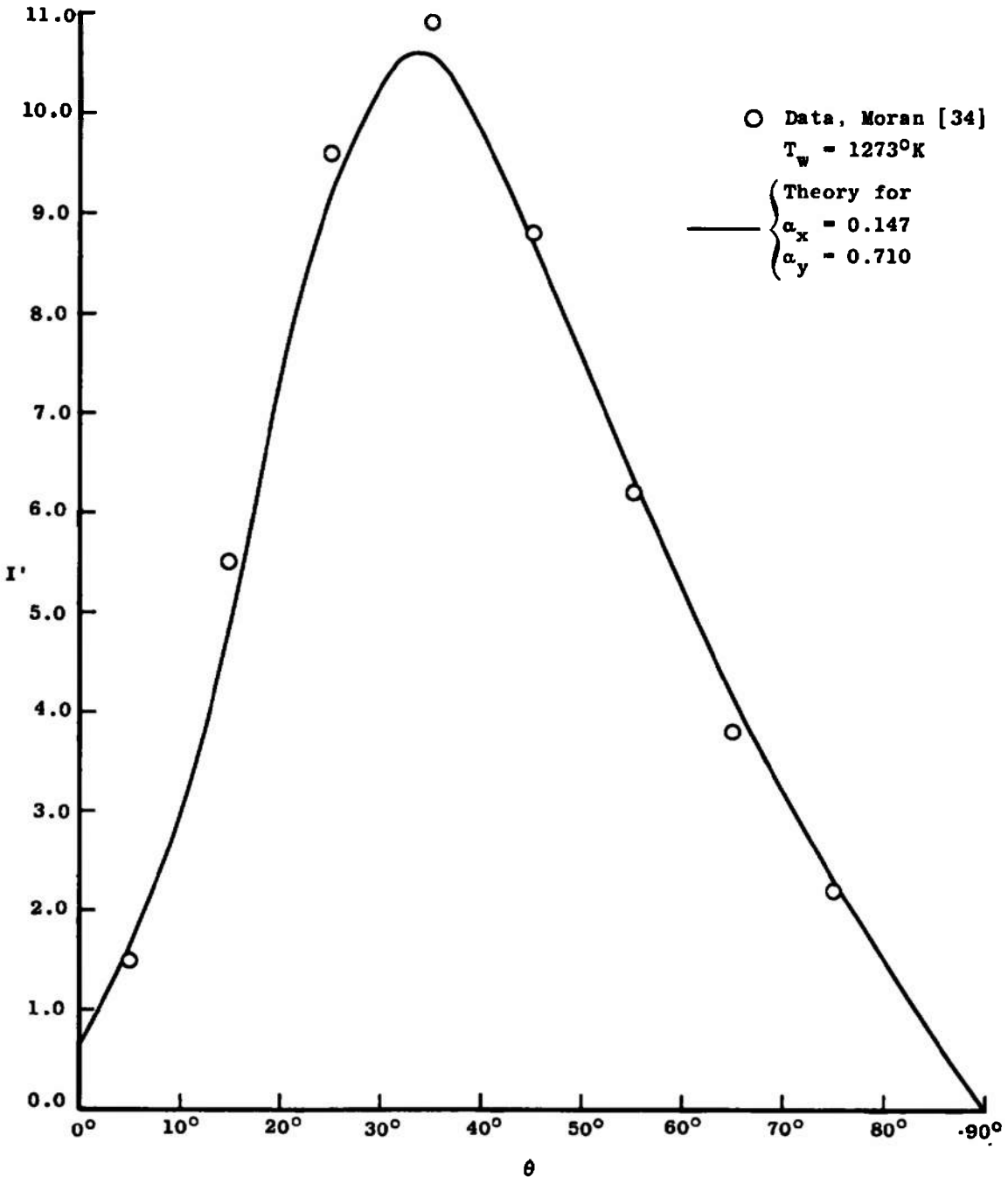

a. Relative Flux.

Figure 40. Comparison of Theory and Data for Argon Scattered from Platium, θ_i = -65°, v' = 5.4 x 10^4 cm/sec.

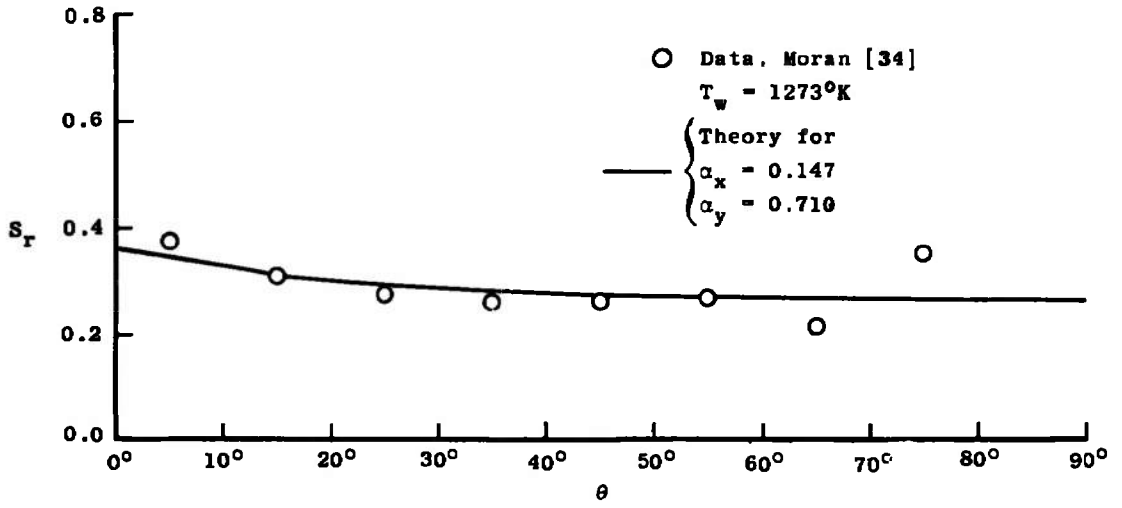

b. Speed Ratio.

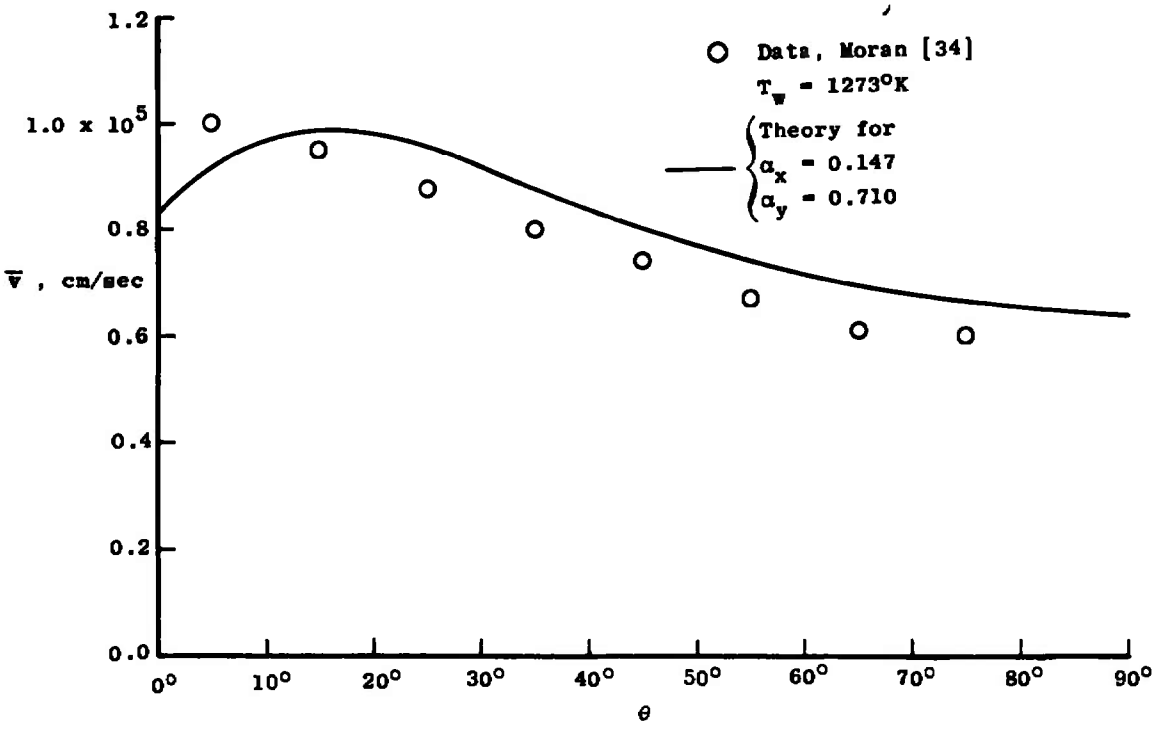

c. Mean Speed.

Figure 40 (Continued).

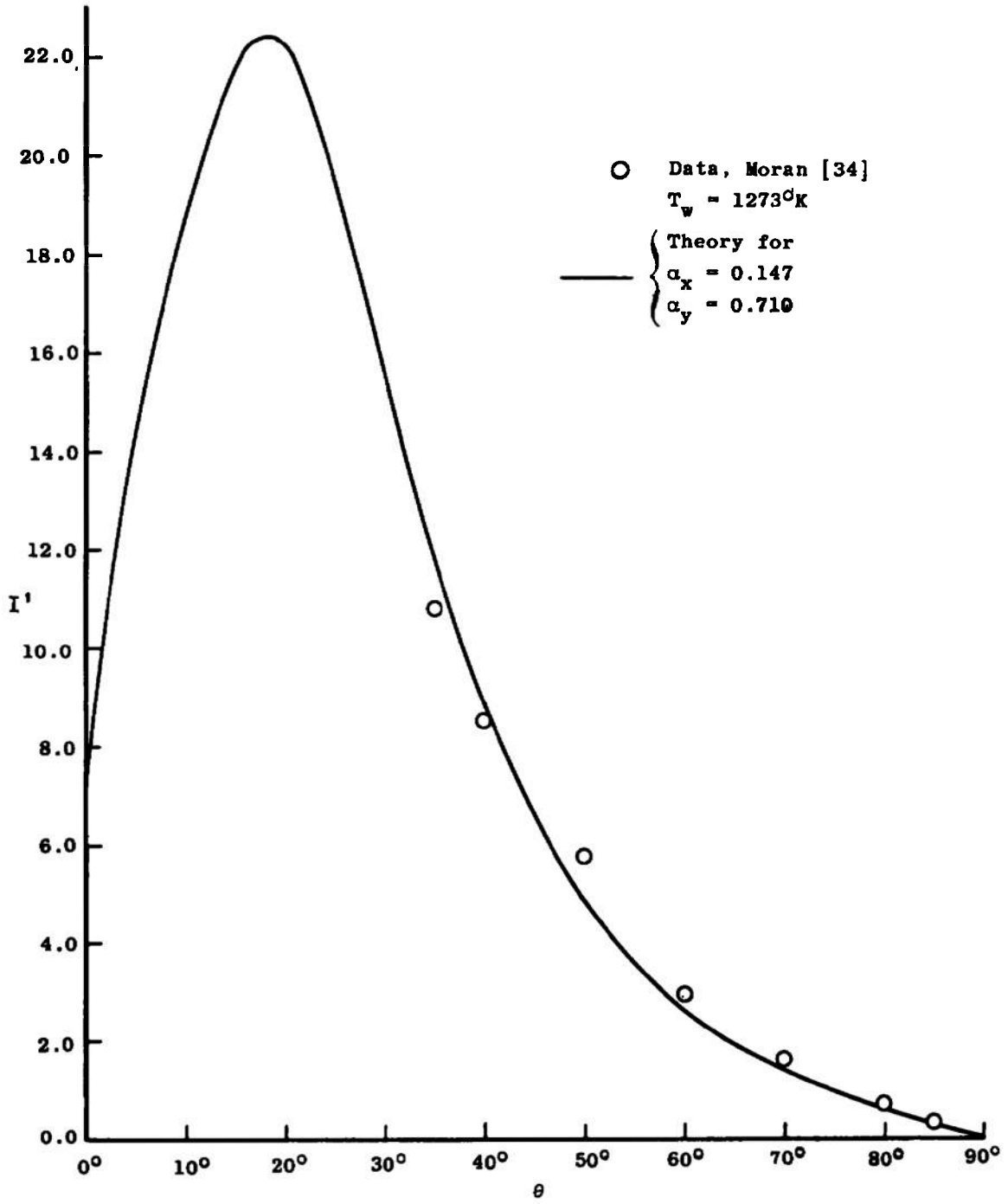

a. Relative Flux.

Figure 41. Comparison of Theory and Data for Argon Scattered from Platinum, θ_i = -20°, v' = 9.55 x 10^4 cm/sec.

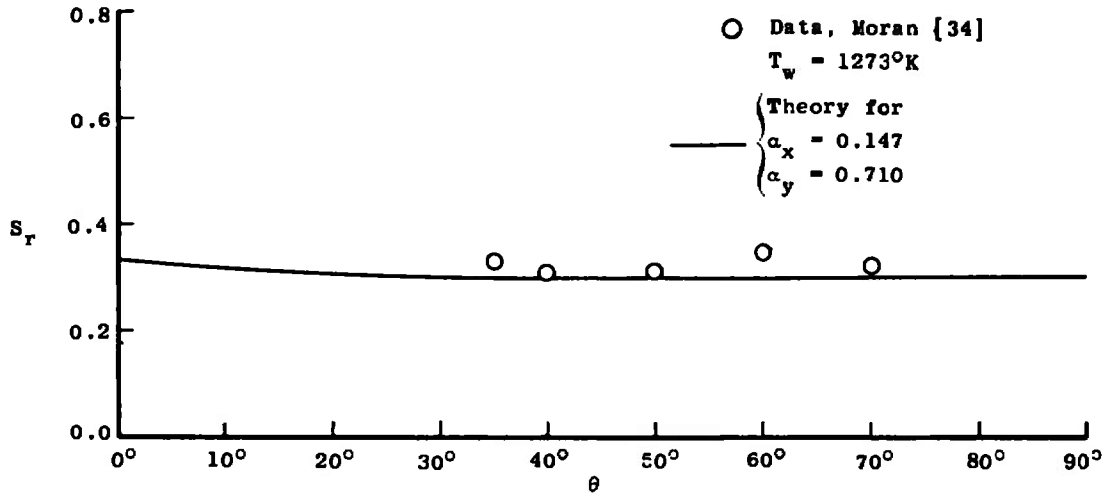

b. Speed Ratio.

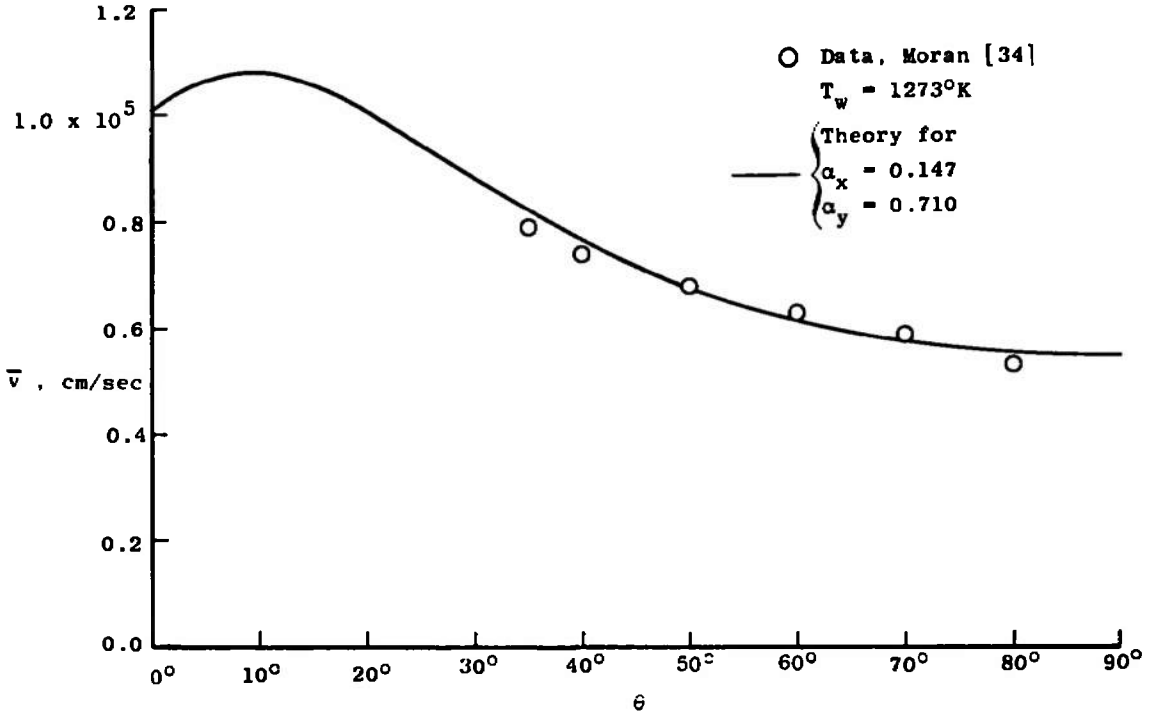

c. Mean Speed.

Figure 41. (Continued).

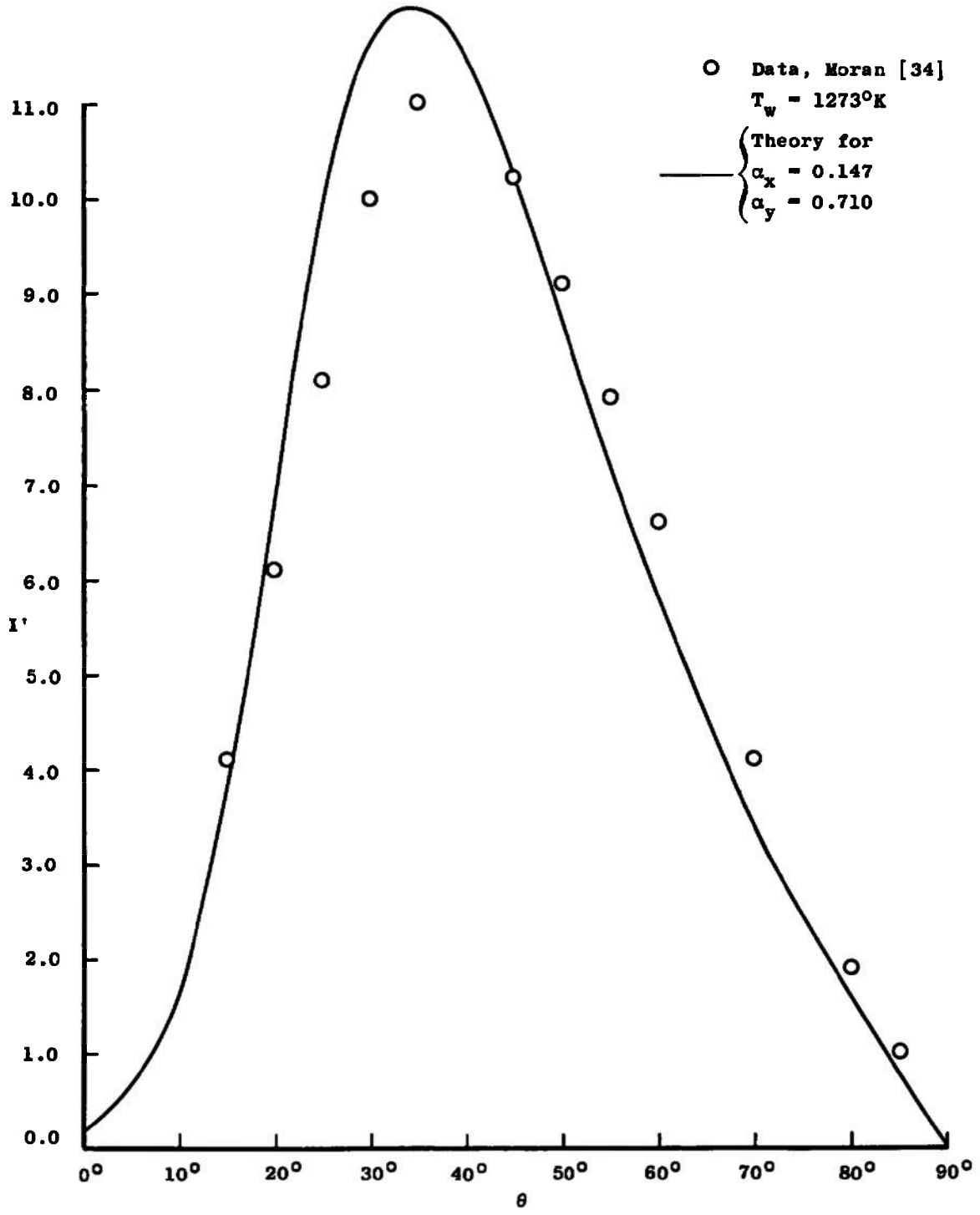

a. Relative Flux.

Figure 42. Comparison of Theory and Data for Argon Scattered from Platinum, θ_i = -40°, v' = 9.55 x 10^4 cm/sec.

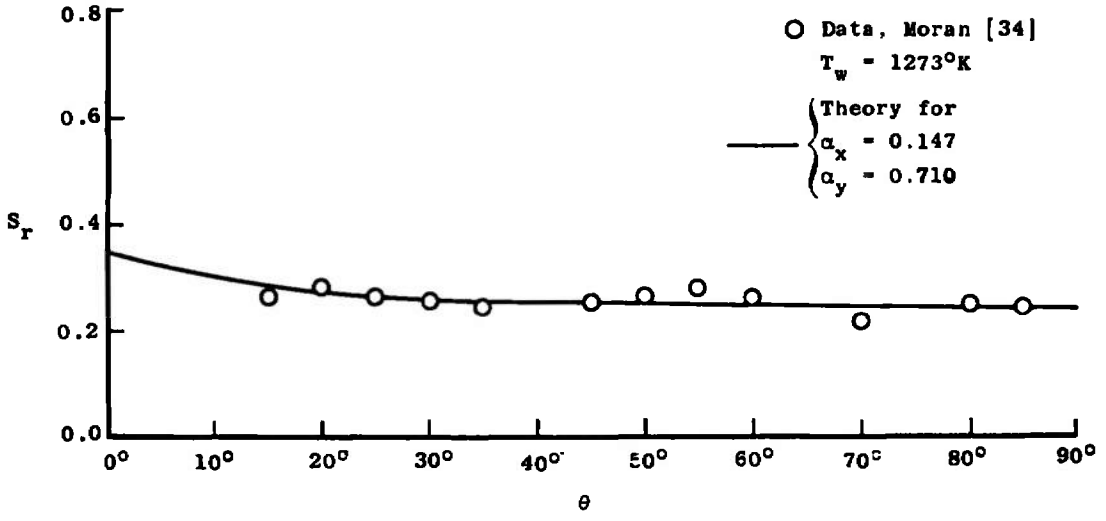

b. Speed Ratio.

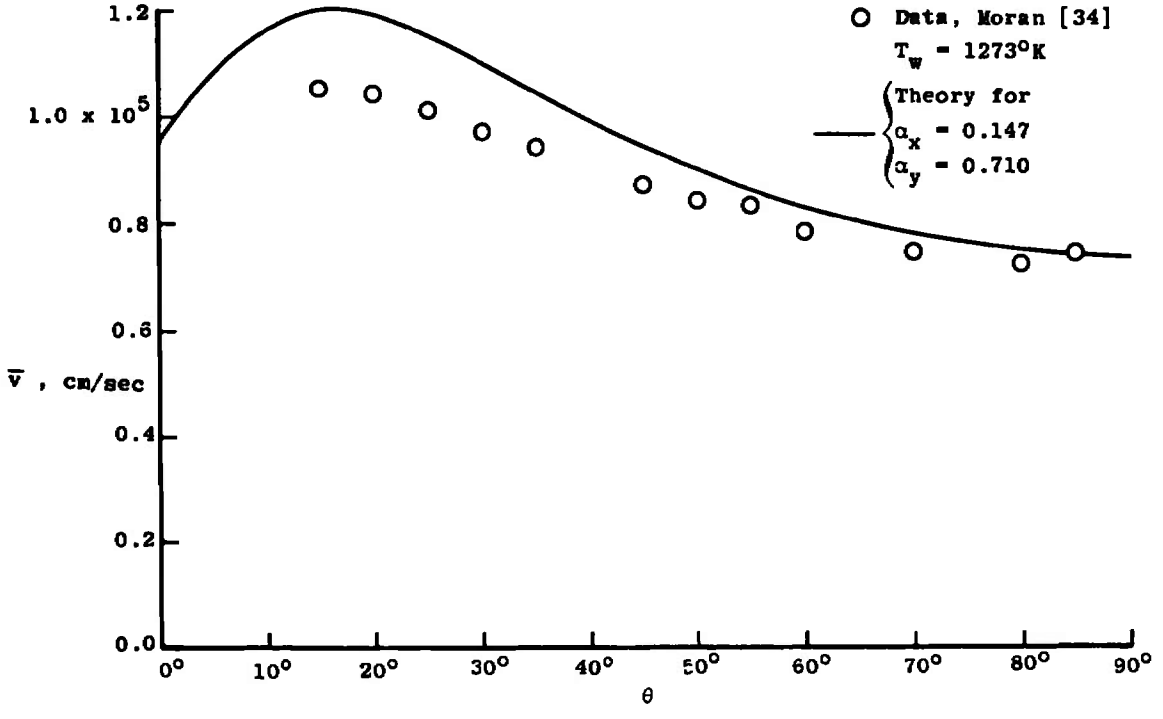

c. Mean Speed.

Figure 42. (Continued).

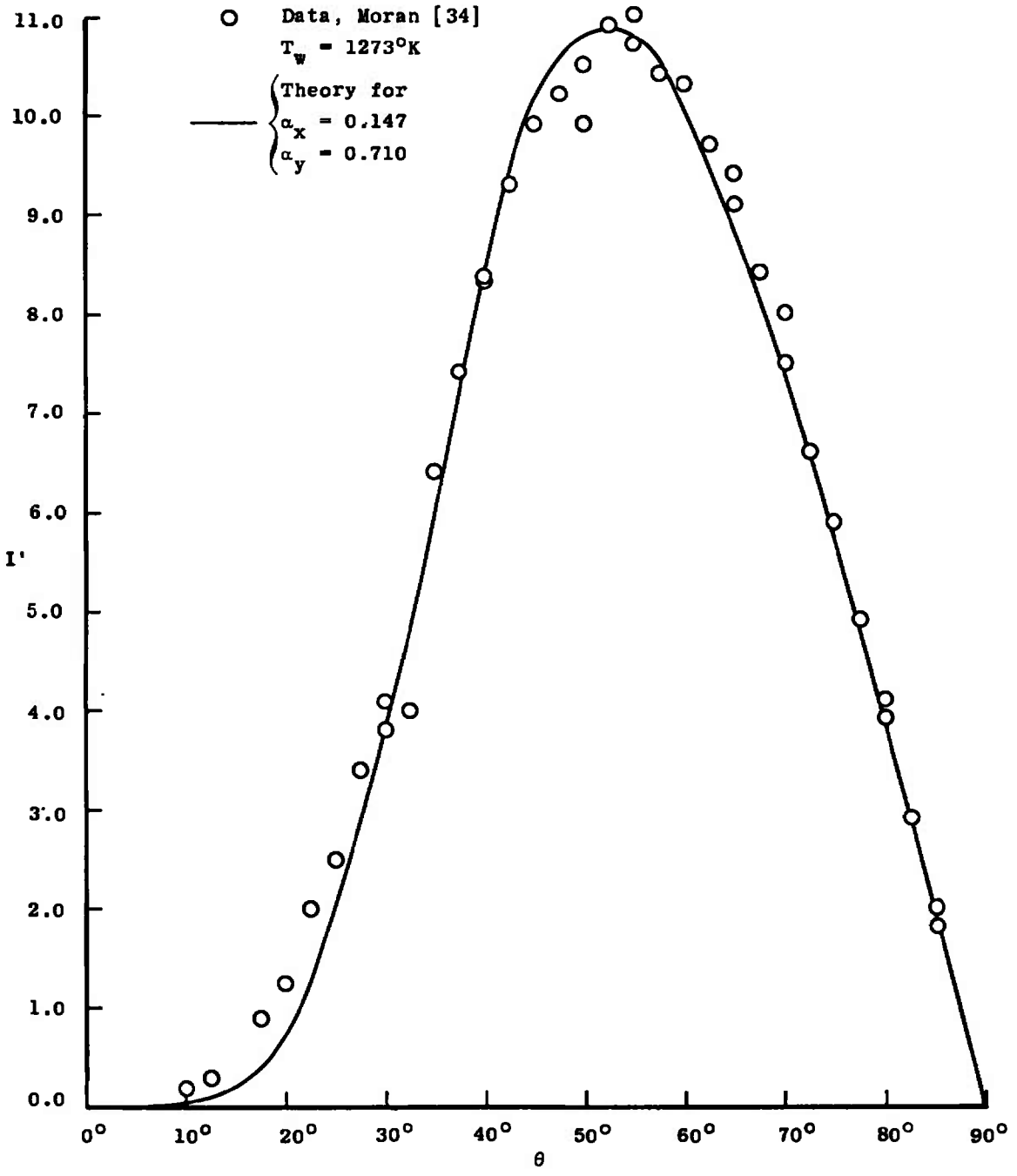

a. Relative Flux.

Figure 43. Comparison of Theory and Data for Argon Scattered from Platinum, θ_i = -65°, v' = 9.55 x 10^4 cm/sec.

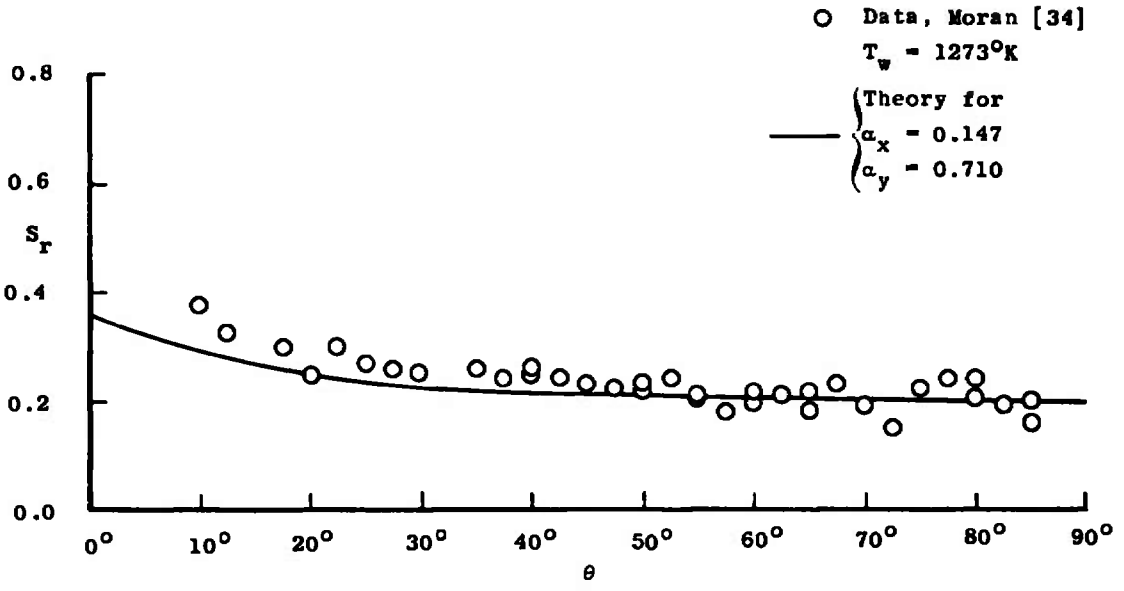

b. Speed Ratio

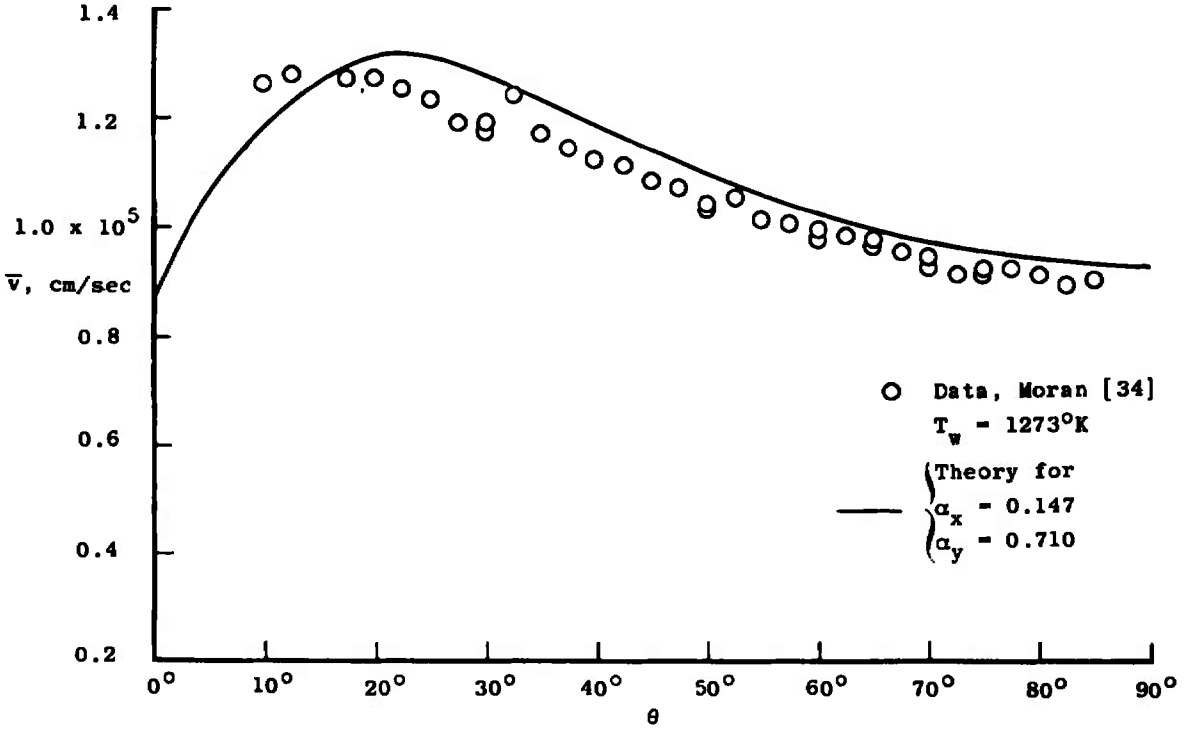

c. Mean Speed.

Figure 43. (Continued).

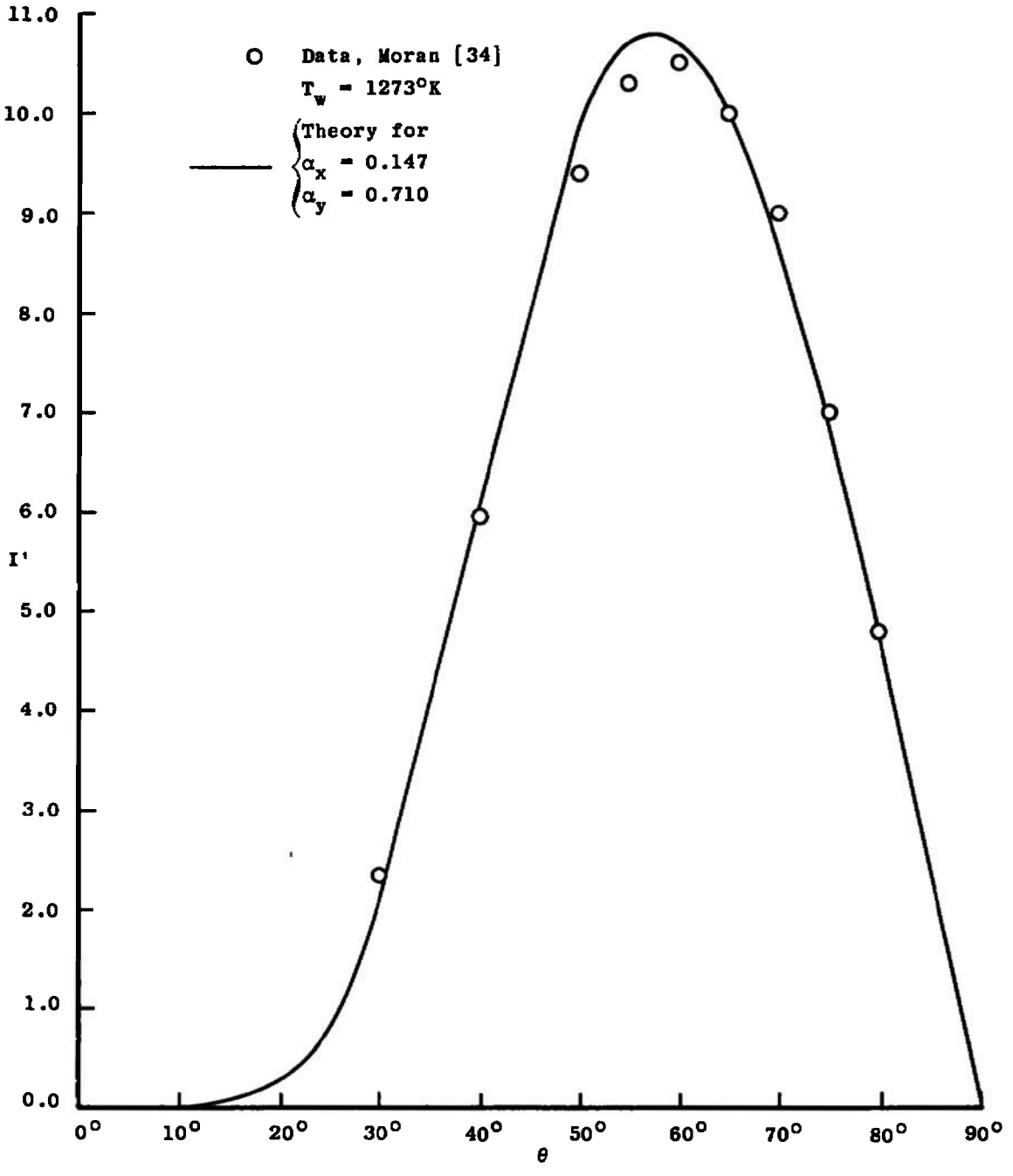

a. Relative Flux.

Figure 44. Comparison of Theory and Data for Argon Scattered from Platinum, θ_i = -80°, v' = 9.55 x 10^4 cm/sec.

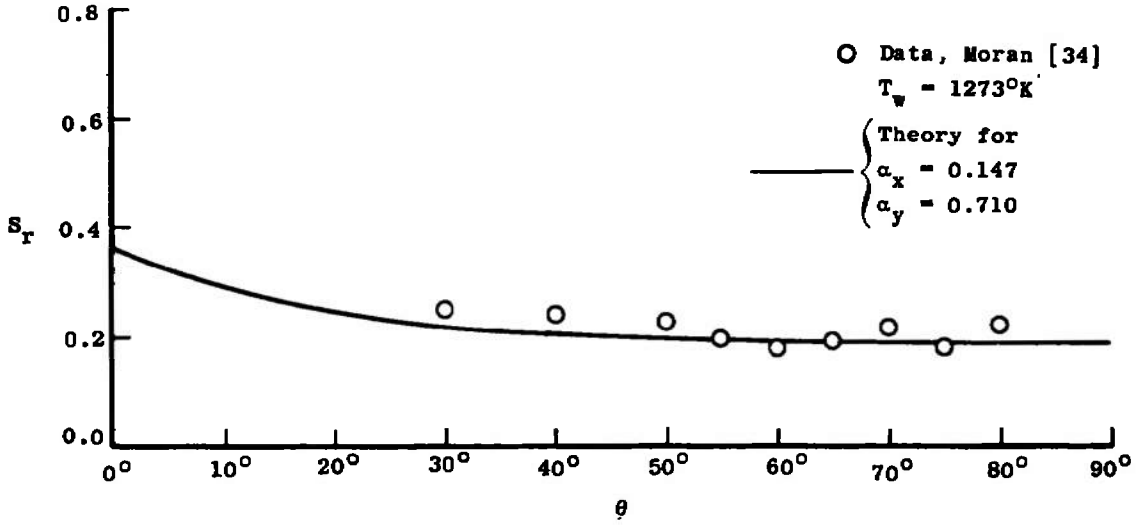

b. Speed Ratio.

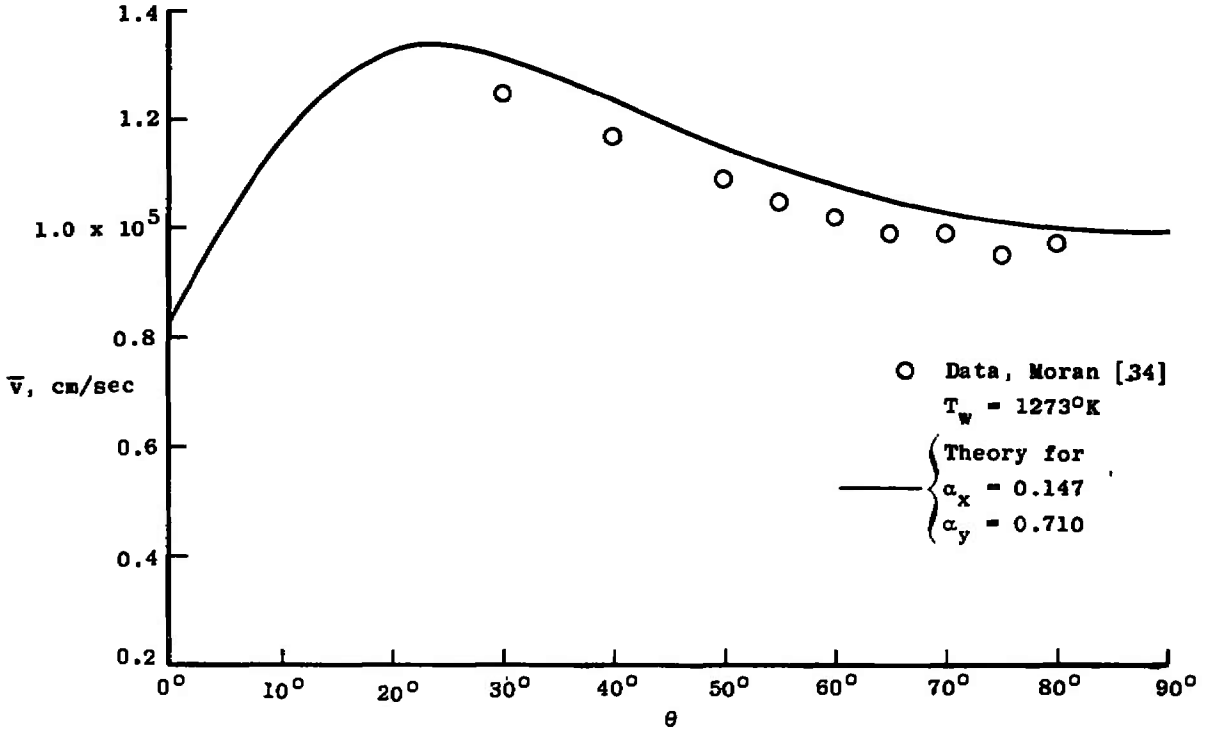

c. Mean Speed.

Figure 44. (Continued).

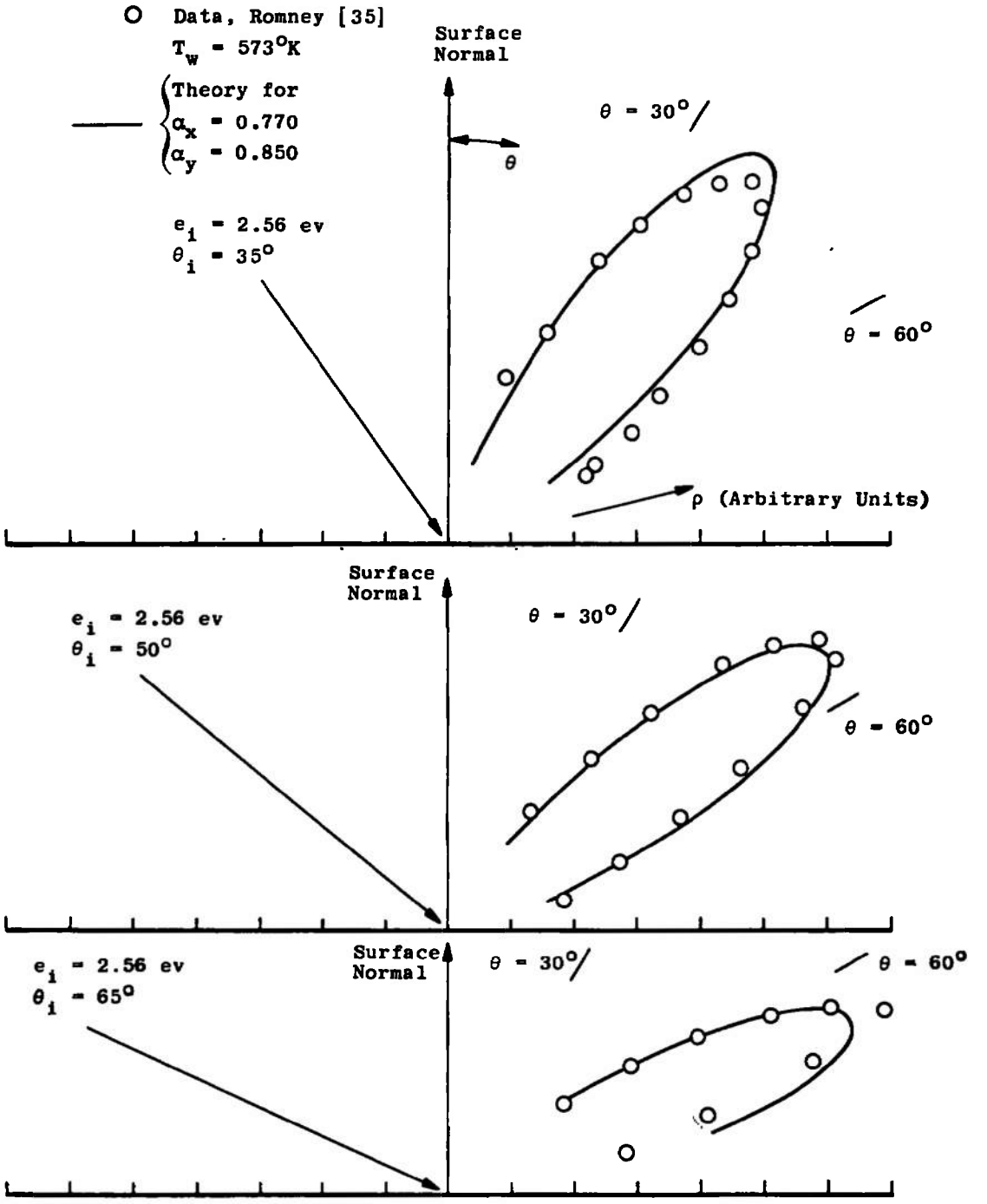

a. Relative Density.

Figure 45. Comparison of Theory with Data of Romney [35].

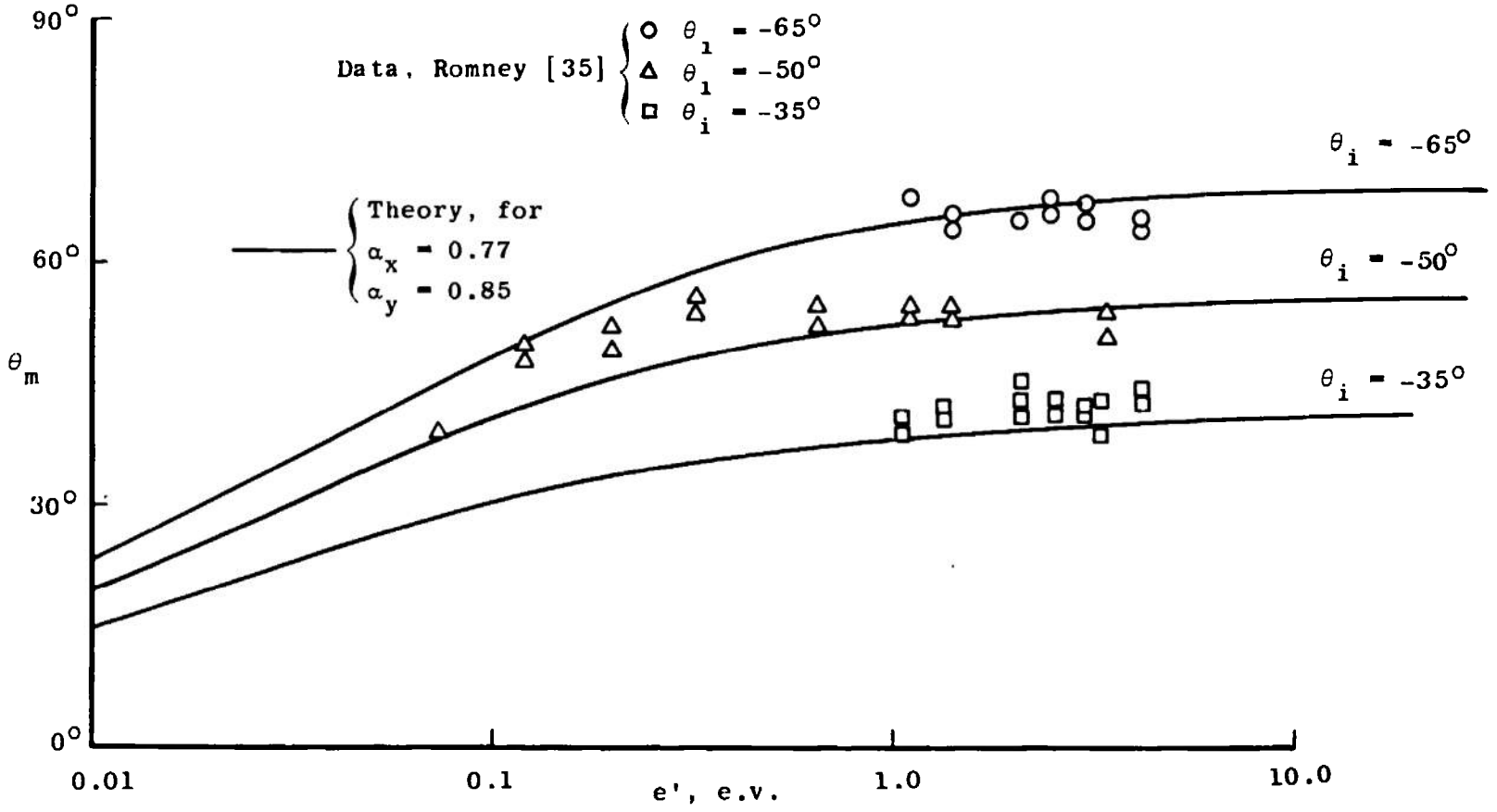

b. Position of Maximum Intensity.
Figure 45. (Continued).

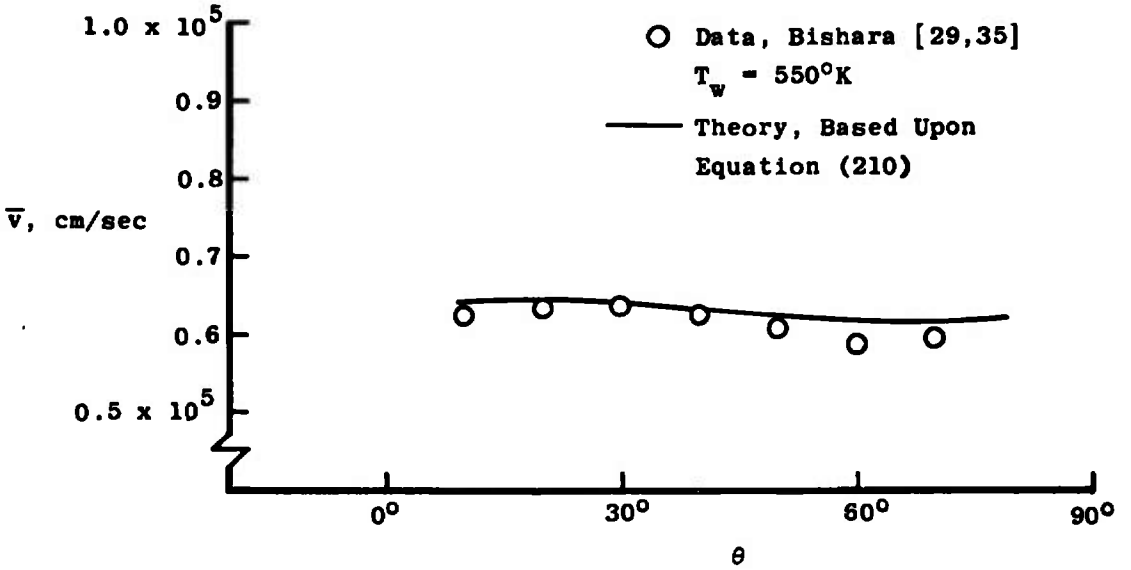

b. Mean Speed, $\phi = 0°$.

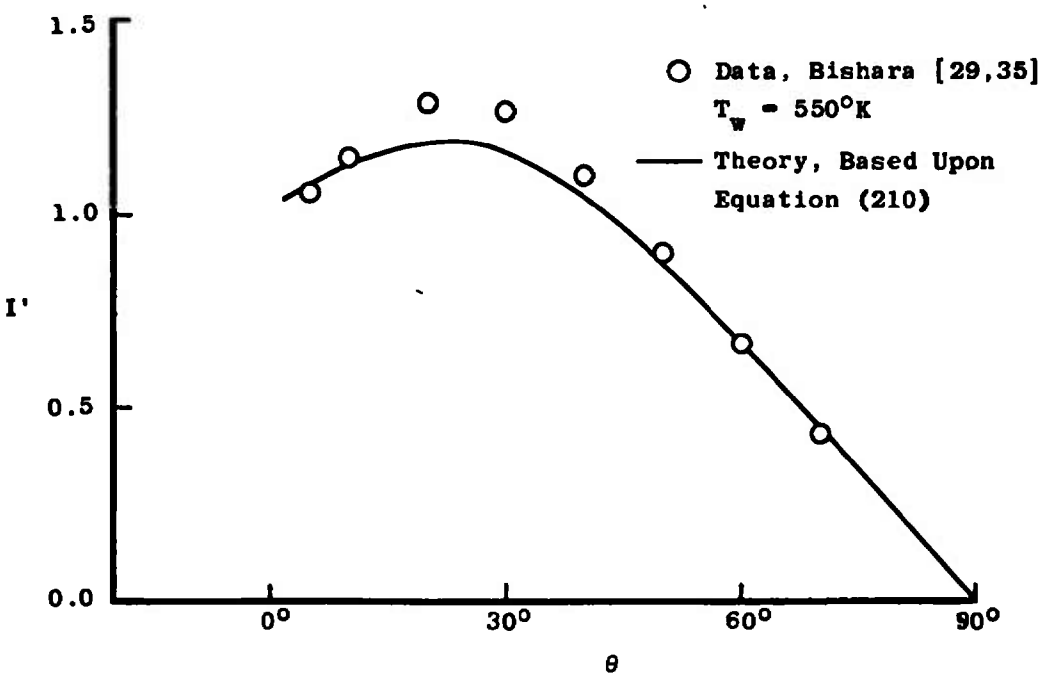

a. Relative Intensity, $\phi = 0°$.

Figure 46 Comparison of Theory and Data for Argon Scattered from Silver, $\theta_i = -40°$, $v' = 5.56 \times 10^4$ cm/sec.

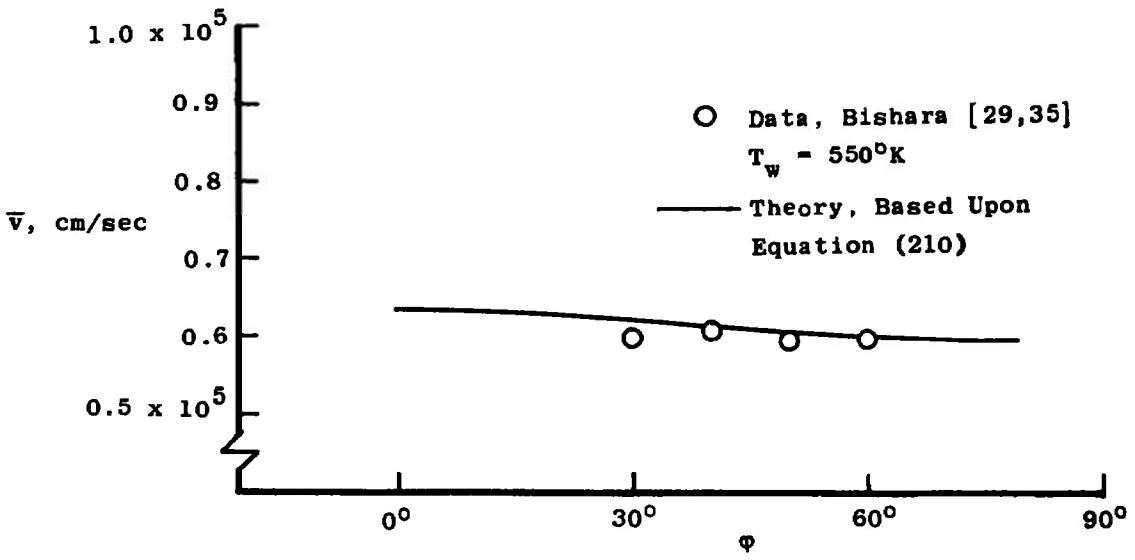

d. Mean Speed, $\theta = 0°$.

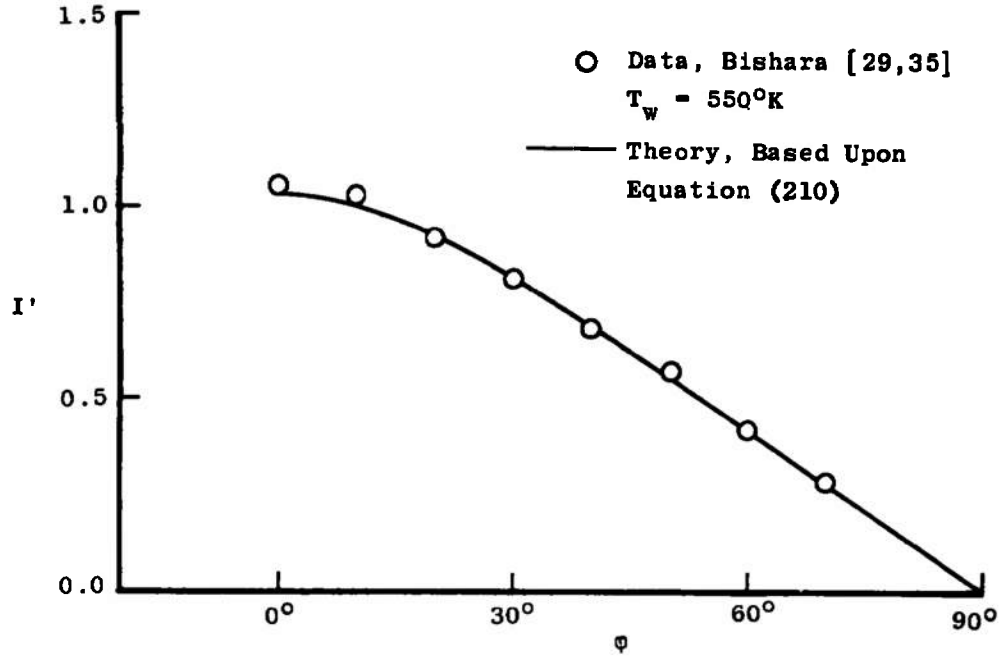

c. Relative Intensity, $\theta = 0°$.

Figure 46. (Continued).

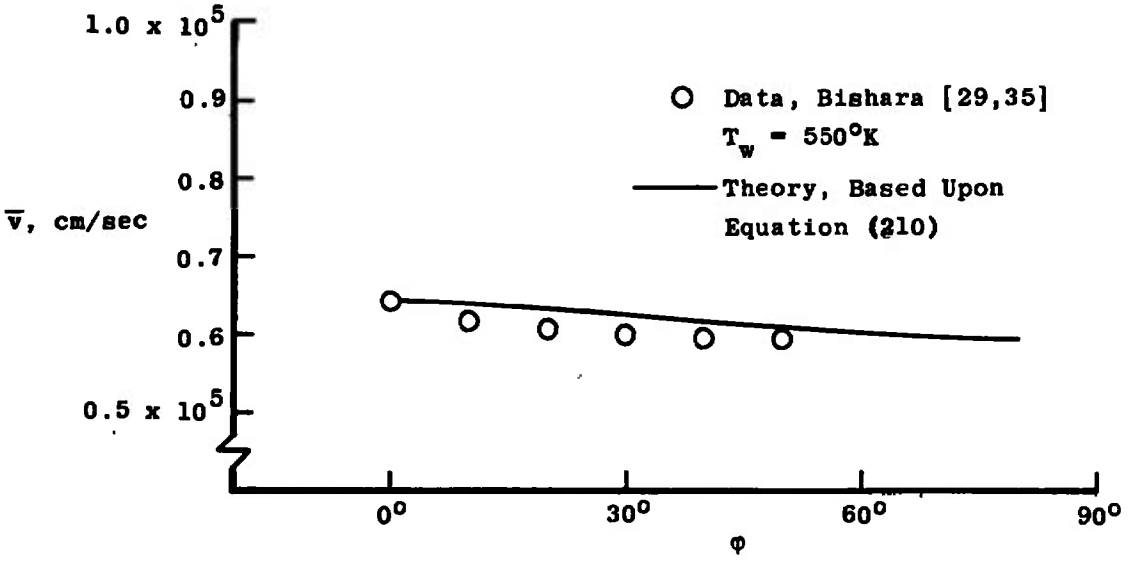

f. Mean Speed, $\theta = 20°$.

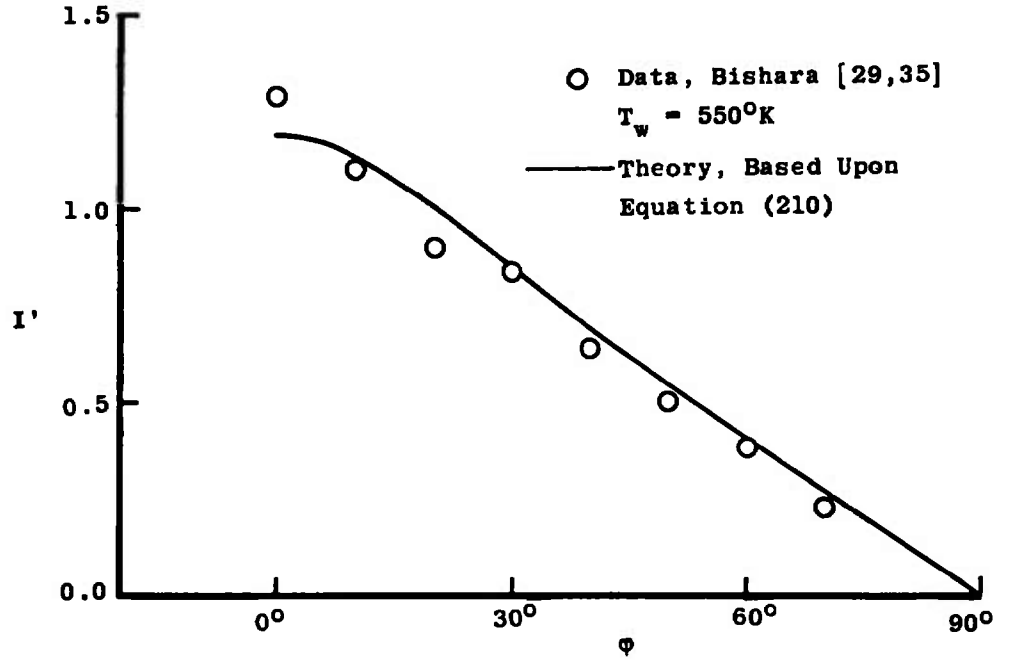

e. Relative Intensity, $\theta = 20°$.
Figure 46. (Continued).

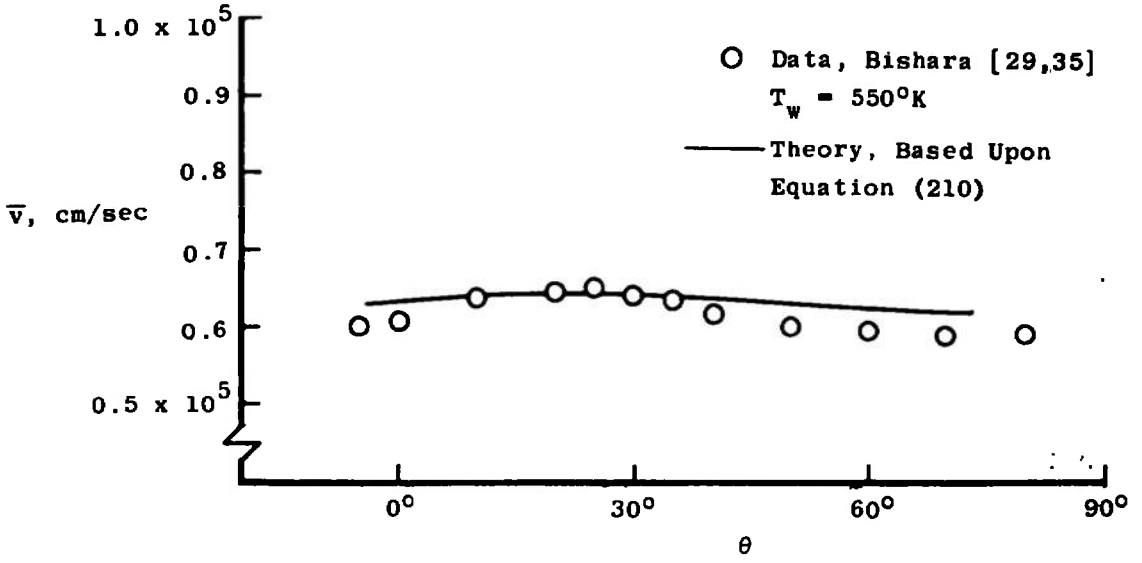

b. Mean Speed, $\phi = 0°$.

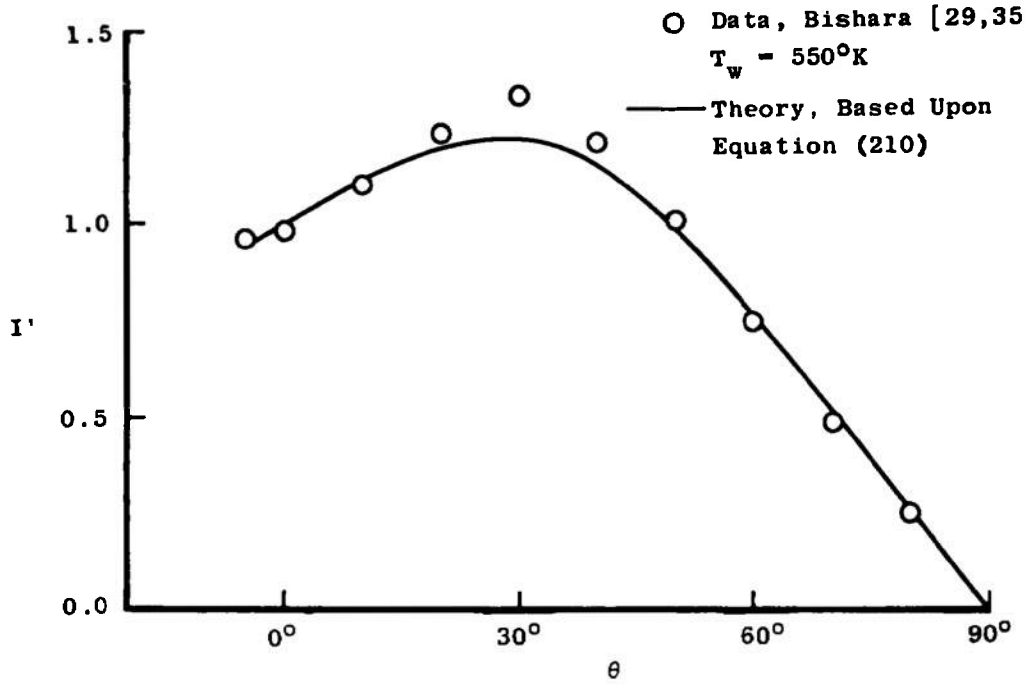

a. Relative Intensity, $\phi = 0°$.

Figure 47. Comparison of Theory and Data for Argon Scattered from Silver, $\theta_i = -50°$, v' = 5.56 x 10^4 cm/sec.

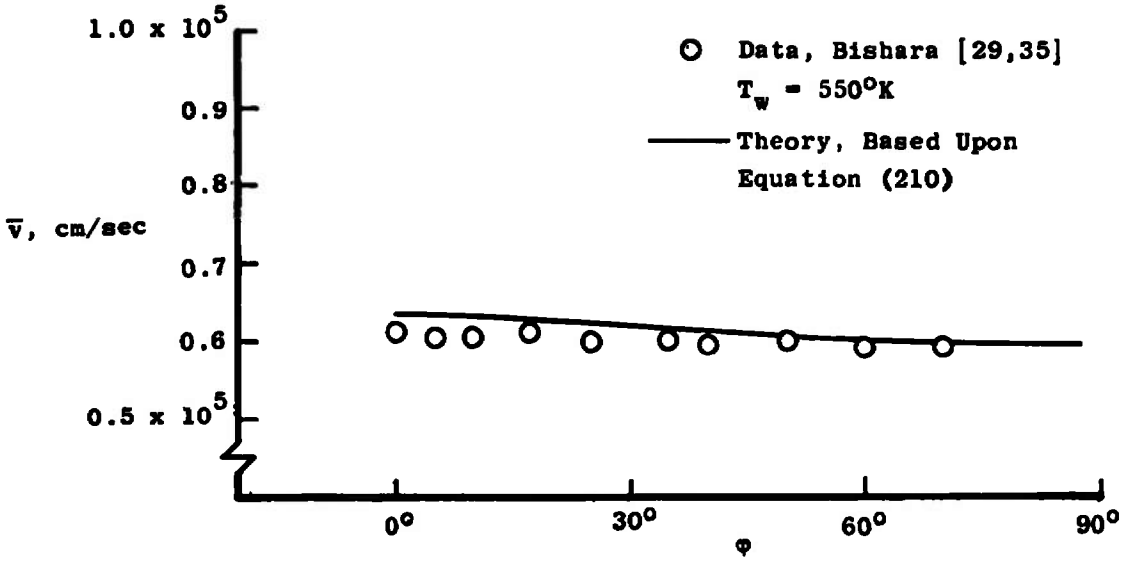

d. Mean Speed, $\theta = 0°$.

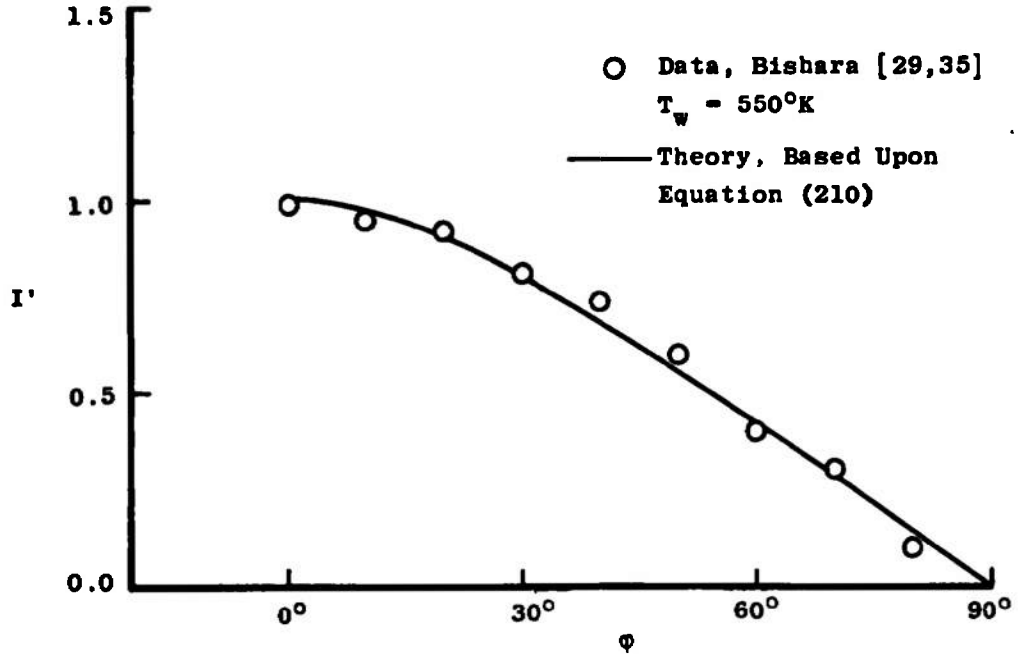

c. Relative Intensity, $\theta = 0°$.

Figure 47. (Continued).

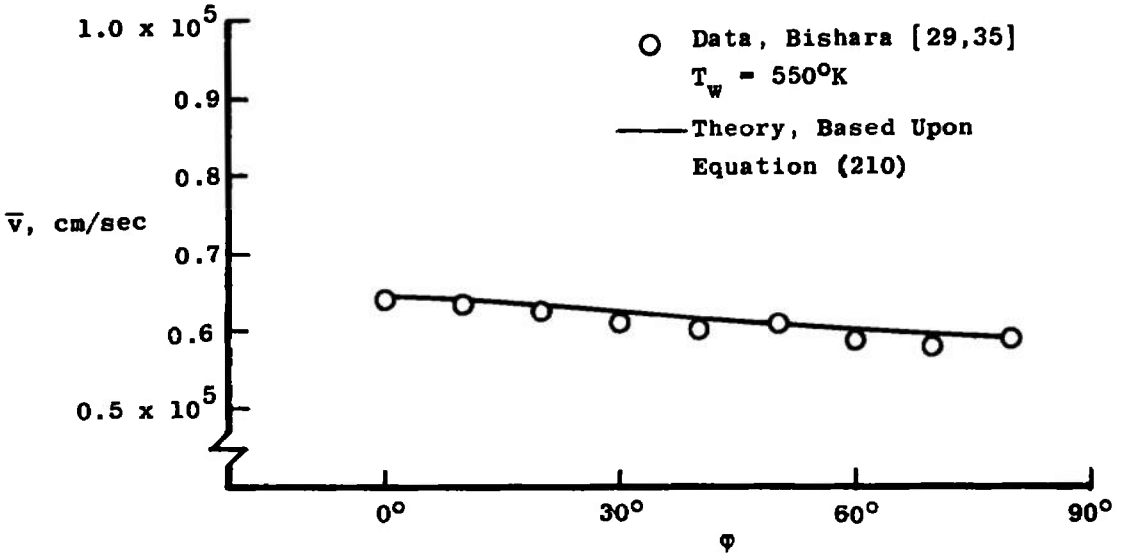

f. Mean Speed, $\theta = 30°$.

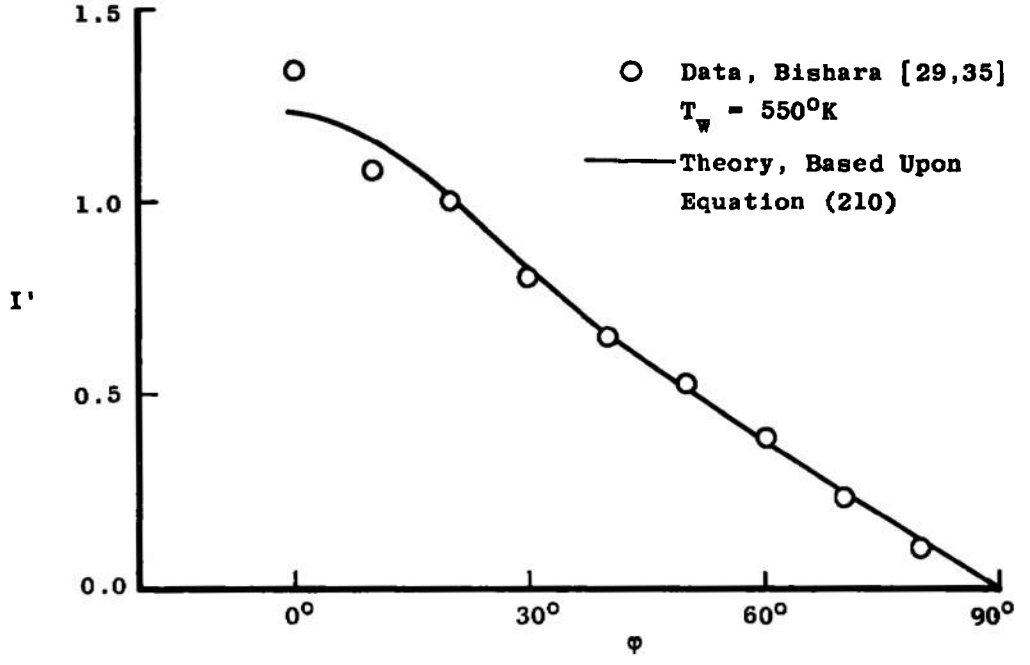

e. Relative Intensity, $\theta = 30°$.

Figure 47. (Continued).

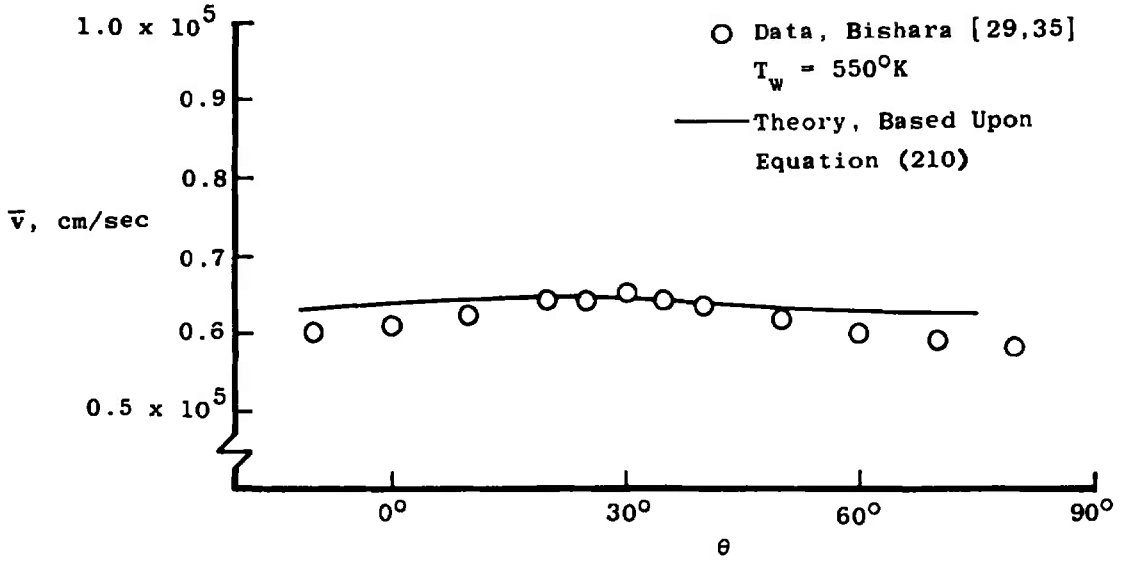

b. Mean Speed, $\phi = 0°$.

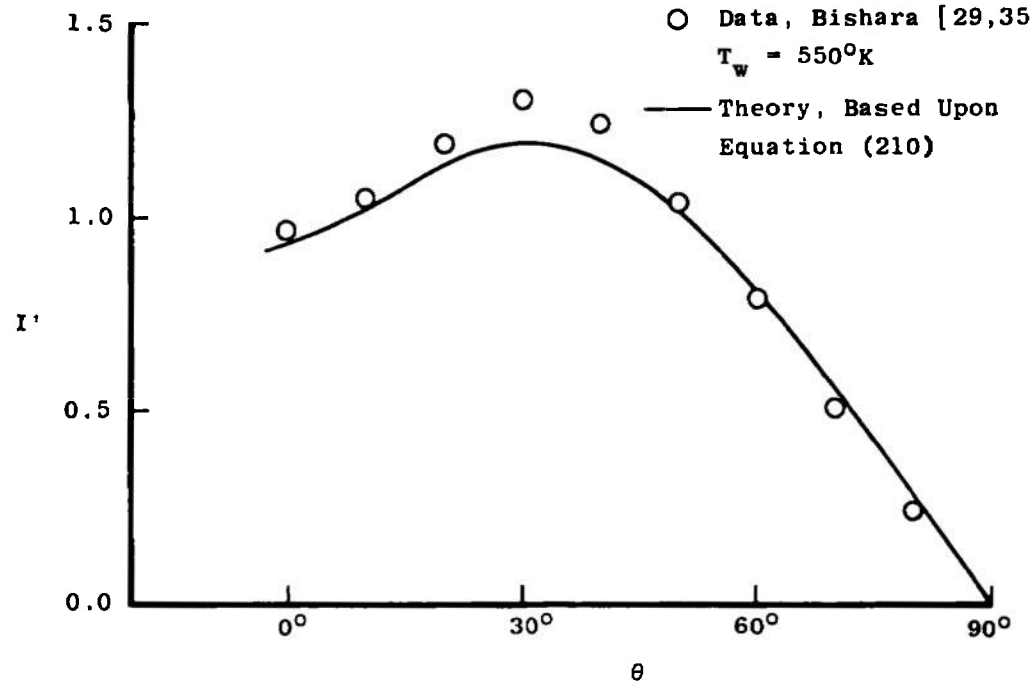

a. Relative Intensity, $\phi = 0°$.

Figure 48. Comparison of Theory and Data for Argon Scattered from Silver, $\theta_i = -60°$, $v' = 5.56 \times 10^4$ cm/sec.

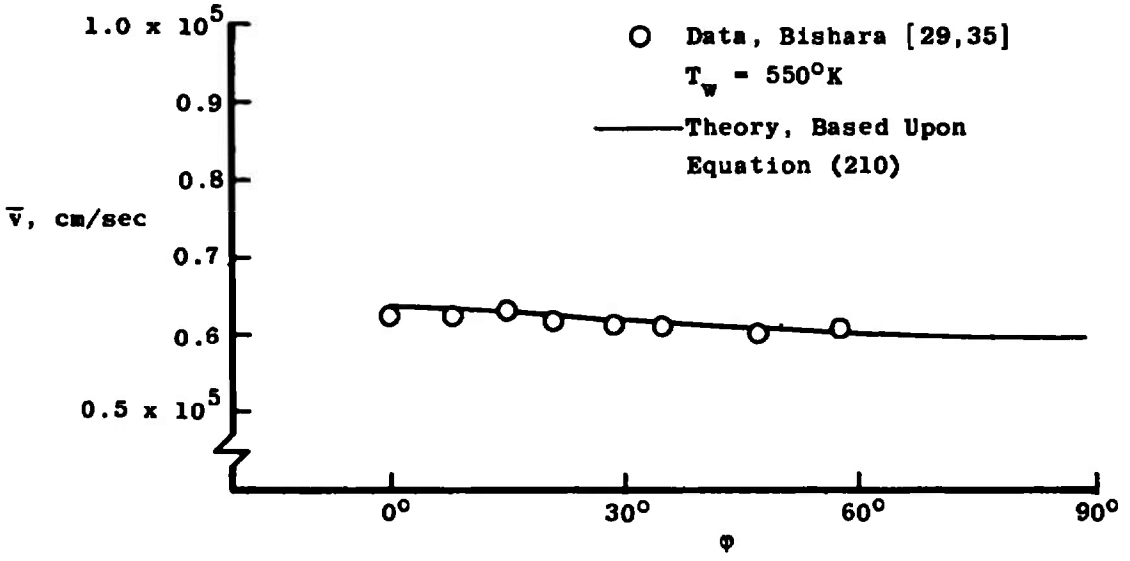

d. Mean Speed, $\theta = 0°$.

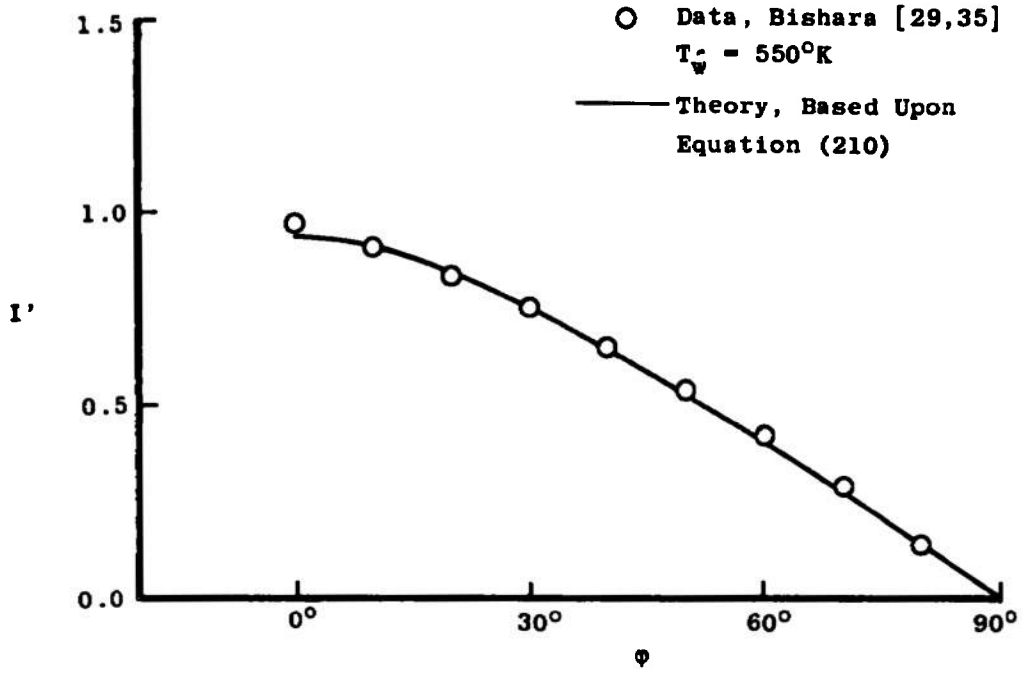

c. Relative Intensity, $\theta = 0°$.

Figure 48. (Continued).

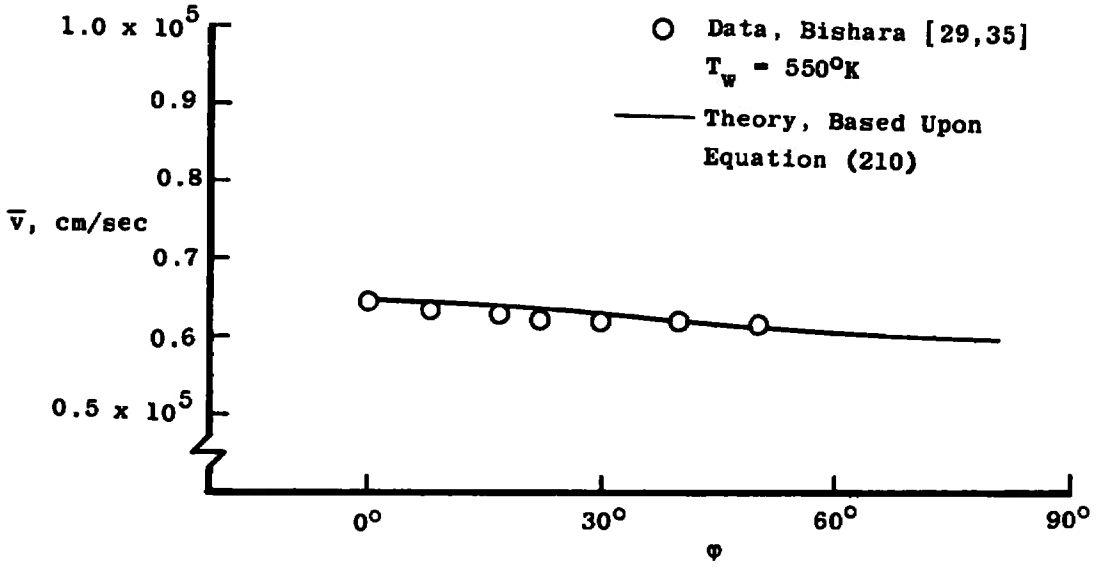

f. Mean Speed, $\theta = 30°$.

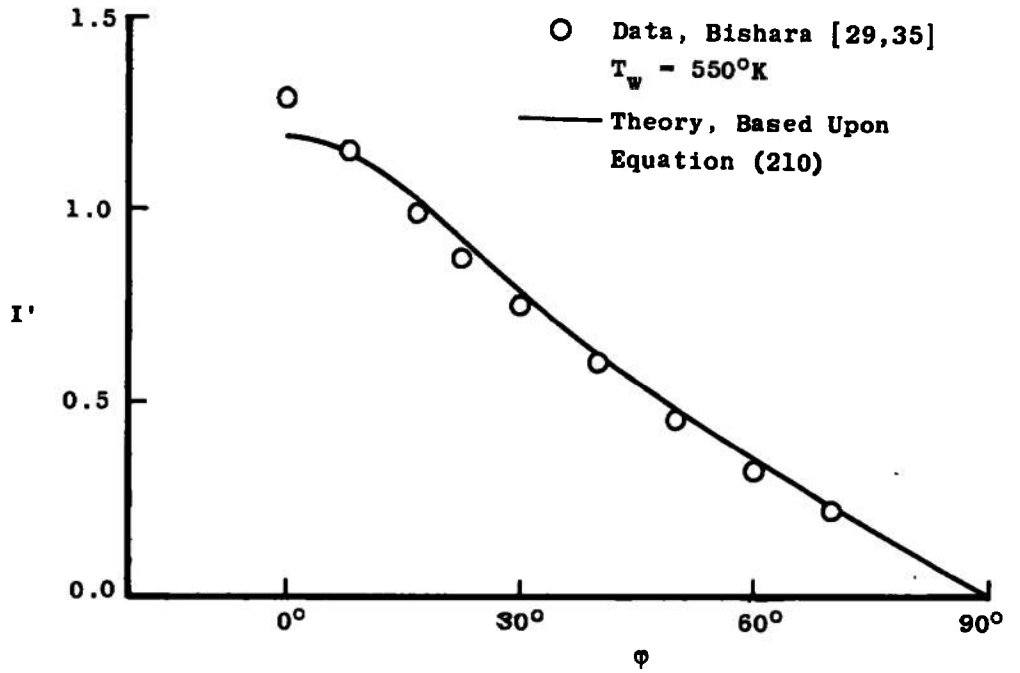

e. Relative Intensity, $\theta = 30°$.

Figure 48. (Continued).

APPENDIX B
EVALUATION OF CERTAIN INTEGRALS OF EXPONENTIALS AND BESSEL FUNCTIONS

At several points in the development of the analysis it was necessary to evaluate infinite integrals of the following type:

$$\int_0^\infty x^n \exp(-ax^2)\ I_\nu(bx)\ dx \qquad \text{(B-1)}$$

Letting $x = t^{1/2}$ expression B-1 becomes:

$$1/2 \int_0^\infty t^{n/2-1/2} \exp(-at)\ I_\nu(bt^{1/2})\ dt \qquad \text{(B-2)}$$

This integral can be evaluated by the use of Equation 6.643-2 of Gradshteyn and Ryzhik [39] and the result is:

$$\Gamma(n/2 + \nu/2 + 1/2)[a^{n/2}\ b\ \Gamma(\nu+1)]^{-1} \exp(b^2/8a) M_{-n/2,\nu/2}(b^2/4a) \qquad \text{(B-3)}$$

where $M_{c,d}(t)$ is Whittaker's Function (see [30], page 505).

The result in expression B-3 can be written in terms of Kummer's Function M(c,d,t) using Equation 13.1.32 of [30] and the final result for the integral is:

$$\Gamma(n/2 + \nu/2 + 1/2)[a^{n/2}\ b\ \Gamma(\nu+1)]^{-1}(b^2/4a)^{(1+\nu)/2} \cdot M(1/2 + \nu/2 + n/2,\ 1 + \nu,\ b^2/4a) \qquad \text{(B-4)}$$

where from [30] Kummer's Function is defined as:

$$M(c,d,t) = \sum_{m=0}^{\infty} \frac{\Gamma(c+m)\ \Gamma(d)\ t^m}{\Gamma(c)\ \Gamma(d+m)\ m!} \tag{B-5}$$

Notice that for c = d Equation B-5 becomes:

$$M(d,d,t) = \exp(t) \tag{B-6}$$

Using these results the following equations are obtained for some integrals of interest:

$$\int_0^{\infty} xe^{-ax^2} I_0(bx)dx = 1/(2a)\ \exp(b^2/4a) \tag{B-7}$$

$$\int_0^{\infty} x^2e^{-ax^2} I_0(bx)\ dx = \pi^{1/2}/(4a^{3/2})\ M(3/2,1,b^2/4a) \tag{B-8}$$

$$\int_0^{\infty} xe^{-ax^2} I_1(bx)\ dx = (b\pi^{1/2}/8a^{3/2})\ M(3/2,2,b^2/4a) \tag{B-9}$$

$$\int_0^{\infty} x^2e^{-ax^2} I_1(bx)\ dx = b/(4a^2)\ \exp(b^2/4a) \tag{B-10}$$

$$\int_0^{\infty} x^3e^{-ax^2} I_1(bx)\ dx = (3\pi^{1/2}b/16a^{5/2})\ M(5/2,2,b^2/4a) \tag{B-11}$$

UNCLASSIFIED

Security Classification

DOCUMENT CONTROL DATA - R & D

(Security classification of title, body of abstract and indexing annotation must be entered when the overall report is classified)

1 ORIGINATING ACTIVITY (Corporate author) Arnold Engineering Development Center Arnold Air Force Station, Tenn. 37389	2a. REPORT SECURITY CLASSIFICATION UNCLASSIFIED 2b. GROUP N/A

3 REPORT TITLE

A MATHEMATICAL DESCRIPTION OF GAS-SURFACE INTERACTION BASED UPON RECIPROCITY

4 DESCRIPTIVE NOTES (Type of report and inclusive dates)

Final Report - July 1970 to July 1971

5 AUTHOR(S) (First name, middle initial, last name)

Max Kinslow, ARO, Inc.

6 REPORT DATE February 1973	7a. TOTAL NO OF PAGES 246	7b. NO. OF REFS 39
8a. CONTRACT OR GRANT NO b. PROJECT NO c. Program Element 65802F d.	9a. ORIGINATOR'S REPORT NUMBER(S) AEDC-TR-72-158 9b. OTHER REPORT NO(S) (Any other numbers that may be assigned this report) ARO-VKF-TR-72-147	

10 DISTRIBUTION STATEMENT

Approved for public release; distribution unlimited.

11 SUPPLEMENTARY NOTES Available in DDC	12 SPONSORING MILITARY ACTIVITY Arnold Engineering Development Center, Air Force Systems Command, Arnold AF Station, Tenn. 37389

13 ABSTRACT The general problem of the interaction between a monatomic gas and a solid surface is investigated from a mathematical point of view by the use of a scattering kernel. This general scattering kernel must fulfill the obvious conditions of normalization and non-negativity and has recently been shown to also satisfy the condition of detailed balancing or reciprocity. Previous gas-surface theories, both analytical and empirical, are considered in view of reciprocity. It is shown that most of these descriptions are satisfactory for gross gas-surface interactions but fail to describe the detailed interaction. By assuming a product solution in each of three coordinate systems, an infinite series of solutions is obtained. The first scattering kernel in each series is obtained in closed mathematical form, while the second and third are evaluated numerically. Recurrence relations are obtained for the coefficients in the infinite series for all rectangular coordinates adequately describes the experimentally observed results of gas-surface interaction. This solution has two parameters which describe the gas-surface interaction. It is shown that these parameters are related to a tangential and a normal thermal accommodation coefficient. The scattering kernels obtained are integrated, in some cases analytically and others numerically, with various weighting functions in order to obtain mean reflected properties, both global and local, such as molecular flux, speed, and energy. These various results are presented for typical gas-surface interaction parameters.

DD FORM 1 NOV 68 1473

UNCLASSIFIED

Security Classification

UNCLASSIFIED

Security Classification

14 KEY WORDS	LINK A		LINK B		LINK C	
	ROLE	WT	ROLE	WT	ROLE	WT
1. gas-surface interaction						
applications of mathematics						
4 argon						
5 platinum						
6 silver						
molecules						
scattering						

2. Gases -- Interaction with

3 Solids -- " "

AFSC
Arnold AFS Tenn

UNCLASSIFIED

Security Classification